



ALMA MATER STUDIORUM  
UNIVERSITÀ DI BOLOGNA

**DOTTORATO DI RICERCA IN**

**MECCANICA E SCIENZE AVANZATE DELL'INGEGNERIA**

Ciclo XXXVI

**Settore Concorsuale: 09/A2**

**Settore Scientifico Disciplinare: ING-IND/13**

**NEW DEVELOPMENTS AND APPLICATIONS BASED ON A NUMERICAL  
MODEL FOR THE OPTIMISATION OF THE CENTRED GEAR  
SKIVING PROCESS**

**Presentata da:** Enea Olivoni

**Coordinatore Dottorato**

Lorenzo Donati

**Supervisore**

Prof. Ing. Rocco Vertechy

**Co-supervisor**

Prof. Ing. Vincenzo Parenti-Castelli

Stefano Fiocchi

Andrea Giannini

Esame finale anno 2024



# Abstract

Gear skiving, known for its high productivity in manufacturing internal gears, has become increasingly popular. Due to complexities including tool profile calculation, kinematics, and variable cutting conditions, and its relatively recent adoption, there is still a lack of in-depth knowledge about the process. Consequently, gear practitioners often rely on their own experience when developing new cutting strategies to mitigate specific process issues and reduce tool wear.

The initial focus of this work is on a thorough literature review of the research and development activities related to gear skiving that was previously missing. Then, a numerical program for the geometric simulation of the process has been developed, enabling analysis of the interplay between setup parameters, and cutting conditions. The simulation has led to new insights and cutting strategies that reduce cumulative machined total cutting length, while keeping the cycle time unchanged or reduced, without significantly impacting the tool load. Experimental tests on annealed steel gears have confirmed that these strategies can reduce tool wear by up to 50%.

Furthermore, the novel numerical program has been developed to assess the impact of re-sharpening conical tools on the process. Re-sharpening alters the tip diameter and the profile of conical tools, affecting cutting performance over their service life. The study identifies tools sensitive to this phenomenon and introduces a strategy to minimize performance variations, validated by experiments.

Finally, this work introduces a novel design methodology for skiving tools using screw theory, a concept previously unexplored in skiving literature. Unlike traditional experience-based design methods, this approach selects the number of teeth, helix angle, and tip diameter based on qualitative indices to enhance tool productivity and cutting conditions. New equations for the tool operating pitch diameter are derived, providing insights into the implications of tip diameter on the full process. While still under investigation, this methodology shows promise.

# Table of Contents

1	Introduction.....	1
1.1	Motivation .....	1
1.2	Geometry and kinematics of centred gear skiving .....	2
1.2.1	Process kinematics .....	2
1.2.2	Tool geometry .....	5
1.2.3	Skiving machine tool and set-up parameters.....	7
1.3	State of the Art .....	11
1.3.1	Cutting process principle and simulation .....	12
1.3.2	Parameters influence on the process .....	14
1.3.3	Tool design.....	16
1.3.4	Miscellaneous.....	17
1.4	Contribution of the Thesis.....	18
2	Numerical model of centred gear skiving .....	20
2.1	Need of an ad hoc program .....	20
2.2	Numerical model workflow.....	20
2.2.1	Input data.....	21
2.2.2	Relative kinematics .....	22
2.2.3	Tool profile calculation .....	25
2.2.4	Surface swept by the tool at each pass .....	29
2.2.5	Workpiece gap at each pass.....	31
2.2.6	Surfaces intersection .....	32
2.2.7	Model of cutting geometry .....	36
2.2.8	Cutting conditions .....	40
2.3	Validation .....	53
2.4	Known limitations and possible uses .....	54
2.5	Conclusions and future perspectives .....	55
3	Process optimisation based on the proposed numerical model .....	56
3.1	Implications of $NoP$ and $h_{MAX}$ on $l_{TOT}$ and on $A_{hp}$ .....	56
3.2	Application 1: novel cutting strategy aimed at tool wear reduction.....	61
3.2.1	Case study 1 .....	63
3.2.2	Case study 2 .....	67
3.3	Application 2: on the implications resulting from re-sharpening of conical skiving tools .....	75
3.3.1	Parameters of the most sensitive tools to the cutting profile change as a result of re-sharpening .....	76



3.3.2	Simulation of cutting profile change based on the proposed numerical model...	77
3.3.3	Benchmarking procedure .....	78
3.3.4	Comparison of cutting performances between SOL and EOL: Case study 1 .....	79
3.3.5	Comparison of cutting performances between SOL and EOL: Case study 2 .....	82
3.3.6	Homogenisations of cutting performances between SOL and EOL: Case study 1 .....	84
3.4	Conclusions and future perspectives .....	87
4	Towards a parameter selection method for conical skiving tools .....	89
4.1	The tool design parameters.....	90
4.1.1	The domain of the tool kinematic parameters .....	91
4.2	Implications of the tool tip diameter on the gear skiving process .....	92
4.2.1	Formulas for the operating pitch diameters.....	93
4.2.2	Implications on the tool profile shape .....	95
4.2.3	Implications on the cutting conditions .....	96
4.3	The common machining operation.....	98
4.4	Tentative tool design quality indices.....	99
4.4.1	Productivity indices.....	99
4.4.2	Performance indices .....	101
4.5	The tool design constraints.....	101
4.6	Conclusions and future perspectives .....	101
	Appendix.....	102
	References.....	107

# List of Figures

<b>Figure 1.1.</b> Gear machining processes: a) Gear skiving; b) Gear hobbing; c) Gear Broaching; d) Gear shaping.....	2
<b>Figure 1.2.</b> a) Off-centred gear skiving with cylindrical tool; b) Centred gear skiving with cylindrical tool; c) Centred gear skiving with conical tool.....	3
<b>Figure 1.3.</b> Centred gear skiving of a) an internal gear; b) an external gear.....	4
<b>Figure 1.4.</b> Velocity triangle at point P.....	5
<b>Figure 1.5.</b> a) Spur cutter; b) helical cutter.....	6
<b>Figure 1.6.</b> Tool constructive angles. a) rake angle; b) clearance and side relief angle; c) tool design planes.....	7
<b>Figure 1.7.</b> Architecture of a skiving machine tool.....	8
<b>Figure 1.8.</b> Planar models to investigate the relationships between set-up parameters and tool parameters in determining $h_{MAX}$ ; a) effect of the number of teeth on $h_{MAX}$ ; b) effect of cross-axis angle on $h_{MAX}$ ....	9
<b>Figure 1.9.</b> Three different strategies for skiving with several passes using the set-up parameter <i>Crot</i> : a) null <i>Crot</i> ; b) <i>Crot</i> only on one side; c) <i>Crot</i> alternated on both sides.....	10
<b>Figure 1.10.</b> Working rake angle relative to two different passes of a 13-passes skiving process. a) Third pass; b) twelfth pass.....	12
<b>Figure 1.11.</b> Computation of the Uncut Chip Geometry.....	13
<b>Figure 2.1.</b> Numerical model workflow.....	21
<b>Figure 2.2.</b> Step procedure to compute the gear gap mesh: a) two-dimensional gear gap point coordinates; b) point cloud of the extruded gear gap; c) triangulated surface $SG(\psi)$ of the gear gap.....	22
<b>Figure 2.3.</b> Reference frames employed in the numerical model for gear skiving of: a) an internal gear; b) an external gear.....	23
<b>Figure 2.4.</b> Tool profile numerical calculation: a) family of discrete gap surfaces sectioned by the tool rake face; b) the tool profile discretized in $NpT$ points resulting from the envelope of the discrete locus of curves.....	27
<b>Figure 2.5.</b> Calculation of conical tool flanks. a) Tool tip diameter reduction caused by re-sharpening; b) tool profile at SOL; c) tool profile at EOL.....	29
<b>Figure 2.6.</b> Surface swept by the tool. Top row: at the first pass; bottom row: at the last pass.....	30
<b>Figure 2.7.</b> Four-step procedure to compute the workpiece gap of each pass: a) first step; b) second step; c) third step; d) fourth step.....	32
<b>Figure 2.8.</b> First surfaces intersection. a) Penetration of the surface swept by the tool on the gear gap; b) gear gap after first surfaces intersection; c) intersection points on the surface swept by the tool; d) penetration during run-in path.....	33
<b>Figure 2.9.</b> Second surfaces intersection. a) Penetration of the surface swept by the tool, sunk by $f_A$ on the gear gap; b) gear gap after second surfaces intersection; c) intersection points on the surface swept by the tool; d) the UCG.....	34
<b>Figure 2.10.</b> Trace carved by the tool on the gear gap relative to three different passes of the same process: a) third pass; b) ninth pass; c) fourteenth and last pass.....	34
<b>Figure 2.11.</b> Calculation of chip thickness through ray intersection. a) Tool profile points and the associated ray vectors, relative to one gear position that make up the surface swept by the tool; b) top view; c) front view.....	35
<b>Figure 2.12.</b> a) Engagement points relative to one process pass; b) chip sections relative to the several cutting positions of the considered pass and representation of the chip area $A_h$ of one chip section; c) working chip thickness values of the engagement points.....	36
<b>Figure 2.13.</b> a) Geometry of the cutting edge in oblique cutting; b) Schematic of the oblique cutting model for skiving.....	38
<b>Figure 2.14.</b> a) Section of the oblique cutting model on the normal plane $\pi_n$ ; b) model of cutting geometry implemented in the numerical model.....	40
<b>Figure 2.15.</b> a) Velocity vectors relative to the engagement points of a finishing pass; b) maximum values of the norm of the relative velocity vectors over the profile points.....	42

<b>Figure 2.16.</b> a) Working angles at the initial cutting position; b) working angles at the final cutting position; c) simulated working rake angle for one pass; d) simulated working clearance angle for one pass. ....	43
<b>Figure 2.17.</b> Minimum working angles for a skiving process of 14 passes: a) minimum working rake angle; b) minimum working clearance angle. ....	45
<b>Figure 2.18.</b> Simulation results of two case studies which show that: a) tools that operates at higher cross axis angle, provide better values of $\gamma_{rMIN}$ ; b) tools with smaller tip diameters, provide better values of $\gamma_{rMIN}$ . ....	46
<b>Figure 2.19.</b> a) Simulated chip thickness values for one skiving pass; b) Values of maximum chip thickness $h_{MAX}$ for a skiving process of 14 passes. ....	47
<b>Figure 2.20.</b> a) values of the working chip area $A_h$ for a skiving process of 14 passes; b) comparison between values of working chip area $A_h$ and normalised working chip area $A_{hP}$ , for one pass. ....	48
<b>Figure 2.21.</b> a) Representation of how $l_{cSING}$ is defined; b) different values of $l_{cSING}$ assumed by the profile points during one pass. ....	50
<b>Figure 2.22.</b> a) Simulated values of $l_{cSING}$ for a skiving process of 14 passes; b) Comparative example to demonstrate that tools with bigger tip diameter may machine smaller $l_{cSING}$ . ....	51
<b>Figure 2.23.</b> a) Variation of the axial feed among the passes of a skiving process which operates with constant $h_{MAX}$ in the roughing passes and fixed axial feed in the finishing; b) corresponding variation of the $NoC$ among the passes. ....	52
<b>Figure 2.24.</b> a) Simulated values of $l_{cSING}(i) \cdot NoC(i)$ for a skiving process of 14 passes; b) corresponding simulated values of $l_{cTOT}$ . ....	53
<b>Figure 2.25.</b> Comparison between desired gear gap and machined gear gap. ....	54
<b>Figure 3.1.</b> Implications of the number of passes and of the maximum chip thickness on: a) the axial feed; b) the number of cuts of one pass. ....	57
<b>Figure 3.2.</b> Simulated values of $A_{hP}$ and $l_{cSING}$ for two different skiving processes, each carried out with different cutting strategies. a) values of $A_{hP}$ for process 1 with $NoP = 33$ and $h_{MAX} = 0.20$ mm; b) values of $A_{hP}$ for process 1 with $NoP = 33$ and $h_{MAX} = 0.25$ mm; c) values of $l_{cSING}$ for process 1 with $NoP = 33$ and $h_{MAX} = 0.20$ mm; d) values of $l_{cSING}$ for process 1 with $NoP = 33$ and $h_{MAX} = 0.25$ mm; e) values of $A_{hP}$ for process 2 with $NoP = 16$ and $h_{MAX} = 0.15$ mm; f) values of $A_{hP}$ for process 2 with $NoP = 32$ and $h_{MAX} = 0.15$ mm; g) values of $l_{cSING}$ for process 2 with $NoP = 16$ and $h_{MAX} = 0.15$ mm; h) values of $l_{cSING}$ for process 2 with $NoP = 32$ and $h_{MAX} = 0.15$ mm. ....	59
<b>Figure 3.3.</b> Comparison of the cumulative total machined cutting length relative to a) process 1 with same $NoP$ and different values of $h_{MAX}$ ; b) process 2 with same value of $h_{MAX}$ and different $NoP$ . ....	60
<b>Figure 3.4.</b> a) Worn tool tooth from the rake face; b) worn tool tooth from the right flank; c) simulated values of $h_{MAX}$ of the relevant process; d) simulated values of $\gamma_{rMIN}$ of the relevant process; e) simulated values of $l_{cTOT}$ of the relevant process. ....	62
<b>Figure 3.5.</b> Simulated values of a) $A_{hP}$ for the standard process; b) $h_{MAX}$ for the standard process; c) $A_{hP}$ for Process 1; d) $h_{MAX}$ for Process 1; e) $A_{hP}$ for Process 2; f) $h_{MAX}$ for Process 2. ....	64
<b>Figure 3.6.</b> Simulated value of a) $l_{cTOT}$ of the three processes; b) the averaged value of $\gamma_{rMIN}$ among the passes of the three processes. ....	65
<b>Figure 3.7.</b> Tool wear from the rake face and the right flank view, after machining 50 workpieces with: a) the standard process; b) Process 1; c) Process 2. ....	66
<b>Figure 3.8.</b> Simulated values of a) $h_{MAX}$ for the standard process; b) $h_{MAX}$ for Process 1; c) $A_{hP}$ for the standard process; d) $A_{hP}$ for Process 1. ....	68
<b>Figure 3.9.</b> Simulated values of a) $l_{cTOT}$ of the standard process and of Process 1; b) the averaged $\gamma_{rMIN}$ among the passes of the standard process and of Process 1. ....	69
<b>Figure 3.10.</b> Tool wear from the rake face and the tip view, after machining 50 workpieces with: a) the standard process; b) Process 1). ....	69
<b>Figure 3.11.</b> Comparison of the simulated values of $\gamma_{rMIN}$ relative to the two tools of Case study 1 and Case study 2 operated with the same set-up parameters: a) tool of Case study 2) b) tool of case study 1. ....	70

<b>Figure 3.12.</b> Simulated values of a) $h_{MAX}$ for Process 2; b) $h_{MAX}$ for Process 3; c) $A_{hP}$ for Process 2; d) $A_{hP}$ for Process 3.....	71
<b>Figure 3.13.</b> a) Radial infeed cutting strategy of Process 2; b) radial infeed cutting strategy of Process 3; c) - e) power readings of the motor spindles of the skiving machine for passes 2,8,14 of Process 2; f) - h) power readings of the motor spindles of the skiving machine for passes 4,16,28 of Process 3.....	72
<b>Figure 3.14.</b> Simulated values of a) $l_{cTOT}$ of Process 2 and of Process 3; b) the averaged $\gamma_{rMIN}$ among the passes of Process 2 and of Process 3; c) $\gamma_{rMIN}$ at all the passes of Process 2; d) $\gamma_{rMIN}$ at all the passes of Process 3.....	73
<b>Figure 3.15.</b> Tool wear from the rake face and the tip view, after machining: a) 50 workpieces with Process 2; b) 70 workpieces with Process 3).....	74
<b>Figure 3.16.</b> Tool wear from the rake face, the tip, and the flank view, after machining: a) 70 workpieces with Process 2; b) 70 workpieces with Process 3).....	75
<b>Figure 3.17.</b> Effect of the profile shift coefficient on gears with different number of teeth.....	76
<b>Figure 3.18.</b> Tool cutting profile at the SOL and at the EOL: a) of tool 1; b) of tool 2.....	77
<b>Figure 3.19.</b> Cutting profile of tool 1: a) at the SOL; b) at the EOL.....	78
<b>Figure 3.20.</b> Comparison of working parameters of tool 1 at SOL (left side) and EOL (right side): a) – b) working chip thickness of pass n° 15; c) – d) working rake angle of pass n° 15; e) cumulative machined total cutting length $l_{cTOT}$ .....	79
<b>Figure 3.21.</b> Comparison of working parameters of tool 1 at SOL (left side) and at EOL (right side) for all the process passes: a) – b) values of $h_{MAX}$ ; c) - d) values of $\gamma_{rMIN}$ ; e) – f) values of $A_{hP}$ .....	80
<b>Figure 3.22.</b> Tool wear from the rake face and the tip view, after machining 30 workpieces with: a) the tool at the SOL; b) the tool at the EOL.....	81
<b>Figure 3.23.</b> Comparison of working parameters of tool 2 at SOL (left side) and EOL (right side): a) – b) working chip thickness of pass n° 9; c) – d) working rake angle of pass n° 9; e) cumulative machined total cutting length $l_{cTOT}$ .....	82
<b>Figure 3.24.</b> Comparison of working parameters of tool 2 at SOL (left side) and at EOL (right side) for all the process passes: a) – b) values of $h_{MAX}$ ; c) - d) values of $\gamma_{rMIN}$ ; e) – f) values of $A_{hP}$ .....	83
<b>Figure 3.25.</b> Tool wear from the rake face and the tip view, after machining 30 workpieces with: a) the tool at the SOL; b) the tool at the EOL.....	84
<b>Figure 3.26.</b> Comparison of working parameters of tool 1 at SOL with the standard process (left side), and with the new process (right side), for all the process passes: a) – b) values of $h_{MAX}$ ; c) - d) values of $\gamma_{rMIN}$ ; e) – f) values of $A_{hP}$ .....	85
<b>Figure 3.27.</b> a) Comparison of the values of machined $l_{cTOT}$ using the tool at the SOL with the standard process and with the new process; b) comparison of the working chip thickness machined by the tool at the SOL, during two different passes with same radial infeed relative to the two compared processes.....	86
<b>Figure 3.28.</b> Tool wear from the rake face and the tip view, after machining: a) 30 workpieces with the tool at SOL using the new process; b) 38 workpieces with the tool at SOL using the new process.....	86
<b>Figure 4.1.</b> The domain of the tool kinematic parameters relative to one workpiece.....	91
<b>Figure 4.2.</b> a) Schematic of a generic gearset made up of a skiving tool and an internal gear; b) schematic of a gearset made up of a skiving tool and an internal gear in the particular case where the tool has been designed to have the tip diameter equal to the operating pitch diameter; c) comparison of the rake face orientation between the theoretical case used to derive the equation for the operating pitch diameter and the real case.....	94
<b>Figure 4.3.</b> Variation of the tool operating pitch diameter as a function of the tool tip diameter: a) for a spur internal gear; b) for a spur external gear.....	96
<b>Figure 4.4.</b> a) Cutting trajectory of a tool designed with the tip diameter bigger than the operating pitch diameter; b) cutting trajectory of a tool designed with tip diameter equal to the operating pitch diameter; c) comparison between the values of $l_{cTOT}$ machined by the two tools.....	97
<b>Figure A.1.</b> Block diagram representing the workflow of the numeric routine for the calculation of the constructive clearance angle.....	103
<b>Figure B.1.</b> a) Schematic of a skew axis gearset; b) gearset axodes; c) schematic of the infinitesimal tooth departed from the ISA.....	105

# List of Tables

<b>Table 1.1:</b> Comparison between gear machining processes.....	2
<b>Table 1.2.</b> Main operating limit values of the Gleason 600PS Machine tool.....	11
<b>Table 2.1.</b> Tool and set-up parameters given as input in the numerical model.....	22
<b>Table 3.1.</b> Implications of set-up parameters on working parameters. ....	57
<b>Table 3.2.</b> Tool and workpiece data of case study 1. ....	63
<b>Table 3.3.</b> Process data of case study 1.....	64
<b>Table 3.4.</b> Tool and workpiece data of case study 2. ....	67
<b>Table 3.5.</b> Process data of case Study 2. ....	68
<b>Table 3.6.</b> Geometrical data of tool 1, tool 2, and the gear they machine.....	78
<b>Table 3.7.</b> Process data of the two case studies. ....	79

# Nomenclature

$\Sigma$	cross-axis angle	$A_{hP}$	normalised working chip area
$a$	centre distance	$h$	working chip thickness
$k$	gear ratio	$h_{MIN}$	minimum working chip thickness
$\omega_T$	tool angular velocity	$h_{MEAN}$	mean working chip thickness
$\omega_G$	gear angular velocity	$h_{MAX}$	maximum working chip thickness
$m_n$	normal module	$\gamma_r$	working rake angle
$\alpha_n$	normal pressure angle	$\gamma_{rMIN}$	minimum working rake angle
$b_G$	gear width	$i$	working inclination angle
$z_G$	number of gear teeth	$\alpha_c$	working clearance angle
$d_{tG}$	gear tip diameter	$\alpha_{cMIN}$	minimum working clearance angle
$d_{rG}$	gear root diameter	$v_c$	cutting velocity
$d_{pG}$	gear pitch diameter	$v_f$	feed velocity
$d_{opG}$	operating gear pitch diameter	$f_A$	axial feed
$\beta_G$	nominal gear helix angle	$f_R$	radial feed
$\beta_{oG}$	gear helix angle at operating pitch diameter	$l_{IN}$	tool run-in path
$H_G$	gear lead	$l_{OUT}$	tool run-out path
$p_G$	gear screw parameter	$t$	cycle time
$h_G$	gear gap height	$N_{pG}$	n° of points in which the gear gap profile is discretised
$x_G$	gear profile shift coefficient	$N_{pT}$	n° of points in which the tool profile is discretised
$z_T$	number of tool teeth	$\phi_{G0}$	variable used to describe the relative motion between tool and gear, named as cutting position
$d_{tT}$	tool tip diameter	$h_s$	re-sharpening step
$d_{rT}$	tool root diameter	$\Delta_{dtT}$	tool tip diameter variation due to $h_s$
$d_{pT}$	tool pitch diameter	SOL	start of life
$d_{opT}$	operating tool pitch diameter	EOL	end of life
$\beta_T$	nominal tool helix angle	$O_{G0}(x_{G0}, y_{G0}, z_{G0})$	fixed reference frame of the gear
$\beta_{oT}$	tool helix angle at operating pitch diameter	$O_G(x_G, y_G, z_G)$	mobile reference frame of the gear
$H_T$	tool lead	$O_{T0}(x_{T0}, y_{T0}, z_{T0})$	fixed reference frame of the tool
$h_T$	tool teeth height	$O_T(x_T, y_T, z_T)$	mobile reference frame of the tool
$x_T$	tool profile shift coefficient	$T_{G G0}$	homogeneous transformation matrix from fixed gear reference frame to mobile gear reference frame
$\gamma_{r0}$	constructive rake angle	$T_{G0 T0}$	homogeneous transformation matrix from fixed tool reference frame to fixed gear reference frame
$\alpha_{c0}$	constructive clearance angle		
$\alpha_{s0}$	constructive side relief angle		
$\tau_{s0}$	constructive step angle		
$NoC$	number of cuts on one pass		
$NoP$	number of radial passes		
$NoW$	number of machined workpieces		
$l_{cSING}$	cumulative machined cutting length during a single penetration of a pass		
$l_{cTOT}$	cumulative machined total cutting length		
$ML$	machined length		
$A_h$	working chip area		

$T_{T0 T}$	homogeneous transformation matrix from mobile tool reference frame to fixed tool reference frame
$T_{G T}$	homogeneous transformation matrix from mobile tool reference frame to mobile gear reference frame
$S_G(\psi)$	gear gap surface
$S_T(\psi)$	tool flank surface
$\{S_G(\psi)\}_T(\phi_G)$	family of gear gap surfaces written in tool mobile reference frame
$\{S_{ST}\}_G(\phi_G)$	surface swept by the tool written in the gear mobile reference frame
$\pi_r$	tool rake plane
$\pi_c$	cutting plane
$\pi_n$	normal plane of the model of cutting geometry
$\pi_f$	tool flank plane
$e_n$	unit edge vector
$t_n$	unit tangent velocity vector
$i_n$	unit inclination vector
$g_n$	unit rake vector
$f_n$	unit flank vector
$n_{cn}$	unit normal vector to $\pi_n$
$n_{rn}$	unit normal vector to $\pi_r$
$n_{fn}$	unit normal vector to $\pi_f$
$r_{aT}$	tool axode throat radius
$\psi_{aT}$	tool axode helix angle
$r_{aG}$	gear axode throat radius
$\psi_{aG}$	gear axode helix angle
$p_{rel}$	pitch of relative motion
$v_{rel}$	relative velocity
$\omega_{rel}$	relative angular velocity
ISA	instantaneous screw axis
$\Delta r$	departure; distance, measured along the centre distance line, between the ISA and the operating pitch diameter
$\Delta\psi$	rotation of the infinitesimal tooth when moved from the ISA of the quantity $\Delta r$

**set-up parameters:** those parameters that the operator, who manages the interface with the skiving machine, can modify depending on the specific machining operation.

**working parameters:** those parameters that depend on the interplay between kinematics and geometry of the process and are used to describe the cutting conditions.

**tool parameters:** parameters used to describe the tool shape.

**tool design parameters:** tool parameters that uniquely determine the geometry of the tool and that are set as input in the tool calculation routine.

**tool kinematic parameters:** subset of the tool design parameters, which affects the process relative kinematics.

**tool constructive parameters:** subset of the tool design parameters, which do not affect relative kinematics, namely the tool constructive angles.





# Acknowledgements

Sincere gratitude is extended to Metalcastello S.p.a. for fully financing this Ph.D. program on gear skiving and for generously providing its facilities and equipment for the experimental trials. Special thanks go to Andrea Giannini and Stefano Fiocchi and all the employees at Metalcastello for their contributions to this research.

Heartfelt thanks go to Professor Vincenzo Parenti-Castelli and Professor Rocco Vertechy. They have not only allowed for this excellent opportunity for a PhD program in collaboration between academia and industry but have also dedicated their time and provided invaluable advice throughout these years.



# 1 Introduction

This opening chapter serves as the introduction to the entire dissertation. Initially, it presents the research topic that is the focus of the manuscript. Subsequently, the chapter describes the geometry and kinematics of the process, supplemented by essential relationships and definitions, to facilitate an understanding of gear skiving technology. Following this, a review of the current state of the art of the gear skiving process is provided. Finally, the context of this work is delineated with respect to the existing literature.

## 1.1 Motivation

Due to the environmental emergency, the current market is demanding an ever-increasing number of electric vehicles. The electric motors of many of these vehicles share the inherent feature of producing power at high speed with relatively low torque which is not suitable for driving the car. Therefore, planetary gearboxes with a high gear ratio must be employed. As a result, the gear market is undergoing a transition to meet the ensuing demand for internal gears featured in most planetary gearboxes.

Historically, the most common processes for producing internal gears were shaping and broaching. Lately, however, another process has started gaining attention. Gear skiving, in the literature also referred to as scudding or slicing, is a machining process for gear production. It was originally developed and patented in 1910 [1]. However, innovative as the patent was at that time, the machining technology of those days was insufficient to meet the highly demanding requirements inherent in the process. Among them, the most problematic ones were the high stiffness of the machining apparatus, the accurate motion synchronisation needed between the tool and the workpiece, and the necessity for durable tool materials. After a dormant period of more than 50 years, the skiving process only found some rare applications in the 1960s and 1970s when it was used for internal gears manufacturing.

With the advancement in manufacturing technology and novel tool coatings, nowadays gear skiving has become a highly competitive technology in gear production. Compared to the most common gear machining processes shown in Figure 1.1, such as hobbing, broaching, and shaping, the gear skiving process offers significant advantages. Unlike gear hobbing, it also allows internal gears to be cut and it is more flexible than broaching. Although shaping is the most applied cutting method for internal gears, the lack of material removal during the back stroke negatively affects the process productivity [2]. In contrast, gear skiving is a continuous cutting procedure. Its uninterrupted material removal increases the production compared to both shaping and hobbing [3,4].

Gear skiving has also some limitations. Specifically, it necessitates a clearance for the tool to disengage from the gear, which, however small, is not negligible as in shaping. Additionally, when machining a wide workpiece, striking a balance between avoiding collisions with the tool holder and attaining an optimal cross-axis angle for ensuring adequate cutting conditions can pose a non-trivial challenge. Despite these drawbacks which may hinder its applicability, the gear skiving process retains several advantages in comparison to the other gear machining processes. This is evident from the comparison shown in Table 1.1, where for each machining process the advantages are labelled in green, the mild issues in orange and the major drawbacks in red.

The gear skiving process offers versatility in its operation. Depending on the application, it can be employed as either a wet or dry process. Additionally, it is adaptable for use on machining centres or dedicated skiving machines. The latter are typically stiffer and more apt for the machining of bigger gear modulus. Finally, gear skiving may be considered as an all-in-one process, since it can also be effectively used for finishing operations on pre-machined hardened gears, in which case it is referred to as hard gear skiving.

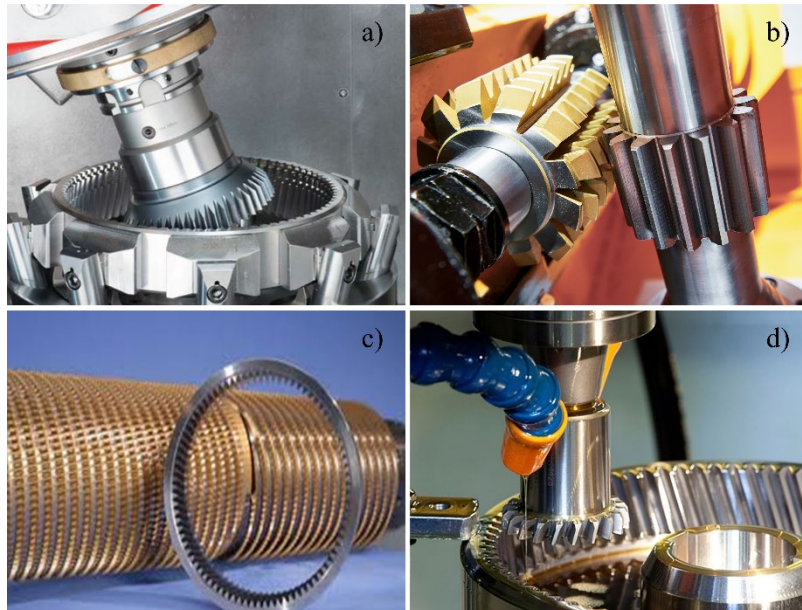


**Figure 1.1.** Gear machining processes: a) Gear skiving; b) Gear hobbing; c) Gear Broaching; d) Gear shaping.

As in many other machining technologies, the successful implementation of gear skiving depends on several issues that are of great research interest. However, due to its recent adoption by gear companies, only a part of these issues has been investigated so far, and there were few published papers before 2010 [5]. Since then, research centres and universities have been putting great attention to this technology and to the factors that influence it.

**Table 1.1:** Comparison between gear machining processes.

<b>Skiving</b>	<b>Hobbing</b>	<b>Broaching</b>	<b>Shaping</b>
<ul style="list-style-type: none"> <li>✓ Productivity</li> <li>✓ Quality</li> <li>✓ Int. and ext. gears</li> <li>✓ Flexibility</li> </ul>	<ul style="list-style-type: none"> <li>✓ Productivity</li> <li>✓ Flexibility</li> </ul>	<ul style="list-style-type: none"> <li>✓ Productivity</li> <li>✓ Int. and ext. gears</li> </ul>	<ul style="list-style-type: none"> <li>✓ Clearance tool exit</li> <li>✓ Flexibility</li> <li>✓ Int. and ext. gears</li> </ul>
<ul style="list-style-type: none"> <li>✗ Clearance tool exit</li> <li>✗ Wide gears</li> </ul>	<ul style="list-style-type: none"> <li>✗ No internal gears</li> <li>✗ Quality</li> <li>✗ Clearance tool exit</li> </ul>	<ul style="list-style-type: none"> <li>✗ Flexibility</li> <li>✗ Clearance tool exit</li> <li>✗ Quality</li> </ul>	<ul style="list-style-type: none"> <li>✗ Productivity</li> <li>✗ Quality</li> </ul>

## 1.2 Geometry and kinematics of centred gear skiving

### 1.2.1 Process kinematics

Gear skiving, in its general configuration, is depicted in Figure 1.2a), illustrating the skiving of an internal gear. The process in the figure is referred to as off-centred gear skiving because the tool operates with an offset, eccentrically relative to the workpiece. The off-centred configuration allows the employment of both conical and cylindrical tools. As shown in Figure 1.2a), at the machining point P, the offset ensures that the outer surface of the tool has clearance and does not interfere with the workpiece. While cylindrical tools may offer certain advantages over conical tools, as will be discussed later, the off-centered setup introduces additional complexities to the process, beginning with the kinematics. Consequently, machine tool manufacturers may choose to restrict the machine to operate exclusively in a centered configuration, as depicted in Figure 1.2b) and 1.2c). This centered configuration significantly simplifies both the process control architecture and tool design. In this scenario, the process is referred to as centered gear

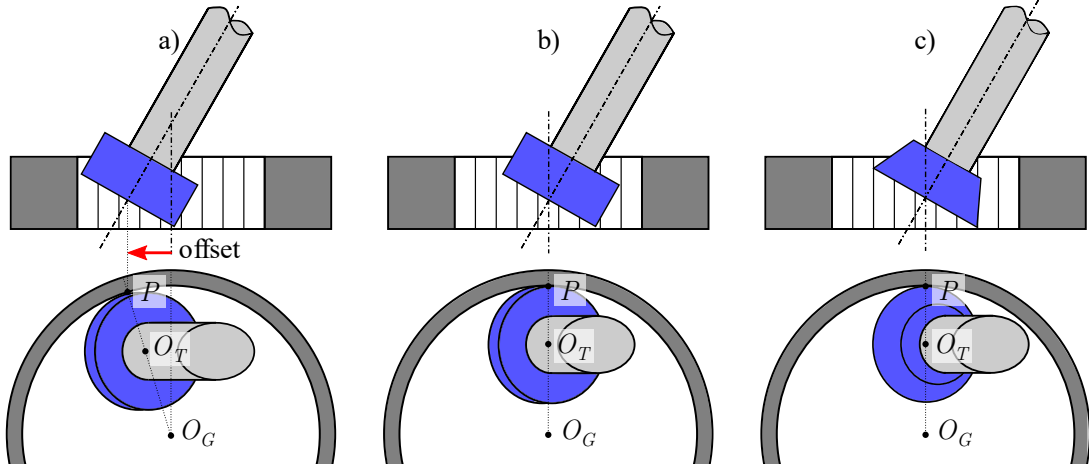


**Figure 1.2.** a) Off-centred gear skiving with cylindrical tool; b) Centred gear skiving with cylindrical tool; c) Centred gear skiving with conical tool.

skiving, which can be considered a special case of the off-centered process, where the offset is set to zero. However, this choice limits the use to exclusively conical tools. As demonstrated in Figure 1.2b), using a cylindrical tool in the centered configuration would result in a collision between the outer surface of the tool and the machined surface of the workpiece. To enable the centered process, conical tools are essential, as their conical shape ensures collision avoidance. This is demonstrated in Figure 1.2c), where at the machining point  $P$ , the conical tool design prevents contact with the outer surface of the tool, thereby eliminating the risk of rubbing.

The company's Gleason 600PS machine tools are designed to perform centred gear skiving exclusively. For this reason, all the work presented in this dissertation focuses on the centred process and its peculiarities. Sometimes the word “centred” may be omitted and only “gear skiving” will be used to refer to the process. However, as suggested by the title of this work, any reference to gear skiving is presumed to pertain to the centered process unless specified otherwise.

Centered gear skiving can be effectively used for machining both internal and external gears, although the operating schemes for these two cases differ. This difference is illustrated in Figure 1.3, which presents both front and top views of the skiving processes for an internal gear (Figure 1.3a) and an external gear (Figure 1.3b). Despite the variance in operational schemes, the fundamental working principle remains consistent: the tool and workpiece rotate synchronously, analogously to a pair of mating gears with skew axes. Initially, the workpiece blank may be either a ring or a cylinder depending on if the gear is internal or external, respectively.

Then, machining is performed in several passes wherein the tool is set at an increasing radial depth at each pass and fed axially along the face width of the gear. At each pass the gear gap is gradually machined, up to the last pass that yields the final shape of the gear gap and where the tool is set at the nominal centre distance  $a$  relative to the gear. The gear ratio  $k$ , the cross-axis angle  $\Sigma$  and the centre distance  $a$  of the assembly tool-gear, can be computed as follows:

$$k = \frac{z_T}{z_G} \quad \Sigma = \left| |\beta_T| + \varepsilon_z \cdot \varepsilon_\beta \cdot |\beta_G| \right| \quad a = \frac{d_{rG} + \varepsilon_z \cdot d_{tT}}{2} \quad 1.1$$

where  $z_T, z_G$  and  $\beta_T, \beta_G$  are the number of teeth and the nominal helix angles, of tool and gear, respectively, whereas  $d_{rG}$  and  $d_{tT}$  are the gear root diameter and the tool tip diameter, respectively. The parameter  $\varepsilon_z$  accounts for the fact the workpiece may be either internal or external. Specifically,  $\varepsilon_z$  has a value equal to 1 if the workpiece is external or -1 if the workpiece is internal. The parameter  $\varepsilon_\beta$  on the other hand, considers the direction of the tool and workpiece

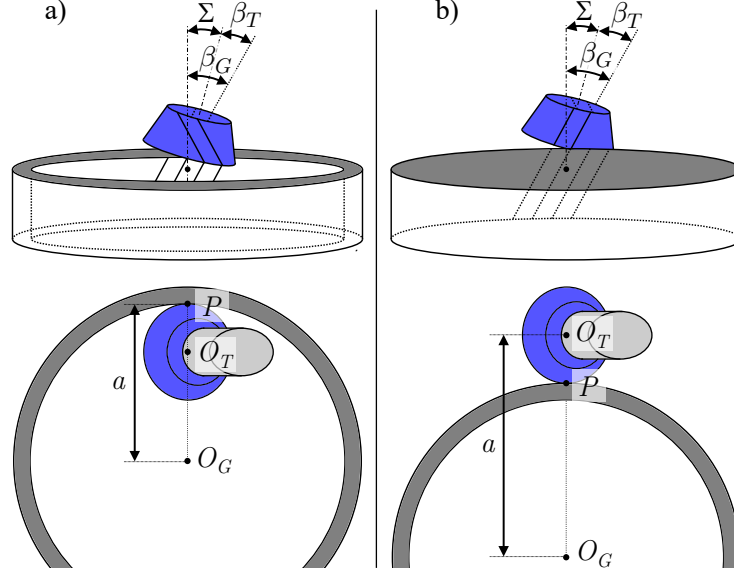


**Figure 1.3.** Centred gear skiving of a) an internal gear; b) an external gear.

helices. If tool and gears have the same helix direction  $\varepsilon_\beta$  is equal to 1, whereas if the helices are opposite  $\varepsilon_\beta$  is equal to -1.

An example of this is portrayed in Figure 1.3. Particularly, in Figure 1.3a) a left-hand internal gear is machined by a left-hand helix tool, hence  $\varepsilon_z$  has value -1 and  $\varepsilon_\beta$  has value 1. Therefore,  $\Sigma$  is given by the difference between the two helices and  $a$  is given by the differences of the two diameters. In Figure 1.3b) on the other hand, a left-hand external gear is machined by a right-hand tool, hence  $\varepsilon_z$  is 1 whereas  $\varepsilon_\beta$  is -1. As a result,  $\Sigma$  is still given by the difference between the two helices, but  $a$  is given by the sum of the two diameters. There are also cases where the helices add up to  $\Sigma$  as well, for example for the case of an internal workpieces with tool and workpieces with opposite helices.

Throughout this work it is employed the convention that the helix of left-hand gears is positive, whereas the helix of right-hand gears is negative, which is the reason for the absolute value in Eq. 1.1. When the cutter or the gear are spur, the respective helix angle is zero. The value of the cross-axis angle  $\Sigma$  is taken either positive or negative depending on the orientation of the fixed tool reference frame w.r.t the gear fixed reference frame. The schematic of the reference frames adopted is reported in Figure 2.3 of next section along with coordinate transformations matrices.

The process cutting action is produced by the cutting velocity  $v_c$ , developed at the machining point between tool and workpiece. Referring to Figure 1.4 which shows the velocity triangle at point P of tangency between the operating pitch diameters lying on the centre distance, the modulus of the cutting velocity  $v_{cP}$  at point P may be written as:

$$v_{cP} = \frac{v_{TP} \cdot \sin(\Sigma)}{\cos(\beta_{oG})} \quad 1.2$$

where  $v_{TP}$  is the modulus of the tool peripheral velocity at point P. From Eq. 1.2 it is clear that when  $\Sigma$  goes to zero, the cutting velocity also vanishes resulting in null cutting action. Therefore, for a given workpiece with nominal helix angle  $\beta_G$ , in order to generate sufficient cutting action, a tool with a proper nominal helix angle  $\beta_T$  must be chosen, based on Eq. 1.1. The shaft angle is usually set to  $20^\circ$  as a trade-off between optimal working parameters and interference avoidance between tool holder and workpiece.

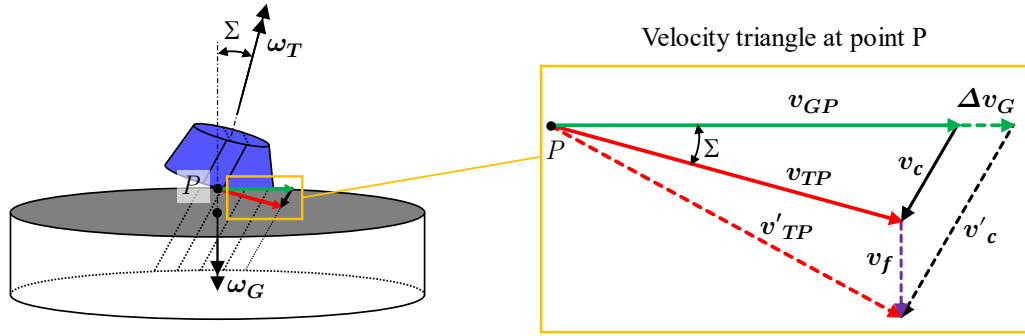


Figure 1.4. Velocity triangle at point P.

From Figure 1.4 it can also be seen another peculiarity of gear skiving. Whenever the gear to be cut is helical instead of spur, and the tool is fed axially with velocity  $v_f$ , the angular velocity of the workpiece gear must be varied in modulus by a quantity  $\Delta\omega_G$ . In particular, in order to remain in mesh, workpiece and tool must have the same velocity component on the normal direction to the helices at the contact point. With reference to Figure 1.4, it can be seen that when the feed velocity  $v_f$  is added to the tool, the peripheral velocity of the cutter at point P changes from  $v_{TP}$  to  $v'_{TP}$ . For the tool and gear to remain in mesh, the cutting velocity  $v_c$  must retain the same direction tangent to the helix. Therefore, at point P, the modulus of the gear peripheral velocity  $v_{GP}$  must be varied by the quantity  $\Delta v_G$  as shown in the figure. Considering the relation between the modulus of the gear peripheral velocity and angular velocity, and the gear operating pitch radius  $r_{opG}$ , the following equation must hold:

$$\Delta\omega_G = \frac{v_f \cdot \tan(\beta_{oG})}{r_{opG}} \quad 1.3$$

### 1.2.2 Tool geometry

The skiving tool resembles a pinion shaper cutter, since it is essentially an external pinion. The macro-geometry of a skiving tool indeed, may be described by the tool number of teeth  $z_T$ , by the tool nominal helix angle  $\beta_T$  and by the tool tip diameter  $d_{iT}$ . However, as it will be shown in Paragraph 2.2.3, the way the tool profile is computed and consequently its micro-geometry, differs from that of a traditional shaping tool.

Skiving cutters may be either spur or helical as shown in Figure 1.5. In the first case the cutter teeth develop parallel to the direction of the tool rotation axis. In contrast, observing a helical tool, the teeth are inclined with respect to the tool rotation axis. This inclination is referred to as the helix angle, which is defined as the acute angle between the tangent to the tooth helix and the straight generator of the cylinder on which the helix lies. The nominal helix angle  $\beta_T$  is measured on the tool pitch cylinder. As already mentioned, the tool helix angle will determine along with the gear helix angle, the cross-axis angle. Therefore, since  $\Sigma$  must be bigger than zero to generate cutting action, spur skiving cutters can machine helical gears only, whereas helical skiving cutters can machine both spur and helical gears.

Skiving cutters usually have constructive angles which aid machining. One of the most relevant is the constructive rake angle  $\gamma_{r0}$ , since it strongly affects the cutting conditions and the tool load. The distinction between spur and helical cutter affects the geometry of the rake face of the tool.

In particular, spur cutters have a conical rake face (Figure 1.5a), whereas helical cutters usually adopt planar rake faces (Figure 1.5b). The tool constructive rake angle  $\gamma_{r0}$  is machined on the front face of each tooth. For spur cutters,  $\gamma_{r0}$  is defined as the angle between the transverse plane,

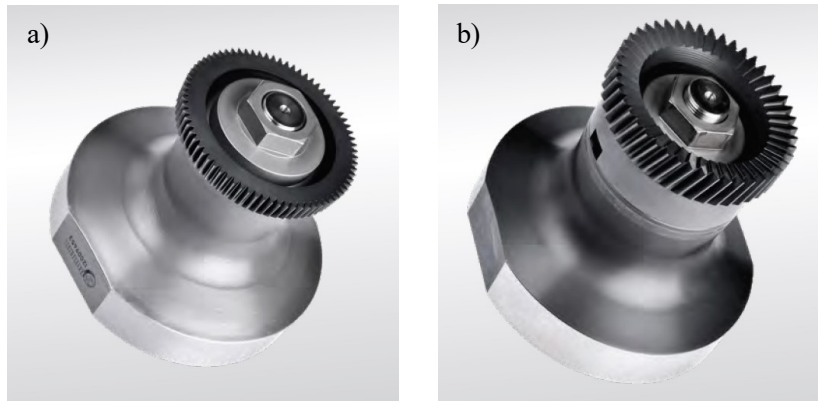


Figure 1.5. a) Spur cutter; b) helical cutter.

orthogonal to the tool rotation axis, and the conical rake face generatrix, which is unique for the tool teeth (Figure 1.6a).

In case of helical tool, its definition is more complex since each tooth has its own rake face whose orientation includes the effects of both the tool constructive step angle  $\tau_{s0}$  and the tool constructive rake angle  $\gamma_{r0}$ . Usually, the constructive step angle is taken coincident to the tool nominal helix angle. This arrangement of the rake face allows an even distribution of the load, and consequently of the wear, on the tool profile [6].

In order to define the rake angle and illustrate its role in defining the rake face in a helical cutter, the steps taken to determine the rake face of a single tooth are presented in what follows. To this end, Figure 1.6c) shows a reference frame  $O(x, y, z)$  attached to a single tooth, with unit vectors  $i, j, k$  and the tool design planes, i.e. the transverse plane and the rake face, based on which the tooth cutting profile is defined. The  $x$  and  $y$  axes lie on the tool transverse plane whereas the  $z$ -axis points upwards. Furthermore, the reference frame origin  $O$  is placed coincident with the tooth tip and the  $x$ -axis is set collinear with the tooth axis of symmetry. By rotating a unit vector originally coincident with the unit vector  $j$  about the  $x$ -axis of the constructive step angle  $\tau_{s0}$ , the vector  $j'$  is found. Similarly, by rotating a unit vector originally coincident with the unit vector  $i$  about the  $y$ -axis of the constructive rake angle  $\gamma_{r0}$ , the vector  $i''$  is determined (Figure 1.6c). It is worth noting that unit vectors  $j'$  and  $i''$  are not perpendicular to each other. Using the cross-product on the calculated vectors, it is possible to determine the unit vector normal to the rake face  $n_r$ . The rake face normal vector  $n_r$  is represented in Figure 1.6c) along with the normal vector  $n_t$  to the transverse plane. The unit normal vector  $n_r$ , along with the reference frame origin  $O(x, y, z)$ , completely define the tool rake face.

From what reported above, it can be concluded that differently from the case of spur cutters, in helical cutters the rake angle alone does not define the orientation of the rake face. The orientation is determined only when both step angle and rake angle are specified.

Another distinction amongst skiving tools can be made based on their external shape, which can be either conical or cylindrical. In conical tools, a constructive clearance angle  $\alpha_{c0}$  is machined on the external surface of the tool to avoid interference with the gear machined, as shown in Figure 1.6b). On the other hand, cylindrical tools have no constructive clearance angle. Thus, to avoid interference, the tool must either be tilted during the operation, requiring an extra degree of freedom to the machine tool, or it must be operated in an eccentric position with respect to the gear, as it was shown in Figure 1.2a).

Among the main advantages that cylindrical tools offer over conical tools, is that the tool profile does not change during the tool service life due to re-sharpening. Indeed, in order to obtain the constructive clearance angle at the tip, conical tools are designed with a decreasing tool tip diameter along the tool width, as shown in Figure 1.6b). As explained later in Paragraph 2.2.3,



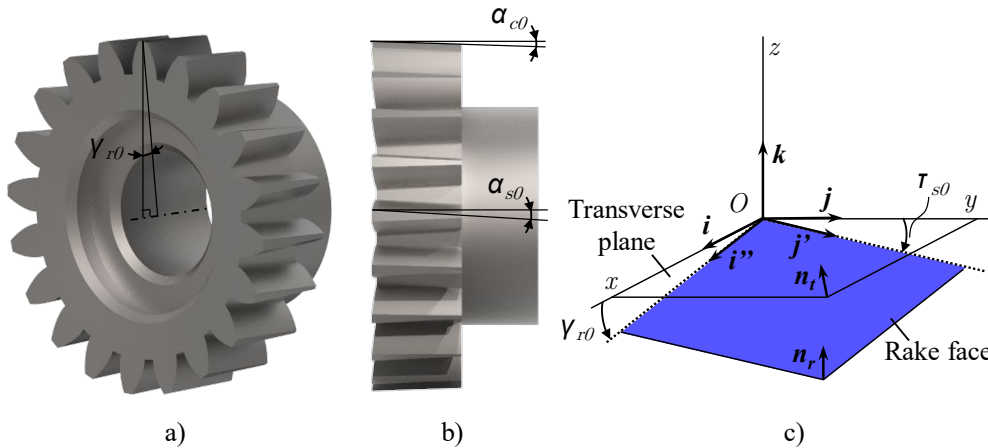


**Figure 1.6.** Tool constructive angles. a) rake angle; b) clearance and side relief angle; c) tool design planes.

the tool tip diameter affects the shape of the entire tool profile. Specifically, a reduction of the tip diameter may be thought as a reduction of the profile shift coefficient of the tool. Having the tool teeth that reduce their thickness along the tool width, conical tools result in also having a constructive side clearance angle  $\alpha_{s0}$  as shown in Figure 1.6b).

Hence, with conical tools, a change of the tool profile shape during the tool service life is unavoidable, with the related risk of impairing cutting performances. With cylindrical tools on the other hand there is not such a risk. However, in practice, due to the added complexity in the machine tool architecture that the use of cylindrical tools entails, not all machine tools on the market today can use cylindrical tools, while virtually all can use the conical ones. Therefore, despite their inherent drawback, conical tools are the most used to date for gear skiving.

As far as the machined profile shape is concerned, a skiving tool may be designed to machine every kind of profile e.g. involute, cycloidal and circular gears among other. However, as it will be clarified in Paragraph 2.2.3 where the procedure for the tool profile calculation is introduced, the theoretical tool profile deviates from that of an ideal involute, cycloid or circle. Therefore, tool manufactures produce tools whose profile slightly deviates from the theoretical one, in order to make the production affordable, employing traditional generating technique.

For what concern the tool material, this may vary depending on the specific machining operation, e.g. if the workpiece material is already hardened and if lubricant is employed. A very popular choice for skiving of not-hardened gears machined with lubricant are tools made of high-speed steel and coated in AlCrN. For hardened gears, carbide tools may be employed instead.

It is important to note that thus far, only the tool constructive angles have been defined. In later sections, the working parameters will be introduced, which include the working angles, such as the working rake angle and working clearance angle. The working angles occur during machining and in gear skiving they vary both during each pass and also for each portion of the tool profile. They are the result of the interplay between tool and workpiece geometry and kinematics. Therefore, they should not be confused with the tool constructive angles, which have constant values and are used to define the tool geometry.

### 1.2.3 Skiving machine tool and set-up parameters

A general architecture of a skiving machine is shown in Figure 1.7, where the tool and the workpiece have been represented in blue and grey respectively. The rails allowing the relative motions between components are coloured light grey whereas the other machine tool parts are depicted in red.

From the figure, it can be seen that both the tool and the gear may rotate around their own axes with angular velocities  $\omega_T$  and  $\omega_G$  respectively. Furthermore, there are four rails that allow the

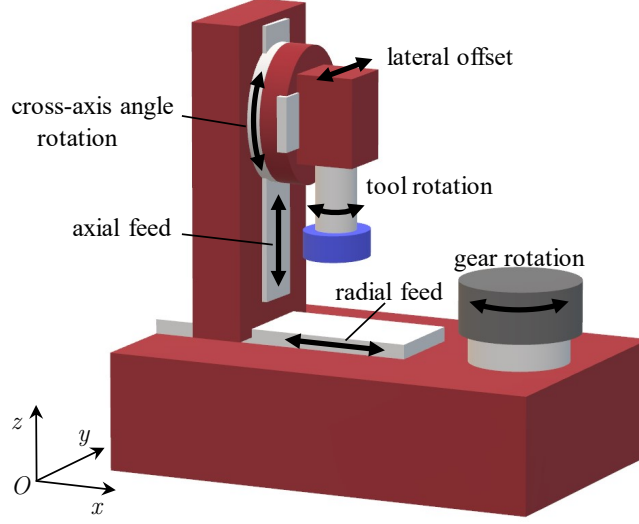


Figure 1.7. Architecture of a skiving machine tool.

relative motion of the tool with respect to the workpiece. In particular, referring to the reference frame  $O(x, y, z)$  in the figure, the tool can be rotated about the  $x$ -axis in order to reach the desired cross-axis angle  $\Sigma$ . In order to machine the entire workpiece width  $b_G$ , the tool is fed axially along the  $z$ -axis with the axial feed  $f_A$ .

Additionally, to reduce the tool load, usually the machining of the gear gap is carried out over a number of passes  $NoP$  in which the workpiece gap is divided radially. Hence the radial infeed  $f_R$  of the tool teeth into the workpiece gap along the  $x$ -axis, does not reach the value of the gear gap height  $h_G$  in one pass. Instead, the radial feeds are cumulated at each pass until the nominal centre distance  $a$  between the rotation axes of tool and gear is reached. It may also be noted that there is a rail for the tool movement in the  $y$ -axis direction. This may be used for off-centred gear skiving and for corrections or modifications of the workpiece gap.

So far, the parameters  $\omega_T, \omega_G, f_A, f_R, NoP$  have been introduced to describe the machine tool motions. In the context of this work such parameters are grouped in the so-called set-up parameters, which are those that the operator, who manages the interface with the skiving machine tool, can set depending on the specific machining operation.

However, there are other set-up parameters among which, notably, are: the modulus of the cutting velocity  $v_c$ , the maximum chip thickness at each pass  $h_{MAX}$ , the tool run-in  $l_{IN}$  and run-out path  $l_{OUT}$ , the cycle time  $t$  and the infeed strategy. All the set-up parameters are related to each other. In the following, the reminder set-up parameters are introduced along with the relationships which bind them to each other.

The modulus  $v_c$  of the cutting velocity is a key parameter for the skiving process and can be computed as follows:

$$v_c = \omega_T \cdot \sqrt{k^2 \cdot \left(\frac{d_{rG}}{2}\right)^2 + \left(\frac{d_{tT}}{2}\right)^2 - \frac{d_{rG} \cdot d_{tT}}{2} \cdot k \cdot \cos(\Sigma)} \quad 1.4$$

For a given workpiece to machine, once the tool design is chosen the values  $k$  and  $\Sigma$  are defined based on Eq. 1.1. Hence, from the Eq. 1.4 it can be seen that  $v_c$  linearly depends on  $\omega_T$ . For a given pair of tool and workpiece materials, there is a limited range of values for the cutting velocity that makes the tool perform at its best in terms of wear and productivity. Hence, in

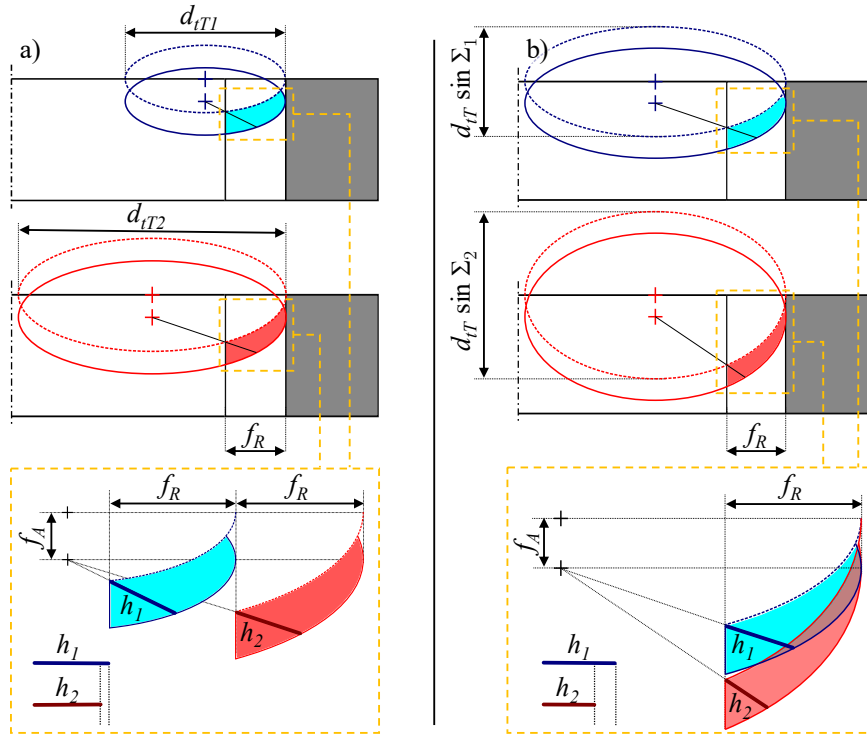


**Figure 1.8.** Planar models to investigate the relationships between set-up parameters and tool parameters in determining  $h_{MAX}$ ; a) effect of the number of teeth on  $h_{MAX}$ ; b) effect of cross-axis angle on  $h_{MAX}$ .

common practice,  $v_c$  is set as the input on the machine tool and  $\omega_T$  is computed accordingly, based on Eq. 1.4.

Another key parameter is  $h_{MAX}$ , namely the maximum value of chip thickness reached during a pass. The value of  $h_{MAX}$  depends on the axial feed  $f_A$ , on the radial feed  $f_R$ , and on the tool design parameters. In the literature, an exact analytical formulation for the skiving process linking these variables is lacking, since the chip thickness varies during the pass and at different points of the profile. Also, the shape of the uncut chip geometry varies at each pass. However, it is known that for a given tool design, an increase in  $f_A$  corresponds to a rise in  $h_{MAX}$  in an almost linear way [7]. Usually, simplified models, e.g. planar models, similar to those represented in Figure 1.8, are used. From such models, relationships linking set-up parameters and tool parameters may be derived.

A clarification must now be made to put into context the figure, which is going to be recalled also in later sections. The schemes represented in the figure, are seen from the section plane passing through the gear axis. From this perspective, the tool has the shape of an ellipse whose bigger diameter corresponds to the tool tip diameter. In each figure there are two tools with different design parameters. In Figure 1.8a) there are two tools operating at the same cross-axis angle with different teeth number, corresponding to different tip diameters,  $d_{tT1}$  and  $d_{tT2}$  respectively. In Figure 1.8b) instead, there are two tools with the same tip diameter  $d_{tT}$ , but with different helix angles. Therefore, the two tools operate at different cross axis angle  $\Sigma_1$  and  $\Sigma_2$  respectively. Each tool is portrayed at two different axial feeds. When the tool is sunk of  $f_A$  on the workpiece, it is represented in continuous line, whereas when it is not sunk is represented in dashed line. The four tools operate with the same axial feed  $f_A$  and the same radial feed  $f_R$ . The shaded coloured areas in light blue and red, correspond to the machined portion during the pass by each tool, on the section plane. On each machined portion has been highlighted the maximum

## 1 Introduction

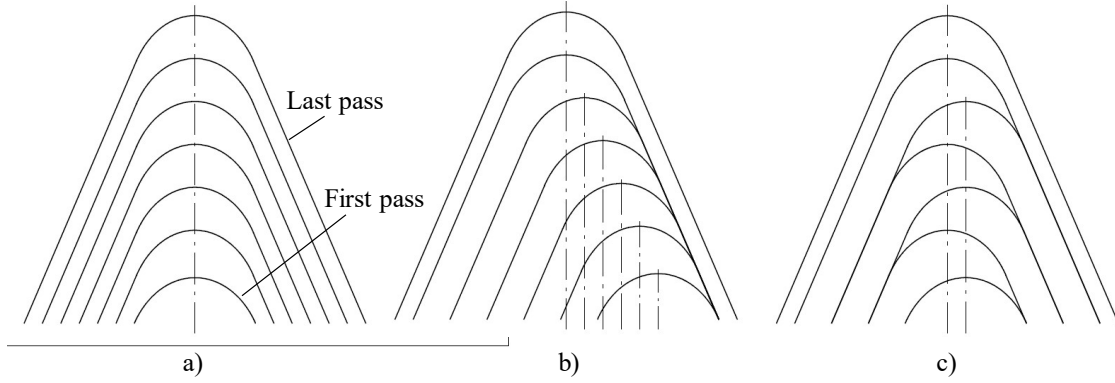


**Figure 1.9.** Three different strategies for skiving with several passes using the set-up parameter  $Crot$ : a) null  $Crot$ ; b)  $Crot$  only on one side; c)  $Crot$  alternated on both sides.

value of the chip thickness. As it can be seen, due to the different designs, the values of the maximum chip thickness, which in the figures has been called  $h_1$  and  $h_2$ , changes.

Machine tools may employ routines based on similar schemes in order to provide the corresponding values of  $f_A$  or  $h_{MAX}$  based on which value is given as the input data. In [7], it was also shown that for the same  $f_A$  and  $f_R$ , a higher gear ratio  $k$  and a higher cross-axis angle  $\Sigma$  yielded a lower  $h_{MAX}$ . This phenomenon can be demonstrated through Figure 1.8a) and b). Specifically, Figure 1.8a) illustrates, that for the same  $f_A$  and  $f_R$ , a larger tool tip diameter  $d_{tT}$ , corresponding to a higher  $k$ , yields smaller values of  $h_{MAX}$ . It must be specified that as will be shown in Paragraph 2.2.8.3, the figure can be misleading. It should not be assumed that in general a larger diameter corresponds to a smaller  $h_{MAX}$ . The figure indeed, aims at showing the implications of a larger number of teeth, which in turn corresponds to a larger tip diameter. This yields a reduction in  $h_{MAX}$ . In a similar manner to Figure 1.8a), Figure 1.8b) shows that for the same  $f_A$ ,  $f_R$  and tool tip diameter  $d_{tT}$ , a higher  $\Sigma$ , produce a longer and leaner chip and smaller values of  $h_{MAX}$ .

As for the cutting velocity, for a given pair of tool and workpiece materials there is a limited range of  $h_{MAX}$  which yield optimal tool performances. Also, the tool load is directly linked to  $h_{MAX}$ . Hence, usually,  $h_{MAX}$  is set as input in the machine-tool, and based on the  $NoP$  and the tool design, the axial feed is computed accordingly by the machine tool. However, in the last passes of finishing operations, in order to reduce the feed-marks on the gear flanks, the axial feed may be set as the input, and the value of  $h_{MAX}$  is computed accordingly. In such case attention must be paid on not reaching too small value of  $h_{MAX}$ , otherwise there is the risk of inducing plastic deformation rather than cutting the material.

Other set-up parameters are the tool run-in path  $l_{IN}$  and the tool run-out path  $l_{OUT}$ . These paths ensure that the tool is freed from the engagement with the workpiece at the initial and at the final cutting phases, respectively. Specifically, they allow avoidance of abrupt impacts at the beginning of the pass and also the prevention from not fully machined gap at the end of the pass. Hence, they concur in determining the cycle time  $t$ , as the tool must follow a longer axial stroke with respect to the gear width  $b_G$  at each pass. As for the case of the chip thickness, the run-in and run-out paths depend the axial feed  $f_A$ , on the radial feed  $f_R$ , and on the tool design, hence on the geometry of the engagement that occur between tool and workpiece within a pass. A precise analytical relationship for computing the run-in run-out paths based on other set-up parameters is lacking in the literature as well, and approximated models as that shown in Figure 1.8 may be used by the machine tools.

For what concern the productivity of the process, the cycle time is crucial, which may be computed as follows:

$$t = \sum_{i=1}^{NoP} \frac{b_G + l_{IN}(i) + l_{OUT}(i)}{f_A(i) \cdot \omega_G} \quad 1.5$$

where the symbol ( $i$ ) close to each set-up parameter stands of the  $i$ -th pass. From Eq. 1.5 it can be seen that the cycle time decrease by increasing the cutting velocity, by machining bigger chip thickness and by reducing the number of passes, in other words by increasing the load on the tool. Hence in production a trade-off between productivity and tool durability must be found.

Finally, a relevant role in the process is played by the infeed strategy. In fact, there are more ways to divide the gear gap height into passes. One way is to make all the passes of the same radial depth, which is named as linear infeed strategy. Alternatively, to reduce the tool dynamic load in the last passes, where most of the cutting profile is engaged, the degressive radial infeed strategy may be chosen. In this case the radial infeed is reduced from the first up to the last pass.

Additionally, it can also be chosen to anticipate the entering of one flank of the tool profile on the workpiece in order to favour cutting conditions and to homogenize the tool wear. This may be done by giving additional side rotation  $Crot$  to the workpiece in the intermediate passes. Figure 1.9 shows the resulting machined gear gaps relative to three different strategies for the parameter  $Crot$ . Figure 1.9a) shows the case where no extra side rotation  $Crot$  is used, and the intermediate passes are centred with respect to the final gap. Figure 1.9b) shows the case where during the intermediate passes the tool profile is set into tangency with the right side of the gear gap machined in the previous pass. Hence, one side of the tool profile is used to carry out most of the machining in this case. Finally, Figure 1.9c) shows the case where the workpiece side rotation  $Crot$  is alternated at each pass.

Those discussed above, are the most relevant set-up parameters based on which a centred gear skiving machining operation may be designed. Lastly, Table 1.2 shows the key characteristics for the Gleason 600PS machine tool which has been used to carry out experiments in this work.

**Table 1.2.** Main operating limit values of the Gleason 600PS Machine tool.

Parameters	min	max
Machinable normal module $m_n$	-	6 mm
External gear tip diameter $d_{tG}$	150 mm	600 mm
Internal gear root diameter $d_{rG}$	100 mm	600 mm
Cross axis angle $\Sigma$	-	25°
Gear angular velocity $\omega_G$	-	700 rpm
Tool angular velocity $\omega_T$	-	2200 rpm

### 1.3 State of the Art

With the aim of summarizing the major findings and highlighting possible new research directions, a paper was authored as part of this doctoral work, to establish the current state of the art in the skiving field. This section presents an updated yet condensed version of what published in [5], to which the reader may refer.

Several aspects are involved in the gear skiving process. Amongst them, the gear quality and the cutting conditions that determine the rate at which the tool wears during the operation are the most relevant ones, thus they are considered as the key issues of the process. The reasons supporting this assertion are that while the gear quality represents the qualitative outcome of the process, the cutting conditions determine its cost in terms of tool wear and cutting time. Therefore, a skiving application should be evaluated considering these two key issues by weighing the quality achieved with the price paid to obtain it.

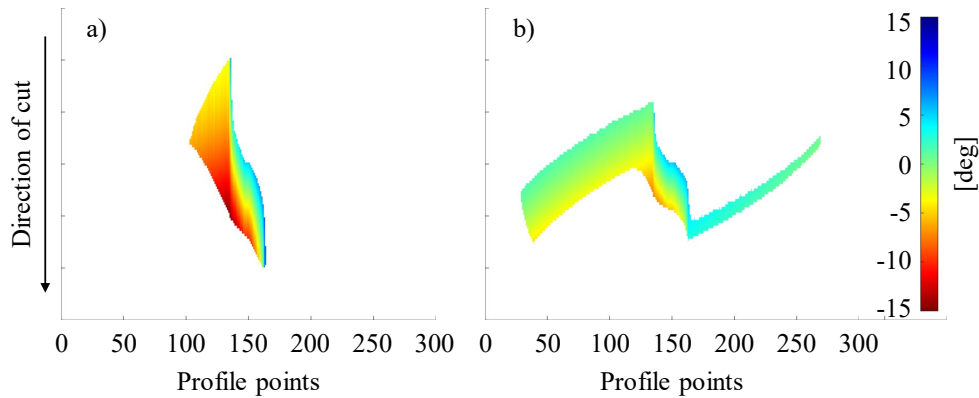


**Figure 1.10.** Working rake angle relative to two different passes of a 13-passes skiving process. a) Third pass; b) twelfth pass.

Many studies on gear skiving are available in the literature aiming at either improving the two key issues, and hence the process, or at helping for a deeper understanding of it. From the literature survey, three major themes emerged which were adopted in [5] to sort papers within corresponding groups. Papers not clearly dealing with the three major themes were reported in a fourth group. In particular, the first group, defined as *cutting process principle and simulation*, includes articles which developed simulation procedures to analyse key factors that would be hard to measure. The second group, defined as *parameter influence on the process*, encompasses articles in which the influence of certain parameters and their variation on the cutting conditions and the gear quality are studied. The third group, defined as *tool design*, comprises articles dealing with the key role of the tool geometry on the full process. The few articles that do not cover any of the above-mentioned major themes were gathered in the fourth group defined as *miscellaneous* group.

A perfect attribution of the analysed papers to only one of the four groups was not always possible since some papers may belong to more than just one group. In these cases, the paper was cited in all pertaining groups. Despite some overlapping, the grouping method resulted highly suitable to provide a clear overview on the state of the art of gear skiving. Therefore, it is used in this thesis as well.

### 1.3.1 Cutting process principle and simulation

The most commonly analysed elements in gear skiving simulations are the working parameters, such as the chip geometry and the working angles. These parameters can be subsequently used to derive more sophisticated parameters such as the cutting forces, the operating temperatures, and also the tool wear. Prediction of the influence of these elements allows the process optimisation in terms of tool durability and workpiece quality, enhancing production and efficiency.

Unfortunately, the interaction between tool and workpiece during the skiving process is very complex. Working parameters including cutting velocity, instantaneous rake angle and chip thickness, vary continuously both along the cutter and at different engagement phases for each process pass. An example of this is portrayed in Figure 1.10 where the values of the working rake angles relative to two different passes of the same process are shown. As it can be seen the shape of the engagement for the two passes is completely different. Furthermore, the working rake angle varies both in the direction of cut and also along the profile points. Therefore, some simplified models have been proposed that allow key working parameters such as chip thickness and working rake angle, to be approximately computed with minimal computational effort [8,9]. Unfortunately, such models, besides being approximate, are limited by the assumptions made to define them.

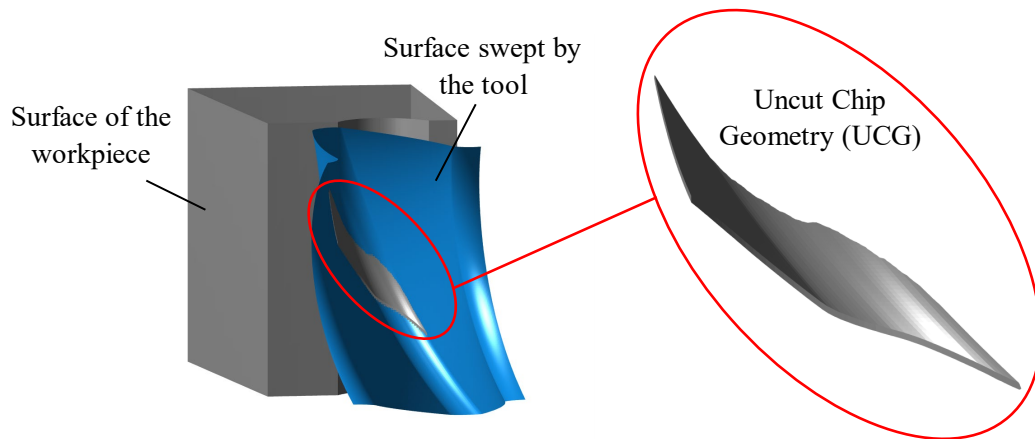


**Figure 1.11.** Computation of the Uncut Chip Geometry.

In order to accurately and thoroughly compute the cutting conditions, regardless of the set-up parameters at hand, simulation software should be used. In [10] Schulze et al. implemented a 3D model of a skiving process in the FEM commercial software ABAQUS, in order to analyse the chip formation mechanism for the case study at hand. However, a process as gear skiving, involves large material deformations, presence of lubricant, complex tool shape and different engagement geometry over multiple passes. The use of commercial FEM models entails the use of simplifications and requires a set-up time that cannot always be met in practice.

In a novel and evolving technology as gear skiving, it is advisable to consider as many parameters as possible. For this reason, ad-hoc software and numerical geometric simulations are considered the best options to simulate several aspects of the process.

Spath et al. [11] were among the first to develop a dedicated software for skiving. This allowed for the design of the tool shape and the computation of the working parameters. Since then, research groups have developed their own ad hoc skiving simulation software to explore different aspects of the process. SPARTApro for example, is a software based on rigid bodies penetration calculation. It was originally developed for hobbing simulations and then adapted to gear skiving. It was used in [7] to study the implications between process parameters and also more recently in [12]. The software simulation results were validated in [13] through a comparison with real machining. Remarkably, very recently, the University of Karlsruhe gave open access to its own skiving simulation software, Openskive. The software was used in recent studies [14,15] and is based on rigid bodies simulation as well.

Despite not considering apparently crucial aspects of the process, e.g. the material deformation, the employment of rigid bodies simulation is a viable option for gear skiving simulation. It allows fast calculation of the working parameters such as the working angles, and of geometrical key factors of the process such as the uncut chip geometry (UCG). The determination of the UCG can then be exploited to predict other process parameters, such as cutting forces and operating temperatures. An example of how to compute the UCG using the numerical program introduced in Chapter 2, is given in Figure 1.11. The figure shows the grey surface corresponding to the workpiece gap being machined, the light blue surface swept by the cutter profile during a machining pass, and the UCG that results from the intersection of the two surfaces.

Several ways of representing the interaction between tool and workpiece have been presented in the literature. The latter can be represented either as surfaces or as volumes. Some researchers used the discrete Z-map method, where vertically oriented line segments describe the workpiece geometry [16,17].

Other authors [18,19] employed the triple Dixel format which is an extension of the Z-map method in three orthogonal directions. The use of the triple Dixel representation, which is computationally more expensive, is justified by a more accurate description of the represented

volume. Interestingly in [18] McCloskey et al. by intersecting the 3D chip with the tool rake face, they obtained the 2D chip geometry, which was used as entry in a Kienzle model to estimate cutting forces.

A different technique that allows UCG computation has been employed by Fang et al. in [20]. The authors used level contour method to thoroughly analyse the 3D chip under different cutting conditions. This method was also used to compute the UCG in [21], from which the working parameters were derived.

An alternative to carry out rigid bodies volume intersection is through CAD software. In [22,23], Antoniadis et al., presented a skiving process simulation in CAD environment. After calculation of the 3D UCG, using the novel code they computed 2D chip sections through the knowledge of the tool rake face position. These were employed in a Kienzle model to predict cutting forces. The UCG and the relative cutting forces were computed in a similar fashion in [24–26]. Despite the interesting results, the use of CAD based software tends to be more arduous to implement than the previously presented simulation methods; thus, good programming skills are required for its efficient use.

As already mentioned, to compute cutting forces, authors often use 2D chip sections within a cutting model, derived by slicing a previously computed 3D UCG. However, there are other options to compute cutting forces. Several researchers directly discretized the cutter in points or micro sections [27–31]. Then, the width and depth of cut relative to each discretized domain is computed. For each of these, it is possible to apply an oblique cutting model to compute local forces, which could be finally summed up to obtain the resulting process forces. This technique has the advantage to be computationally faster with respect to the solid modellers for volume intersection methods since volume representation is not required during the simulation.

With the calculated forces and the knowledge of the material properties, some scholars proposed advanced models to derive the working temperature of the process [17,31,32] and also to predict tool wear [17].

### 1.3.2 Parameters influence on the process

Achieving a better knowledge of the cause-effect relations that exist among process parameters means acquiring a deeper comprehension of the machining process. Before listing the various research works that were conducted in this area, the definitions of the different sets of addressed parameters must be given since they vary across the literature.

In the context of this thesis, the parameter sets are distinguished between *set-up parameters*, *tool parameters* and *working parameters*. In particular, the *set-up parameters* are those that the operator, who manages the interface with the skiving machine, can modify depending on the specific machining operation. These include the tool cross-axis angle  $\Sigma$ , the centre distance  $a$ , the tilt angle  $\delta$ , the axial and radial feeds of the tool, respectively  $f_A$  and  $f_R$ , and the angular velocities of tool and gear, respectively  $\omega_T$  and  $\omega_G$ . Moreover, the set-up deviations, namely the variations of each set-up parameter from its nominal value, are part of this group. The *tool parameters* are intended as those describing the tool shape. These encompass all gear characteristic elements, such as: the tool number of teeth  $z_T$ , the normal module  $m_n$ , the tool nominal helix angle  $\beta_T$  and the tool profile shift coefficient  $x_T$ . Tool constructive angles like the rake angle  $\gamma_{r0}$ , the clearance angle  $\alpha_{c0}$ , the side relief angle  $\alpha_{s0}$  and the step angle  $\tau_{s0}$  are also included in this group. Finally, the *working parameters* are those that depend on the interplay between kinematics and geometry of the process and are used to describe the cutting conditions. These are the working rake and clearance angles, chip thickness, cutting velocity and all the other elements which result from the tool and workpiece instantaneous interaction.

Depending on which implications due to parameter variations have been addressed, it is possible to make three distinctions among articles of this paragraph. Indeed, a significant number of papers focus on the influence that the set-up and tool parameters have on working parameters.



A second portion focuses on their effect on gear modifications and tooth surface quality, whereas the last portion addresses their influence on tool wear.

As far as the influence on working parameters is concerned, the effect of set up and tool parameters on the working top and side relief angles has been assessed in [33]. In [34], the influence of tool rake angle, relief angle and feed motion on the interference between tool and workpiece was studied. A similar study was conducted in [35], in which the effect of the tooth number, tool modification factor, rake angle and relief angle on the interference was analysed. In [36], Guo et al. studied the effect of the tool teeth number and the cross-axis angle on the working rake angle. They also investigated the influence of different tool teeth numbers and the axial feed on the lead deviation of the machined gear.

In [7], Klocke et al. investigated, qualitatively, how, the tilt angle, cross-axis angle, tool teeth number and tool modification factor affected the chip thickness, the rake angle, and the cutting and sliding velocities. In [37], the influence of the tool teeth number, tilt angle and the profile shifting coefficient in working parameters were analysed. In [38] Moriwaki et al. studied the effect of the cross-axis angle and the tool face offset on the working rake angle, the clearance angle and on the depth of cut. Soon after, Uriu et al. continued the study of the research group in gear skiving [39]. They gave foundation for the common choice of setting the cross-axis angle to 20°. The analysis of the working parameter values demonstrated that such an angle implies moderate cutting conditions.

Wang et al. studied the effect of tool teeth number, relief angle, centre distance, cross-axis angle and feed motion on the interference between tool and workpiece, and on the machining deviation [40]. Then, they developed an optimization algorithm to compute the optimal set of working parameters.

In his latest work [25], Tapoglou investigated the effect of different feed rate, rake angle and inclination angle values on cutting force components and chip geometry.

After establishing the calculation model for the UCG, Fang et al. [20] analysed how different radial and feed rates affect the uncut chip shape. Then, in [41], they proposed a fast radial infeed planning by linking the desired working chip thickness with the radial feed, through the proposed calculation of the UCG.

In [42], Hilligardt et al. established a geometrical model to evaluate the meshing interference between tool and workpiece. In this study, the authors also estimated the effect of set-up and tool parameters on interference. Moreover, in [14], they showed the impact that a smaller tool profile shift coefficient may have on working parameters and tool load through a case study.

As previously mentioned, several research groups have concentrated on examining how set-up and tool parameters impact the gear quality in terms of gear modifications, quality and surface roughness. The goal is to potentially lower the costs associated with achieving specific gear quality standards.

Tachikawa et al. [43] studied the effect of the run out and the pitch deviation on the machined gear profile. In [44], an optimal parameters setting of the machine was computed by constructing a sensitivity matrix and using a linear regression method. Furthermore, in a recent study [45], Guo et al. analysed the effect of tool-workpiece position misalignments on tooth profile deviation. In [46], Li et al. studied a parameter selection method for the tool in order to improve machining accuracy.

In [47], the influence of both rake angle and re-sharpening depth on gear tooth profile errors were thoroughly analysed. Following this, a later work [48] demonstrated the influence of the relative position and orientation between tool and workpiece on profile deviations. In [49], in order to explore the skiving process flexibility, it was analysed the profile errors produced when using the same skiving tool when machining gears with different number of teeth.

Zheng et al. [50] were among the first to investigate the influence of tooth modification parameters on the tooth surface deviation, contact pattern and transmission error. In [51], Trübswetter et al. analysed the effect of different axial feeds on the gear flanks microstructure,

demonstrating a correlation between axial feed and surface waviness. Similarly, in [52] Jia et al. simulated the machined surface topography after the computation of the contact occurring between tool and workpiece surfaces. Recently, Ren et al. investigated the effect of tool eccentricity on gear profile errors [53]. The authors then explored how feed and eccentricity affected surface roughness. These studies on surface roughness can help developing ad-hoc cutting strategies based on the requested gear quality.

In [12], Janßen et al. were among the firsts to explore the possibility to modify the set-up parameters in order to generate flank modifications on the machined gear. The gear modifications can aid the meshing behaviour in operation. However, gear flank modification e.g. flank crowning, when produced by the skiving process, results in twisted flank. Therefore, in [15,54] two different methods for adjusting the tool design and the setup parameters were proposed, in order to minimize the undesired twist.

Another key aspect for the successful application of gear skiving is the tool durability, due to the high cost of skiving tools. Hence the implication of the parameter variation on the tool wear has been investigated by different scholars.

In [28] Guo et al. compared the effect of using different radial infeed strategies on the tool load which has direct implications on tool wear. In [55], Balabanov et al. investigated the influence of cutting edge radius on tool wear. They compared the results of a simulation with real cutting tests and determined the optimal edge radius for the case study analysed. In [56], Astashchenko et al. determined the most durable combinations of tool materials and coatings to machine an internal gear made of 38H2MYuA (equivalent to 34CrAlMo5) by gear skiving. Interestingly, in [57], Arndt et al. compared dry and wet gear skiving using different cutting strategies in terms of both tool wear and gear surface quality. Recently, in [58], Olivoni et al. proposed a method to analyse the differences in tool performances due tool re-sharpening, since they have direct correlation with tool wear. Then, the authors tuned set-up parameters in order to homogenise wear on tools at different re-sharpening phase so that to increase tool life.

### 1.3.3 Tool design

As in many generative machining processes, in gear skiving the tool plays a role of primary importance. Gear teeth are obtained as the envelope of the surface family spanned by the tool teeth while they move relative to the workpiece [59]. Therefore, errors in the tool geometry or in the relative motion will reflect as errors in the geometry of the machined gear.

It is well known from the theory of gearing that the machined gear profile would be error free if the cutter profile is calculated as the intersection between the conjugate surface of the gear to be cut and the rake surface. This applies regardless of the shape of the profile, which may for example be involute [6,60,61], cycloid [62] or circular [62–64].

Many research papers address tool geometry calculation employing conjugate theory, which is one of the pillars in the theory of gearing. Based on this, in [65,66] Jia et al. presented a numerical method for the calculation of the cutting profile. However, the theoretical tool profile could result as being non-involute, asymmetric and eventually unpractical to produce. Consequently, in industrial practice, it is common to find cutters whose profiles deviate from the theoretical shape to streamline tool production. However, this practice may cause errors on the machined gears.

As a result, several authors focused their attention on tool profile modifications in order to reduce the resulting gear errors. For example, in [67], Kojima et al. determined the exact tool profile for cutting an involute gear along with its deviation from an ideal involute. Then, they employed a standard involute shape as the tool profile, and computed the corresponding conjugated gear, showing that this latter presented profile errors. Eventually, they proposed a correction of the tool base circle radius to reduce such errors.

Guo et al. made important contributions in the field of gear skiving and published relevant articles concerning tool profile modifications. In [6] they presented a novel correction method for

the tool profile by altering the pressure angle. In [68], they developed a method to correct the twist of modified tooth flanks by optimizing the cutter profile. In particular, the cutter profile was represented as data points and formulated as a B-spline curve whose correction polynomial coefficients were computed. Polynomial coefficients were also employed in [69], where a new correction method for the tool profile was proposed to obtain an even grinding allowance on the machined gear flanks. Interestingly, recent studies focused on tool designs that allow for gear modifications while producing minimal errors [15,54].

Other scholars focused on new tool designs that aim at improving the cutting conditions of the process. In order to reduce the tool profile load and consequently its wear, for example, the design and performances of a multiblade cutter for gear skiving were investigated in [70–73]. The basic idea of a multiblade cutter is to divide the cutting action, which occurs within a pass, among different sub-blades. Experiments showed that, as far as soft steel gears were machined, the multiblade tool design may outperform a standard tool design in terms of wear by 6 times. However, the advantage reduces with the workpiece hardness. Recently, Olivoni et al. [74], proposed a novel parameter selection method for the design of skiving tool which aims at improving cutting conditions while considering specific process requirements.

One question which remains open is which type of skiving tool is the most convenient. Skiving tools can be distinguished based on their external shape which can be either conical or cylindrical. In conical tools, a constructive clearance angle is machined on the external surface of the tool to avoid interference with the gear machined. This type of tool simplifies the interference avoidance with the workpiece and requires a simpler machine setup. However, the conicity involves a change in profile shape with re-sharpening which if not properly designed leads to errors on the machined gear. Therefore, several studies have been made on the design of conical tools to prevent errors on the workpiece due to re-sharpening [37,60,75].

On the other hand, cylindrical tools have no constructive clearance angle. The cylindrical shape allows the elimination of issues caused by re-sharpening as the profile remains the same throughout the tool service life. However, to avoid interference, the tool must either be tilted during the operation, requiring an extra degree of freedom to the machine tool, or it must be operated in an eccentric position with respect to the gear. Each of these approaches requires a different way of designing the tool, which was the topic covered in [63,76–78].

Finally, some authors have investigated the effects of the rake face shape on the process. Usually, tools with spur teeth, have the rake faces of the teeth belonging to a common conical surface. In the case of tools with helical teeth instead, each tooth has a planar rake face oriented by the tool helix and the constructive rake angle, as shown in Paragraph 1.2.2. However, in [79,80], Wang et al. demonstrated that a curved rake face results in better performance. Additionally, in [64], a free-form rake face was studied to further improve the cutting conditions. Despite the promising results, however, such shapes have not yet found widespread practical use, as they involve additional difficulties in both the tool design and the re-sharpening phase.

#### 1.3.4 Miscellaneous

Due to the presented grouping method, some articles have not been included in the three groups reported above. These papers are considered in this miscellaneous section. They aim at solving other, so far less investigated, gear skiving issues.

In particular, in [81], Chen et al. presented a grinding method for the flank faces of a spur slice cutter. The geometrical characteristics of the flank faces were analysed. Then, the grinding motion model based on a five axis CNC machine tool for grinding was developed.

Similarly, in [82], a mathematical approach for generating the NC code required to grind the flanks and the rake face of skiving tools was proposed. The same author also proposed a methodology for the generation of the NC code required to manufacture gears by gear skiving on a conventional six-axis CNC turn-mill machining centre [83]. The study emphasized that the

quality of gears produced by gear skiving using dedicated machine was better than that produced using conventional machine tools. The machining accuracy that was reached in the experimental trial was insufficient for practical applications. However, this study represented a first step toward the employment of gear skiving process in general purpose CNC machines.

Tachikawa et al. [84] were the first to direct their interest toward the complex problem of vibrations in gear skiving. They proposed a simple method to compute the time series of cutting forces, considering the simultaneous mesh of multiple cutting edges. After establishing a mathematical model for the cutting forces power spectrum, the authors estimated the frequency at which these fluctuated. Considering the natural frequencies of the cutter and the clamped workpiece, they predicted the rotational speed of the cutter that was most likely to reduce vibrations.

In [21], Ren et al. investigated the correlation between local working parameters and the surface integrity of the machined gear flanks. In this study the deformation level and microstructural alterations of the access and recess gear flanks were gauged. The authors gave a rational explanation of the greater deformation on the recess flank.

Lately, some research group started analysing the possibility of applying the skiving process for the production of face gears, which are mainly used in helicopter transmission and vehicles differentials. Up to date the studies remain at a simulative phase, though the results seem promising [85–88].

### 1.4 Contribution of the Thesis

This section aims at outlining the context of this work in relation to the state of the art of gear skiving presented in the previous section.

Gear skiving has gained popularity among gear manufacturing companies relatively recently. Hence, in the last two decades, researchers have focused on addressing process-related issues, resulting in a considerable number of published articles. In order to foster research in the field and avoiding overlapping, it is paramount to have a benchmark that summarizes the major findings and that highlights possible new research directions. Since a systematic review outlining the state of the art of gear skiving was lacking, a first contribution of this doctoral work was to generate one [5].

As emerged from the review, a key aspect of the process are the cutting conditions since they determine both the tool wear and the cycle time determining the cost of the skiving operation. Hence, one objective of this thesis was to develop new cutting strategies aimed at reducing tool wear while maintaining or enhancing productivity. To this end, an ad hoc numerical program was developed to replicate the skiving process performed by the machine tool owned by the company. The numerical program is presented in Chapter 2.

With the aid of the numerical program, new implications between set-up parameters and working parameters are investigated. In the study presented in the first part of Chapter 3, it emerged that by simultaneously increasing the number of radial-passes and the nominal chip thickness, the cumulative machined total cutting length would significantly decrease. This while either maintaining or reducing the cycle time and by minimally increasing the predicted qualitative tool load. Therefore, experiments on annealed steel workpieces with different geometries have been carry out to prove the effectiveness of the proposed method showing good results in terms of wear reduction.

Additionally, a known issue related to the skiving process is the risk of performance impairment due to re-sharpening of conical tools. Despite being reported in the literature in [11,78], to the best Authors' knowledge this issue has not yet been adequately addressed.

The simulation program enabled for the first time a detailed analysis of the issue associated with re-sharpening of conical tools. Specifically, it revealed that due to the way conical skiving tools are designed, their re-sharpening leads to a variation in the tip diameter, resulting in a

corresponding change in the tool profile shape. A significant alteration in the profile shape, in turn, results in notable variations in cutting conditions and consequently impacts the tool's performance in terms of wear.

Therefore, in the second part of Chapter 3, tools design that are more sensitive to the effect of re-sharpening have been first identified. Thus, the implications on tool wear caused by the change in tool profile shape were analysed with the aid of simulation and then experimentally demonstrated. Additionally, an effective ad hoc cutting strategy to homogenize the wear of tools at different re-sharpening stage, have been proposed and tested, to show its effectiveness [58].

Overall, Chapter 3 shows the potential of the devised simulation program in enhancing the skiving process by aiding the development of new cutting strategies aimed at optimising specific cutting conditions.

However, in several case studies analysed throughout this PhD, it emerged that at the root of machining issues there was poor tool design. Having developed a simulation program, it is natural to question the effect of different tool designs on the process. This was the second objective of this work and is presented in Chapter 4. Specifically, to date a standard design methodology for skiving tools is lacking, and tool designs are mainly based on experience and best practice rules e.g. tools are designed to provide cross-axis angle of  $20^\circ$ . This may lead to tools that yield average, non-optimal, cutting conditions and also issues in some cases. Therefore, in our prior work, a first design methodology was proposed [74]. However, the study entailed several simplifications.

For this reason, a new methodology for the design of skiving tools was conceived which is still under investigation. Chapter 4 outlines the method in all its points, although only some of them are discussed in detail. The method lays foundation on screw theory, which is widely used in the literature related to gear design, but that has not yet been exploited in the study of gear skiving. The concept of infinitesimal teeth introduced in [89] are exploited, to derive novel equations for the operating pitch diameter of skiving tools. These have then been used to investigate implications of the tool tip diameter on the process.

The proposed approach should offer key benefits, enabling the resulting tool design to meet specific performance requirements in terms of both productivity and cutting conditions, which cannot be considered by a parameter selection based on practical experience. Additionally, the outlined methodology promises to be time-efficient, preventing the need for extensive simulations and their subsequent post-processing for comparison.

## 2 Numerical model of centred gear skiving

### 2.1 Need of an ad hoc program

As already mentioned, in gear skiving the interaction between tool and workpiece at each pass is very complex. The working parameters vary both along the cutter and at different positions for each pass. Hence, in order to investigate the cutting conditions for the enhancement of different aspects of the process, from tool design to cutting strategy, numerical simulations must be used.

As mentioned, different research centres investigating the gear skiving process have internally developed their own simulation software. Typically, these programs are not publicly available and may be provided upon considerable license fees.

In order to provide the company, with a tool for analysing the skiving process, in the context of this doctoral work, an ad hoc simulation program for skiving was developed in Matlab environment. The numerical program is presented in this chapter and is used to replicate the skiving process performed by the company's Gleason 600PS machine tool.

It is important to emphasise that the purpose of the following sections is not to explain in detail the numerical procedures that have been developed. This would in fact require extensive time. Rather, the aim is to show the main logic behind each numerical routine.

### 2.2 Numerical model workflow

The workflow of the whole numerical model is shown in the block diagram of Figure 2.1. In the following paragraphs, the theoretical background and definitions regarding each constituent block will be presented in detail. Firstly however, a high-level explanation of how the numerical model operates is provided to aid its comprehension.

As shown in the figure legend, the blocks in green represent the input data while the blocks in orange represent the elements calculated through simulation. Overall, the model workflow can be summarised as follows. Given as input the tool design parameters, the workpiece parameters, and the set-up parameters, the relative kinematics of the tool with respect to the workpiece is computed for each pass. Also, by setting as input the workpiece geometry and the tool design parameters, using the relative kinematics of the last pass, the tool profile is uniquely determined, and it is discretised into a finite number of points in space.

Then, by moving the tool profile with its relative motion with respect to the gear, the surface swept by the tool profile points at each pass is computed. Using the swept surface, the corresponding workpiece gap geometry is derived. By computing the intersection between the surface of the workpiece gap relative to the previous pass with the surface swept by the tool at the current pass, it is possible to determine the tool engagement points, the chip thickness they machine and the uncut chip geometry. The tool engagement points are defined as those points of the surface swept by the tool that penetrate the workpiece gap during the current pass. As it will be shown, such points can be exploited to compute the cumulative machined cutting length.

Also, by knowing the relative kinematics and the surface swept by the tool it is possible to establish the model of the cutting geometry. This allows the computation of the working angles based on the relative orientation between the velocity vectors and the cutting edges in which the tool profile has been discretized. Finally, the working angles are associated to the respective engagement points.

Therefore, for each engagement point all the working parameters, namely: the working angles, the chip thickness, the cumulative machined cutting length and the relative velocity vectors, are known. In other words, the cutting conditions, which are described by the working parameters, are determined. As it will be seen in later chapters, an in-depth analysis of the working parameters allows the detection of criticalities in the machining operations and the process optimisation.

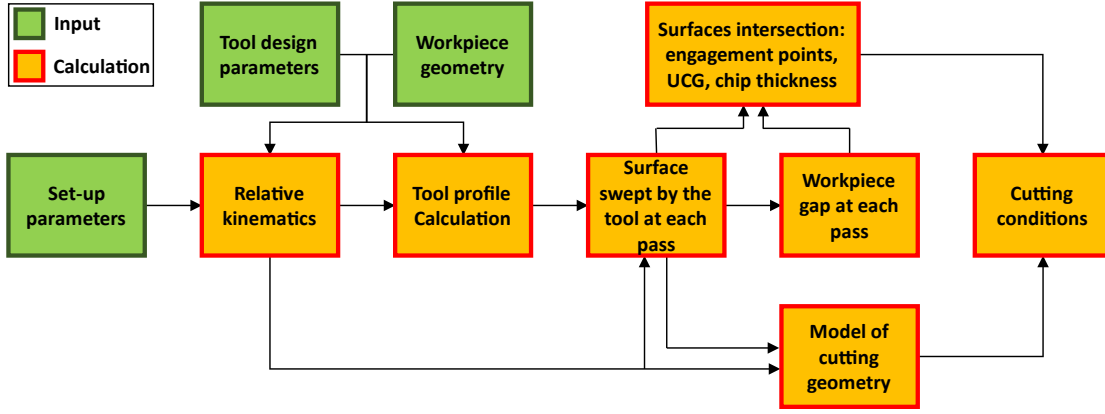


Figure 2.1. Numerical model workflow.

### 2.2.1 Input data

In the previous paragraph it was mentioned that the workpiece geometry is given as input. With workpiece geometry it is meant that not only the gear parameters are given as input, as for the case of the tool. A text file containing the point coordinates of a single gear gap in the transverse plane are also given as input to the program. The coordinate points may come from any external program.

The choice to generate the coordinate points of the gear gap outside the Matlab environment is due to the fact that often gears have specific profile modifications or in other cases some machining stock must be left in the gap. The corresponding gap geometries are not trivial to replicate except with ad hoc software, such as [90], which has been used in this work to generate the gear gap profile.

Once the text file has been read by the program, the gap profile is discretized in  $N_{pG}$  points specified as input via numerical interpolation. Furthermore, the program extracts data from the file concerning the gap geometry such as the diameters and the tooth thickness. In addition to the file with the gear gap point coordinates, the gear geometry data that cannot be measured from the file, such as the number of teeth, helix angle and gear width, are also provided as input to the program. With the input data, it is possible to extrude each point  $[x_G \ y_G \ z_G \ 1]^T$  of the discretized gear gap profile, written in homogenous coordinates, along the gear width by means of homogeneous matrix transformation. In this way, the points of the gear gap are obtained as follows:

$$\begin{bmatrix} x_{S_G}(\psi) \\ y_{S_G}(\psi) \\ z_{S_G}(\psi) \\ 1 \end{bmatrix} = \begin{bmatrix} \cos(\psi) & -\sin(\psi) & 0 & 0 \\ \sin(\psi) & \cos(\psi) & 0 & 0 \\ 0 & 0 & 1 & p_G \cdot \psi \\ 0 & 0 & 0 & 1 \end{bmatrix} \begin{bmatrix} x_G \\ y_G \\ z_G \\ 1 \end{bmatrix} \quad 2.1$$

In the above equation, for each value  $\psi_0$ ,  $[x_{S_G}(\psi_0) \ y_{S_G}(\psi_0) \ z_{S_G}(\psi_0) \ 1]^T$  represents a point of the gear gap written in homogenous coordinates. Furthermore,  $p_G = \frac{H_G}{2\pi}$  is the screw parameter of the gear,  $H_G$  is the gear lead, and  $\psi$  is the variable describing the rotation about the gear axis during the screw motion; specifically, the value of  $\psi$  will be within the range  $[0; \frac{b_G}{p_G}]$ , in order to span the entire gear width  $b_G$ .

Using a triangulation technique [91] allows the generation of a triangular mesh that binds all the gear gap points of Eq. 2.1 as part of a unique surface. Therefore, throughout this work reference is made not to the gear gap points, but rather to the gear gap surface  $S_G(\psi)$ . The symbol

## 2 Numerical model of centred gear skiving

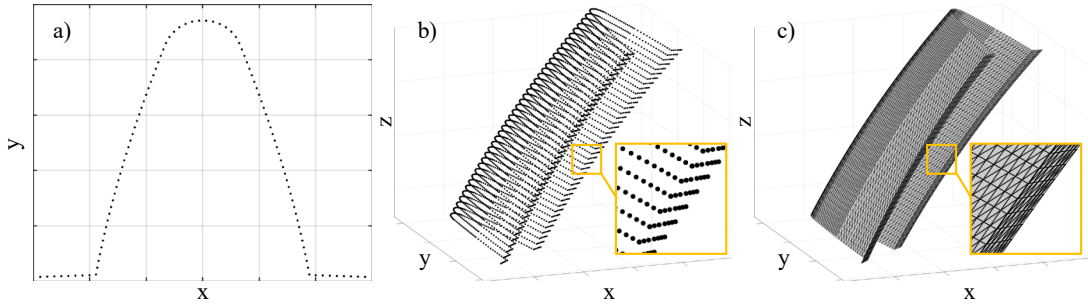


**Figure 2.2.** Step procedure to compute the gear gap mesh: a) two-dimensional gear gap point coordinates; b) point cloud of the extruded gear gap; c) triangulated surface  $S_G(\psi)$  of the gear gap.

$S_G(\psi)$  serves to indicate the whole of the points and the mesh which bind them. As shown in later sections, the use of a mesh allows, among other things, operations between surfaces to be carried out, such as surface intersection. This is key to model the penetration which arises in machining. Figure 2.2 shows the procedure to define the gear gap mesh, starting from the imported two-dimensional gap to the gear gap point cloud resulting from its extrusion and finally to the triangulated surface  $S_G(\psi)$  of the gap.

With regard to the tool design parameters some clarifications must be made. In the literature review, the tool parameters were defined as those describing the tool shape. However, in the contest of this work, reference is made to the tool design parameters. These parameters are defined as those that uniquely determine the geometry of the tool and that must be set as input in the tool calculation routine. They are given as input to the program through a template and are summarised in the left column of Table 2.1. Regarding the setup parameters, as the skiving process is typically operated in multiple passes, input vectors comprising each parameter for all passes are used. The set-up parameters set as input into the program are summarized in the right column of Table 2.1.

**Table 2.1.** Tool and set-up parameters given as input in the numerical model.

Tool design parameters	Set-up parameters
Number of teeth $z_T$	Vector of radial infeed $f_R$
Nominal helix angle $\beta_T$	Vector of axial feed $f_A$
Tip diameter $d_{tT}$	Modulus of tool angular velocity $\omega_T$
Constructive rake angle $\gamma_{r0}$	Vector of workpiece side rotation $Crot$
Constructive step angle $\tau_{s0}$	Machine tool axes corrections
Constructive clearance angle $\alpha_{c0}$	-

### 2.2.2 Relative kinematics

In this paragraph, the rigid body matrix transformations used to describe the relative motion between tool and gear are introduced, as well as the calculation of the relative velocity vectors. The reference frames employed in the numerical program in order to compute the rigid body matrix transformations are defined at first.

Figure 2.3a) and b) shows the reference frames relative to the schemes of Figure 1.3a) and b) for centred gear skiving of an internal and an external gear, respectively. Specifically, in Figure 2.3 are shown two fixed reference frames:  $O_{G0}(x_{G0}, y_{G0}, z_{G0})$  of the gear and  $O_{T0}(x_{T0}, y_{T0}, z_{T0})$  of the tool. The fixed reference frame origins are coincident with the mobile reference frames  $O_G(x_G, y_G, z_G)$  and  $O_T(x_T, y_T, z_T)$ , solidly attached to the gear and to the tool respectively. The two fixed reference frames lie on the line of shortest distance between the two



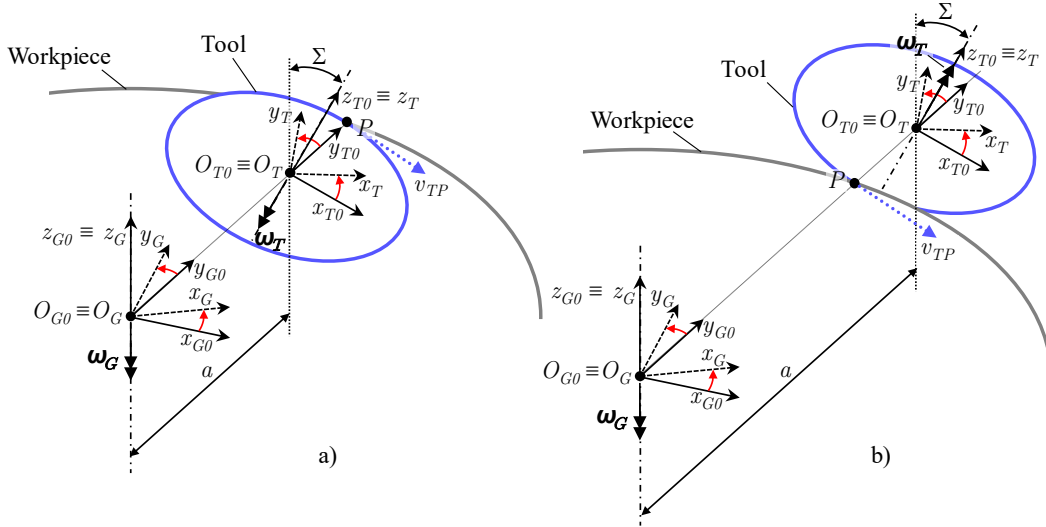


**Figure 2.3.** Reference frames employed in the numerical model for gear skiving of: a) an internal gear; b) an external gear.

rotation axes at the centre distance  $a$ . Furthermore, the tool mobile reference frame is inclined w.r.t. the tool fixed reference frame at the cross-axis angle  $\Sigma$ . The value of both  $a$  and  $\Sigma$  may be computed following Eq. 1.1 using the tool and the gear parameters as shown in the workflow of Figure 2.1.

The direction of rotation of tool and gear shown in Figure 2.3 refer to the case portrayed, where  $\Sigma$  is positive since the tool mobile reference frame is rotated counterclockwise about the  $y$ -axis w.r.t. to the tool fixed reference frame. Clearly, it is also possible to have the tool inclined on the opposite direction. In this case  $\Sigma$  assumes negative value and the direction of rotation of the tool and the workpiece is reversed. As a general rule it is sufficient to observe that the tool peripheral velocity  $v_{TP}$  at point P, which must enter the workpiece material. This determines the direction of rotation of the tool, whereas that of the gear is determined accordingly depending on if the gear is internal, or external.

In order to operate the coordinate transformations between the reference frames of Figure 2.3 three homogeneous coordinate transformation matrices of size  $4 \times 4$ , may be defined. Particularly,  $T_{T_0 T}$  transforms homogenous coordinates from the tool mobile reference frame to the tool fixed reference frame,  $T_{G_0 T_0}$  transforms homogenous coordinates from the tool fixed reference frame to the gear fixed reference frame and  $T_{G G_0}$  transforms homogenous coordinates from the gear fixed reference frame to the gear mobile reference frame. The three homogeneous matrices may be composed together to describe the coordinate transformation  $T_{G T}$ , from the tool mobile reference frame to the gear mobile reference frame, following the convention of rotations about body fixed axes, hence by post multiplying the matrices as shown in Eq. 2.2, where  $\mathbf{r} = [r_x \ r_y \ r_z \ 1]^T$  represents a generic vector written in homogenous coordinates.

$$\begin{aligned} \{\mathbf{r}\}_G &= T_{G G_0} \cdot T_{G_0 T_0} \cdot T_{T_0 T} \cdot \{\mathbf{r}\}_T \\ \{\mathbf{r}\}_G &= T_{G T} \cdot \{\mathbf{r}\}_T \end{aligned} \quad 2.2$$

The matrices above may be written in the following form:

## 2 Numerical model of centred gear skiving

$$\begin{aligned}
 T_{G G_0} &= \begin{bmatrix} c(\phi_G + Crot(i) + \Delta\omega_G(i)) & -s(\phi_G + Crot(i) + \Delta\omega_G(i)) & 0 & 0 \\ s(\phi_G + Crot(i) + \Delta\omega_G(i)) & c(\phi_G + Crot(i) + \Delta\omega_G(i)) & 0 & 0 \\ 0 & 0 & 1 & 0 \\ 0 & 0 & 0 & 1 \end{bmatrix} \\
 T_{G_0 T_0} &= \begin{bmatrix} c(\Sigma) & 0 & s(\Sigma) & 0 \\ 0 & 1 & 0 & a(i) \\ -s(\Sigma) & 0 & c(\Sigma) & f_A(i) \\ 0 & 0 & 0 & 1 \end{bmatrix} \\
 T_{T_0 T} &= \begin{bmatrix} c(\phi_T) & -s(\phi_T) & 0 & 0 \\ s(\phi_T) & c(\phi_T) & 0 & 0 \\ 0 & 0 & 1 & 0 \\ 0 & 0 & 0 & 1 \end{bmatrix}
 \end{aligned}$$

where  $\phi_G$  and  $\phi_T$  stands for the variables representing the rotation about the axes of the gear and of the tool respectively. Also, the symbol  $(i)$  close to each set-up parameter stands of the  $i$ -th pass, whereas the symbols  $c(\ )$  and  $s(\ )$  stand for the cosine and the sine of the corresponding parameter. Considering that the variables  $\phi_G$  and  $\phi_T$  are linked to each other by the gear ratio  $k$  as:

$$k = \frac{\phi_G}{\phi_T} \quad 2.3$$

it can be concluded that once the tool and the set-up parameters for machining a specific workpiece have been defined, the variable describing the motion of a point whose coordinates are transformed from the tool mobile reference frame to the gear mobile reference frame, is  $\phi_G$  and Eq. 2.2 may be written as:

$$\{\mathbf{r}\}_G(\phi_G) = T_{GT}(\phi_G) \cdot \{\mathbf{r}\}_T \quad 2.4$$

Specifically, being a numerical program, each process pass will be analysed by discretizing the relative angular span performed by the gear in a discrete number of positions  $\phi_{G_0}$ .

For what concern the relative velocity vectors, relating to the schemes shown in Figure 2.3, the cutting velocity of the tool with respect to the gear at point P may be computed as:

$$\mathbf{v}_{cP} = \mathbf{v}_{TP} - \mathbf{v}_{GP} \quad 2.5$$

Where the peripheral velocities of tool and gear  $\mathbf{v}_{TP}$  and  $\mathbf{v}_{GP}$  respectively, are computed as follows:

$$\begin{aligned}
 \mathbf{v}_{TP} &= \boldsymbol{\omega}_T \times \overline{\mathbf{O}_T \mathbf{P}} + \mathbf{v}_f \\
 \mathbf{v}_{GP} &= \boldsymbol{\omega}_G \times \overline{\mathbf{O}_G \mathbf{P}}
 \end{aligned}$$

As it will be shown in later sections, the relative velocity vectors relative to the tool profile points that penetrate the gear at each pass, i.e. the engagement points, are conveniently written in the gear reference frame using Eq. 2.4, in order to compute the cutting conditions.

As already mentioned, there are intermediate passes in which the gear gap height is divided, in order to ease the load on the tool during machining. At each pass the tool is set at an increasing radial depth from the first to the last pass, which cause an augment of the centre distance at each pass. The cross-axis angle and the angular velocities remain constant during the passes instead.

Therefore, the relative motion between tool and gear as well as the velocity vectors change throughout the passes due to the variation in centre distance, which affects the cutting conditions. As a result, the calculation of the homogenous transformation matrices and of the velocity vectors relative to the profile points at the different cutting positions, must be iterated and stored for each pass by the numerical program.

### 2.2.3 Tool profile calculation

This paragraph provides an overview of the theoretical concepts that form the basis for the tool profile calculation routine. Particular emphasis is put in clarifying the role that each tool design parameter has on the calculation procedure. This is done for two main reasons. Firstly, a procedure for selecting skiving tool parameters will be proposed in Chapter 4, and this paragraph is used to provide the relevant foundations. Secondly, the understanding of the procedure to compute the tool profile is crucial in order to fully grasp the gear skiving process.

Based on the theory of gearing [92,93], two conjugated surfaces are such if they remain in mesh, without penetrating, while relatively moving. Hence, in order to properly machine the desired gear gap at the last pass, the tool profile must belong to the surface conjugated to the workpiece gap. Given two mobile reference frames  $O_1(x_1, y_1, z_1)$  and  $O_2(x_2, y_2, z_2)$ , set at different positions and with different orientation, each attached to a surface,  $S_1$  and  $S_2$  respectively, one of the main problems in gear design consists in computing the unknown conjugate surface  $S_2$  to the known surface  $S_1$ . From the theory of gearing, the conjugate surface  $S_2$  to  $S_1$  may be computed as the envelope of the family of surface  $S_1$  written in reference frame  $O_2(x_2, y_2, z_2)$ .

Hence, for the theoretical computation of a skiving tool, the conjugate surface to the gear gap must be computed. In this context, the known gear gap surface  $S_G(\psi)$  computed as in Eq. 2.1, can be regarded as the known surface. The family of gear gap surfaces, expressed in the tool reference frame, which needs to be enveloped for computing the conjugate surface to  $S_G(\psi)$ , depends solely on the geometry of the gear gap and on the relative kinematics. Based on this, it may be stated that in gear skiving the tool geometry depends uniquely on the shape of the gear gap and on the relative kinematics. However, this is not completely accurate. Indeed, the portion of the tool that participates in the cutting action is not the tooth flank, but only the profile on the rake face. The tool flanks are not responsible for material removal. This applies to both conical and to cylindrical tools.

Therefore, the cutting profile must be computed as the curve resulting from the intersection between the plane of the tool rake face with the conjugate surface to the gear gap, also named as the generating gear [6,76]. As a result, the statement made above may be rectified as follows. In gear skiving, three elements concur in determining the geometry of the tool profile: the geometry of the workpiece to machine, the relative kinematics between the tool and the gear and the tool constructive angles. The first two elements concur in determining the generating gear and the last element determines the orientation of the rake plane used to section it.

Those just mentioned are the main theoretical concepts on which the tool profile calculation is based. Before addressing the numerical computational method, a few points must be made. In the tool profile calculation only the relative kinematics of the last pass is considered, since it is the one which shapes the desired gear gap. Additionally, the tool profile must not depend on the specific axial feed employed during the process. Hence, referring to the transformation matrix of Eq. 2.4, when the coordinates of the gear gap are written in the tool reference frame, both  $f_A$  and  $\Delta\omega_G$  are set to zero. Also, in the tool design of centred gear skiving the value of  $Crot$  is typically set to zero. As a result, the tool profile is independent on the set-up parameters.

It can therefore be concluded that, since the workpiece geometry is given as the input to the program, the relative kinematics and consequently the generating gear, depend uniquely on the tool design parameters  $(z_T, \beta_T, d_{iT})$ . In fact, based on Eq. 1.1, they determine the centre distance

$a$ , the cross-axis angle  $\Sigma$  and the gear ratio  $k$ , namely the relative kinematics of the last pass. For this reason, the parameters  $(z_T, \beta_T, d_{iT})$  are referred to as the tool kinematic parameters. The tool constructive angles instead, are named as the tool constructive parameter. As shown in Paragraph 1.2.2, the tool constructive rake angle and the tool constructive step angle determine the orientation of the rake plane. Such distinction on the tool design parameters will be used again in Chapter 4. Notably, the tool kinematics parameters and the tool constructive parameters are unrelated and can be chosen independently to each other. They both concur in determining the shape of the tool profile.

The numerical computation of the tool profile is carried out as follows. Firstly, the inverse of the homogeneous matrix shown in Eq. 2.4 is computed. Then, it is possible to calculate the coordinates of the gear gap surface  $\mathcal{S}_G(\psi)$ , written in the tool reference frame, for each considered position  $\phi_G$ , as follows:

$$\{\mathcal{S}_G(\psi)\}_T(\phi_G) = T_{GT}(\phi_G)^{-1} \cdot \{\mathcal{S}_G(\psi)\}_G \quad 2.6$$

where  $\{\mathcal{S}_G(\psi)\}_T(\phi_G)$  is the family of gear gap surfaces  $\mathcal{S}_G(\psi)$  written in the tool reference frame. In a numeric program the variable  $\phi_G$  which is theoretically a continuous variable describing the gear rotation about its axis, must be discretized in a finite number of positions. This yields an approximation to theory. Therefore, the finest the discretisation for a given angular span, the more accurate the calculation. However, about two discrete positions per degree of angular span results to yield a good accuracy of the computed profile.

It should be specified that each surface  $\mathcal{S}_G(\psi)$  of  $\{\mathcal{S}_G(\psi)\}_T(\phi_G)$  has different coordinate points but has the same triangular mesh. This is due to the fact the gear gaps of the family of surfaces are rigidly transformed, hence the relative location of the points within a single surface  $\mathcal{S}_G(\psi)$  does not change. Consequently, the gear gap mesh needs to be computed only once.

Once the discrete surface family is computed, instead of calculating its envelope, namely the generating gear, and section it with the rake plane  $\pi_r$ , it results convenient to compute the intersection among the rake plane and the family of surfaces first, as proposed in [65]. The intersection between  $\pi_r$  and  $\{\mathcal{S}_G(\psi)\}_T(\phi_G)$  yields a discrete locus of curves. Then, the envelope of the discrete locus of curves on the rake plane is computed and the tool profile is determined. Finally, the tool profile is discretized into the desired number of points  $N_{pT}$  by numerical interpolation.

A graphical representation of the numerical tool profile calculation just described is given in Figure 2.4. Specifically, Figure 2.4a) shows the family of the discrete gap surfaces intersected by the tool rake plane, depicted in blue, and the resulting discrete curve locus, depicted in red. Figure 2.4b) shows the view, normal to the rake plane, which portrays the discrete locus of curves and the  $N_{pT}$  discrete tool profile points in black, resulting from its numerical envelope. It may also be noticed that there are fillet radii that extend beyond the discrete locus of curves in the root area of the profile. Such radii have only an aesthetic purpose and do not participate in the cut.

From the above procedure, it is clear that for a given gear gap to be machined, by affecting either the generating gear, hence by changing one or more of the tool kinematic parameters  $(z_T, \beta_T, d_{iT})$ , or by altering the orientation of the rake plane, hence by varying one of the constructive parameters, yields a different tool profile. Therefore, in phase of tool design, each set of tool design parameters corresponds to a different tool profile.

In Chapter 4, it will be outlined an approach for the selection of the tool design parameters in order to enhance the process. In the following paragraph and in Chapter 3 however, it is analysed a commonly encountered scenario to gear manufacturers. In this context, the tool has already been designed, and its shape must be determined in order to carry out simulations to analyse and enhance the process.

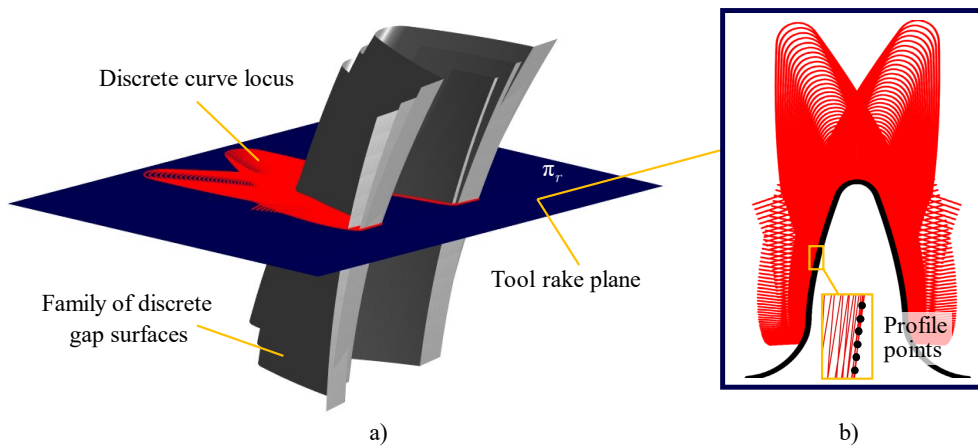


**Figure 2.4.** Tool profile numerical calculation: a) family of discrete gap surfaces sectioned by the tool rake face; b) the tool profile discretized in  $N_{pT}$  points resulting from the envelope of the discrete locus of curves.

Before going on with the computation of the entire tool flanks, it is worth stressing that given a tool profile computed as above, can only produce the desired gear gap if it is used under the same conditions for which it has been designed. Varying the centre distance or the cross-axis angle during machining, for instance, yields a different profile with respect to the one desired. Similarly, it is not possible to use the same tool to machine a workpiece that has the same profile of the workpiece for which the tool has been designed, but that has a different number of teeth. This is because the gear ratio would change and consequently also the generating gear. A study of the error produced by a skiving tool when machining gears with a tooth number different from the nominal one is shown in [49].

What has been said clarifies the fact that skiving is a fundamentally different process from hobbing or shaping. In fact, these traditional processes simulate the behaviour of a rack. As a result, one tool may be used to machine several types of gears. Furthermore, it is possible to alter the process kinematics, in order, for instance, to realise gears with different profile shift coefficient. This is not possible with a skiving tool, which can only machine the gear gap for which it was designed, without altering the kinematics.

### 2.2.3.1 Tool flanks calculation

The procedure above allows the calculation of the cutting profile of a skiving tool, which in turn it is sufficient to carry out the process simulation shown in Figure 2.1, since, as already explained, it is only the profile that machines the gear gap. However, in order to provide a deeper insight into tool design, it is interesting to show how the tool flanks may be computed. This is done using two points of views. First a theoretical approach is presented. Then, it is compared with the practical considerations.

The tool machines the workpiece only with the profile on the rake face. However, after a re-sharpening step, there must be a new profile on the new rake face capable of machining the same gear gap. This is trivial for cylindrical tools. As mentioned in Paragraph 1.2.2, such tools maintain the same profile shape throughout their service life, which can therefore be high.

In the case of centred skiving, however, only conical tools can be employed to avoid interference with the workpiece during machining. Looking at the enlargement in Figure 2.5a), it can be seen that, due to the tool conicity, each re-sharpening step  $h_s$  in which the tool service life is divided, corresponds to a variation  $\Delta_{dtT}$  of the tool tip diameter, which may be computed as:

$$\Delta_{dtT} = 2 \cdot h_s \cdot \tan(\alpha_{c0}) \quad 2.7$$

## 2 Numerical model of centred gear skiving

Since the tool tip diameter varies, the centre distance varies according to Eq. 1.1 and also the relative kinematics and the generating gear vary. Theoretically at each re-sharpening height, the tool profile must be computed using a different generating gear sliced by the rake plane. Thus, the profile calculation must be iterated to compute the entire tool flank. An example of this is shown in Figure 2.5b) and c) in which the tool profile corresponding to the start of life (SOL) and the end of life (EOL), respectively, are portrayed. It can be seen that the two profiles are different due to the different re-sharpening stage.

In the phase of process analysis in which the tool is already designed, the value of the constructive clearance angle  $\alpha_{c0}$  for interference avoidance is provided. Therefore, it is possible to iterate the computation of the tool profile and to extrude the tool flanks surface  $\mathcal{S}_T(\psi)$  similarly to Eq. 2.1. This is achieved by extruding each point  $\mathbf{r}_T = [x_T \ y_T \ z_T \ 1]^T$  of the discretized tool profile, relative to each re-sharpening step, following the tool lead  $H_T$ , as follows:

$$\begin{bmatrix} x_{S_T}(\psi) \\ y_{S_T}(\psi) \\ z_{S_T}(\psi) \\ 1 \end{bmatrix} = \begin{bmatrix} \cos(\psi) & -\sin(\psi) & 0 & 0 \\ \sin(\psi) & \cos(\psi) & 0 & 0 \\ 0 & 0 & 1 & p_T \cdot \psi \\ 0 & 0 & 0 & 1 \end{bmatrix} \begin{bmatrix} x_T \\ y_T \\ z_T \\ 1 \end{bmatrix} \quad 2.8$$

In the equation above, for each value  $\psi_0$ ,  $[x_{S_T}(\psi_0) \ y_{S_T}(\psi_0) \ z_{S_T}(\psi_0) \ 1]^T$  represents the homogenous coordinates of a point of the tool flank surface  $\mathcal{S}_T(\psi)$ ; whereas  $p_T = \frac{H_T}{2\pi}$  is the screw parameter of the tool and  $\psi$  is the variable describing the rotation about the tool axis during the screw motion; the value of  $\psi$  for each re-sharpening step  $h_s$ , spans the range  $[0; \frac{h_s}{p_T}]$ .

In the design phase, however, difficulties arise. It is necessary to define a unique value  $\alpha_{c0}$  of the constructive clearance angle that ensures, at each re-sharpening height, that collision with the workpiece is avoided. In particular, each generating gear relative to each tool profile corresponding to a re-sharpening height must not collide with the other profiles that make up the tool flanks. In order to verify this, a basic numerical routine, external to the numerical program workflow of Figure 2.1 and which is meant exclusively to explore the complex world of tool design, has been developed and is presented in Appendix A.

Obviously, the larger the constructive clearance angle, the easier it is to avoid interference with the workpiece. However, with reference to Eq. 2.7, it can be seen that the higher the value of  $\alpha_{c0}$  is, the more the tip diameter of the tool varies and thus the centre distance. As will be shown in Chapter 3, for certain tool geometries, a too large change in diameter during the tool life can significantly affect the shape of the profile, which is then associated with a significant change in tool performances. For this reason, conical tools typically have constructive clearance values that range between  $3^\circ$  and  $10^\circ$  and a tool service life between 5 and 15 mm.

Finally, for the sake of completeness, it is interesting to compare theory and practice from what concern tool design. As mentioned in the state of the art, the theoretical tool profile could result as being non-involute, slightly asymmetric and eventually unpractical to produce. Consequently, in industrial practice, it is common to find tools whose profiles deviate from the theoretical shape, since skiving tools can be realised using generative techniques, making their production cost-effective.

The general idea for the practical production of skiving tools is the following. Having to theoretically compute several profiles for several re-sharpening heights, a nominal profile is established as a reference. This profile is computed as a modified involute that replicates the shape of the theoretical profile, corresponding to the nominal cross-axis angle as accurately as possible. The tool flanks are machined by generating process, while a variable profile shift coefficient is

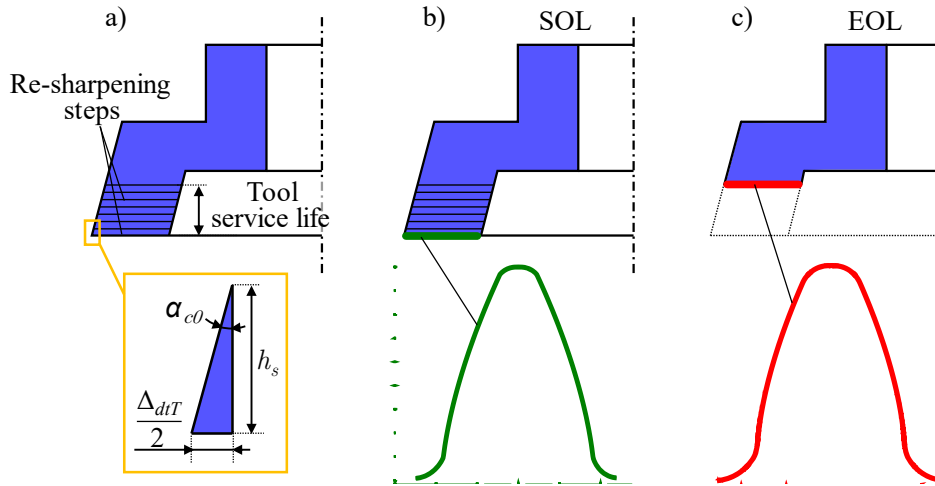


**Figure 2.5.** Calculation of conical tool flanks. a) Tool tip diameter reduction caused by re-sharpening; b) tool profile at SOL; c) tool profile at EOL.

applied along the tool width to generate the conicity. This is done while using a unique base diameter corresponding to the nominal involute profile and a constant tool lead.

Consequently, apart from when the tool re-sharpening stage corresponds to the nominal profile, the real tool must be inclined in the machine tool with a cross-axis angle that will deviate from the nominal one depending on the state of re-sharpening. Such variations are also implemented in the skiving machine tool and result in machine tool axes deviations with respect to nominal set-up parameters. Hence, corrective values for the machine tool axes have been introduced into the set-up parameters in Table 2.1. By doing so it is possible to faithfully replicate the process.

It is worth clarifying that in the simulations presented in this work, the theoretical profile is always used for two main reasons. Firstly, the real profile deviates from the theoretical one by a small margin, otherwise it would generate errors on the workpiece. Secondly, the real profile geometry is unknown as only the tool manufacturer knows how the specific tool has been produced. In the following, when reference is made to the tool profile it is meant the theoretical profile of the tool at the start of life. When the end of life or other re-sharpening stages of the tool are considered, it will be specified.

#### 2.2.4 Surface swept by the tool at each pass

Once the tool profile and the relative kinematics have been calculated, referring to the workflow of Figure 2.1, the surfaces swept by the tool during the process for each pass can be computed. A clarification must now be made. By surface swept by the tool, it is meant, the whole of the point cloud, generated by the tool profile points in relative motion with respect to the gear and written in the gear mobile reference frame  $O_G(x_G, y_G, z_G)$ , along with the relative mesh which bind the point cloud. As explained in Paragraph 2.2.1, the definition of a mesh is needed to carry out numerical calculations such as the intersections between tool and gear surfaces to simulate machining. For the sake of clarity, in the following figures the lines of the meshes relative to the gear gap and the surface swept by the tool will be concealed. Nevertheless, it is important to bear in mind that are the meshes who enable the execution of many of the numerical operations described in this work.

The choice of adopting the mobile reference frame of the gear allows an easier interpretation of the process. Since the tool and the gear are in relative motion, it is not easy to visualise the interaction while one penetrates into the other. Instead, visualising the gear as stationary and the

## 2 Numerical model of centred gear skiving

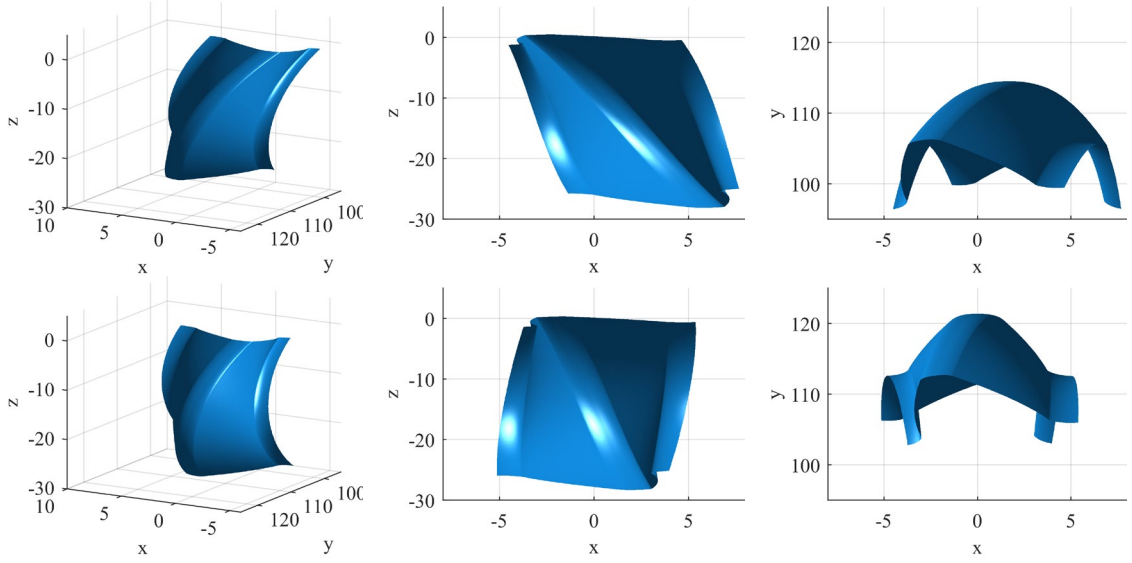


**Figure 2.6.** Surface swept by the tool. Top row: at the first pass; bottom row: at the last pass.

tool moving relative to it allows the skiving process to be associated with the well-known schemes of the mechanics of cutting.

Therefore, by using Eq. 2.3-2.4, it is possible to describe the relative motion of the tool profile, in the gear mobile reference frame, for each pass. This yields for each pass, what here is referred to as the surface swept by the tool  $\{\mathcal{S}_{ST}\}_G(\phi_G)$ . Therefore, the coordinates of each point  $\{\mathbf{r}_T\}_T = [x_T \ y_T \ z_T \ 1]^T$  in which the tool profile has been discretized, written in the tool mobile reference frame  $O_T(x_T, y_T, z_T)$ , are transformed in the gear mobile reference frame as follows:

$$\{\mathbf{r}_T\}_G(\phi_G) = T_{GT}(\phi_G) \cdot \{\mathbf{r}_T\}_T \quad 2.9$$

where  $\{\mathbf{r}_T\}_G(\phi_{G0}) = [x_{TG}(\phi_{G0}) \ y_{TG}(\phi_{G0}) \ z_{TG}(\phi_{G0}) \ 1]^T$ , represents one point, relative to the considered discrete gear position  $\phi_{G0}$ , of the surface swept by the tool  $\{\mathcal{S}_{ST}\}_G(\phi_G)$ , written in the gear mobile reference frame. Since the relative motion of the tool with respect to the gear is described by the discrete variable  $\phi_{G0}$ , from here on the term cutting position, is used to refer to  $\phi_{G0}$ . To sum up, all the coordinates of the  $N_{pT}$  points in which the tool profile has been discretized, are transformed from the tool mobile reference frame to the gear mobile reference frame via Eq. 2.9. This happens for all positions  $\phi_{G0}$  in which the gear rotation relative to each pass has been discretized. The whole coordinates transformation generates the surface swept by the tool. Each cutting position  $\phi_{G0}$  corresponds to a different configuration of the  $N_{pT}$  tool profile points along the surface swept by the tool.

There is one surface swept by the tool for each pass. Each of them is different with respect to the other, since the tool set-up parameters, e.g. the centre distance and the  $Crot$  among others, vary at each pass. In other words, at each pass the transformation matrix  $T_{GT}(\phi_G)$  of Eq. 2.4 changes. An example of this is given in Figure 2.6, where the figures in top row show from three different perspectives, the surface swept by the tool relative to the first pass of a multi pass process. In the figures in bottom row instead, it is shown the surface swept by the tool at the last pass from the same three perspectives. It can be noticed here that at the first pass, the surface swept by the tool apart from being shifted with respect to the gap centre at  $x = 0$ , due to a side rotation  $Crot$ , appears to develop more horizontally. The last pass, on the other hand, tends to be straighter and is centred to the gap due to null  $Crot$ . Also, from the figure, it can be seen how peculiar it is the relative motion of the tool with respect to the gear in the skiving process.



It is worth to point out, that the arrangement of the points in relation to each other remains the same for all the passes. Hence, it is possible to compute a single mesh for all the surfaces  $\{\mathcal{S}_{ST}\}_G(\phi_G)$  relative to the several passes.

Finally, it must be pointed out that in order to carry out the surface intersection routine, two swept surfaces must be computed for each pass. The first surface is calculated at a certain height with respect to the gear gap, in order to assure that all the penetration points are contained in the gear gap. Then, a second surface is computed at a height reduced by the axial feed of the pass, so that the engagement points can be accurately computed, as explained in the relevant section.

### 2.2.5 Workpiece gap at each pass

The computation of the workpiece gap is essential as it allows, along with the previously computed surface swept by the tool, the computation of the surfaces intersection which yields the engagement points. The workpiece gap calculation is divided into four steps and requires the surfaces swept by the tool in each pass to have been previously computed, as shown in Figure 2.1. The entire procedure is depicted in Figure 2.7, which shows the four-step procedure for the ninth pass of process of thirteen passes.

The first step involves projecting the points of the surface swept by the tool onto the transverse plane of the gap. To do this, it must be considered that in the real process, if the gap to be machined is helical, while the tool plunges in the axial direction of the gear by an amount  $\Delta z$  an extra rotation  $\Delta\phi_G$  of the gear must be produced, as follows:

$$\Delta\phi_G = \frac{\Delta z \cdot \tan(\beta_G)}{r_{pG}} \quad 2.10$$

in agreement to what reported in Paragraph 1.2.1. Hence, for each surface swept by the tool, the quantity  $\Delta\phi_G$ , about which rotate the points of  $\{\mathcal{S}_{ST}\}_G(\phi_G)$  during their projection on the gap traverse plane, is computed accordingly to the relevant  $z_{TG}(\phi_G)$  through Eq. 2.10. The projection may be computed as follows:

$$\begin{bmatrix} x_{TGp}(\phi_G) \\ y_{TGp}(\phi_G) \end{bmatrix} = \begin{bmatrix} \cos(\Delta\phi_G) & -\sin(\Delta\phi_G) \\ -\sin(\Delta\phi_G) & \cos(\Delta\phi_G) \end{bmatrix} \cdot \begin{bmatrix} x_{TG}(\phi_G) \\ y_{TG}(\phi_G) \end{bmatrix} \quad 2.11$$

Where  $[x_{TGp}(\phi_G) \ y_{TGp}(\phi_G)]^T$  are the projected points of  $\{\mathcal{S}_{ST}\}_G(\phi_G)$  on the gear transverse plane. Figure 2.7a) shows the result of the projection for one pass. Obviously if the gear gap is spur as the case of the figure, the following relation holds:

$$[x_{TGp}(\phi_G) \ y_{TGp}(\phi_G)]^T = [x_{TG}(\phi_G) \ y_{TG}(\phi_G)]^T$$

It is hence possible to proceed with the second step, which consists in enveloping the outer edge of the projected points. This edge is shown as a thick blue line in Figure 2.7b) and represents the shape of the gap in the transverse plane after the pass has been performed throughout the gear width.

Then, it is possible to proceed with the third step, in which the intersection and merging between the edges machined by successive passes are computed. In Figure 2.7c) it can be seen that the ninth pass, widens the gap only on the left-hand side in the highlighted red area. This is because the right-hand side of the gap has already been machined by the previous pass, represented in dashed line, due to the workpiece side rotation  $Crot$ . Once the shape of the current pass gap has been determined, it is numerically interpolated into  $N_{pG}$  points.

## 2 Numerical model of centred gear skiving

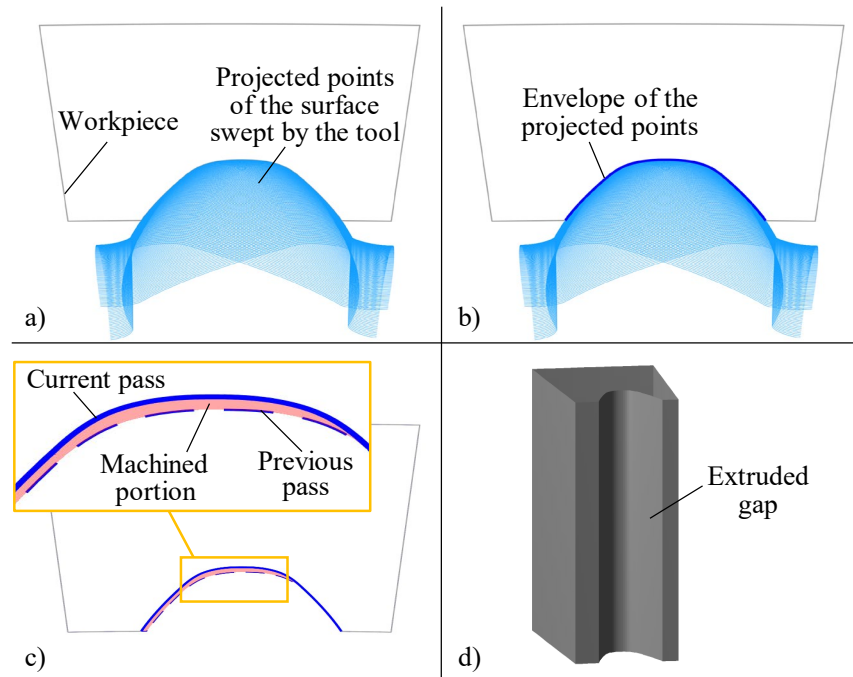


**Figure 2.7.** Four-step procedure to compute the workpiece gap of each pass: a) first step; b) second step; c) third step; d) fourth step.

Finally, in the fourth and final step, the gaps computed in the third step are extruded by means of Eq. 2.1. This allows the surfaces of the gaps relative to each pass to be computed and also their corresponding mesh. It should be pointed out that the programme does not extrude the gear gap relative to the entire gear width. In fact, as will be seen in the next paragraph, only a portion of the gear gap width is required in the computation. Therefore, to reduce the computational cost, only a portion of the real gear gap is considered. Hence for the same density, the resulting triangular mesh is made up of less elements.

### 2.2.6 Surfaces intersection

This routine represents the core of the numerical program as it allows the penetration between tool and workpiece to be computed. The output of the routine are the engagement points, namely those points of the surface swept by the tool that penetrate the workpiece gap during the pass, the relative chip thickness and the UCG. The computation of the penetration is crucial for analysing the process and determining the cutting conditions.

The routine is divided into two steps. Each step is repeated for each pass of the process. At the first step, the first surfaces intersection is calculated. The gear gap of a certain pass is penetrated by the surface swept by the tool of the next pass. An example is shown in Figure 2.8 a), where the surface swept by the tool at the third pass penetrates the gear gap resulting from the second pass. Using the Matlab function [94] adapted to this routine, it is possible to compute the intersection between the two surfaces. The result of the first surfaces intersection is shown in Figure 2.8b) and c). In particular, Figure 2.8b) shows the surface of the gear gap after the first intersection. From the figure it can be seen that the gear gap is carved by the surface swept by the tool. The area relative to the points of the trace carved on the gear gap has been represented in blue. Figure 2.8c) instead, shows the surface swept by the tool in blue colour and the region relative to the points on it that have penetrated the gear gap, namely the intersection points, in grey colour. These intersection points just shown are not the engagement points that are used to compute the cutting conditions. To determine the engagement points, it is necessary to perform

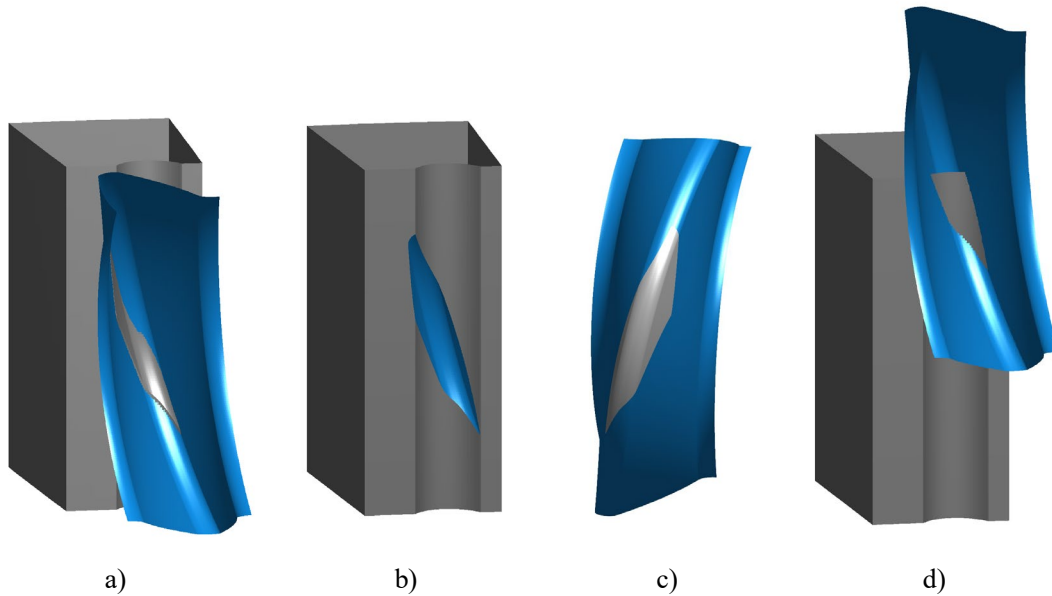


**Figure 2.8.** First surfaces intersection. a) Penetration of the surface swept by the tool on the gear gap; b) gear gap after first surfaces intersection; c) intersection points on the surface swept by the tool; d) penetration during run-in path.

the second step of this routine. The first surfaces intersection just shown is in fact an ideal condition and serves merely as a preliminary computation to carry out the second step.

In the real process, during the run-in tool path the tool first comes into contact with the workpiece. At this stage, the shape of the trace carved on the gear gap is not complete since full penetration has not been achieved. The same thing happens during the run-out path when the tool disengages from the workpiece. An example of the penetration during the run-in path is given in Figure 2.8d), where it can be seen that the trace carved on the gap is incomplete. From this situation, the tool advances axially until it reaches the full penetration into the workpiece shown in Figure 2.8a). From here on, the shape of the penetration remains the same during the advancement of the tool throughout the gear width. This is crucial for what concern the logic of the numerical routine.

In fact, since the shape of the trace carved on the gap remains constant once full penetration is achieved, the second step of the routine consists in computing another surfaces intersection. The latter is referred to as the second surfaces intersection and involves the surface of the gear gap carved by the first surfaces intersection, and the surface swept by the tool sunk by the axial feed  $f_A$  with respect to the previous surface swept by the tool.

An example is shown in Figure 2.9. In particular, Figure 2.9a) shows the surface swept by the tool, sunk by  $f_A$  compared to the one shown in Figure 2.8a). It can be seen that due to the axial feed, the surface swept by the tool penetrates further the gear gap already carved by first intersection. Figure 2.9 b) shows the surface of the gear gap after the second surfaces intersection. The region relative to the points of the new trace carved in the gear gap are depicted in blue. Figure 2.9c) depicts, on the surface swept by the tool, in red shadow the area relative to those points who penetrate the gear gap during the second surfaces intersection; whereas in grey colour the region relative to the intersection points of the first surfaces intersection. From the enlargement in the figure, the red area compared to the grey one appears to expand slightly downwards, which is due to the axial feed. In the upper part instead, the red area is reduced considerably compared to the grey one. This is due to the fact that at the first surfaces intersection of Figure 2.8, the gear gap was at an ideal condition, namely without traces carved by the previous axial pass. In the second step of the routine instead, a more realistic situation is being considered, where the penetration pattern of the current pass is affected by the one of previous pass.

## 2 Numerical model of centred gear skiving

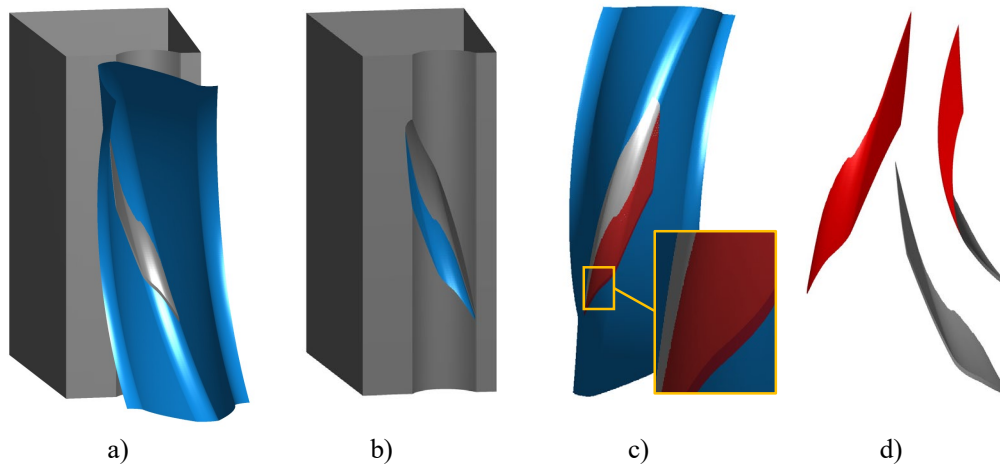


**Figure 2.9.** Second surfaces intersection. a) Penetration of the surface swept by the tool, sunk by  $f_A$  on the gear gap; b) gear gap after second surfaces intersection; c) intersection points on the surface swept by the tool; d) the UCG.

The engagement condition yielded by the second surfaces intersection just shown is repeated identically if the surface swept by the tool is sunk by another amount  $f_A$ . As already said, this situation persists throughout the entire gear width except for the two transitional phases of run-in and run-out tool paths. These two phases, as detailed later, are negligible with good approximation. Therefore, the red coloured points in Figure 2.9c) are the engagement points relative to the considered pass, with which the cutting conditions can be computed.

Additionally, considering the penetration in Figure 2.9a), by combining the portion of the surface swept by the tool that penetrates the gear gap with that of the surface of the gear gap that is penetrated, it is possible to assemble the UCG. Figure 2.9d) shows the UCG from three perspectives, where the portion of the surface swept by the tool is shown in red and that of the gear gap in grey. As mentioned in the state of the art, the UCG is a significant parameter and can be exploited for process analysis.

A clarification should thus be made. The numerical program does not consider the transitional phases to achieve full penetration. This happens for two main reasons. Firstly, it would complicate the routine considerably and would also increase the number of results to be analysed, which is

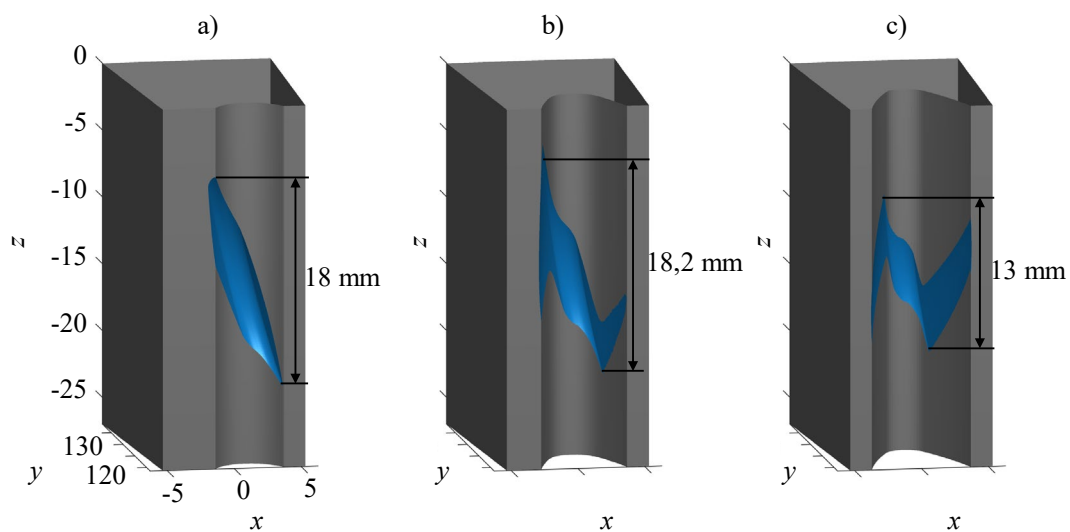


**Figure 2.10.** Trace carved by the tool on the gear gap relative to three different passes of the same process: a) third pass; b) ninth pass; c) fourteenth and last pass.

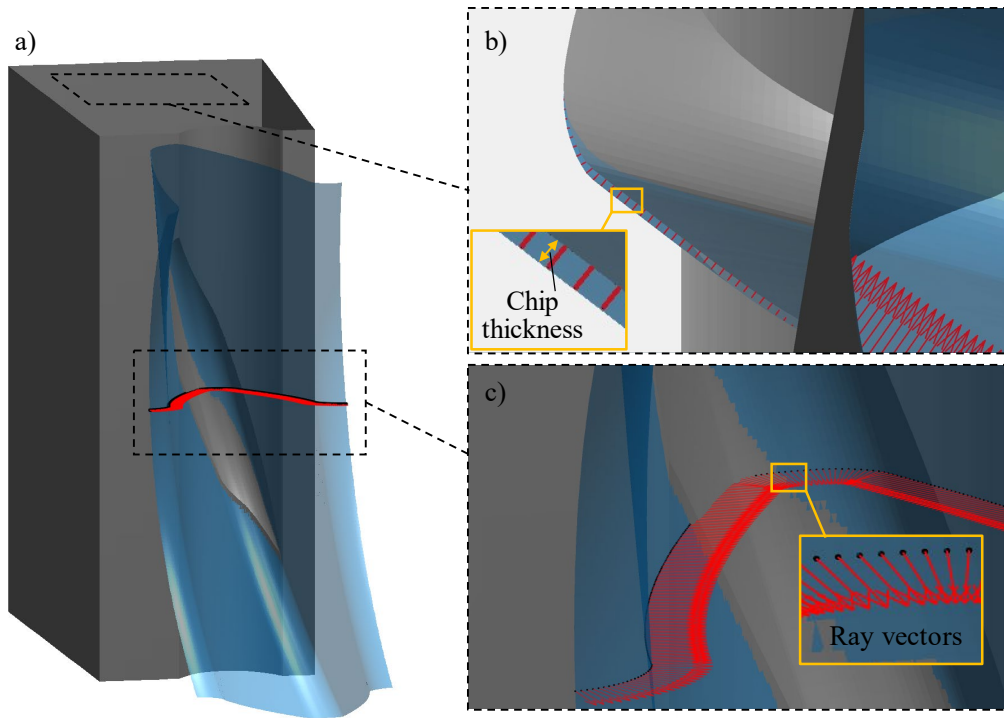


**Figure 2.11.** Calculation of chip thickness through ray intersection. a) Tool profile points and the associated ray vectors, relative to one gear position that make up the surface swept by the tool; b) top view; c) front view.

already high. In fact, the penetration pattern of each pass is different and in one process there may be more than thirty passes. In this regard, Figure 2.10 shows the shape of the trace carved on the gear gap at three different passes of the process. As it can be seen the penetration pattern evolves at each pass. Secondly, for common gear geometries the run-in and run-out path are negligible with respect to the whole gear width within a good approximation. Figure 2.8 d), however, seems to suggest the opposite. This is due to the fact that, as mentioned in the previous paragraph, to reduce the computational cost, only a portion of the real gap is considered in the calculation. Specifically, only the portion of the gap sufficient to contain the traces carved relative to full penetration at all the passes is considered.

The height of the trace in the example analysed in Figure 2.10 never exceeds 18.2 mm and has an average among all the passes of about 15mm. Considering that the real gap in the example has a module of 3.5 mm and a width of 76 mm, the run-in and run-out path account on average for about 20% of the whole height. Therefore, also considering that the penetration of the transitional phase is a sub-case of that relative to full penetration, its neglect does not yield a large approximation. For those cases in which the gear width is comparable to the run-in and run-out paths it is necessary to interpret the simulation results differently. This point will be taken up in Paragraph 2.2.8.5 after the cutting conditions have been introduced.

### 2.2.6.1 Calculation of the working chip thickness and working chip area

Within the presented routine it is also implemented the calculation of the working chip thickness  $h$  and of the working chip area  $A_h$ . The chip thickness is the amount of material that each point in which the profile has been discretized, machines at each position, from the gear gap. Hence, it is related to the local load on the single tool profile points. As it will be seen in the following chapters, is one of the most relevant for the process.

To compute the chip thickness, the function [95] has been adapted for the present routine. It is based on the algorithm proposed in [96], which allows the intersection between ray vectors and the triangles of a mesh to be computed. Specifically, among other things, it is possible to calculate

## 2 Numerical model of centred gear skiving

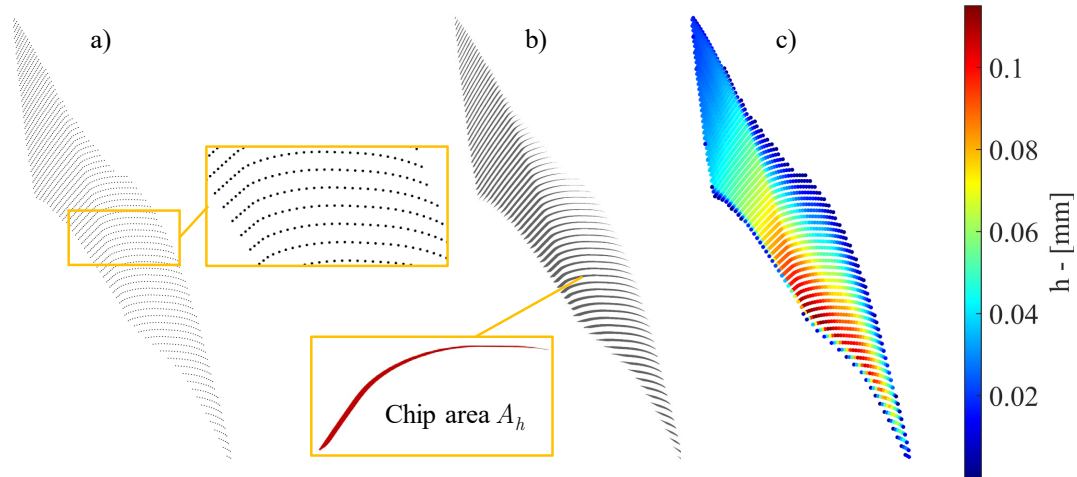


**Figure 2.12.** a) Engagement points relative to one process pass; b) chip sections relative to the several cutting positions of the considered pass and representation of the chip area  $A_h$  of one chip section; c) working chip thickness values of the engagement points.

the penetration length of a ray within the considered mesh. Therefore, for each position of the tool profile on the surface swept by the tool, ray vectors are associated with the tool profile points. These vectors have as direction, the normal to the tool profile at the considered point, lie in the rake plane and point towards the tool centre. Therefore, the measurement of the working chip thickness  $h$  is carried out along the ray vectors thus defined.

Figure 2.11 shows an example of this. In particular, in Figure 2.11 a) the profile points relative to one single cutting position  $\phi_{G0}$  are shown in black. These points belong to the surface swept by the tool sunk by the axial feed, which is shown in transparency, and which penetrates the gear gap already carved by the first surfaces intersection. Figure 2.11b) and c), represent two magnifications of the top and front views, respectively. In particular, Figure 2.11 c) shows the ray vectors associated to each profile point on the rake plane relative to the gear position considered. Some of the profile points, specifically, the engagement points, intersect the left side of the gap. Figure 2.11b) shows the magnification of the left side of the gap from the top view. It can be seen that the engagement points penetrate the gap to different degrees, i.e. each point machines a different chip thickness.

For what concern the working chip area  $A_h$  this is defined as the area of the chip section machined by the tool rake face at each cutting position  $\phi_{G0}$  considered. As shown later, this is also a key parameter as it is linked to the tool load. Referring to the UCG of Figure 2.9, the chip area corresponds the area of the chip sections resulting from the intersections between the UCG and the tool rake face at each cutting position considered.

To have a graphic representation of the parameters just introduced reference could be made to Figure 2.12. Particularly, Figure 2.12a) shows the engagement points relative to the pass examined in this paragraph. Figure 2.12b) shows the chip sections machined at several cutting positions. From the enlargement it can also be seen the working chip area  $A_h$  coloured in red, relative to one chip section. Finally, Figure 2.12c) shows the values of the working chip thicknesses relative to each engagement point.

### 2.2.7 Model of cutting geometry

In this paragraph the model of cutting geometry employed by the numerical program is introduced. It is based on what presented in [18,97] for skiving and shaping respectively. Reference can be made to [59] for a general and more in-depth discussion. The model allows the definition of working angles, that describe how a certain process is performing, namely its cutting

conditions. As already observed in Figure 2.12, in gear skiving the cutting conditions greatly vary both along the pass and at each profile portion.

The model of cutting geometry is based on two basic factors: the cutting edge, and the relative velocity vector associated to it. The former is relative to a single discretised portion of the tool cutting profile, which machines the workpiece. A representation of the geometry of cutting edge is shown in Figure 2.13a), where the tool is represented in light blue and the workpiece in grey.

As mentioned in Paragraph 2.2.3, the tool profile is discretized by a number of points  $N_{pT}$ . Except for the initial and the final point, each profile point is associated to a cutting edge. The exclusion of the first and last points is justified by the fact that the two points belong to the fillet radii and do not participate in cutting. For simplicity in the proposed model, the cutting edges are considered as straight segments. In particular, the cutting edge of a point  $P_n$ , may be computed as the difference between the position vector  $r_{P(n-1)}$  relative to the previous profile point  $P_{n-1}$  and that of  $r_{P(n+1)}$  relative the next profile point  $P_{n+1}$ . Therefore, the unit cutting edge vector  $e_n$  describing the direction of the cutting edge relative to point  $P_n$  may be computed as follows:

$$e_n = \frac{r_{P(n+1)} - r_{P(n-1)}}{\|r_{P(n+1)} - r_{P(n-1)}\|} \quad 2.12$$

For what concern the relative velocity  $v_c$  of point  $P_n$ ,  $v_{cP_n}$ , associated to the cutting edge, this can be computed according to Eq. 2.5. The associated unit tangent vector  $t_n$  is defined with opposite direction to the relative velocity and can be computed using Equation 2.13.

$$t_n = -\frac{v_{cP_n}}{\|v_{cP_n}\|} \quad 2.13$$

Two main cases may be distinguished in the literature. Orthogonal cutting occurs when the unit vector  $t_n$  of relative velocity is orthogonal to the unit cutting edge vector  $e_n$ . Conversely, when there is an angle other than the right angle between the vectors, oblique cutting occurs which is the case portrayed in Figure 2.13a). It is clear, that due to the peculiar relative motion between tool and gear, and considering also the complex profile geometry, gear skiving falls in the case of the oblique cutting processes.

Figure 2.13b) shows the schematic of the oblique cutting model for skiving. From the figure, it can be seen the cutting edge relative to point  $P_n$  along with the defined unit vectors  $e_n$ ,  $t_n$  in blue and red respectively. The figure also shows other vectors and planes, defined in what follows, based on these two initial vectors.

In particular, it is possible to define the cutting plane  $\pi_c$  as the plane passing through the unit vectors  $e_n$  and  $t_n$ . Cutting action occurs on this plane. The unit normal vector  $n_{cn}$ , depicted in green in Figure 2.13b), is normal to the cutting plane and can be computed using as follows:

$$n_{cn} = \frac{e_n \times t_n}{\|e_n \times t_n\|} \quad 2.14$$

Using  $n_{cn}$  it is possible to compute the unit inclination vector  $i_n$ , represented in orange, as:

$$i_n = n_{cn} \times e_n \quad 2.15$$

which in turn may be exploited to compute the working inclination angle  $i$  through Eq. 2.16. The angle  $i$  describes how much the oblique model deviate with respect to the orthogonal model and heavily affects chip evacuation.



## 2 Numerical model of centred gear skiving

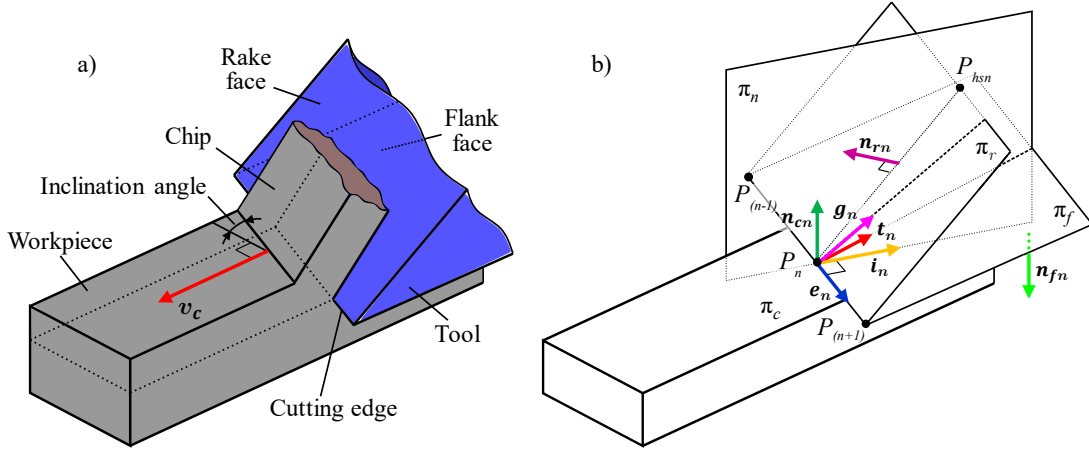


**Figure 2.13.** a) Geometry of the cutting edge in oblique cutting; b) Schematic of the oblique cutting model for skiving.

$$i = \cos^{-1}(\mathbf{i}_n \bullet \mathbf{n}_{cn}) \quad 2.16$$

Then, the normal plane  $\pi_n$  passing through unit vectors  $\mathbf{n}_{cn}$  and  $\mathbf{i}_n$  is defined. In the case of orthogonal cutting, where  $i = 0$ , the normal plane is the sole plane of the model. In many analyses relative to oblique cutting models, it is assumed that the mechanics of cutting in the normal plane is equivalent to that of orthogonal cutting [98]. Therefore, it is common to project vectors and calculate parameters onto  $\pi_n$ , which assumes particular significance. For this reason, Figure 2.14a) reports the section of the oblique cutting model of Figure 2.13b) taken in the normal plane. Figure 2.14a) aids in visualizing the working angles yet to be defined.

Referring to Figure 2.13b), it can be seen the unit rake vector  $\mathbf{g}_n$ , depicted in magenta, lying in the direction defined by the intersection of the rake plane with the normal plane. The rake vector is by definition orthogonal to the cutting edge and can be calculated as follows:

$$\mathbf{g}_n = \mathbf{n}_{rn} \times \mathbf{e}_n \quad 2.17$$

where  $\mathbf{n}_{rn}$ , in violet, is the unit normal vector to the rake plane  $\pi_r$ . The unit rake vector may be exploited to compute the working rake angle  $\gamma_r$  using Eq. 2.18.

$$\gamma_r = \cos^{-1}(\mathbf{i}_n \bullet \mathbf{g}_n) \quad 2.18$$

The sign of  $\gamma_r$  is given by the following convention:

$$(\mathbf{i}_n \bullet \mathbf{g}_n) < 0 \implies \gamma_r < 0$$

$$(\mathbf{i}_n \bullet \mathbf{g}_n) > 0 \implies \gamma_r > 0$$

It should be emphasized that in this work the working rake angle has been defined on the normal plane  $\pi_n$ , as shown in Figure 2.14a). As mentioned, this is a fairly common choice, but it is not the only option. Indeed, it is possible to define the working rake angle on alternative planes, such as the one generated by  $\mathbf{t}_n$  and  $\mathbf{n}_{cn}$  commonly referred to as the velocity plane. There is no definitive right or wrong, but it is crucial to specify the plane where the angles are measured, as their values depend on this choice.

A clarification must now be made. In Paragraph 2.2.3, it has been stated that, for the purpose of process analysis, it is sufficient to compute the tool profile only, and there is no need to compute



the tool flanks. In fact, as shown so far in this paragraph and in the previous one, by exclusively employing the tool profile points and the corresponding relative kinematics, the chip thickness, relative velocity, working inclination angle, and working rake angle have been computed.

However, it might be useful to compute the working clearance angle  $\alpha_c$  as well. This parameter provides a measure of the distance with respect to the interference condition of the tool flanks with the machined gap. It should be noted that for a comprehensive calculation ensuring that the entire tool flank avoids collision with the workpiece, a thorough and rather complex verification is necessary, as explained in Appendix A. This involves checking that the generating gear corresponding to various re-sharpening steps does not collide with the tool flanks at any pass. As mentioned, the routine is implemented externally to the numerical program of Figure 2.1. It is not required during the process analysis, as the tool has already been designed by manufacturers who guarantee its usability.

Hereafter, a calculation is proposed, which is implemented in the numerical program. It allows for the evaluation of the working clearance angle which generates in the proximity of the cutting profile. This calculation can prove to be useful both in the design phase and during analysis to assess the risk of potential rubbing. To perform the calculation however, it is necessary to compute a second cutting profile related to the re-sharpening step  $h_s$ , thus with a reduced tip diameter, according to Eq. 2.7. Such profile is part of the tool flanks and is discretized in the same number of points  $N_{pT}$  as the nominal profile. As explained in the relevant section, this second profile is extruded along the tool axis by the amount  $h_s$  following the tool lead, using Eq. 2.8. This calculation is performed together with the nominal tool profile calculation.

It is thus possible to define the flank direction of a point  $P_n$  of the tool profile by taking the vector difference between corresponding points of the two profiles. Specifically, given two corresponding points  $P_n$  and  $P_{h_s n}$ , relative to the nominal profile and the re-sharpening profile, respectively, considering their relative position vectors  $\mathbf{r}_{P(n)}$  and  $\mathbf{r}_{P_{h_s(n)}}$ , the flank direction is described by the unit vector  $\mathbf{f}_n$ , which may be computed as follows:

$$\mathbf{f}_n = \frac{\mathbf{r}_{P_{h_s(n)}} - \mathbf{r}_{P(n)}}{\|\mathbf{r}_{P_{h_s(n)}} - \mathbf{r}_{P(n)}\|} \quad 2.19$$

For the sake of clarity, the unit vector  $\mathbf{f}_n$  has not been represented in Figure 2.13b). However, on the normal plane of Figure 2.14a) its projection on  $\pi_n$  has been reported in brown.

Thus, the plane  $\pi_f$  tangent to the flank at point  $P_n$  and passing through unit vectors  $\mathbf{f}_n$  and  $\mathbf{e}_n$  can be defined. Referring to Figure 2.13b), it can be seen the unit normal flank vector  $\mathbf{n}_{fn}$  in light green, normal to  $\pi_f$  and which may be computed as:

$$\mathbf{n}_{fn} = \frac{\mathbf{f}_n \times \mathbf{e}_n}{\|\mathbf{f}_n \times \mathbf{e}_n\|} \quad 2.20$$

Notably,  $\mathbf{n}_{fn}$  points outward the tool flanks. Then, it is possible to compute the working clearance angle as:

$$\alpha_c = \frac{\pi}{2} - \cos^{-1}(\mathbf{i}_n \bullet \mathbf{n}_{fn}) \quad 2.21$$

where the sign of  $\alpha_c$  is given by the following convention:

$$\begin{aligned} (\mathbf{i}_n \bullet \mathbf{n}_{fn}) < 0 &\implies \alpha_c < 0 \\ (\mathbf{i}_n \bullet \mathbf{n}_{fn}) > 0 &\implies \alpha_c > 0 \end{aligned}$$

## 2 Numerical model of centred gear skiving

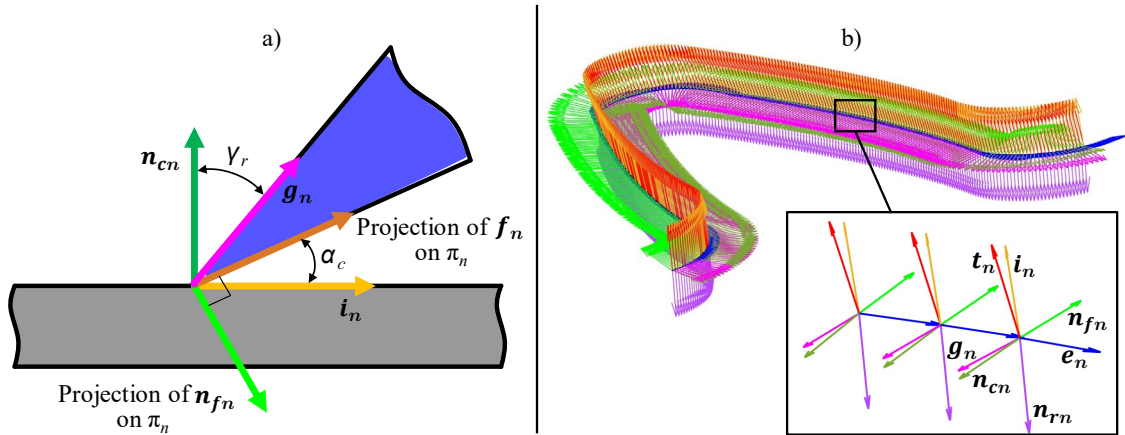


**Figure 2.14.** a) Section of the oblique cutting model on the normal plane  $\pi_n$ ; b) model of cutting geometry implemented in the numerical model.

In [59], it is talked about mandatory relationship, referring to the necessity of having a positive value for the working clearance angle. Indeed, if this is not the case, referring to Figure 2.14a) there would be rubbing between workpiece and tool with the risk of damage both.

As for the working rake angle, it should be emphasized that with the above procedure the clearance angle is defined on the normal plane  $\pi_n$ . Additionally, this calculation considers the surface relative the tool flank locally as a plane. Therefore, it is accurate only when considering a small re-sharpening step  $h_s$  and a high number of profile points  $N_{pT}$ .

Finally, Figure 2.14b) shows a plot from the numerical model, relative to the model of cutting geometry implemented for gear skiving. The same colours of Figure 2.13b) have been used to portray the unit vectors of Figure 2.14b). By looking at the enlarged area, the unit vectors relative to the cutting edges of the discrete tool points, can clearly be seen.

### 2.2.8 Cutting conditions

This paragraph describes the main output of the numerical programme workflow of Figure 2.1. Specifically, the working parameters used which describe the cutting conditions are presented. Additionally, the evolution of the working parameters during the relative motion between tool and gear is analysed. This is done with regard to the different profile portions and also across the various passes of the process.

It should be clarified that in the following discussions and figures, reference is always made to the cutting conditions of a single tooth of the tool. This is because the cutting conditions repeat identically on all teeth. However, to prevent any distortion in perceiving the process, it is essential to keep in mind that, except for the initial passes, there are always multiple teeth engaged with the workpiece in one pass.

As pointed out in the introduction, the working parameters depend on both the set-up parameters and the tool parameters. Therefore, some of the principal relationships, most of which already known in the literature, which connect these sets of parameters, will be also addressed in the following discussion. This lays the foundation for the following chapters.

Particularly in Chapter 3, novel cutting strategies will be introduced to optimize the process. In this context, the tool is already designed, and thus, the tool parameters cannot be modified. The objective is to manipulate the set-up parameters to minimize wear without compromising productivity. Conversely, in Chapter 4, an opposite approach is adopted. Specifically, the innovative concept of the common machining operation is introduced, with the aim of isolating and studying the effect of tool parameters on working parameters.

### 2.2.8.1 Cutting velocity

The cutting velocity is crucial as it significantly influences the tool wear. To machine a workpiece composed of a certain alloy with a tool specifically coated, there exists an optimal range of values of relative velocity within which to balance productivity and tool wear. Consequently, the desired cutting velocity is set as input into the machine tool. Then, based on Eq. 1.4, the rotational speeds of the spindles are calculated accordingly. The higher the relative velocity, the faster the spindles rotate. Considering that the axial feed, governing the various passes, is measured in  $\frac{\text{mm}}{\text{gear rev}}$ , the cutting velocity also determines the feed velocity. Thus, the cutting velocity is relevant not only for tool wear but also for the productivity, as it can be observed by Eq. 2.5.

With the possible exception of the finishing pass, machining passes are typically conducted at a constant cutting speed. The machine tool, therefore, calculates a unique spindles rotation speed for all passes. This results in a slight variation of the relative velocity between successive passes. Specifically, referring to Figure 2.3 and Equation 2.5, for internal gears where the centre distance increases at each pass due to the increasing radial feed, the relative velocity increases accordingly. For external gears instead, the cutting velocity slightly decreases with the passes. However, such variation is usually negligible. This holds while comparing corresponding points lying on the surfaces swept by the tool of each pass. However, as explained below, also the point position where the relative velocity is computed plays a role.

It is crucial to remark that, for the model of cutting geometry, it is significant the direction of the relative velocity vectors, not their magnitude. Therefore, changing the process velocity in the machine tool does not affect the working angles. However, referring to the relative velocity vectors, a consideration must be made. The engagement points for which the relative velocity vectors are computed are located in different positions in space. Consequently, referring to Eq. 2.5, the velocity vector of each point slightly varies in both direction and magnitude. As a result, it is not possible to have a uniform speed for all the engagement points of a pass. This can be explained from the plot in Figure 2.15. Specifically, Figure 2.15a) shows the relative velocity vectors corresponding to the engagement points during the finishing pass of an internal gear. Since the engagement points are located differently, they have different velocity vectors.

Due to the different velocity vector directions and also to the shape of the tool profile, the working angles will vary both across different portions of the profile and throughout the pass, as shown in the next paragraph. Figure 2.15b) portrays the maximum values of the norm of the relative velocity vectors for that pass, plotted over the tool profile points.

A clarification should be made on this type of figure, since it will be used frequently throughout this work. In order to better associate the cutting conditions to the profile portions, the tool profile projection on its rake face has also been reported in the figure. The profile is intended as in operation, hence referring to the scheme of Figure 1.3, with the face pointing downwards. Therefore, the profile portion on the left of the plot is actually the profile right flank (RF), the portion in the middle is the tip (T) and the portion on the right side of the plot relates to the profile left flank (LF).

As it can be noticed, the points at the radii of the tool tip T are those which reach the greater magnitude, which in this case is close to the  $60 \frac{\text{m}}{\text{min}}$  set as input in the machine tool. This is because, referring again to Equation 2.5, for internal gears, the radii at the tool tip of the profile are the points farthest from the gear axis and thus have higher relative velocity. For external gears, the opposite holds, with the tooth tip having a lower cutting speed.

A final remark concerns the possibility of analysing the component of relative velocity parallel to the cutting edge, known as the sliding component. This component does not contribute to the cutting action but is solely responsible for wear. Depending on the tool design, specifically, depending on the relative position of the tool operating pitch radius with respect to the tool profile, a different distribution of the sliding speed may be obtained. This component is not usually critical for skiving of standard workpieces. In such cases the wear affects mostly the tool tip region and

## 2 Numerical model of centred gear skiving

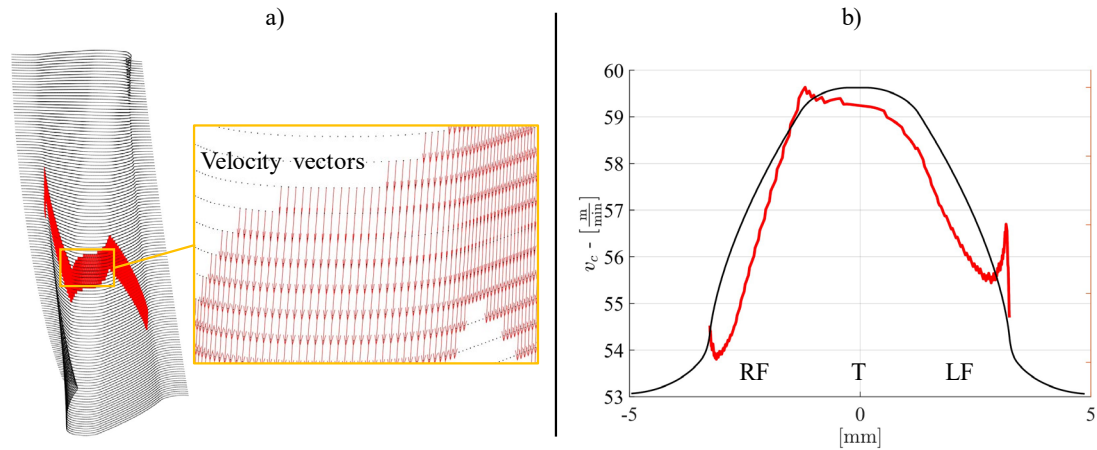


**Figure 2.15.** a) Velocity vectors relative to the engagement points of a finishing pass; b) maximum values of the norm of the relative velocity vectors over the profile points.

is caused by material removal. However, in the case of hard skiving, where pre-machined gears are processed, the sliding speed can play a crucial role.

### 2.2.8.2 Working angles

The working angles defined in Paragraph 2.2.7 are of great relevance in skiving as they influence the overall process. Specifically, the working rake angle  $\gamma_r$  plays a pivotal role. It is well-established from conventional processes, e.g. turning, that  $\gamma_r$  impacts the load on the cutting tool. Notably, positive values of the rake angle are linked to a reduction of the tool load and in good surface finishing, whereas negative values relate to excessive stress on the tool [99]. For what concern the clearance angle  $\alpha_c$ , its primary function is to avoid the collision between the tool flanks and the machined gear gap. Therefore, extreme values of  $\alpha_c$  do not alter cutting conditions, the imperative is to avoid reaching negative values.

Among the peculiarities of the gear skiving process, there is a significant variation of the values assumed by the working angles at the different cutting positions of each pass. A representation of this phenomenon is shown in Figure 2.16a) and b). The figures schematically portray the tool at the initial and at the final cutting positions. In the figures have also been reported the working angles and the unit vectors of Paragraph 2.2.7 employed for their definition. From Figure 2.16a), it can be seen that at the beginning of the pass, both angles  $\gamma_r$  and  $\alpha_c$  are positive. Figure 2.16b) on the other hand, illustrates an increase of the clearance angle at the end of the pass, accompanied by a decrease of the rake angle which becomes negative. This pattern is typical of the skiving process and summarizes two major challenges for skiving tool designers. Specifically, a skiving tool must be interference free at all the passes and should also work with positive values of  $\gamma_r$  so that to avoid overloads. This must hold throughout the tool service life.

In Figure 2.16c) and d) are shown, respectively, the values of the working rake angle and the working clearance angle, relative to a single pass, calculated using the numerical program. Using the model of cutting geometry previously presented, these values were computed for all points on the surface swept by the tool. Now instead, they are filtered relatively to the engagement points determined with the surfaces intersection model. This approach allows the analysis of the cutting conditions uniquely of those profile points which are actively involved in the process. From the Figure 2.16c) and d), it is possible to observe the trend described through Figure 2.16a) and b). At the beginning of the pass the rake angle is positive, as shown in the blue area of Figure 2.16c). Then it decreases until reaching values less than  $-6^\circ$  corresponding to the red region. Figure 2.16d), shows the clearance angle with small positive values at the beginning of the cut, which increase with the advancement of the cut.

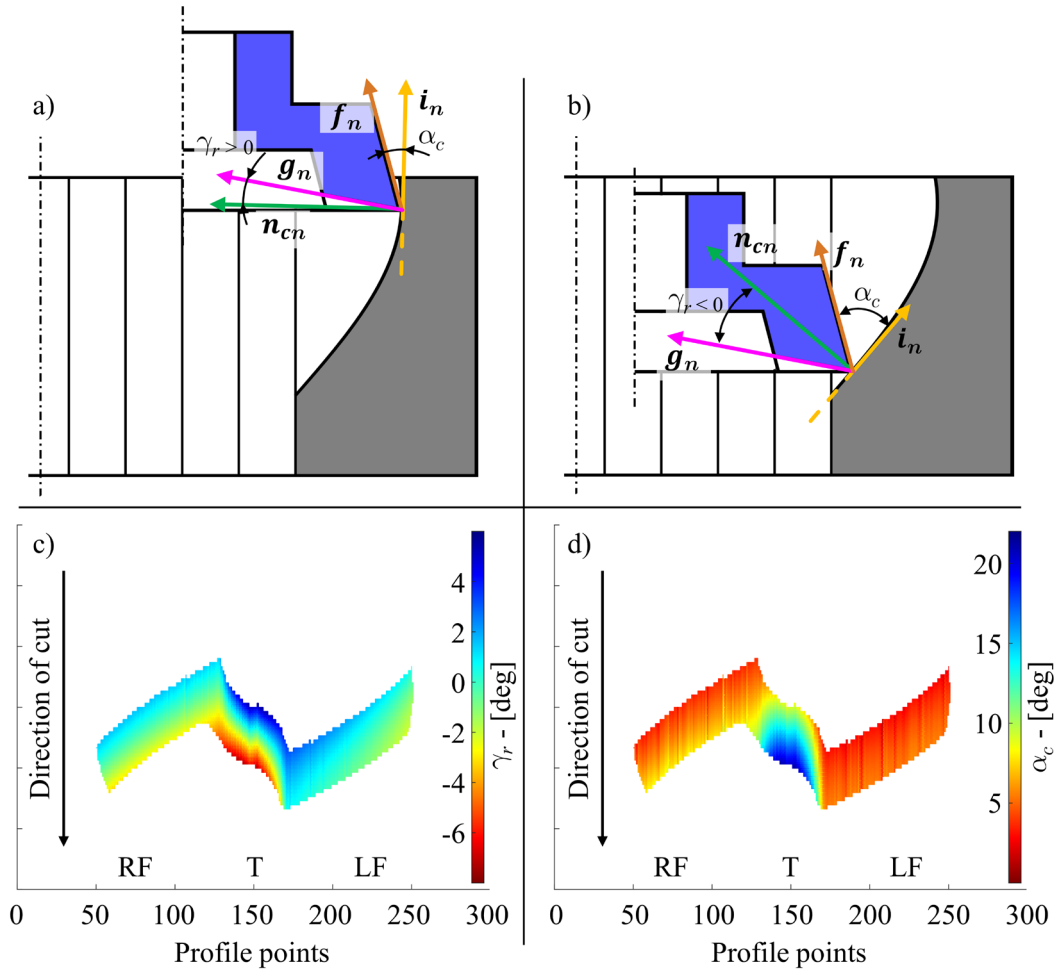


**Figure 2.16.** a) Working angles at the initial cutting position; b) working angles at the final cutting position; c) simulated working rake angle for one pass; d) simulated working clearance angle for one pass.

Furthermore, from Figure 2.16c) and d), it is possible to observe the different values assumed by the engagement points across the portions of the tool profile. Specifically, the rake angle reaches minimum values at the tip (T), at about midpoint of the tool profile points. This is due to the fact that the tip region, having a larger diameter, remains engaged in the gear gap for longer. Indeed, referring to the schematic in Figure 2.16b), it can be seen that the longer the profile remain engaged in the pass, the more  $\gamma_r$  decreases. Regarding the clearance angle, the greatest risk of collision occurs on the right and left flanks RF and LF respectively. However, from Figure 2.16d),  $\alpha_c$  never drops below 2 degrees.

As shown in Paragraph 2.2.4, due to the different set-up parameters employed, both the surfaces swept by the tool and the relative kinematics change with each pass (Figure 2.6). Furthermore, also the shape of the gear gap to be machined changes with each pass, gradually resembling that of the final gap. Consequently, for each pass, there are different engagement points and different direction of the unit vectors, yielding different working angles.

Since it is crucial to avoid negative values of  $\alpha_c$  and also to avoid low values of  $\gamma_r$ , usually the minimum values of these two angles are analysed over each pass. Figures 2.17a) and b) portray the values of  $\gamma_{rMIN}$  and  $\alpha_{cMIN}$ , respectively, relative to the tool profile points of a gear skiving process with 14 passes. Such process will be used as a case study to illustrate also the other key working parameters, not only the working angles.

Referring to Figure 2.17a), it is observed that the value of  $\gamma_{rMIN}$  increases at each pass. Notably, there is a difference of about  $10^\circ$  at the tool tip between the first and last passes. This

phenomenon may be conveniently explained by examining the relative position of the instantaneous screw axis (ISA) for each pass with respect to the machined gap. In Chapter 4, this topic will be further explored. For now, it can be stated that, during the passes, due to the deviation of the centre distance from its nominal value, i.e. that of the last pass, there is an alteration in the relative kinematics. The effect of such alteration directly affects the surface swept by the tool, as it was shown in Figure 2.6. From this figure, it can be noticed that at the first pass, the surface swept by the tool tends to develop more horizontally than in the last pass. This causes to the tool tip portion to remain engaged with the gap for longer at the initial passes. Therefore, referring now to Figure 2.16b), this explains the more negative values of  $\gamma_{rMIN}$  during the firsts passes, which improve with subsequent passes as the centre distance approaches its nominal value.

In relation to the effects of the set-up parameters on  $\gamma_r$ , referring to Figure 2.16b), it is possible to draw the following. When the effect of the set-up parameter is to increase or reduce the penetration with the gap, the working rake angle value correspondingly reduces or increases. It must be clarified here that it is meant that if  $\gamma_r$  improves also its minimum and average values increase. Referring to Figure 1.8, for the same axial feed  $f_A$ , increasing the number of passes and thus reducing the radial infeed  $f_R$  of each pass, decreases the duration of engagement, hence improving the working rake angle. For the same radial feed, reducing the axial feed also decreases the duration of engagement, leading to improvement in the values of  $\gamma_r$ . However, the effect of  $f_A$  is less pronounced than that of  $f_R$  even considering the extent to which these two parameters can be tuned in the process.

For what concern  $\alpha_{cMIN}$ , Figure 2.17b) shows minimal variation across passes. As mentioned earlier, this parameter is crucial during tool design, but once interference with the workpiece is ensured, higher values of working clearance angle do not necessarily enhance the process.

It must be highlighted, that the extent to which the working angles can be varied by tuning the set-up parameters is limited compared to the influence that the tool parameters have on them.

Regarding the effects of the tool constructive parameters ( $\gamma_{r0}, \alpha_{c0}, \tau_{s0}$ ) on the working angles, it can be asserted the following. Referring to Figure 2.16 a) and b), it can be seen that by increasing the values of the tool constructive angles,  $\gamma_{r0}$  and  $\alpha_{c0}$ , cause an increase of the working angles  $\gamma_r$  and  $\alpha_c$ , since the unit vectors  $\mathbf{g}_n$  and  $\mathbf{f}_n$  are changed. However, adopting high values for the constructive angles entails the risk of excessively weakening the tool wedge. Additionally, high values of  $\gamma_{r0}$  may negatively interfere with the practical feasibility of the tool. Therefore, tools with  $\gamma_{r0}$  exceeding  $5^\circ$ - $10^\circ$  are rarely produced. As for  $\alpha_{c0}$ , using high values of the constructive clearance angle would ease the problem of interference avoidance. However, depending on Eq. 2.7, the value of  $\alpha_{c0}$  influences the value of the tool tip diameter with re-sharpening. As explained in Paragraph 2.2.3, a tip diameter variation leads in turn to a change in the tool profile shape (Figure 2.5), which is related to a variation in cutting conditions. Thus, excessive values of  $\alpha_{c0}$  may result in a tool that significantly varies performance throughout its service life, an issue which is addressed in Chapter 3, or may even be hard to manufacture. For this reason, routines such as that in Appendix A, are key to design tools with minimum constructive clearance angle. For what concern the implications of the constructive step angle  $\tau_{s0}$  on the working angles, it has been shown that by setting it at about the value of the tool nominal helix angle  $\beta_T$ , may help in balancing the cutting conditions between the profile flanks [6]. In fact, the tool of the process shown in Figure 2.17 was designed with  $\tau_{s0} = \beta_T$ . As it can be seen from the figure, the working angle values on the profile flanks are evenly balanced.

The effect of the tool kinematic parameters ( $z_T, \beta_T, d_{tT}$ ) on the working angles can be summarized as follows. Based on Eq. 1.1,  $z_T$  and  $\beta_T$  correspond to  $k$  and  $\Sigma$ , respectively. In [7], it was documented that an increase in  $z_T$  results in an improvement of  $\gamma_{rMIN}$  which is the case. However, in the same study it was also reported a reduction of  $\gamma_{rMIN}$  corresponding to a reduction of  $\Sigma$ , which is not accurate. In fact, previously, in [36], it was shown that by using the

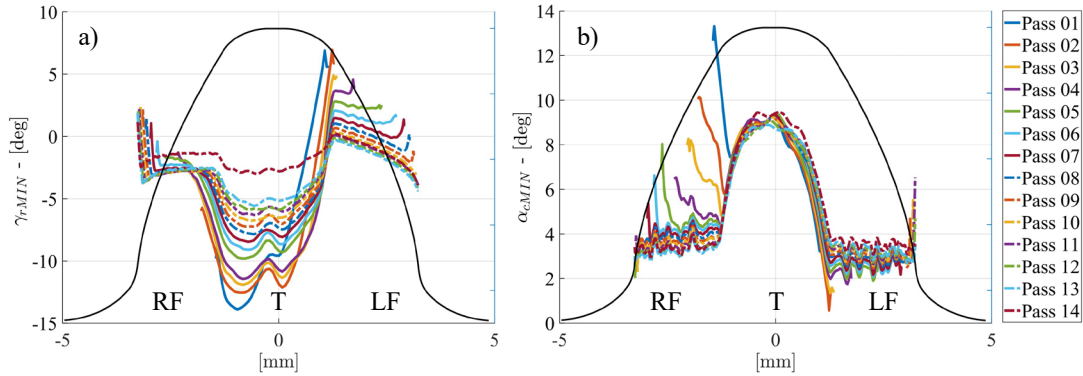


**Figure 2.17.** Minimum working angles for a skiving process of 14 passes: a) minimum working rake angle; b) minimum working clearance angle.

same axial and radial feed, both increasing  $k$  and  $\Sigma$  leads to an increase in  $\gamma_{rMIN}$ . An example of this, computed with the numerical program is shown in Figure 2.18a). This illustrates a comparison of the working rake angle values of the last pass relative to two different tools designed to produce the same gear. The two tools operate both with  $f_R = 0.3$  mm and  $f_A = 0.4 \frac{\text{mm}}{\text{gear rev}}$ . They also have the same number of teeth  $z_T = 37$  but have different values of  $\beta_T$ . Therefore, tool 1 operates with  $\Sigma_1 = 15^\circ$ , whereas tool 2 with  $\Sigma_2 = 25^\circ$ . As a result, the tool profiles are also different. As shown in Figure 2.18a), the tool 2, with the higher  $\Sigma$ , whose profile and rake values are depicted in dashed line, operates with higher values of  $\gamma_{rMIN}$ .

However, in [36], it was stated that the larger the value of the tool tip diameter  $d_{tT}$ , the better  $\gamma_{rMIN}$ . This is not entirely accurate. In fact, as will be shown in Chapter 4, it is helpful to consider the tool operating pitch radius to choose a suitable  $d_{tT}$  for the specific application. In Figure 2.18b) it is reported a second example computed with the numerical program. The figure shows the comparison between the values assumed by  $\gamma_{rMIN}$  by two different tools, designed to machine the same gear which employ the same set-up parameters. Specifically, for the pass shown the two tools operate with  $f_R = 0.8$  mm and  $f_A = 0.3 \frac{\text{mm}}{\text{gear rev}}$ . Additionally, the two tools have the same number of teeth  $z_T = 31$  and the same helix angle  $\beta_T = 20^\circ$  but have been designed with different diameters  $d_{tT1} = 126$  mm and  $d_{tT2} = 123$  mm respectively. As it can be seen, contrary to the reported findings, the tool with the smaller tip diameter provides better values of  $\gamma_{rMIN}$ , which happens especially in the first passes.

From what reported it is evident that there is still some confusion in the literature regarding the impact of tool design parameters on working parameters. In Chapter 4, a new approach is introduced, based on the instantaneous kinematics of the process. The approach aims to explore the effects of tool kinematic parameters on working parameters. In particular, it will be argued that, during the tool design phase, it is beneficial to optimize tool kinematic parameters. This enables the generation of relative kinematics that inherently provides favourable cutting conditions, which may be beneficial for tool design. Indeed, it is not rare in practice to observe tools with sub optimal kinematic parameters, along with large tool constructive angles, to make up for the poor relative kinematics.

It may be noticed that in this paragraph no discussion was made on the inclination angle. This parameter has a significant impact on the direction of chip evacuation and may be used to compute it [100]. However, more sophisticated models are needed for detailed considerations regarding material flow on the rake face.

Eventually it should be remarked, that for each working angle, not only the minimum values but also the average, weighted average, and maximum values are calculated. This approach allows for a detailed analysis of the machining process.



## 2 Numerical model of centred gear skiving

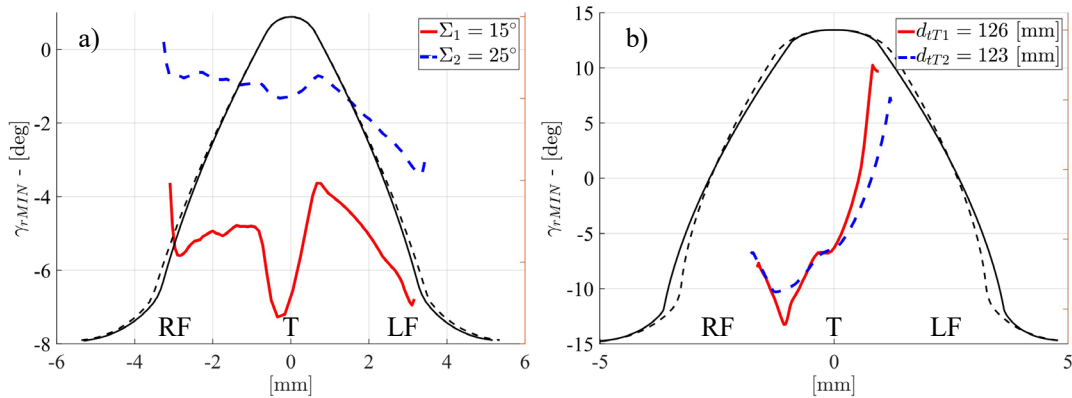


**Figure 2.18.** Simulation results of two case studies which show that: a) tools that operates at higher cross axis angle, provide better values of  $\gamma_{rMIN}$ ; b) tools with smaller tip diameters, provide better values of  $\gamma_{rMIN}$ .

### 2.2.8.3 Working chip thickness

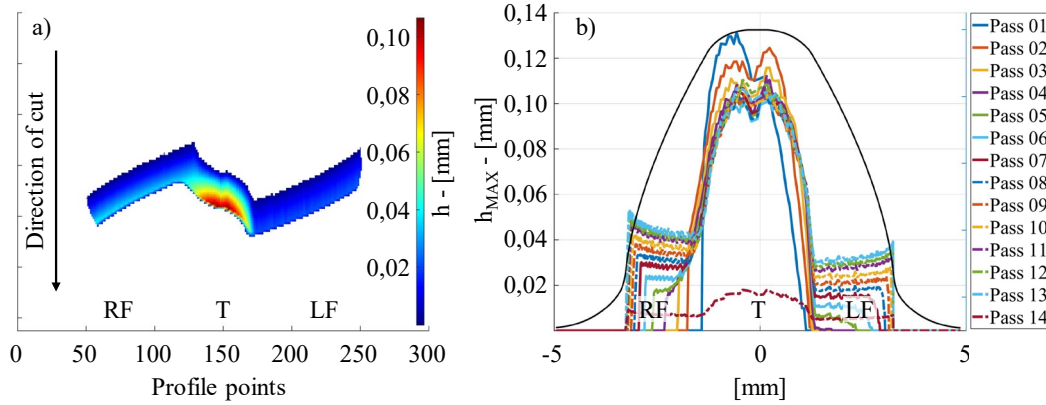
The working chip thickness defined in Paragraph 2.2.6.1, is a main parameter for the skiving process since it is strictly related to the load experienced by the tool. For each gear alloy there exists a limited range of values of chip thickness within which to operate to balance tool wear and productivity, depending also on the cutting strategy.

Figure 2.19a) illustrates the working chip thickness values  $h$  relative to one skiving pass, calculated by the numerical program. As observed, the highest values of chip thickness are worked by the tool tip T. Additionally, the chip thickness values evolve with the cutting positions. To explain this, reference can be made to any of the 4 diagrams of Figure 1.8, detailed in Paragraph 1.2.3. As shown in the diagrams, during a pass, the chip thickness increases until reaching its maximum value  $h_{MAX}$  towards the end of the pass. Then it follows an abrupt reduction of  $h$  until the final cutting positions which ends the pass. The same behaviour may be observed in the simulation results of Figure 2.19a). Therefore, in order to avoid excessive loads on the tool, the maximum value of chip thickness at each pass is typically the chip parameter most analysed.

For the same setup parameters and tool design, the chip thickness increases with the axial feed. Typical values for  $h_{MAX}$  used for skiving common gear alloys, range between [0.1 - 0.3] mm. Usually, to prevent high loads on the tool profile, in the machine tool a limiting value of  $h_{MAX}$  is set for the roughing passes, which determine the axial feed. Then,  $h_{MAX}$  is reduced in the finishing passes to achieve better surface roughness. The simulation results relative to the maximum chip thickness for the process of 14 passes of Figure 2.17, are presented in Figure 2.18b). In this case, the nominal value of  $h_{MAX}$  set on the machine tool for the roughing passes 1-13, was  $h_{MAX} = 0.12$  mm. However, in the final pass, it was set as input  $f_A = 0.1 \frac{\text{mm}}{\text{gear rev}}$ , due to surface finishing requirements. Such axial feed corresponds to  $h_{MAX} = 0.02$  mm for the finishing pass. From the figure, it can be seen that  $h_{MAX}$  remains approximately constant across the roughing passes. To achieve this, the machine operates with different values of  $f_A$  and  $f_R$  for each pass.

Regarding the influences of tool kinematic parameters ( $z_T, \beta_T, d_{tT}$ ) on chip thickness, they have been discussed in Paragraph 1.2.3 with the aid of Figure 1.8. In brief, for the same  $f_A$  and  $f_R$ , the larger the gear ratio  $k$  achieved by the tool, the lower the value of  $h_{MAX}$ . A similar behaviour is observed for tools that achieve a greater cross-axis angle  $\Sigma$ . This has a significant impact on process productivity and will be considered in the tool design method proposed in Chapter 4. For what concern the implications of the tool tip diameter  $d_{tT}$  on the chip thickness a





**Figure 2.19.** a) Simulated chip thickness values for one skiving pass; b) Values of maximum chip thickness  $h_{MAX}$  for a skiving process of 14 passes.

clarification must be made. Indeed, Figure 1.8a) is used to represent the effect of a bigger tool teeth number  $z_T$  on the machined chip thickness, where to a bigger  $z_T$  corresponds a larger  $d_{tT}$ . However, the figure may be misleading. Indeed, from Figure 1.8a) it may appear that a larger tip diameter generally corresponds to lower chip thickness, which is not accurate. For the same values of tool teeth number and helix angle  $z_T, \beta_T$ , increasing the tool tip diameter of a tool, would not reduce the machined chip thickness. On the contrary, it would increase it. This implication cannot be seen through the schemes of Figure 1.8 which must be therefore used only to show the implications of  $z_T$  and  $\beta_T$  on the chip thickness.

In addition to the value of  $h_{MAX}$ , the numerical program also computes the mean and the minimum chip thickness values,  $h_{MEAN}$  and  $h_{MIN}$ , respectively. Indeed, it is key to ensure that  $h_{MIN}$  does not reach excessively low values, as there is a risk of material forming instead of machining.

#### 2.2.8.4 Working chip area and normalised working chip area

The working chip area  $A_h$  defined in Paragraph 2.2.6.1, similarly to the working chip thickness  $h$  is linked to the tool load [21,101,102]. Despite being related to each other,  $A_h$  and  $h$  represent two rather different entities. Specifically, while the working chip thickness is the amount of material machined by a single tool profile point at one cutting position, the working chip area is relative to all the engagement points that in one cutting position machine a certain chip section, as shown in Figure 2.12b). During a single pass, the chip thickness describes the penetration of an individual profile point, whereas  $A_h$  describes the penetration of an entire tool tooth.

The working chip area is a relevant parameter as it enables the assessment of implications on tool load, arising from strategies with a different number of passes. For instance, considering two skiving strategies with the same nominal maximum chip thickness, e.g.  $h_{MAX} = 0.15$  mm, one carried out in five passes and the other in ten passes, the first strategy exerts a higher flexional load on the cutting tool. By solely observing the values of the working chip thickness however, this phenomenon is not captured. Therefore, while the chip thickness is linked to the measure of the local stress experienced by each profile points during one pass, the working chip area is related to the flexional load experienced by the whole rake face during the pass, which in turn is linked to the whole tool dynamic load.

In Figure 2.20a), are reported the values of the working chip area over the cutting positions relative to the 14 passes of the skiving process shown in the previous figures. As evident, except for the finishing pass which is carried out at a different  $h_{MAX}$ , the value of the chip area tends to increase with successive passes. This happens because, as the nominal centre distance is approached, the portion of the tool profile engaging with the workpiece becomes bigger.

## 2 Numerical model of centred gear skiving

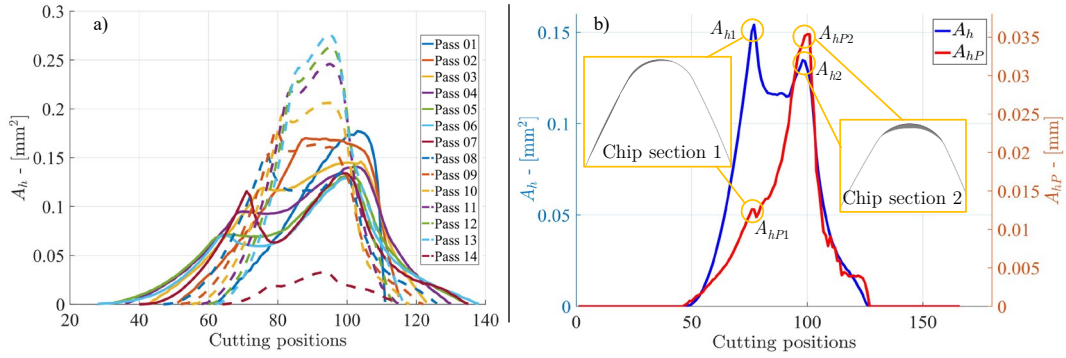


**Figure 2.20.** a) values of the working chip area  $A_h$  for a skiving process of 14 passes; b) comparison between values of working chip area  $A_h$  and normalised working chip area  $A_{hP}$ , for one pass.

Such an increase of  $A_h$  with successive passes, occurs despite the depicted process adopts a digressive infeed strategy, involving progressively reduced values of  $f_R$  from the first to the last pass. This aids the understanding of the logic of the digressive infeed strategy and its advantages over the linear one. In fact, employing a linear infeed strategy would result in even larger chip sections areas during the final passes compared to those shown in Figure 2.20a), leading to high dynamic loads on the tool which may cause premature wear.

A clarification must now be made. When reference is made to the tool load, it is crucial to consider that the chip area just shown, pertains to the engagement of a single tool tooth with the workpiece. If the aim is to estimate the actual tool load at each pass, it is necessary to add up the values of  $A_h$  relative to the several number of tool teeth in engagement, at different phases, with the gear. However, this is not the primary objective in this context. What is sought, is a parameter that qualitatively describes the load experienced by an individual tooth of the tool during each pass for the purpose of developing strategies to reduce its wear.

In this context, Figure 2.20b) shows with a blue line the values of the working chip area for a single pass of another skiving process. Two chip sections corresponding to different cutting positions are also shown, whose working chip areas are denoted as  $A_{h1}$  and  $A_{h2}$ , respectively. From the graph,  $A_{h1}$  results slightly bigger than  $A_{h2}$ . In addition, the two chip sections are very different in shape. Specifically, chip section 1 relative to  $A_{h1}$  is spread through a bigger tool profile portion, whose points machine small chip thicknesses. On the contrary, chip section 2 relative to  $A_{h2}$  is condensed at the tool tip whose points machine bigger chip thicknesses.

This trend of the chip section may be observed both for a single pass, as shown in the figure, and also by comparing chip sections from the initial passes to those of the later passes when a digressive infeed strategy is employed. Clearly, the two different types of chip sections load the tool tooth differently. In particular, chip section 2 exerts greater flexional load on the tool tooth, since a larger amount of material is removed from less profile points at the tip. However, as shown in Figure 2.20b) the working chip area  $A_h$  is not capable of capturing this phenomenon.

Hence, a shape factor of the chip section should also be considered. Therefore, in the context of this work, another working parameter is used, the normalised working chip area  $A_{hP}$ , which is defined as follows:

$$A_{hP} = \frac{A_h}{p_h} \quad 2.22$$

where  $p_h$  is the value of the perimeter relative to the considered chip section. The values of the normalised chip area  $A_{hP}$  have been reported in Figure 2.20b) with a red line. As it can be seen from the graph, the value of the normalised chip area of section 1,  $A_{hP1}$ , results far smaller than that of section 2,  $A_{hP2}$ .

The working normalised chip area  $A_{hP}$  is measured in [mm] and may be associated to the amount of load per unit of tool profile length. The trend of  $A_{hP}$  more closely describe, on a qualitative level, the flexional load caused by chip removal on the whole tool tooth during the pass. Indeed, similarly to the working chip area  $A_h$ , and contrarily to the chip thickness  $h$ ,  $A_{hP}$  enables the assessment of implications on the flexional load applied on the tool teeth, arising from strategies with a different number of passes. Also  $A_{hP}$ , accounts for the differences in load caused by chip sections with different shape but similar area.

Therefore, when the cutting conditions are analysed, it is recommended to check both  $h_{MAX}$  and  $A_{hP}$ . The former along with values of  $\gamma_{rMIN}$  help in the understanding of how the individual points on the tool profile are stressed. However, once  $h_{MAX}$  and  $\gamma_{rMIN}$  are set within acceptable values for the material being machined by the tool at hand, it is necessary to also check how the cutting strategy employed affects  $A_{hP}$ . In this way, cutting passes that excessively load the tool teeth are avoided. As it will be shown in the next chapter, the parameter  $A_{hP}$  proves to be highly effective in helping to devise new cutting strategies.

Regarding the implications of the set-up parameters on  $A_h$  and  $A_{hP}$ , they have not yet been analysed in the literature. In the context of Chapter 3 the effect of the set-up parameters on  $A_{hP}$  will be shown and exploited using the proposed numerical program in order to devise novel cutting strategies aimed at reducing tool wear.

#### 2.2.8.5 Cumulative machined cutting length

For what concern the definition of the cumulative machined cutting length, a distinction must here be made. There is indeed the cumulative machined cutting length during a single penetration of a pass  $l_{cSING}$  and the cumulative machined total cutting length  $l_{cTOT}$ .

Specifically,  $l_{cSING}$  is defined as the length of the distance covered by one engagement point during its penetration on the gear gap in a single pass. A representation of  $l_{cSING}$  can be seen in Figure 2.21a). The figure illustrates the engagement points that make up the UCG for a single pass. By measuring the distance covered by each engagement points, it is possible to obtain the value of  $l_{cSING}$  for each point in which the tool profile is discretized. Therefore, for one pass, each point on the profile, will machine a different  $l_{cSING}$ . An example can be seen in Figure 2.21b), which shows the value of  $l_{cSING}$  for the engagement points of Figure 2.21a).

The  $l_{cSING}$  is a relevant parameter for the skiving process as it is a complementary measure to  $A_h$  of the UCG. Specifically, the higher the  $l_{cSING}$ , the longer the chip to be removed, which results in a longer contact time between the cutting edge and the gear material, leading to increased heating in the cutting zone. Another reason that makes  $l_{cSING}$  relevant for the process is its role in determining  $l_{cTOT}$ , which will be introduced shortly, and which is closely related to tool wear.

From Figure 2.21b), it may be observed a tendency of  $l_{cSING}$  to accumulate at the tool tip. This occurs especially in the early passes, both because the tip is the only portion engaging with the workpiece, due to the reduced radial feed, and also because, as explained for working angles, the tip remains engaged longer compared to the profile flanks. Additionally, since the UCG varies at each pass,  $l_{cSING}$  also changes with the passes. In Figure 2.22a), the values of  $l_{cSING}$  for the 14-pass process of Figures 2.17 and 2.19 are reported. A progressive decrease in  $l_{cSING}$  across the passes can be observed. This is due to the evolution of the geometry of the engagement and, consequently, to the UCG shape.

Regarding the implications of set-up parameters on  $l_{cSING}$ , the latter is, by definition, linked to the length of the engagement between the tool and the workpiece. Therefore, the discussions made for the working angles apply here as well. Increasing the radial feed and the axial feed increases the penetration and consequently increases  $l_{cSING}$ .

## 2 Numerical model of centred gear skiving

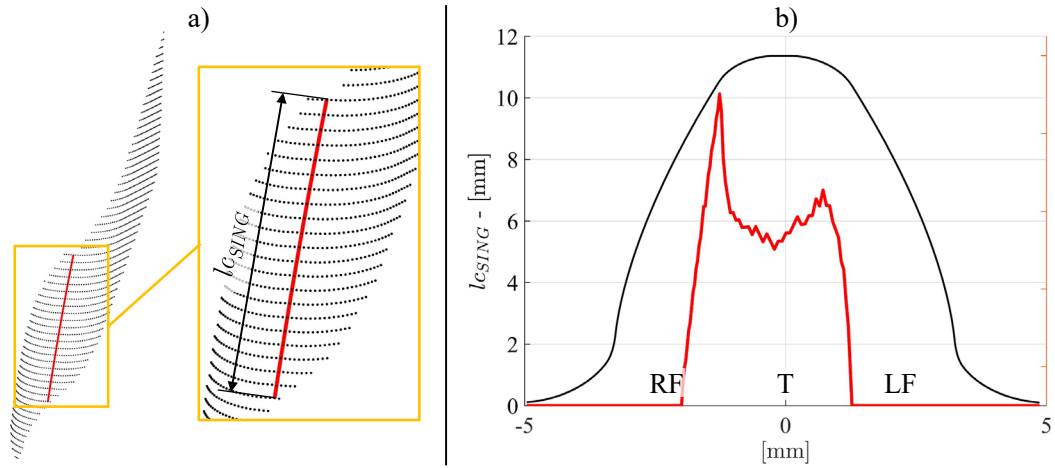


**Figure 2.21.** a) Representation of how  $l_{cSING}$  is defined; b) different values of  $l_{cSING}$  assumed by the profile points during one pass.

A clarification must be made regarding the dependence of  $l_{cSING}$  on the tool kinematic parameters ( $z_T, \beta_T, d_{tT}$ ). In the literature there is a lack of studies investigating how the tool kinematic parameters affects the geometry of the engagement of the skiving passes. Furthermore, in [5], it was highlighted a tendency in papers in analysing the implications of one parameter at a time on working parameters. Generally, when considering different tool designs, by varying the tool teeth number and the tool helix angle, in order to produce higher  $k$  and  $\Sigma$ , respectively, results in a higher engagement length and hence also a higher  $l_{cSING}$ .

By increasing the parameters  $z_T$  and  $\beta_T$ , the tool tip diameter also increases. Moreover, as will be discussed in Chapter 4 on tool design, the tip diameter of skiving tools can be chosen within a certain range. Such range has an additional influence on the length of engagement. Specifically, with for the same  $z_T$  and  $\beta_T$ , a larger  $d_{tT}$  increases the engagement length. For this reason, one may be led to believe that, in general, the engagement is proportional to the tool tip diameter.

However, this may be misleading. In fact, for a given criterion for the selection of  $d_{tT}$ , both  $z_T$  and  $\beta_T$  simultaneously contribute to the value of the tool tip diameter. As mentioned earlier, each one has its own effect on  $l_{cSING}$ . Therefore, it may happen that larger diameters correspond to a shorter engagement length and thus a reduced  $l_{cSING}$ . In Figure 2.22b), it is shown a comparative example computed with the numerical program. The figure shows the values of  $l_{cSING}$  machined by two different tools which operate with the same radial and axial feed, specifically  $f_A = 0.4 \frac{\text{mm}}{\text{gear rev}}$  and  $f_R = 0.3 \text{ mm}$ . The two tools have different number of teeth,  $z_{T1} = 50$  and  $z_{T2} = 57$ , and also different helix angle  $\beta_{T1} = 20^\circ$  and  $\beta_{T2} = 10^\circ$ , which results in different cross axis angles,  $\Sigma_1 = 20^\circ$  and  $\Sigma_2 = 10^\circ$ . Both tools have the tip diameter chosen with the same criterion, specifically,  $d_{tT}$  is set equal to the tool operating pitch diameter, which gives  $d_{tT1} = 184.6 \text{ mm}$  and  $d_{tT2} = 200.8 \text{ mm}$ . In Figure 2.22b), the profile relative to tool 1 is depicted in continuous black line, whereas that of tool 2, with dashed black line. From the figure, it is shown that, contrary to what one might be led to believe, tool 2 with larger tip diameter, machines smaller values of  $l_{cSING}$ , depicted in dashed blue line, compared to tool 1  $l_{cSING}$  values depicted in continuous red line.

Therefore, when analysing the geometry of engagement between tool and gear, it is advisable to analyse the effect of multiple parameters simultaneously. On this regard, in Chapter 4, a novel approach is outlined to describe the simultaneous effect of tool kinematic parameters on working parameters through a model deriving from the instantaneous process kinematics.

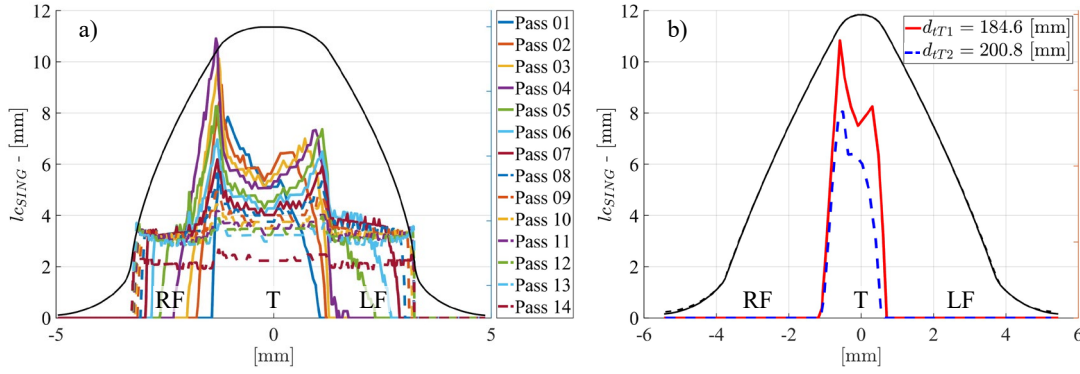


**Figure 2.22.** a) Simulated values of  $l_{cSING}$  for a skiving process of 14 passes; b) Comparative example to demonstrate that tools with bigger tip diameter may machine smaller  $l_{cSING}$ .

Moving on to the definition of the cumulative machined total cutting length  $l_{cTOT}$ , it is necessary to first establish the number of cuts  $NoC$ , which for the  $i$ -th pass may be computed as follows:

$$NoC(i) = \frac{b_G}{f_A(i) \cdot k} \quad 2.23$$

where it should be recalled that  $b_G$  is the gear width. The parameter  $NoC(i)$  represents the number of times that, in the considered  $i$ -th pass, each individual tooth of the tool penetrates the workpiece. It should be noted that if the operation is carried out, as often happens, at a constant  $h_{MAX}$  during the roughing passes,  $f_A$  varies with each pass, and therefore  $NoC$  also varies. An example of such variation is illustrated in Figure 2.22. The figure pertains the case study of the 14-pass skiving process shown so far in Figures 2.17, 2.19b) and 2.22a). In Figure 2.23a), the values of  $f_A$  for each pass are shown. It can be observed that after a slight decrease,  $f_A$  increases with the passes and then decreases in the final one, since it is set at  $f_A = 0.1 \frac{\text{mm}}{\text{gear rev}}$  for finishing. This leads to an opposite trend of  $NoC$  at each pass, as shown in Figure 2.23b).

Hence, given the value of  $l_{cSING}(i)$  relative to the  $i$ -th pass, it is possible to define the cumulative machined total cutting length  $l_{cTOT}$  for a process of  $NoP$  passes as:

$$l_{cTOT} = \sum_{i=1}^{NoP} l_{cSING}(i) \cdot NoC(i) \quad 2.24$$

The value of  $l_{cTOT}$  plays a crucial role in the process. It represents the total distance machined by the profile portions of the tool throughout all the passes to produce a single workpiece. It is therefore a parameter intimately related to tool wear. It is worth emphasizing that, unlike the working normalized chip area  $A_{hp}$ , which is a parameter to be analysed individually, over a single pass,  $l_{cTOT}$  is a parameter describing the whole process. It considers all the cutting positions of all the process pass through the summation of  $NoC$  for each pass.

Additionally, it should be remarked that  $l_{cTOT}$  must not be confused with the well-known machined length  $ML$ , calculated as follows:

$$ML = NoP \cdot b_G \cdot NoW \quad 2.25$$

where  $NoW$  is the number of machined workpieces. The parameter  $ML$  is widely spread as it is derived from traditional machining processes like turning, which are often characterised by

## 2 Numerical model of centred gear skiving

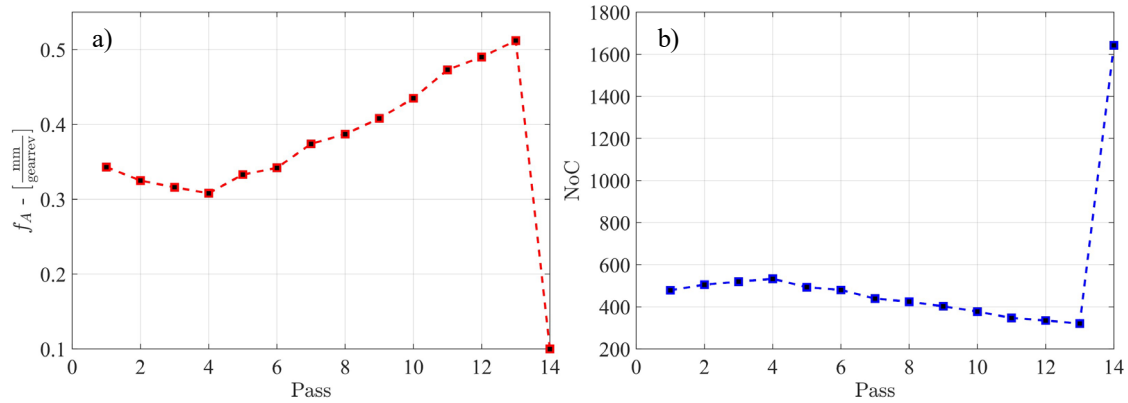


**Figure 2.23.** a) Variation of the axial feed among the passes of a skiving process which operates with constant  $h_{MAX}$  in the roughing passes and fixed axial feed in the finishing; b) corresponding variation of the  $NoC$  among the passes.

constant chip thickness and continuous cutting. In such cases,  $ML$  can have a similar meaning as  $l_{cTOT}$  for a single workpiece.

However, in gear skiving, the two parameters have very different meanings and values. The machined length  $ML$  does not require simulation for calculation, whereas  $l_{cTOT}$  cannot be computed otherwise. As an example of the difference between the two parameters, it is sufficient to consider an example of set-up parameter variation for the skiving process. If either the  $NoP$  is increased or the axial feed is varied,  $ML$  remains constant, whereas  $l_{cTOT}$ , as will be shown in the next chapter, varies considerably. Due to its ease of calculation,  $ML$  is also computed by the skiving machine tool to provide an indication of the amount a tool has been used. However, for a detailed analysis like that conducted with simulation,  $l_{cTOT}$  proves to be more precise.

Considering the way  $l_{cTOT}$  is computed, its trend over the tool profile points, may resemble that of  $l_{cSING}$ . In particular, Figure 2.24a) shows the simulated values for the products  $l_{cSING}(i) \cdot NoC(i)$  for each pass, while Figure 2.24b) shows their sum, i.e.,  $l_{cTOT}$ . From Figure 2.24a), a similar trend to Figure 2.22a) is observed for all the roughing passes except the last finishing pass. The reason is linked to the values of the  $NoC$  shown in Figure 2.23b). In the roughing passes, the  $NoC$  does not vary significantly among passes, maintaining the trend of Figure 2.24a) relatively unchanged compared to Figure 2.22a). In the last pass, however, due to the low value of the axial feed, the value of  $NoC$  surges. Despite the values of  $l_{cSING}$  being the smallest in the final pass, they are enlarged by  $NoC$ . As a result, the finishing pass result in being one of the most relevant passes in terms of  $l_{cTOT}$ , comparable to the initial ones. From this it may be deduced, that it is not recommended to use too low values of the axial feed for finishing, unless strictly necessary.

Regarding the implications of the set-up parameters and the tool parameters on  $l_{cTOT}$ , there is a lack of publications on this matter. Such implications appear to be quite complex. For instance, considering the effect of the axial feed on  $l_{cTOT}$ , while keeping unchanged the other parameters, an increase of  $f_A$  leads to an increase in  $l_{cSING}$  and a reduction of  $NoC$ . Hence the behaviour of  $l_{cTOT}$  remains ambiguous. Moreover, the way such variations occur differs for the various passes. The implications of the tool design parameters on  $l_{cTOT}$  are even more complex. In the next chapter, the effect of the set-up parameters on  $l_{cTOT}$  is assessed with the aid of the proposed numerical program. Based on the derived implications, new cutting strategies aimed at reducing tool wear, while keeping the cycle time unchanged are developed.

From the above discussion on working parameters, it has been observed that the tool tip is the tool profile portion that operates simultaneously with the lowest values of  $\gamma_{rMIN}$ , with the higher values of chip thickness, and also machines to the majority of  $l_{cTOT}$ . These are the reasons which explain one of the main peculiarities of gear skiving, namely the tip is the tool profile portion



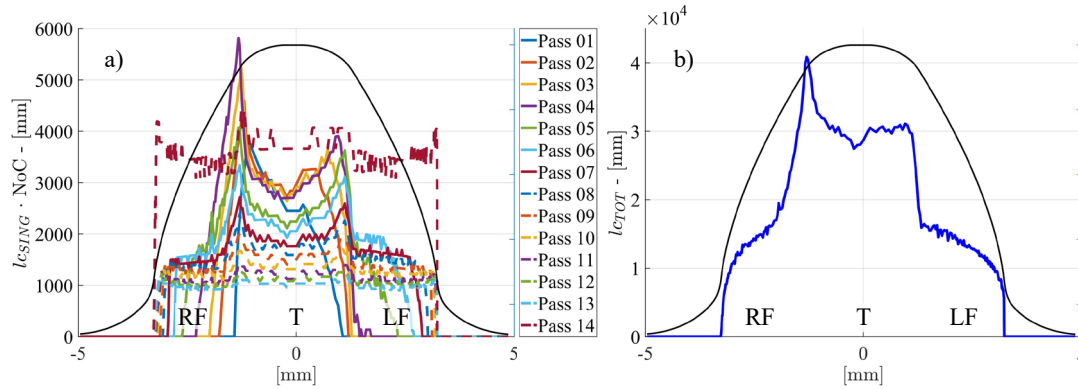


**Figure 2.24.** a) Simulated values of  $l_{c_{SING}}(i) \cdot NoC(i)$  for a skiving process of 14 passes; b) corresponding simulated values of  $l_{c_{TOT}}$ .

most prone to wear. In gear skiving of not pre-machined gears, the tip is usually the portion which determines tool replacement.

Finally, in Paragraph 2.2.6, it was discussed that the numerical program does not account for the transitional phase of the run-in and run-out paths of the tool (Figure 2.8d) as they are usually negligible compared to the gear width. For workpieces with particularly low gear width  $b_G$ , it is possible to proceed as follows. The working parameters are computed as in a standard case. The value of  $l_{c_{TOT}}$  is not correct in absolute terms. Therefore, it is not possible to compare it with values relating to processes of other workpieces. However, in relative terms,  $l_{c_{TOT}}$  maintains its significance. In fact, for workpieces with low  $b_G$ , if the simulated values of  $l_{c_{TOT}}$  are reduced through novel cutting strategies, or a novel tool design, the same wear reduction benefits are achieved as for a normal-sized gear. Regarding the other working parameters, it is advisable to consider maximum and minimum values since the engagement pattern is mostly incomplete and average values may be misleading.

## 2.3 Validation

A basic first check that may be done in order to verify the model, is to move the calculated tool profile according to the proposed relative kinematics model, and to compare the generated gear gap with the desired one. An example of this is shown in Figure 2.25, which portrays the desired gear gap, the machined gear gap, and an enlargement of the deviation between the gaps. As it can be seen, the computed tool profile is able to accurately replicate the desired gear gap.

Moreover, as explained in Paragraph 1.2.3, the machine tool is able to compute certain set-up parameters based on others set as input, through mathematical models that are implemented in it. Therefore, a further trial that might be done is to compare the parameters computed by the numerical model, with those computed by the machine tool, relative to the same machining operation. Referring to Figure 2.15b) for instance, the norm of the computed velocity vectors at the tip closely matches the desired cutting velocity of  $60 \left[ \frac{m}{min} \right]$  which was set as input on the machine tool for that pass. This procedure despite being pretty, straightforward is key, as suggests the validity of the relative kinematics model on which the model of cutting geometry is based on.

A similar test can be made to verify the correctness of the intersection model. Figure 2.19b) showed the simulated  $h_{MAX}$  for the process passes, relative to different radial feeds and axial feeds computed by the machine tool to operate with  $h_{MAX} = 0.12$  mm. As it can be seen the results of the simulation match closely those of the machine tool.

Based on what above, both the penetration model used to compute the engagement points and the kinematic model used to compute the velocity vectors seem to be accurate. The working

## 2 Numerical model of centred gear skiving

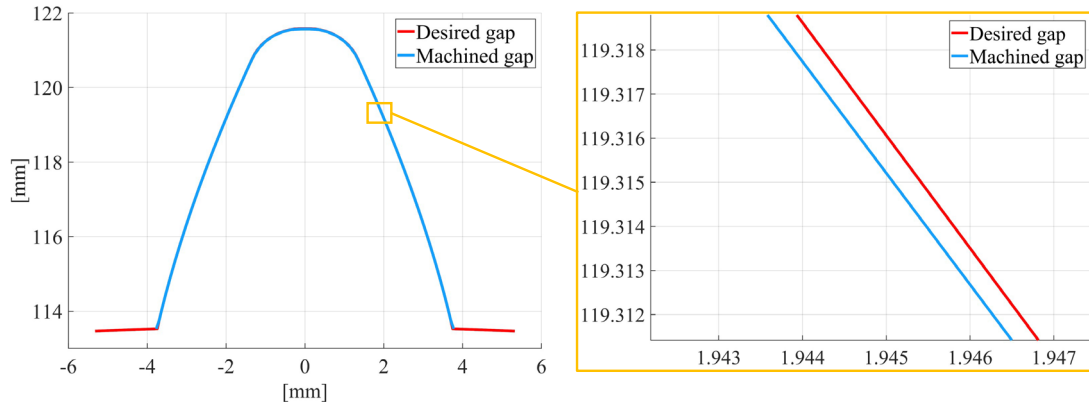


Figure 2.25. Comparison between desired gear gap and machined gear gap.

parameters are derived directly from the results of these two models. However, unfortunately, working parameters cannot be measured directly.

Hence, as a more general approach for the validation of the proposed numerical model, comparisons were made between skiving experiments and simulation results. This is done by comparing the simulated working parameters with tool wear photographs taken with the aid of a digital microscope. The proposed approach has been repeated for several case studies, some of which are presented in Chapters 3 and 4. They aim at investigating different phenomena, yet always related with working parameters. As clarified in the next section, the numerical model is only able to replicate the process from a geometric point of view and omits several process aspects. However, as demonstrated in later chapters, within its limitations, there is a remarkable correlation between experiments and simulation results which proves its validity.

### 2.4 Known limitations and possible uses

To understand the limitations of the proposed numerical model it is sufficient to consider the multitude of variables involved in a real skiving process. The cutting profile is not really a sharp edge, but it is characterized by a small edge radius. The tool wears at each machined workpiece and the size of the edge radius increases while its shape becomes irregular. This happens on a different ratio for each portion of the tool profile, hence continuously altering the cutting behaviour. During a pass, the tool induces plastic deformation in the workpiece material until the chip is separated. The chip flows across the rake face, which is not a uniform plane but possesses its own surface roughness depending on the re-sharpening process adopted. Moreover, the mechanism of chip formation depends on the geometry of each pass, by the materials of the gear and of the tool coating, as well as the speed at which the process is carried out. Additionally, the lubricant affects both the chip formation and its removal as well as the temperatures within the cutting zone.

The numerical model proposed in this chapter instead, is purely geometrical and it does not consider any of the mentioned aspects. It is by definition an approximate model. To account for the variables previously mentioned, a simulation employing FEM or other numerical techniques more adept at handling large deformations, such as Smoothed Particle Hydrodynamics (SPH), could be implemented. Using such sophisticated methods in the attempt to reproduce even some of the above process aspects, however, requires a simulation set-up and a computational time that may not always be justifiable in a corporate setting.

Conversely, geometric simulation, by deliberately excluding such variables, results to be extremely time efficient as it is fast in computation and do not require set-up time. However, by not considering material properties, the geometric simulation fails in providing suitable parameters for skiving parts made of alloys about which there is no previous experience. In such



cases a trial-and-error phase may be required to determine, for instance, an acceptable cutting speed or chip thickness, which may be optimised later on also through the numerical simulation.

Within the company environment where this PhD was conducted, the expertise of the shop floor employees regarding set-up parameters relative to several alloys was integrated with the results derived from the geometric simulation. This synergy has enabled the effective use of the proposed numerical model to mitigate challenges and concretely optimize the process, as shown in the following.

In Chapters 3 and 4, the numerical program is used to devise new cutting strategies aimed at reducing tool wear while maintaining or improving productivity, and also to aid tool design. However, other uses are possible, such as investigating gear quality and geometric modifications or solving clearance related issues.

## 2.5 Conclusions and future perspectives

In this chapter, a numerical model that allows replication of the skiving process performed by the company's machine skiving tool has been presented. The logic behind each main numerical routine constituting the model workflow has been introduced. The model conducts a geometric simulation of the centred gear skiving process, enabling the analysis of the local cutting conditions in which the tool operates.

Moreover, the main relationships, most of which already known in the literature, linking set-up parameters and tool design parameters with the working parameters, have been discussed. By doing so, some discrepancies between reported studies have been highlighted. The numerical program and the discussed relationships lay the foundation for the following chapters, where different aspects of the skiving process are addressed and optimised.

Regarding further developments of the numerical program, in the future, the transitional phases concerning the tool run-in and run-out paths will be considered. This will allow for more precise simulations relative to workpieces with small gear width. Additionally, the routine presented in Appendix A, will be optimised, and implemented in the main model workflow. By doing so a comprehensive and more accurate perspective on tool design and on the risk of collision in operation may be achieved.

### 3 Process optimisation based on the proposed numerical model

In a common gear manufacturing context, for a given machining operation, the tool is typically designed by external companies. Therefore, usually, it is not possible to tune the tool design parameters at will. However, adjustments can be made to the set-up parameters in order to devise new cutting strategies which enhance the cutting conditions and optimize the performance of the available tools.

As mentioned, the numerical model is unable to simulate the effect of the cutting speed. This parameter is chosen based on trial-and-error experiments conducted at the company. Thus, the set-up parameters that can both be tuned on the machine tool, and whose implications on working parameters can be analysed through simulation, include: the number of passes  $NoP$ , the maximum chip thickness at each pass  $h_{MAX}$ , and the infeed strategy. From previous tests conducted at the company, the digressive radial infeed strategy with additional workpiece side rotation  $Crot$  has proven to yield the best results. Therefore, all the cutting strategies presented below adopt this approach. Based on what presented in Paragraph 1.2.3, by choosing the  $NoP$  and the infeed strategy, the radial feed  $f_R$  is uniquely determined. Also, by selecting  $f_R$  and the chip thickness for a specific tool design determines the axial feed  $f_A$ . As a result, the set-up parameters that determine the cutting strategy and that are tuned in the following discussion, are  $NoP$  and  $h_{MAX}$ . Clearly, it is also possible to use  $f_R$  and  $f_A$  as inputs and compute  $NoP$  and  $h_{MAX}$  accordingly. This approach is usually employed for the finishing passes.

Regarding implications of  $NoP$  and  $h_{MAX}$  on working parameters, as discussed in Paragraph 2.2.8, the extent to which working angles can be improved using novel cutting strategies is limited, as tool design is the main determinant. Therefore, in the context of this work, it resulted natural to focus also on their implications on other working parameters, such as the normalised chip area, introduced in this work, and the cumulative total machined cutting length. This represents a novelty within the gear skiving field and is the subject of the first section of this chapter. In later sections, two main applications of the numerical program are presented. Each application exploits, in a different way, the new implications found in the first section. Additionally, for each application, different case studies are presented, where the numerical program has been used to enhance specific aspects of the skiving process. The general approach followed in both applications, is to improve the tool cutting performances without increasing the cycle time or even attempting to reduce it. Specifically, the tool cutting performances are measured in terms of amount of wear per number of machined parts.

Regarding the experimental tests that are presented, some clarifications must be made. Each experiment was conducted at least twice to ensure repeatability. After each trial, photos of the most worn tool teeth were taken using a digital microscope. These photos are used for comparisons with the simulation results and with other experiments. Lastly, the tools have always been replaced before producing parts out of the specified tolerance class. Therefore, each tool shown below has machined its last workpiece while still adhering to the customer's specifications.

#### 3.1 Implications of $NoP$ and $h_{MAX}$ on $l_{cTOT}$ and on $A_{hP}$

In this section, the implications of  $NoP$  and  $h_{MAX}$  on the cumulative machined total cutting length  $l_{cTOT}$  and on the normalised chip area  $A_{hP}$  are addressed. However, it is also necessary to analyse their implications on other working parameters in order to have a comprehensive overview of the process.

**Table 3.1.** Implications of set-up parameters on working parameters.

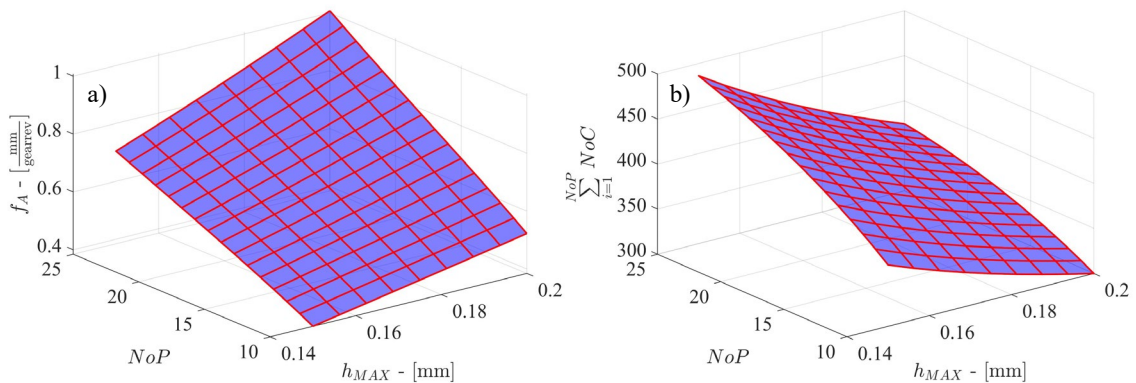
Working parameters Set-up parameters	$\sum_{i=1}^{NoP} NoC(i)$	$l_{cSING}$	$A_{hP}$	$l_{cTOT}$	$t$
$h_{MAX}$ ↑	↓	↑	↑	↓	↓
$NoP$ ↑	↑	↓	↓	↑	↑

Reference can be made in advance to Table 3.1, which summarises all the implications discussed in what follows. The first column of the table features the two set-up parameters  $NoP$  and  $h_{MAX}$ , the implication of which on working parameters are addressed. Close to both set-up parameters there is a red arrow pointing up. In the other columns there are other arrows pointing either up or down. The arrows describe the trend of the considered set-up parameter on the working parameter at the top of each column. Specifically, the red arrows pointing up stand for an increase of the working parameter, whereas blue arrows pointing down stand for a reduction of the working parameter. Hence, each row in the table illustrates the consequences of increasing the corresponding set-up parameter on working parameters, with the other set-up parameter held constant.

Some further clarifications need to be made. It should be remarked that the way in which each working parameter varies, changes from parameter to parameter. Hence, the arrows in Table 3.1 indicate merely a trend. Additionally, in the second column of the table, the symbol  $\sum_{i=1}^{NoP} NoC(i)$  has been used, to represent the sum of the  $NoC$  of each pass over all the passes. This parameter aids in investigating the implications of the set-up parameters on  $l_{cTOT}$ . In the following, the implications of the set-up parameters variation are addressed through skiving simulations computed with the numerical program. The simulations are related to real trials carried out at the company. The results of some of them are given in the following sections.

Starting from the first row of Table 3.1, an increase in  $h_{MAX}$ , with  $NoP$  held constant, results in a reduction of  $NoC$  at each pass. Consequently, also the sum over the passes  $\sum_{i=1}^{NoP} NoC(i)$ , is reduced. This can be easily explained by referring to the diagrams of Figure 1.8. To increase  $h_{MAX}$  at a constant  $f_R$ , a deeper penetration into the workpiece is required, leading to an increase in  $f_A$  at each pass. From Eq. 2.23, it is clear that an increase in  $f_A$  corresponds to a reduction in  $NoC$  at each pass.

Regarding the effect of  $NoP$  on  $\sum_{i=1}^{NoP} NoC(i)$ , the relationship is less straightforward. Referring again to Figure 1.8, a pass with lower  $f_R$  resulting from a higher  $NoP$ , requires a higher  $f_A$  to generate the same  $h_{MAX}$ . Therefore, a bigger  $f_A$  causes a reduction in the  $NoC$  of all the


**Figure 3.1.** Implications of the number of passes and of the maximum chip thickness on: a) the axial feed; b) the number of cuts of one pass.

### 3 Process optimisation based on the proposed numerical model

passes, while the passes increase in number. However, in general, doubling  $NoP$  would not yield a halving of  $f_A$ . Hence, overall, the increase of  $NoP$  overcomes the reduction of  $NoC$  of the single passes and causes a significant increase in  $\sum_{i=1}^{NoP} NoC(i)$ . Figures 3.1a) and b) respectively depict the qualitative trends of  $f_A$  and of  $\sum_{i=1}^{NoP} NoC(i)$ , as functions of the two set-up parameters  $h_{MAX}$  and  $NoP$ . The figures yield a graphic representation of the trends just discussed.

Addressing the implications of increasing  $h_{MAX}$  on  $l_{cSING}$  and  $A_{hP}$ , the following observations can be made. As mentioned, at constant  $NoP$ , increasing  $h_{MAX}$  leads to a rise on  $f_A$  and thus of the penetration between tool and workpiece. Consequently, it is not hard to imagine that both parameters,  $l_{cSING}$  and  $A_{hP}$ , also increase, since they are both measures of the penetration. However, it should be emphasized that, although this implication may seem trivial, without the use of a numerical program like the one presented in this work, it is not possible to quantify the extent of such an increase.

To give an example, Figures 3.2a) - d) illustrate a case study, addressed as process 1, related to two cutting strategies performed with the same tool, while holding fixed the  $NoP$  to 33 passes and by varying  $h_{MAX}$  exclusively. In particular, Figures 3.2a) and c), showing the values of  $A_{hP}$  and  $l_{cSING}$  respectively, are relative to the cutting strategy with  $h_{MAX} = 0.2$  mm. Figures 3.2b) and d) instead, respectively related to the same parameters, concern the cutting strategy with the same  $NoP$  and  $h_{MAX} = 0.25$  mm. As observed from the comparison between Figure 3.2a) and b),  $A_{hP}$  increases approximately up to 20% between the two cutting strategies. As mentioned in Paragraph 2.2.8.4,  $A_{hP}$  is associated to the tool load per unit of profile length, which is qualitatively linked to the dynamic load on the tool teeth at each pass. Regarding  $l_{cSING}$ , a negligible increase is observed when comparing Figures 3.2c) and d).

The example just presented suggests that an increase in the nominal chip thickness value on the machine tool, for the same number of passes, results in a shape of the UCG that remains approximately of the same length but becomes thicker. Overall, the chip appears stockier.

Referring now to the effect of an increase in  $NoP$  on  $l_{cSING}$  and  $A_{hP}$ , a different situation emerges. Increasing  $NoP$  at constant  $h_{MAX}$  results in lower  $f_R$  and, as explained above, in a higher  $f_A$ . Such variations alter the shape of the penetration between the tool and the workpiece. Specifically, the chip shortens and becomes thicker, assuming, once again, a stockier shape. As an example, Figures 3.2 e) - h) are considered. Such figures pertain to a second case study, addressed as process 2, related to two cutting strategies performed with the same tool, with  $h_{MAX}$  fixed to 0.15 mm and carried out at a different  $NoP$ . As can be seen also from the figures, the tool employed in process 2 is different to that employed in process 1. Figures 3.2 e) and g), shows the values of  $A_{hP}$  and  $l_{cSING}$  respectively, and relate to a cutting strategy carried out with 16 passes. Figures 3.2 f) and h) instead, portray the same parameters, respectively, but relate to a cutting strategy with 32 passes. Comparing Figures 3.2 e) and f), it can be seen that the increase in  $NoP$  causes a reduction in  $A_{hP}$  of about 20%. In this case, there is a reduction of the load per unit of tool profile length. From the comparison of Figures g) and h), it is evident that  $l_{cSING}$  also decreases appreciably. It should be specified that the values of  $A_{hP}$  and  $l_{cSING}$  for the finishing passes of the individual processes 1 and 2, do not change with the cutting strategy, since finishing was always performed with the same  $f_R$  and  $f_A$  to reach the same surface quality.

An analysis of the behaviour of  $l_{cTOT}$ , in response to the variation of the discussed set-up parameters may now be conducted. From Table 3.1, it can be seen that in both rows corresponding to  $h_{MAX}$  and  $NoP$ , the trends of the two elements which based on Eq. 2.24 account for  $l_{cTOT}$ , namely  $NoC$  and  $l_{cSING}$ , are opposite. This divergence complicates the analysis of  $l_{cTOT}$ . Nevertheless, the discussion provided aids in explaining the behaviour of  $l_{cTOT}$  as a function of the set-up parameters.

### 3.1 Implications of NoP and hMAX on lcTOT and on AhP

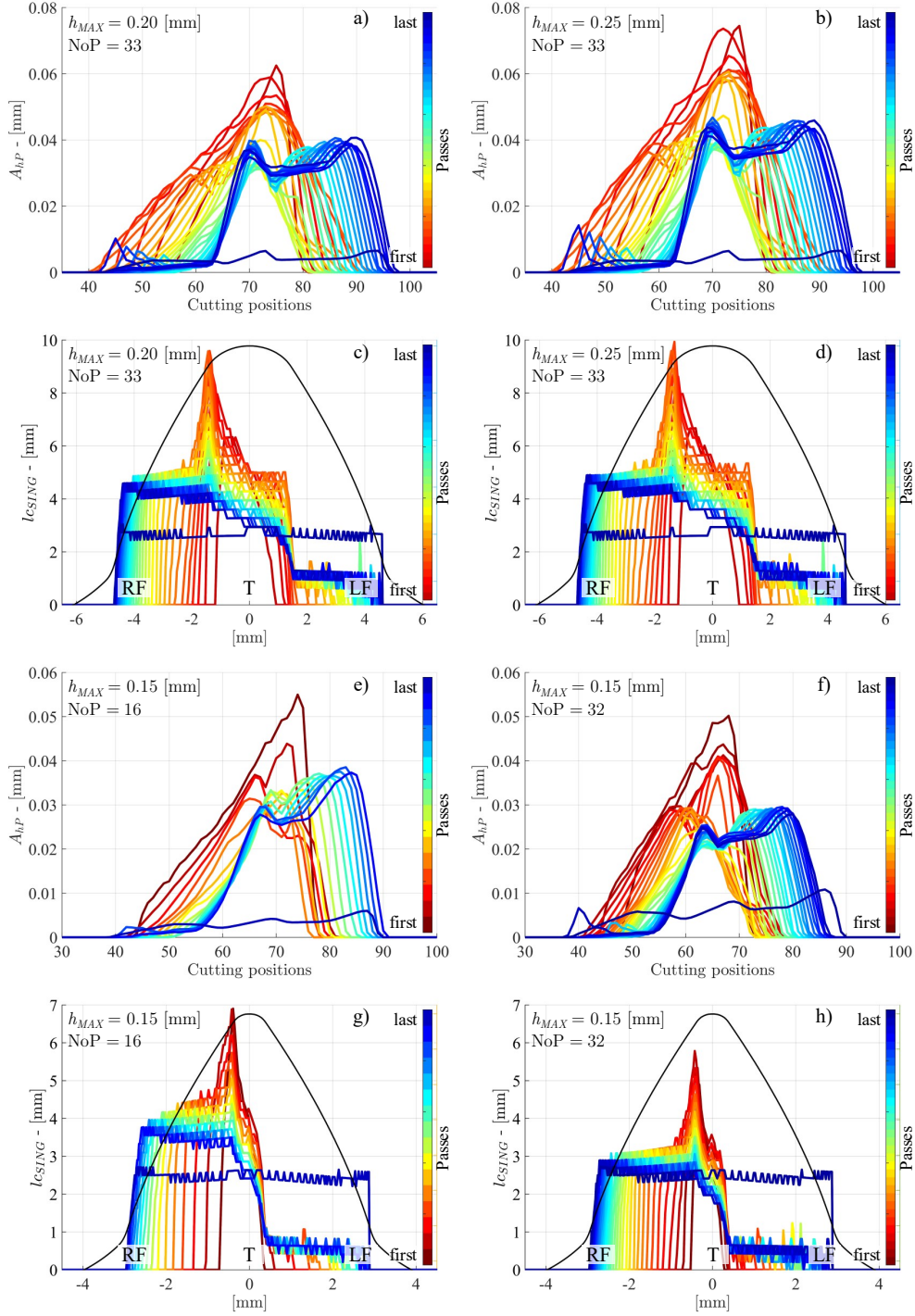


**Figure 3.2.** Simulated values of  $A_{hP}$  and  $l_{cSING}$  for two different skiving processes, each carried out with different cutting strategies. a) values of  $A_{hP}$  for process 1 with NoP = 33 and  $h_{MAX} = 0.20$  mm; b) values of  $A_{hP}$  for process 1 with NoP = 33 and  $h_{MAX} = 0.25$  mm; c) values of  $l_{cSING}$  for process 1 with NoP = 33 and  $h_{MAX} = 0.20$  mm; d) values of  $l_{cSING}$  for process 1 with NoP = 33 and  $h_{MAX} = 0.25$  mm; e) values of  $A_{hP}$  for process 2 with NoP = 16 and  $h_{MAX} = 0.15$  mm; f) values of  $A_{hP}$  for process 2 with NoP = 32 and  $h_{MAX} = 0.15$  mm; g) values of  $l_{cSING}$  for process 2 with NoP = 16 and  $h_{MAX} = 0.15$  mm; h) values of  $l_{cSING}$  for process 2 with NoP = 32 and  $h_{MAX} = 0.15$  mm.

As shown, an increase in  $h_{MAX}$  does not correspond to a significant rise in  $l_{cSING}$ . Conversely, a noticeable decrease in  $NoC$  has been observed. Therefore, referring again to Eq. 2.24, an overall increase in  $h_{MAX}$  causes a significant reduction in  $l_{cTOT}$ .

To illustrate this, Figure 3.3 a) displays the value of  $l_{cTOT}$  for the cutting strategy of Figures 3.2a) and c), compared to that of Figures 3.2b) and d). As it can be seen,  $l_{cTOT}$  is highly

### 3 Process optimisation based on the proposed numerical model

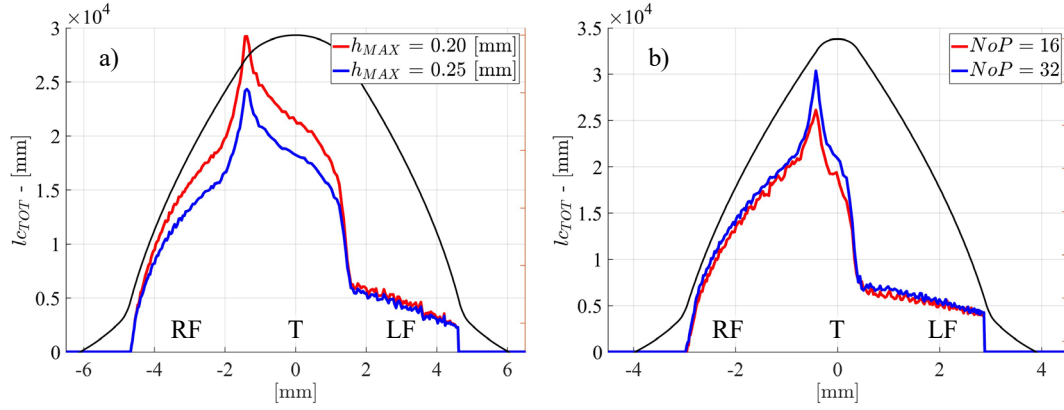


**Figure 3.3.** Comparison of the cumulative total machined cutting length relative to a) process 1 with same  $NoP$  and different values of  $h_{MAX}$ ; b) process 2 with same value of  $h_{MAX}$  and different  $NoP$ .

influenced by  $h_{MAX}$ . In this case, a 25% increase in  $h_{MAX}$  led to a reduction of up to 17% in  $l_{cTOT}$ . Furthermore, with reference to Eq. 1.5, the increase in  $h_{MAX}$  at constant  $NoP$ , by causing a rise in  $f_A$ , leads to a significant reduction in the cycle time. In particular, the cutting strategy with  $h_{MAX} = 0.2$  mm requires a cycle time of 10' 29'', whereas that with  $h_{MAX} = 0.25$  mm only takes 8' 37''.

It is interesting to note that cycle time is approximately directly proportional to  $\sum_{i=1}^{NoP} NoC(i)$ . Indeed, still referring to Eq. 1.5, for a given tool design, the run-in and run-out tool paths from the workpiece change little with the cutting strategy. Therefore, for a given cutting velocity, cycle time is primarily linked to  $f_A$  and  $NoP$ .

It should be remarked that the two advantages in terms of reducing  $l_{cTOT}$  and cycle time come at the expense of increased load on the tool profile, as previously demonstrated by the comparison with Figures 3.2a) and b).

Examining the impact of  $NoP$  on  $l_{cTOT}$ , from the prior discussion an increase in  $NoP$  for the same  $h_{MAX}$  was associated to a significant rise in  $\sum_{i=1}^{NoP} NoC(i)$ , accompanied by a reduction in  $l_{cSING}$ . The comparison made in Figures 3.2 e)-h) was intentionally exaggerated and the  $NoP$  was doubled from 16 to 32. This resulted in a noticeable decrease of  $l_{cSING}$ . However, the corresponding increase in  $\sum_{i=1}^{NoP} NoC(i)$  is much more pronounced. Consequently, an elevated  $NoP$  generally corresponds to an increased  $l_{cTOT}$ . Figure 3.3b) illustrates the values of  $l_{cTOT}$  for the two cutting strategies related to Figures 3.2 e) - h) with 16 and 32 passes and conducted with the same  $h_{MAX}$ . The plot in Figure 3.3b) indicates that a 100% increase in  $NoP$  results in a smaller variation of  $l_{cTOT}$  compared to the variation observed in Figure 3.3a) relative to an increase of 25% of  $h_{MAX}$ . This example suggests that  $l_{cTOT}$  has a different dependency from the two set-up parameters, with a higher sensitivity to variations in  $h_{MAX}$  than in  $NoP$ .

Concerning the impact of  $NoP$  on cycle time, the cutting strategy with 16 passes requires 9' 16'', while that with 32 passes takes 13' 27''. Therefore, it may be concluded that increasing  $NoP$  allows for a reduction of the load per tool profile length, albeit at the cost of a significant increase in cycle time and a less pronounced rise in  $l_{cTOT}$ .

It should be remarked that the relations presented above serve to provide an overview of how the addressed working parameters evolve in relation to the set-up parameters. However, the exact influence of individual working parameters on the process changes depending on the specific geometry of the tool and workpiece at hand. For instance, an increase of the axial feed, significantly enhances the productivity of processes related to workpieces with a higher gear width. On the contrary, for workpieces with reduced gear width the majority of the process cycle

time is spent on the run-in and run-out tool paths. Therefore, in such cases, for a given cutting speed,  $NoP$  becomes the key factor for the productivity of the cutting strategy.

In the following two applications of the numerical program are presented. In both applications the implications of  $NoP$  and  $h_{MAX}$  on working parameters are used, especially the newly established on  $l_{cTOT}$  and  $A_{hP}$ . Although the two applications are inherently different, the ultimate goal remains the same, namely, to reduce tool wear without compromising productivity. To achieve this, the two set-up parameters,  $NoP$  and  $h_{MAX}$ , are tuned according to the specific application at hand.

### 3.2 Application 1: novel cutting strategy aimed at tool wear reduction

This section introduces the first practical application of the devised numerical model. It consists in the development of a novel cutting strategy which have been proved effective in reducing tool wear for the machining of gears made of annealed steel. At the company shopfloor, skiving tools which machine this kind of material has been reported to lose their sharpness as the main issue which determine tool replacement. This happens despite the workpiece hardness results far lower compared to other skiving processes.

Considering the different scenario arising when analysing the wear conditions on skiving tools, two are the most recurring at the company. In the first scenario, tool wear is distributed unevenly along the profile portions of the tool with the presence of small cracks and craters. In this case, the tool wear is associated with excessive localized loads on the profile points. These may be caused by various factors, such as poor tool design or an overly aggressive cutting strategy. Based on the presented work, in this scenario, working parameters such as  $h_{MAX}$ ,  $\gamma_{rMIN}$ , are the primary contributors since they are linked to local stress on the tool profile points. In the second scenario the tool profile is worn rather homogenously. In this case, the wear is associated to repeated rubbing under non-extreme load conditions, and the wear leading phenomenon is abrasion. In this scenario, based on the studies conducted in this work,  $l_{cTOT}$  emerges as the key working parameter.

An example of a worn skiving tool after machining 50 workpieces made of annealed steel is reported in Figure 3.4a) and b). The figures show a single tooth of a worn skiving tool from its rake face and from its right flank view respectively. The cutting profile portions, right flank (RF), tip (T), and left flank (LF) are also reported in the figure. As it can be seen, the wear distribution on the tool profile is rather homogenous, with the portion at the right tip radius which is slightly more worn. At this wear status the tool profile starts producing parts with low surface quality and towards the limit of the required geometrical tolerance. Due to the homogeneity of the wear distribution along the tool profile, the main cause of tool wear is supposed to be related to the cumulative machined total cutting length  $l_{cTOT}$ . The rationale for this statement is the following.

In Paragraph 2.2.8 it was discussed that the tool profile portions work in completely different cutting conditions. In Figure 3.4c) and d) have been reported, respectively, the simulation values for  $h_{MAX}$  and  $\gamma_{rMIN}$  over the tool profile, relative to the process passes carried out by the tool of Figure 3.4a) and b). As explained, such parameters both influence the local load of the tool profile points and are used to assess the cutting conditions along the profile. If the main reason for tool wear was caused by an excessive localized load along the tool profile, then according to the simulated values, the profile portion at the right tip radius, should be much more worn than the right flank portion. Indeed, from the simulation the right tip radius highlighted with an orange rectangle, machines values of  $h_{MAX}$  that are double as those of the right flank highlighted with the pink rectangle. In addition, simultaneously, the right tip radius operates at the lowest values of  $\gamma_{rMIN}$ . However, from the enlargement of Figure 3.4a) and from Figure 3.4b) such a marked difference between the two profile portions is not observed.



### 3 Process optimisation based on the proposed numerical model

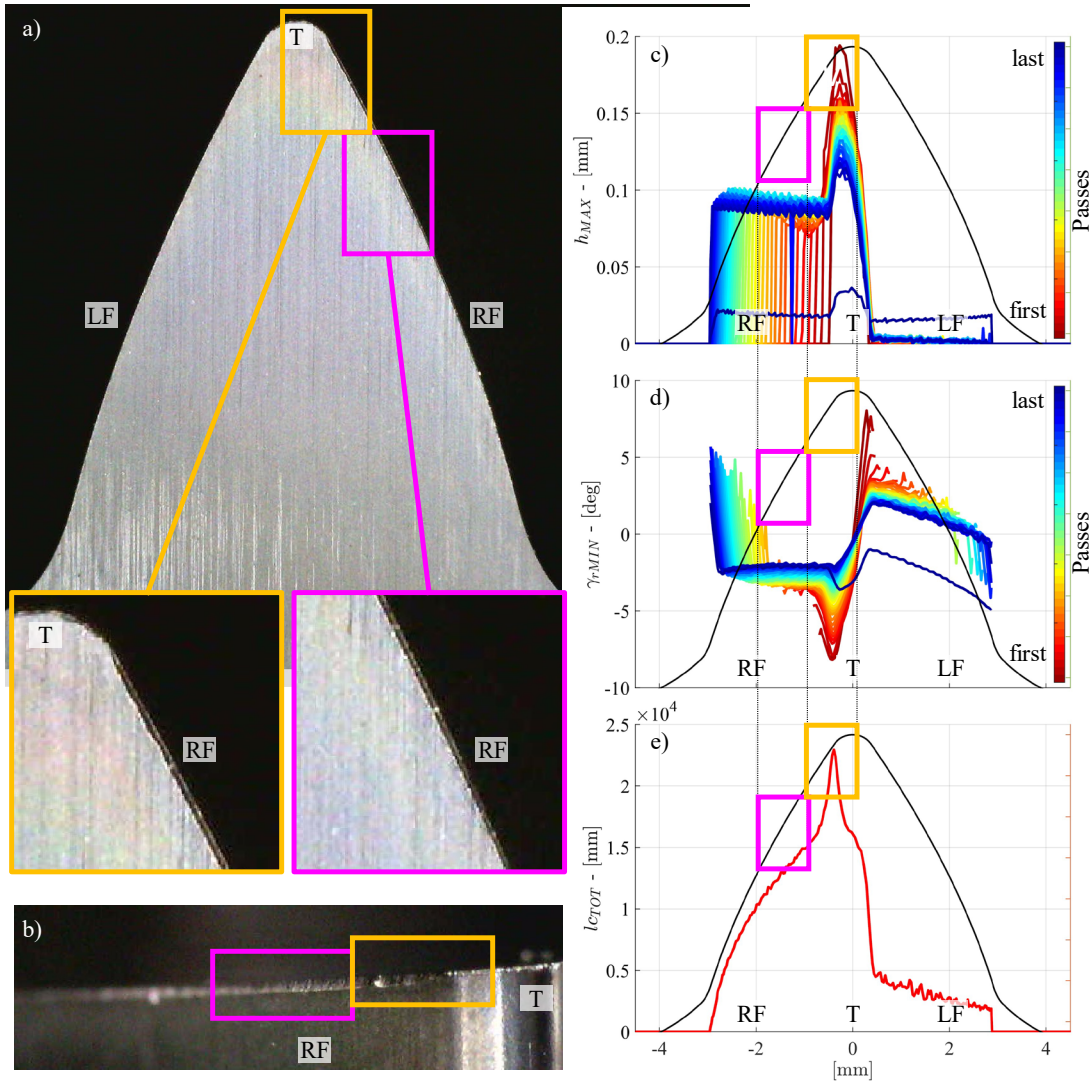


**Figure 3.4.** a) Worn tool tooth from the rake face; b) worn tool tooth from the right flank; c) simulated values of  $h_{MAX}$  of the relevant process; d) simulated values of  $\gamma_{rMIN}$  of the relevant process; e) simulated values of  $l_{cTOT}$  of the relevant process.

By referring to Figure 3.4d) instead, which portrays the values of  $l_{cTOT}$  over the tool profile, it can be seen that it follows approximately the same distribution of the tool wear of Figure 3.4a) and c). According to the simulated values of  $l_{cTOT}$ , the profile portion at the right tip radius, is the most worn part, but the difference with respect the right flank is not so marked, as it happens also in practice.

Hence, the main idea of the novel cutting strategy, is to reduce  $l_{cTOT}$  in order to reduce tool wear. To achieve this, based on what presented in the previous section, the two set-up parameters  $NoP$  and  $h_{MAX}$  should be respectively reduced and increased. However, by naively doing so, the dynamic load of each pass, associated at the working normalised chip area  $A_{hP}$ , would significantly increase. This may result in higher tool vibrations during the process passes, which causes premature tool wear and a poor surface finish. Since  $l_{cTOT}$  result to be more sensitive to the variation of  $h_{MAX}$  than  $NoP$ , the nominal maximum chip thickness of the process is increased. This would simultaneously, reduce the cycle time  $t$  and the cumulative machined total cutting length  $l_{cTOT}$  at the expenses of  $A_{hP}$  which rises. Then, in order to relieve the load per unit of profile length, the number of passes are increased. The amount of how much to increase



### 3.2 Application 1: novel cutting strategy aimed at tool wear reduction

the  $NoP$  comes from a trade-off between not exceeding the original process cycle time, which set the upper limit for  $NoP$ , and to provide enough relieve to the increase of  $A_{hP}$  caused by the augment of  $h_{MAX}$ . The latter condition sets the lower limit for  $NoP$ .

As it will be demonstrated through two different case studies, the proposed cutting strategy allows the nominal value of  $h_{MAX}$ , to be brought closer to its optimal value for balancing productivity and tool wear by reducing  $l_{cTOT}$ . Furthermore, as discussed above by simultaneously increasing  $h_{MAX}$  and  $NoP$  the shape of the UCG tends to become stockier, which has been reported to be beneficial for the skiving process [103].

The reason why the proposed strategy is recommended for annealed steel gears, is that when machining such material, compared to other gear materials, the tool tolerates higher values of  $h_{MAX}$ . Hence, unless the process is already operated at its optimal  $h_{MAX}$ , it is possible to increase  $h_{MAX}$  and  $NoP$  with the novel cutting strategy to a larger extent, thus significantly affecting  $l_{cTOT}$  and consequently the tool wear. For other gear materials, as in Application 2, this cutting strategy may not be effectively applied.


#### 3.2.1 Case study 1

With this first case study, the effectiveness of the proposed cutting strategy is tested. Table 3.2 presents geometric and material data related to the workpiece and the tool. The workpiece is an internal gear made of case hardening steel. Prior to the skiving process, the workpiece undergoes isothermal annealing at  $T > 950^\circ$ , reaching hardness between 143-179 HB. Then the skiving process is carried out prior to case hardening.

Starting from the standard process employed at the company, two processes, Process 1, and Process 2, respectively, are presented. Both processes employ the novel proposed cutting strategy, with Process 2 featuring the biggest deviations from the standard process. For the sake of conciseness, the process data and the simulative and experimental results are shown together for all the three processes. However, in the following, firstly, the comparison between Process 1 and the standard process is discussed. Then, Process 2 is addressed and compared with the other processes.

The process main data are reported in Table 3.3. With the aim to reduce  $l_{cTOT}$ , compared to the standard process, in Process 1 the value of  $h_{MAX}$  have been increased from 0.15 to 0.18 mm.

**Table 3.2.** Tool and workpiece data of case study 1.

Data	Tool	Gear	Gear photo
Normal module $m_n$ [mm]	3.2173	3.2173	
Normal pressure angle $\alpha_n$ [deg]	25	25	
Number of teeth	30	-69	
Helix angle [deg]	20 RH	Spur	
Tip diameter [mm]	109	219.32	
Root diameter [mm]	94.1	232.64	
Tool usable height / gear width [mm]	13	71.7	
Profile shift coefficient (SOL / EOL)	0.3 / 0	-0.2724	
Constructive Rake angle [deg]	5	-	
Constructive clearance angle [deg]	5	-	
Constructive step angle [deg]	20	-	
Material	S390	20NiCrMo2-2	
Coating	AlCrN	-	
Gear quality required	-	AGMA class 8	

### 3 Process optimisation based on the proposed numerical model

**Table 3.3.** Process data of case study 1.

Data	Standard process	Process 1	Process 2
$NoP$	32	39	39
$h_{MAX}$ [mm]	0.15	0.18	0.20
Cross-axis angle $\Sigma$ [deg]	20	20	20
Cutting velocity [m/min]	80	80	80
Cooling	Oil	Oil	Oil
N° of machined parts	50	50	50
Cycle time $t$ [min sec]	13' 27''	13' 04''	12' 04''

In order to prevent the values of  $A_{hP}$  to significantly rise, with the aid of the numerical program the  $NoP$  of Process 1 has been increased from 32 to 39. The finishing pass remains the same. By doing so, the cycle time of Process 1 reduces of about 20 seconds with respect to the standard process, which is positive for productivity.

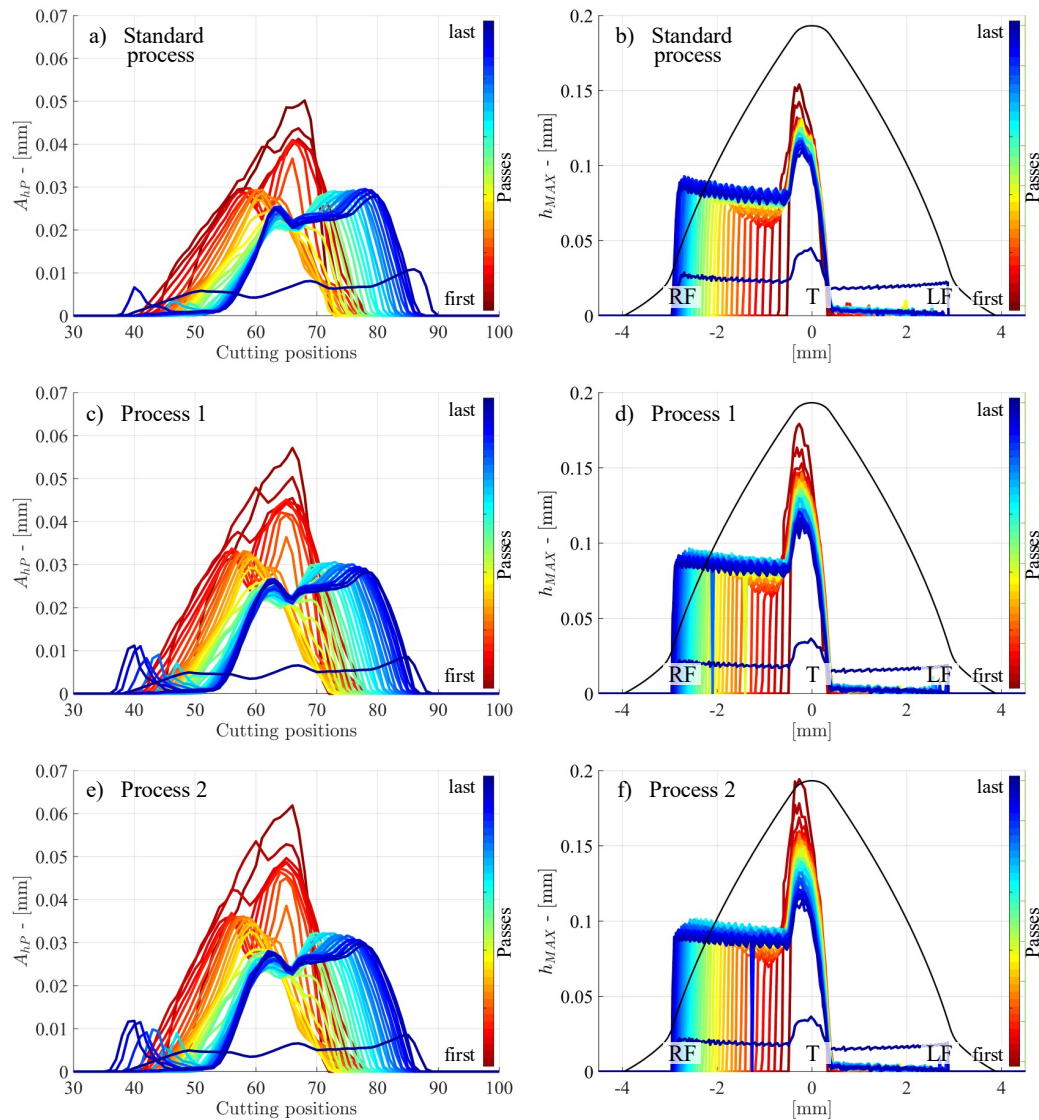


**Figure 3.5.** Simulated values of a)  $A_{hP}$  for the standard process; b)  $h_{MAX}$  for the standard process; c)  $A_{hP}$  for Process 1; d)  $h_{MAX}$  for Process 1; e)  $A_{hP}$  for Process 2; f)  $h_{MAX}$  for Process 2.

### 3.2 Application 1: novel cutting strategy aimed at tool wear reduction

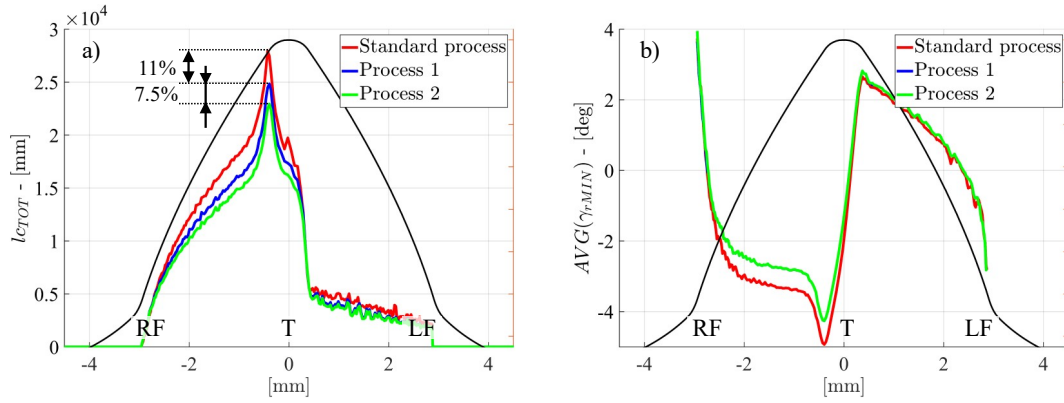


**Figure 3.6.** Simulated value of a)  $l_{cTOT}$  of the three processes; b) the averaged value of  $\gamma_{rMIN}$  among the passes of the three processes.

In Figure 3.5, some of the most relevant working parameters for this case, resulting from the simulation, are shown. Specifically, Figure 3.5a) and b) show respectively the simulated values of  $A_{hP}$  and  $h_{MAX}$  relative to the standard process. By comparing such values with the relevant simulated values for Process 1, portrayed in Figure 3.5c) and d), respectively, it can be seen that the values of  $h_{MAX}$  has been increased.

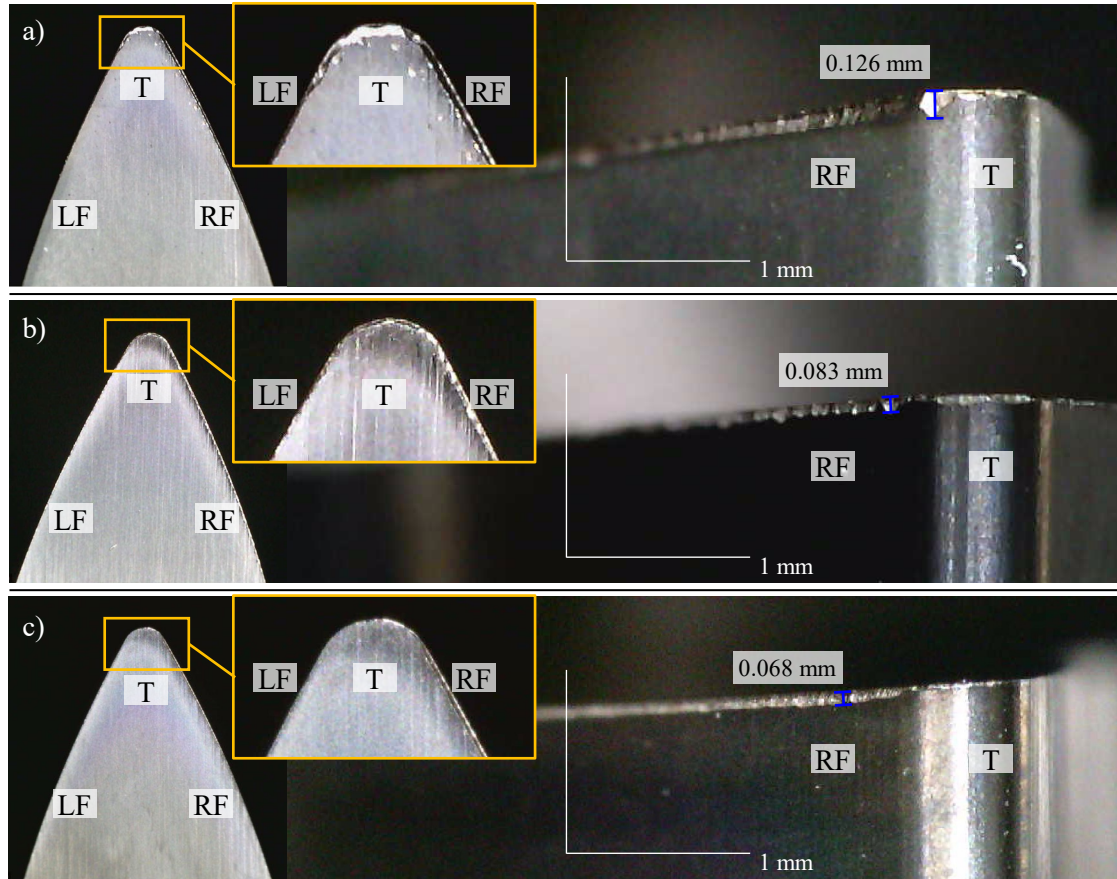
In contrast, as intended, comparing the values of  $A_{hP}$  of homologous passes of the two processes, apart for the first pass, the increase of  $A_{hP}$  for the passes of Process 1 is minimum. This suggests that the load per profile length should not increase significantly for the passes of Process 1 with respect to the standard process. As it will be discussed in Case Study 2, an increase of  $A_{hP}$ , is somehow inevitable in order to maintain the cycle time unchanged from process to process.

Figure 3.6a), shows the cumulative machined total cutting length of the three processes. Comparing the values of  $l_{cTOT}$  relative to the standard process, depicted in red line, with those relative to Process 1, depicted with the blue line, a reduction of about 11% is observed. In addition, by increasing the  $NoP$ , the tool in Process 1 operates with increased values of  $\gamma_{rMIN}$  which also help relieving the stress on the tool. This may be observed from Figure 3.6b), which shows with the same colours, the averaged value of  $\gamma_{rMIN}$  among all the passes for the three processes.

Then, experimental trials have been carried out for both the standard process and Process 1. Specifically, each tool employed on each cutting trial, machined 50 workpieces. The photos of tool wear after machining 50 workpieces for all the three processes are reported in Figure 3.7. By comparing Figure 3.7a) and b), respectively related to the standard process and to Process 1, it can be observed a significant reduction of tool wear from both the rake face and from the tool flank views. The most worn profile portion for both processes is that at the right tip radius, between tip and right flank, as also suggested by the values of  $l_{cTOT}$  in Figure 3.6a). Such profile portion reaches 0.125 mm of tool wear in the standard process, whereas in Process 1, it reaches only 0.085 mm. Thus, Process 1 yields a 30% improvement in wear as well as a cycle time reduction of 20 seconds, compared to the standard process.

Given the promising result, a new process, Process 2, was devised. In this case it was decided to further increase  $h_{MAX}$  from 0.18 mm to 0.20 mm, in order to further reduce  $l_{cTOT}$ . However, from the simulation, the benefit in terms of  $l_{cTOT}$  reduction was not as pronounced as the previous case. Additionally, an augment of  $NoP$  aimed at balancing the values of  $A_{hP}$  would diminish the gain in terms of  $l_{cTOT}$ . Hence, for Process 2 it was decided to favour the reduction of  $l_{cTOT}$  at the expenses of a more significant rise in  $A_{hP}$ . Therefore, the  $NoP$  was maintained to 39 passes as in Process 1. As a result, the cycle time of Process 2 is reduced of one minute

### 3 Process optimisation based on the proposed numerical model



**Figure 3.7.** Tool wear from the rake face and the right flank view, after machining 50 workpieces with: a) the standard process; b) Process 1); c) Process 2.

compared to Process 1 and of one minute and twenty seconds with respect to the standard process, as shown in Table 3.3.

Figure 3.5e) presents the simulated values of  $A_{hP}$  for Process 2. Upon comparing Figure 3.5e) with 3.5c), it becomes apparent that, despite the smaller increase in  $h_{MAX}$  compared to the change made between the standard process and Process 1, the values of  $A_{hP}$  exhibit a more substantial increase. This is due to the lack of the balancing effect given by an augment of  $NoP$ . Referring to Figure 3.6a) where the values of  $l_{cTOT}$  relative to Process 2 have been depicted with the green line, it can be seen that Process 2 operates with a reduced  $l_{cTOT}$  compared to Process 1. However, the 7.5% reduction in  $l_{cTOT}$  is less marked than the 11% reduction of the previous case. Additionally, referring to Figure 3.6b) the values of the averaged minimum working rake angle remain substantially the same as in Process 1 and the green and blue lines are overlapped.

Overall, comparing the parameters of Process 2 and Process 1 with those measured in the comparison of Process 1 with the standard process, it is observed a less marked reduction in  $l_{cTOT}$ , a lack of improvement in  $\gamma_{rMIN}$  and a higher rise in the values of  $A_{hP}$  associated to higher dynamic load. Hence, it is expected that Process 2 would yield a smaller benefit in terms of tool wear over Process 1 compared to the improvement observed from the previous comparison. By comparing the tool wear measured after machining 50 workpieces with Process 2 shown in Figure 3.7c), with that relative to Process 1, shown in Figure 3.7b), the prediction is confirmed. As it can be seen, Process 2 yields a smaller benefit in terms of wear reduction over Process 1. This suggests the effectiveness of the simulation results and of the proposed cutting strategy.

Also, it must be remarked that Process 2 is one minute faster than Process 1 which is a significant advantage in terms of productivity. By comparing Figure 3.7c) with Figure 3.7a), it may be observed a tool wear reduction of about 50% accompanied by a cycle time reduction of



### 3.2 Application 1: novel cutting strategy aimed at tool wear reduction

about 10%. As a result, Process 2 was implemented on the company shop floor, replacing the standard process. Finally, it is worth noticing that while by employing the standard process the limit for tool replacement is set at 50 workpieces, by using the Process 2 tool replacement can be delayed. An illustrative example of this is presented in the upcoming case study.

#### 3.2.2 Case study 2

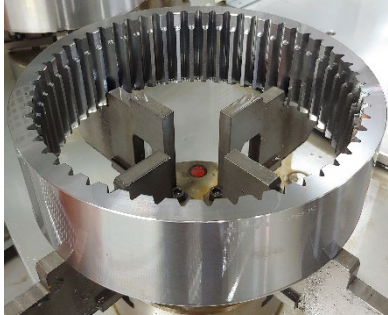
To demonstrate the effectiveness of the proposed cutting strategy across different workpiece geometries, a second case study is presented. Table 3.4 shows the relevant data for the tool and workpiece under consideration. The workpiece material is the same as in the previous case study, as well as its annealed state, which results in the same workpiece hardness of 143-179 HB. However, now the gear module is significantly larger. Additionally, despite the tool has the same number of teeth, the workpiece has less teeth than in case study 1. As a result, the tool-gear pair exhibits a different gear ratio compared to the previous case study, while maintaining the same cross-axis angle. Consequently, as discussed in Paragraph 2.2.3, the tool profile and the cutting conditions are substantially different.

For this case study four different processes are discussed, the standard process, employed at the company and three new processes, whose data are reported in Table 3.5. The first comparison is made between the standard process and Process 1.

Specifically, Process 1 adopts the novel cutting strategy to reduce  $l_{cTOT}$  while preventing the working normalized chip area  $A_{hP}$  to increase significantly. Process 1 of Case Study 1 employed the same logic. However, in Process 1 of Case study 1,  $A_{hP}$  slightly increased compared to the relevant standard process (Figure 3.5a) and c). In Process 1 of Case study 2 instead, the  $NoP$  is computed in order to maintain the values of  $A_{hP}$  at the same level of the standard process.

With the aid of the numerical program, considering an increase in  $h_{MAX}$  from 0.15 mm of the standard process to 0.18 mm of Process 1, it results that the  $NoP$  must be increased from 17 to 27 to balance the increased values of  $A_{hP}$ . As a result, the cycle time for Process 1 becomes of 14' 22''. Therefore, Process 1 takes one minute longer than the standard process. This example has been purposely chosen to show that to counteract the rise in  $A_{hP}$  due to an increase in  $h_{MAX}$ , a perfect balancing of  $A_{hP}$  by increasing the  $NoP$  is not possible, unless a longer cycle time is adopted. An increase in cycle time does not align with the proposed philosophy of process optimization.

**Table 3.4.** Tool and workpiece data of case study 2.

Data	Tool	Gear	Gear photo
Normal module $m_n$ [mm]	4.8542	4.8542	
Normal pressure angle $\alpha_n$ [deg]	25	25	
Number of teeth	30	-55	
Helix angle [deg]	20 RH	Spur	
Tip diameter [mm]	162.5	258.45	
Root diameter [mm]	139.65	278.26	
Tool usable height / gear width [mm]	14.7	88.9	
Profile shift coefficient (SOL / EOL)	-0.1 / -0.4	0	
Constructive Rake angle [deg]	5	-	
Constructive clearance angle [deg]	5.5	-	
Constructive step angle [deg]	20	-	
Material	S390	20NiCrMo2-2	
Coating	AlCrN	-	
Gear quality required	-	AGMA class 8	

### 3 Process optimisation based on the proposed numerical model

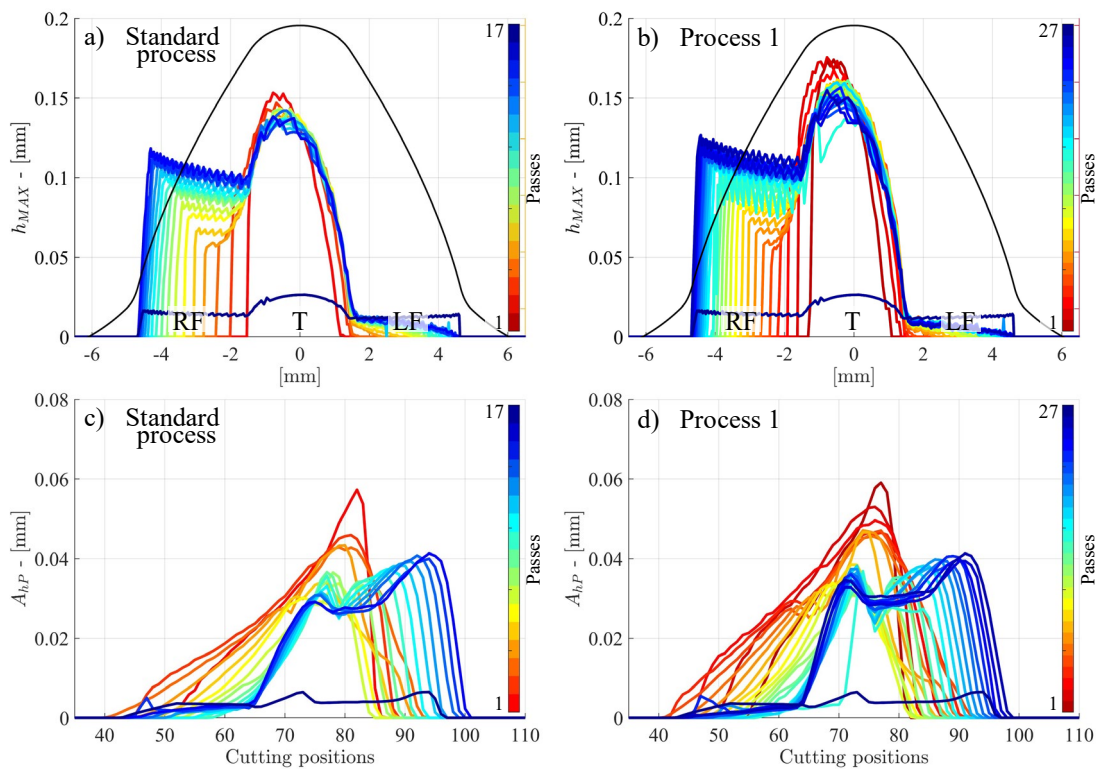
**Table 3.5.** Process data of case Study 2.

Data	Standard process	Process 1	Process 2	Process 3
$NoP$	17	27	17	33
$h_{MAX}$ [mm]	0.15	0.18	0.15	0.25
Cross-axis angle $\Sigma$ [deg]	20	20	20	20
Cutting velocity [m/min]	80	80	120	120
Cooling	Oil	Oil	Oil	Oil
N° of machined parts	50	50	50 and 70	70
Cycle time $t$ [min sec]	13' 22''	14' 22''	9' 03''	8' 47''

Thus, Process 1 should not be considered as a potential substitute for the standard process but rather as a preliminary experiment to assess whether the cutting strategy works also for the present Case study 2.

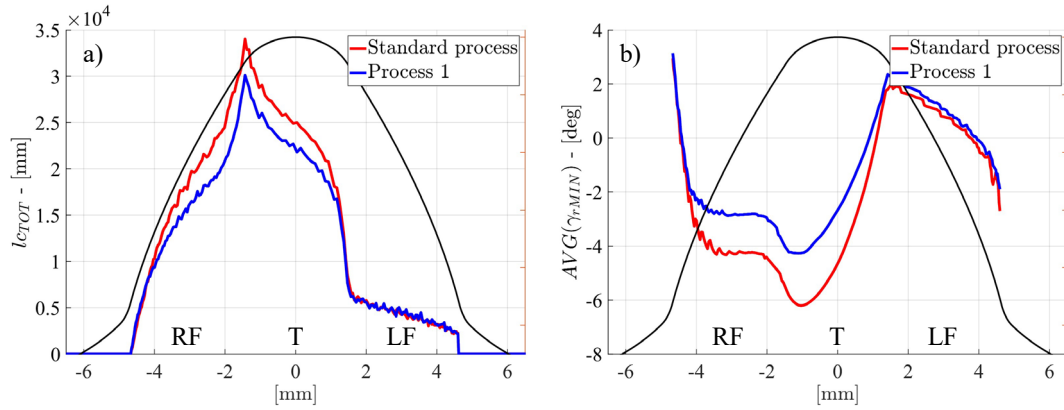
Figure 3.8 presents simulation results for the two processes under consideration. In Figure 3.8a) and b), are reported respectively, the simulated values of  $h_{MAX}$  for the standard process and for Process 1. As it may be observed, the values of  $h_{MAX}$  relative to Process 1 has increased both at the tip, which reaches the nominal value of  $h_{MAX} = 0.18$  mm, and on the tool right flank. Figure 3.8c) and d) instead, show the values of  $A_{hP}$  among the passes for the standard process and for Process 1, respectively. Notably, in Process 1, the values of  $A_{hP}$  are not increased compared to those of the standard process, which is due to the substantial rise in  $NoP$ . As a result, the dynamic load on the tool should remain at the same level for the two processes.

Figure 3.9 presents another comparison between other simulation results of the two processes. In Figure 3.9a), the values of  $l_{cTOT}$  over the tool profile are compared for the two processes. The



**Figure 3.8.** Simulated values of a)  $h_{MAX}$  for the standard process; b)  $h_{MAX}$  for Process 1; c)  $A_{hP}$  for the standard process; d)  $A_{hP}$  for Process 1.

### 3.2 Application 1: novel cutting strategy aimed at tool wear reduction



**Figure 3.9.** Simulated values of a)  $l_{cTOT}$  of the standard process and of Process 1; b) the averaged  $\gamma_{rMIN}$  among the passes of the standard process and of Process 1.

values of  $l_{cTOT}$  for Process 1 are depicted with the blue line and result lower than those relative to the standard process shown with the red line. The maximum difference is observed at the right radius of the tip and is close to 10%. Additionally, Figure 3.9b) portrays with the same colours, the average values of  $\gamma_{rMIN}$  over the passes for the two processes. It is evident that Process 1, due to the greater number of passes which cause a reduction in the engagement duration of each pass, exhibits higher values of the averaged  $\gamma_{rMIN}$ .

Overall, by comparing the results of Figure 3.9 with those of Figure 3.6, related to Case Study 1, it may be predicted that the present machining process will undergo a significant improvement in terms of wear. Indeed, it may be predicted an improvement comparable to what was observed in the transition from the standard process to Process 1 in Case Study 1.

In Figure 3.10, are presented the tool wear photographs corresponding to the two processes of the present case study, after machining 50 workpieces. Specifically, Figure 3.10a) shows the tool wear related to the standard process, while Figure 3.10b) shows the tool wear related to Process 1. It may be noticed that differently from Case Study 1, the orthogonal view to the tip has been

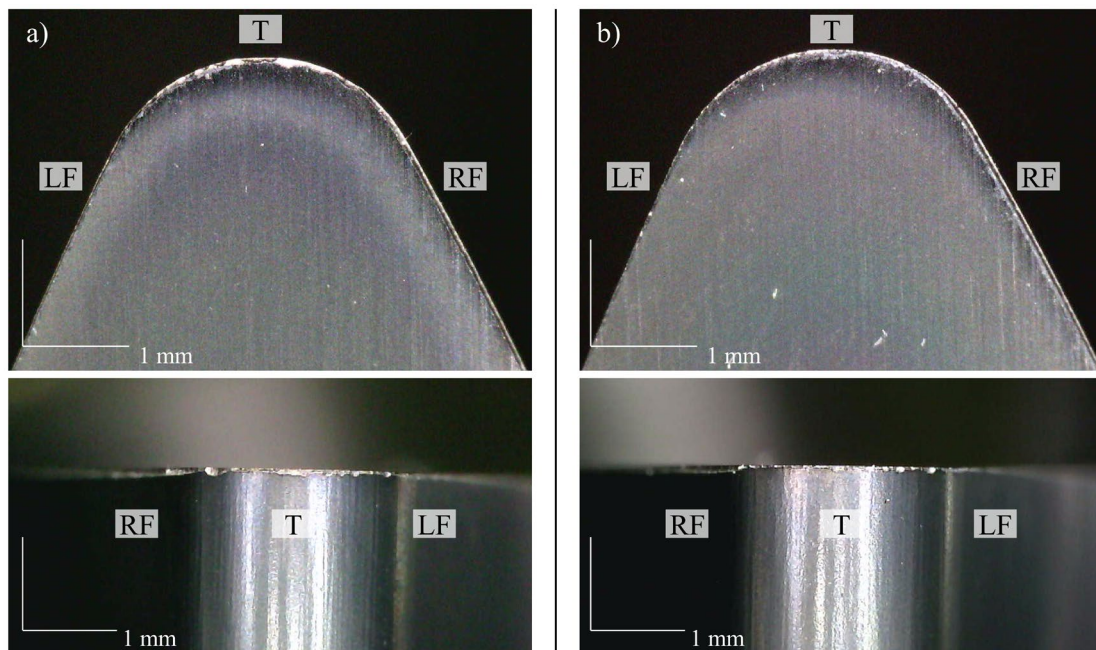


**Figure 3.10.** Tool wear from the rake face and the tip view, after machining 50 workpieces with: a) the standard process; b) Process 1).

### 3 Process optimisation based on the proposed numerical model

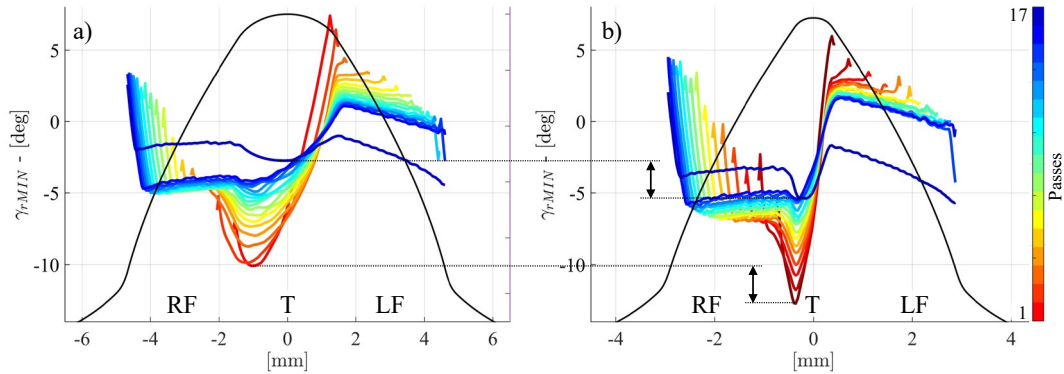


**Figure 3.11.** Comparison of the simulated values of  $\gamma_{rMIN}$  relative to the two tools of Case study 1 and Case study 2 operated with the same set-up parameters: a) tool of Case study 2 b) tool of case study 1.

reported instead of the flank view. The reason is that, given the broader tool tip in Case Study 2, the point with the most wear, which according to both the wear photos and to the simulations, is the right radius of the tip, is better represented from this perspective.

As it may be observed, the tool related to Process 1 appears less worn, but the improvement is minimal and not comparable to that of Case Study 1. The rationale for the smaller improvement in tool wear for the present case study, may be explained as follows. Despite the material of the workpiece being the same for both case studies, the two tools have different designs due to the different gear ratio and also to the different shape of the gear gap to machine. Consequently, even if the same set-up parameters were used, the cutting conditions for the two case studies would be different.

To give an example, in Figure 3.11a) and b), are reported the values of  $\gamma_{rMIN}$  relative to two simulations, one conducted with the tool from Case Study 2 and the other with that of Case Study 1, respectively. Both tools operate with the same set-up parameters, namely  $h_{MAX} = 0.15$  mm and  $NoP = 17$ . As observed in the figures, the values of  $\gamma_{rMIN}$  for the tool of Case Study 1 are lower than those relative to the tool in Case Study 2. In the figure, the differences in the first and in the last passes are indicated with black arrows. Remarkably, a difference of about  $3^\circ$  for each of the passes addressed can be spotted. Additionally, considering the different tool profile shape, the different relative kinematics, and the different shape of the gear gap, also the engagement pattern changes.

By comparing the profile shapes of the two tools of Figure 3.11 it can be noted that the tool in Case Study 2 has a broader tip than that of Case study 1. The wider tool tip removes material more homogeneously, relieving the right radius of the tip and balancing the amount of  $l_{cTOT}$  removed by the profile portions. Hence, in Case Study 2, the cutting conditions are even more uniform than in Case Study 1. This is made evident by comparing the values of  $l_{cTOT}$  portrayed in Figure 3.9a) with those of Figure 3.6a).

In the light of the above discussion, it is not surprising that, despite in the standard process in Case Study 2, the values of  $l_{cTOT}$  are higher than those machined with the standard process of Case Study 1, the wear in Figure 3.7a) is greater than that observed in Figure 3.10a). The above comparison between the two case studies serves to reveal that in gear skiving, even when working with identical materials, it is not possible to linearly transfer the results obtained from one machining process to another if they operate at different cutting conditions.

Nevertheless, from Figure 3.10, it may be concluded that even for the workpiece geometry relative to Case study 2, the novel cutting strategy has been effective. To further enhance the improvement in terms of tool wear reduction, it is necessary to increase the reduction of  $l_{cTOT}$  from the standard process. As a result, the value of  $h_{MAX}$  must be further increased.



### 3.2 Application 1: novel cutting strategy aimed at tool wear reduction

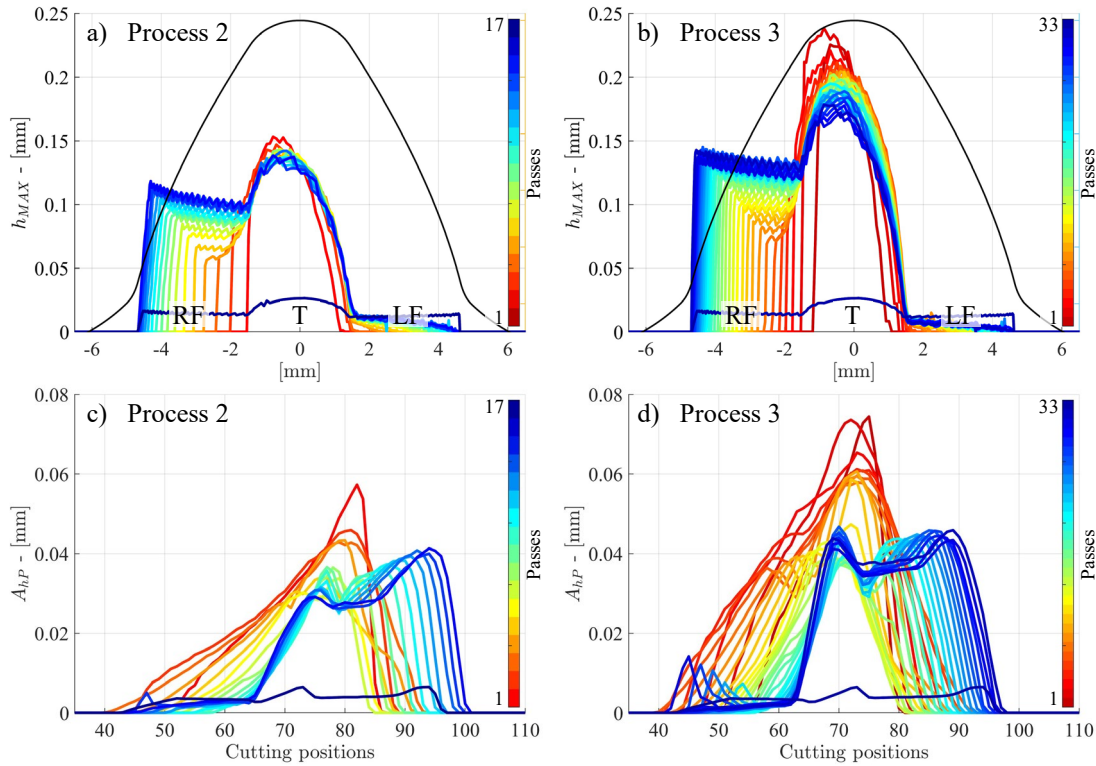


**Figure 3.12.** Simulated values of a)  $h_{MAX}$  for Process 2; b)  $h_{MAX}$  for Process 3; c)  $A_{hP}$  for Process 2; d)  $A_{hP}$  for Process 3.

The following consideration must thus be made. At this stage, it may be worth trying increase the cutting speed of the process. The rationale is that even if the new speed leads to a deterioration in terms of wear, this may be partially compensated by the reduction of tool wear provided by the novel cutting strategy, as it has proven to be effective. The advantage would be a reduced cycle time. It should be emphasized that this is a trial-and-error test, and the numerical program is not capable of predicting the changes in terms of wear due to the new cutting velocity.

From the results later shown, it is observed that increasing the cutting velocity of the standard process from 80 to 120  $\left[\frac{m}{min}\right]$  does not cause a deterioration in tool wear. Instead, the wear status almost improves. This indicates that the process at the company, was being performed at a sub-optimal speed. Therefore, at the company, the standard process is replaced by Process 2, which cycle time is 9' 03''. It should be remarked that, from a geometric point of view, Process 2 is identical to the standard process and only the module of the cutting velocity  $v_c$  changes, as shown in Table 3.5. Hence, the simulated working parameters for Process 2, excluding the norm of the velocity vectors, are identical to the standard process.

Thus, Process 3 is defined as the new process aimed at improving Process 2 through the novel cutting strategy. Obviously, also Process 3 is carried out at  $v_c=120 \left[\frac{m}{min}\right]$ . In order to significantly reduce the values of  $l_{cTOT}$  in the process, an even higher value for the nominal  $h_{MAX}$  used in Case Study 1 is employed in the present case study. Specifically, it is decided to employ for Process 3,  $h_{MAX} = 0.25$  mm. To limit the growth of the dynamic load associated to  $A_{hP}$ , the number of passes is increased to  $NoP = 33$ . Overall Process 3 has a cycle time of 8' 47'', which is approximately unchanged compared to Process 2.

In Figures 3.12a-d), comparisons between simulated values of  $h_{MAX}$  and  $A_{hP}$  for Process 2 and Process 3 are presented. As observed from Figures 3.12a) and b), which respectively depict the values of  $h_{MAX}$  for Process 2 and Process 3, it is evident that the new process operates with a significantly greater chip thickness. Regarding  $A_{hP}$  instead, there is an increase, but it is not

### 3 Process optimisation based on the proposed numerical model

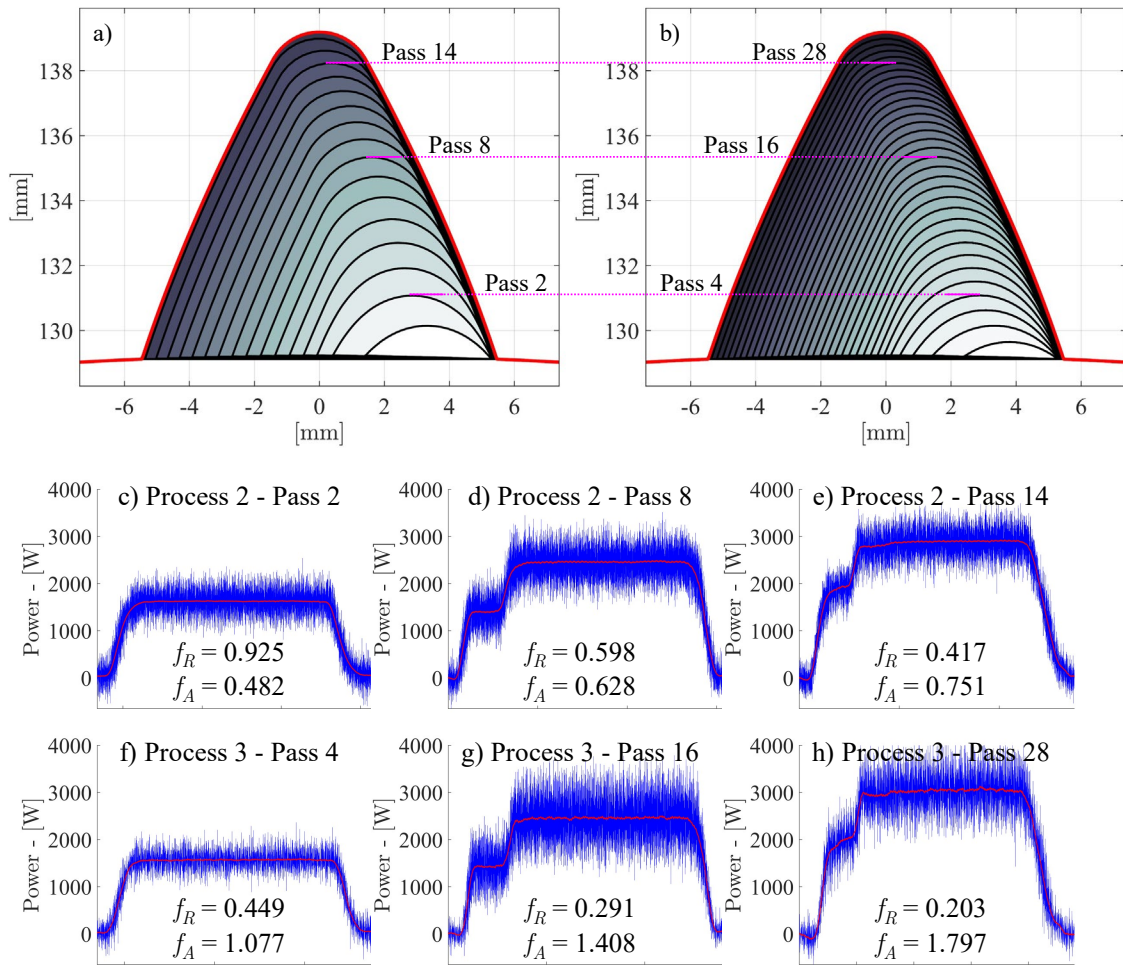


**Figure 3.13.** a) Radial infeed cutting strategy of Process 2; b) radial infeed cutting strategy of Process 3; c) - e) power readings of the motor spindles of the skiving machine for passes 2,8,14 of Process 2; f) - h) power readings of the motor spindles of the skiving machine for passes 4,16,28 of Process 3.

particularly pronounced due to the higher  $NoP$  which are almost doubled with respect to Process 2.

To provide a demonstration of the fact that thanks to the novel cutting strategy the load on the tool does not significantly increase despite the significant rise of  $h_{MAX}$ , reference can be made to Figure 3.13. In particular, Figures 3.13a) and b) show the infeed strategy of Process 2 and Process 3, respectively. Both processes employ a digressive infeed strategy with an extra side rotation  $Crot$  of the workpiece, ensuring that the access flank of the tool is tangent to the gear gap machined in the previous pass.

Due to the almost double  $NoP$  of Process 3 respect to Process 2, to compare two passes with the same radial infeed into the gear gap among the two processes, it is necessary to consider for Process 3 passes with an index double that of the pass considered in Process 2. For example, the fourth pass of Process 3 has penetrated the gear gap with almost the same depth as the second pass of Process 2. In 3.13a) and b) three passes have been highlighted, namely 2,8,14 for Process 2 and the corresponding 4, 16 and 28 for Process 3.

Then, in Figures 3.13c) – h), the power readings of the motor spindles of the Gleason 600PS skiving machine tool for the considered passes of the two processes are shown. The readings concern the tools while machining the first workpiece, hence at the same wear status. Additionally in the figures, the values of  $f_A$  and  $f_R$  for the considered passes of the two processes are reported.

### 3.2 Application 1: novel cutting strategy aimed at tool wear reduction

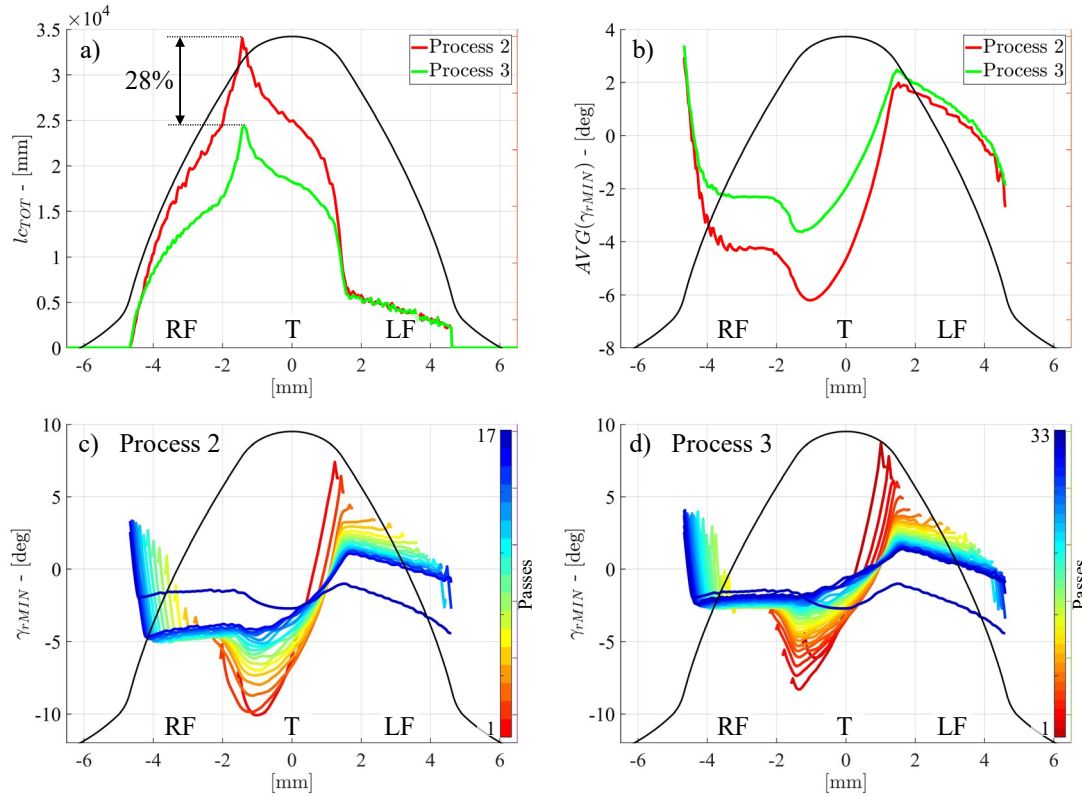


**Figure 3.14.** Simulated values of a)  $l_{cTOT}$  of Process 2 and of Process 3; b) the averaged  $\gamma_{rMIN}$  among the passes of Process 2 and of Process 3; c)  $\gamma_{rMIN}$  at all the passes of Process 2; d)  $\gamma_{rMIN}$  at all the passes of Process 3.

As observed, Process 3, by employing approximately a double  $NoP$  and a much greater  $h_{MAX}$  than Process 2, has much lower values of  $f_R$  and much higher values of  $f_A$  than Process 2.

It is evident from the comparison between equivalent passes that Process 3, despite working with much higher values of  $h_{MAX}$ , does not require greater power from the spindles compared to Process 2 during machining. This example demonstrates the effectiveness of the novel cutting strategy, from the point of view of not increasing the tool load despite increasing the values of  $h_{MAX}$ . Additionally, the example shows the relevance of the working normalized chip area. Indeed,  $A_{hP}$  results well suited in qualitatively describing the tool load applied on the tool teeth relative to different cutting strategies. As explained at the end of Paragraph 2.2.8.4, in this context,  $A_{hP}$  is more effective than  $h_{MAX}$ , which, similarly to  $\gamma_{rMIN}$ , is best suited to describe the local stress of the tool profile points.

In Figure 3.14, additional simulation results of the two processes are presented. Specifically, Figure 3.14a) illustrates the differences between Process 2 and Process 3 in terms of  $l_{cTOT}$ . As observed, the values of  $l_{cTOT}$  are reduced up to 28% in Process 3. This is a far more pronounced difference than that shown in Figure 3.9, relative to the comparison between the standard process and Process 1. Furthermore, Figure 3.14b) shows the values of the averaged values of  $\gamma_{rMIN}$  over the passes for the two processes. In this case, the higher  $NoP$  reduces the engagement duration. On the other hand, high values of  $h_{MAX}$  increase  $f_A$ , causing an opposite effect. Nevertheless, the figure shows that the higher  $NoP$  has a predominant effect, leading to a significant improvement in the averaged values of  $\gamma_{rMIN}$  of Process 3 with respect to Process 2. In this regard, Figure 3.14c) and d) respectively show the values of  $\gamma_{rMIN}$  of all the passes of Process 2 and Process 3. As observed, excluding the finishing pass, which is the same for the two processes, each pass in Process 3 operates with higher  $\gamma_{rMIN}$ , resulting in a reduced load on the tool profile.



### 3 Process optimisation based on the proposed numerical model

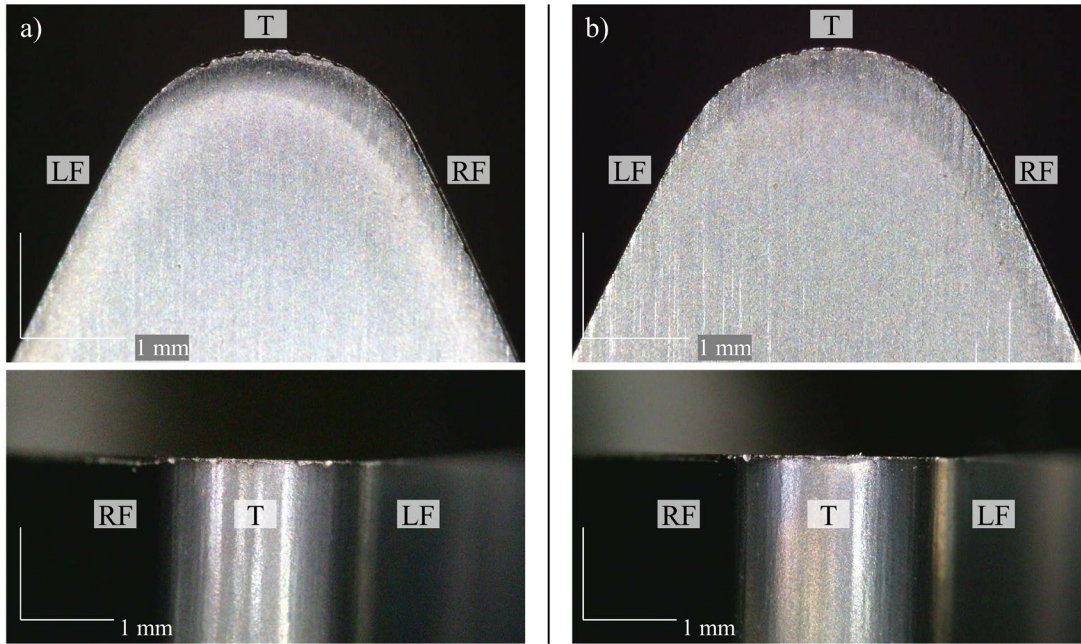


**Figure 3.15.** Tool wear from the rake face and the tip view, after machining: a) 50 workpieces with Process 2; b) 70 workpieces with Process 3).

In light of what shown in Figure 3.14, a significant difference in terms of wear is expected. Given the substantial reduction in the cumulative total machined cutting length, a cutting trial is conducted for the two processes by machining a different number of workpieces  $NoW$  based on the simulated values of  $l_{cTOT}$ . Referring to Figure 3.14a), with Process 2, the machined  $l_{cTOT}$  per workpiece is 34m, while with Process 3 the  $l_{cTOT}$  per workpiece is 24 m. Therefore, 50 workpieces are machined using Process 2, and 70 workpieces using Process 3, which gives the same result in terms of  $l_{cTOT} \cdot NoW$ . The resulting tool wear is shown in Figure 3.15.

From the comparison between the worn tool used in Process 2, shown in Figure 3.15a) and the tool used in Process 3, shown in Figure 3.15b), it emerges that the tool of Process 3 is slightly less worn. The difference is thin, but it can be seen that the tool of Process 3 has less cracks at the tip. This, happens, despite the tool of Process 3 has machined 20 workpieces more than the tool of Process 2. Such difference is attributed to the improved values of  $\gamma_{rMIN}$  shown in the comparison of Figure 3.14c) and d) for the two processes.

Finally, a last cutting trial is conducted, to compare Process 2 and Process 3 when machining the same number of workpieces. Figure 3.16a) and b) shows the tool wear relative to Process 2 and 3 respectively, after machining 70 gears. As it can be seen due to the reduced  $l_{cTOT}$  and the improved values of the working minimum rake angle shown in Figure 3.14, the tool of Process 3 wears significantly less.

It is noteworthy that, as anticipated earlier, by comparing the wear in Figure 3.15a) corresponding to Process 2 with the tool wear in Figure 3.10a) relative to the standard process, it can be observed that the higher cutting speed, with all other parameters being equal, do not worsen the tool wear. On the contrary, the tool of Process 2 results slightly less worn respect to that used in the standard process. As mentioned, this type of phenomenon is not captured by the geometric model presented and the optimal cutting velocity must be determined by trial and error, as in this case. After this finding, also the Process 2 of case study 1 has been employed at increased cutting velocity showing the same good results and a reduced cycle time.

From the reported experiments, the advantages of the proposed cutting strategy have been observed at both the cutting speed employed, namely  $v_c=80 \left[ \frac{m}{min} \right]$  for the standard process and Process 1 and  $v_c=120 \left[ \frac{m}{min} \right]$  for Process 2 and Process 3. In addition, it has proved effective for

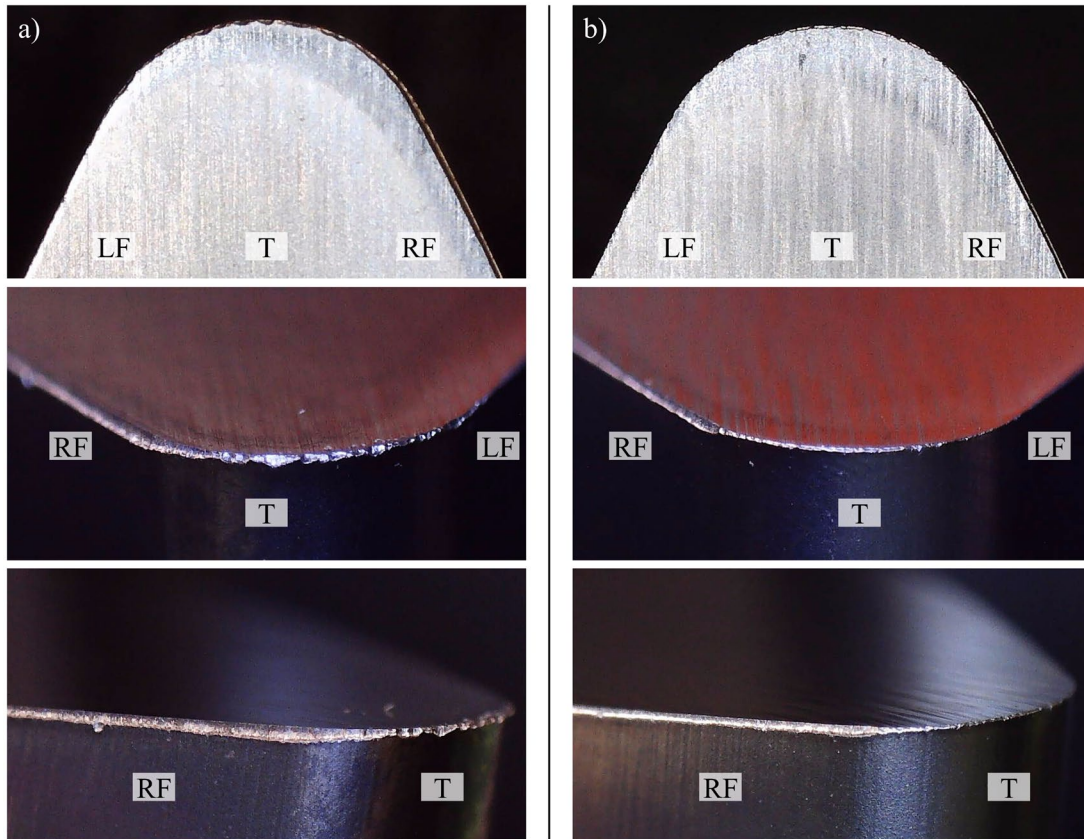


**Figure 3.16.** Tool wear from the rake face, the tip, and the flank view, after machining: a) 70 workpieces with Process 2; b) 70 workpieces with Process 3).

both the geometries relative to the two case studies 1 and 2. This suggests the effectiveness of the proposed cutting strategy which is based purely on geometrical considerations.

### 3.3 Application 2: on the implications resulting from re-sharpening of conical skiving tools

In this section, a second application of the devised numerical model is presented. Specifically, the implications that the re-sharpening of conical tools has on cutting conditions are addressed.

As discussed in Paragraph 1.2.2, skiving tools can be distinguished in conical and cylindrical tools. The latter have the advantage of preserving the tool profile shape with re-sharpening. However, they also entail drawbacks. Indeed, especially with workpieces that allow small cross-axis angle, the design of interference free cylindrical tools which rely uniquely on their off-centred position, may become highly challenging. Additionally, conical tools require machine tools able to handle the complexities related to the off-centred skiving process.

Conical tools on the other hand, having a constructive clearance angle, more easily allow interference avoidance with the flanks of the machined gear. However, due to their constructive clearance angle, as explained in Paragraph 2.2.3, they inevitably entail a change in their cutting profile shape with re-sharpening. In particular, referring to Figure 2.5, if the change of tool profile caused by re-sharpening is significant, the cutting conditions between the tool start of life (SOL) and the tool end of life (EOL) may undergo substantial alterations. This may potentially lead to drawbacks in terms of tool performances, which, as in the previous section, are assessed in terms of tool wear per number of machined parts.

Since conical tools are currently the most widely used for gear skiving, their cutting profile change represents a significant issue in the industrial field. Despite the problem has been documented in the literature [11,78], to date it has not yet been adequately addressed.

The content of this section, represents the extended version of what was presented in [58] as part of the contributions of this doctoral work. In the following, firstly, the geometric parameters of tools most sensitive to the cutting profiles change as a result of re-sharpening are identified. Then, with the aid of the proposed numerical program, simulations and the relative experiments are carried out on two case studies. This allows to assess to which extent the cutting performances, evaluated in terms of tool wear, may be affected by the change of cutting profile caused by re-sharpening. Finally, by using the novel implications introduced in Section 3.1, a novel cutting strategy to homogenise the differences in cutting performances between the tool at SOL and the tool at the EOL of one case study is presented.

### 3.3.1 Parameters of the most sensitive tools to the cutting profile change as a result of re-sharpening

In the following, knowledge regarding the theoretical calculation procedure of a conical skiving tool is assumed, for which reference can be made to Paragraph 2.2.3.

From the theory of gearing [92], the profile shift coefficient  $x_G$  of a gear gap profile generated by its rack can be defined as follows:

$$x_G = \frac{e}{m_n} \tag{3.1}$$

where  $e$  is the displacement of the rack relative to the pitch diameter of the generated gear profile and  $m_n$  is the normal module of the rack. Considering the calculation method of a skiving tool profile, it is possible to think of the generating gear as the rack that defines the skiving tool profile. Therefore, the variation in centre distance that produces the tool conicity is equivalent to apply a profile shift coefficient  $x_T$  with the generating gear which acts as the rack to the skiving tool profile being generated. As a result, referring to Figure 2.5 and considering Eq. 2.7, Eq. 3.1 may be rewritten for the tool as:

$$x_T = \frac{\sum_{i=1}^n h_s(i) \cdot \tan(\alpha_{c0})}{m_n} \tag{3.2}$$

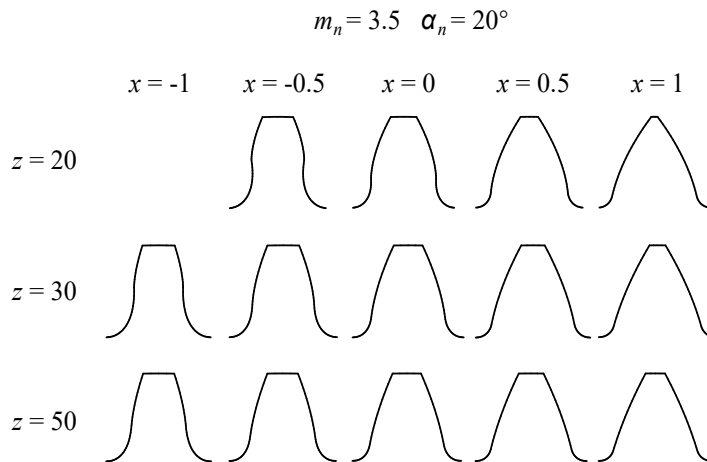
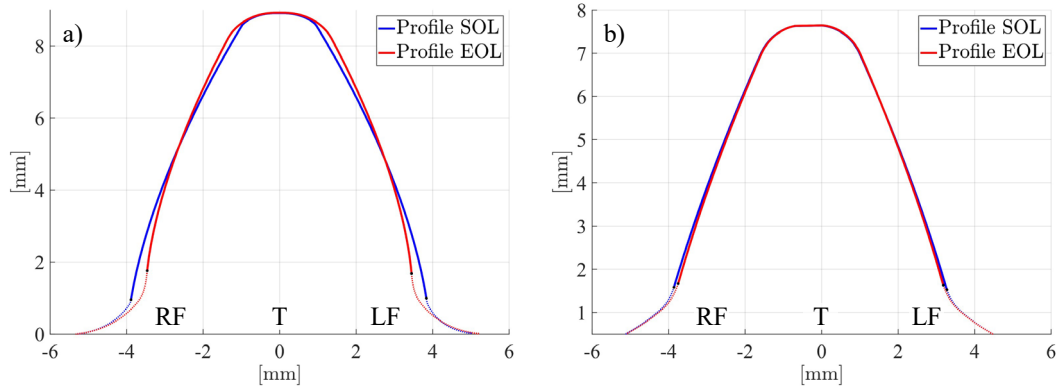


Figure 3.17. Effect of the profile shift coefficient on gears with different number of teeth.

### 3.3 Application 2: on the implications resulting from re-sharpening of conical skiving tools



**Figure 3.18.** Tool cutting profile at the SOL and at the EOL: a) of tool 1; b) of tool 2.

where  $n$  is the number of re-sharpening step  $h_s$ . During the tool profile calculation, the generating gear is brought closer to the tool profile with the increase of the re-sharpening depth. Hence, the tool profile shift coefficient  $x_T$  of Eq. 3.2 decreases at each re-sharpening step from the tool SOL to its EOL.

Also, from Eq. 3.2, it emerges that for the same re-sharpening depth and clearance angle, tools with a lower normal module experience a higher variation of profile shift coefficient during their service life. In addition, it is known from the theory of gearing that gears with a low number of teeth change the shape more significantly for the same amount of profile shift coefficient, as shown in Figure 3.17. It can therefore be concluded that conical tools with a few teeth and smaller normal module are those whose profile changes the most between the tool SOL and EOL.

For commercial reasons, tool manufacturers try to guarantee a usable tool height of about 5-20 mm. Then, during the tool design phase, a value for the constructive clearance angle  $\alpha_{c0}$  in the range of  $2^\circ$ - $10^\circ$  that allows collision avoidance is chosen. As a result, it is not rare in practice to find tools with the highlighted geometric features, i.e. few teeth and a small normal module, that undergo a considerable variation in the cutting profile shape during their service life.

Interestingly, in a recent study [14], it has been shown through experiments that a skiving tool with a reduced profile shift coefficient may perform better. According to this, conical tools should perform better at the EOL with respect to the SOL.

#### 3.3.2 Simulation of cutting profile change based on the proposed numerical model

In this paragraph the numerical model presented in this work, is used to compute the tool cutting profile at the SOL and EOL of two types of tools taken from the company shopfloor. Two case studies are then investigated. In each case study one type of tool, i.e. tool 1 and tool 2, at two re-sharpening stage, the SOL and the EOL, respectively, is used. The tools data for each case study are reported in Table 3.6.

In Figure 3.18a), the simulated profiles at the SOL and at the EOL of tool 1, are represented with a blue and red line respectively. The tool profile portions towards the root diameter have been represented in dashed line since they are merely a fitting and do not effectively participate in cutting the workpiece.

From the figure, the cutting profile of tool 1 undergoes a significant change on its shape during its service life. This is due to the fact that tool 1 has a large clearance angle which, despite the normal module not being particularly small, results in a variation of the profile shift coefficient of 0.5 over the service life. Referring to Figure 3.17, such variation is significant for a pinion with 31 teeth and so it is also for tool 1.

Photographs of the real tool 1 at the SOL and at the EOL are shown in Figure 3.19a) and b), respectively. The effect of the bigger profile shift coefficient at the SOL which yields a tooth



### 3 Process optimisation based on the proposed numerical model

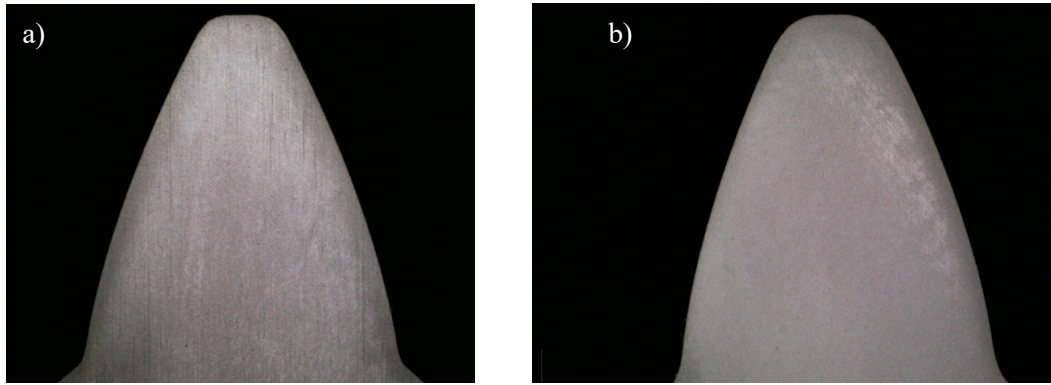


**Figure 3.19.** Cutting profile of tool 1: a) at the SOL; b) at the EOL.

thicker at the base and more tapered at the tip can clearly be observed. Furthermore, referring to Figure 3.18a), when the tool is at the EOL it has a smaller active area of the cutting profile. Such features make a significant difference in tool performances as shown in the following paragraph.

In Figure 3.18 b) the simulated profiles of tool 2 are shown. As it can be noticed, in this case the change in cutting profile between the SOL and the EOL is not relevant. Compared to tool 1, the tool 2 has a smaller clearance angle. Therefore, tool 2 undergoes a smaller variation in the profile shift coefficient, which amounts to 0.3. However, the main difference with respect to tool 1 is that tool 2 has 52 teeth, which makes it less sensitive to the effect of the profile shift coefficient as shown in Figure 3.17.

**Table 3.6.** Geometrical data of tool 1, tool 2, and the gear they machine.

Data	Tool 1	Gear 1	Tool 2	Gear 2
Normal module $m_n$ [mm]	3.5	3.5	3.5	3.5
Normal pressure angle $\alpha_n$ [deg]	20	20	20	20
Number of teeth	31	-67	52	-78
Helix angle [deg]	20 RH	Spur	20 RH	Spur
Tip diameter [mm]	126	227.2	204.5	272.5
Root diameter [mm]	109.6	243.2	189.2	285.7
Tool usable height / gear width [mm]	10	76	10	49
Profile shift coefficient (SOL / EOL)	0.5 / 0	0.03	0.85 / 0.55	-0.62
Constructive Rake angle [deg]	5	-	5	-
Constructive clearance angle [deg]	8.5	-	5	-
Constructive step angle [deg]	20	-	20	-
Material	S390	31CrMoV9	S390	40CrMo4
Coating	AlCrN	-	AlCrN	-

#### 3.3.3 Benchmarking procedure

For a skiving operation, the same set-up parameters, such as number of passes, axial feeds and cutting speeds, are computed by the machine tool, and used regardless of the re-sharpening stage of the tool. As a result, when a skiving tool, undergoes a considerable variation in the cutting profile shape between the SOL and the EOL, it yields sub-optimal tool performances.

In what follows, Case study 1 and Case study 2 relative to tool 1 and tool 2, respectively, are investigated. For each case study, two process simulations, one with the tool at the SOL and one at the EOL are carried out with the numerical program. Then within each case study, the simulations results are compared.



### 3.3 Application 2: on the implications resulting from re-sharpening of conical skiving tools

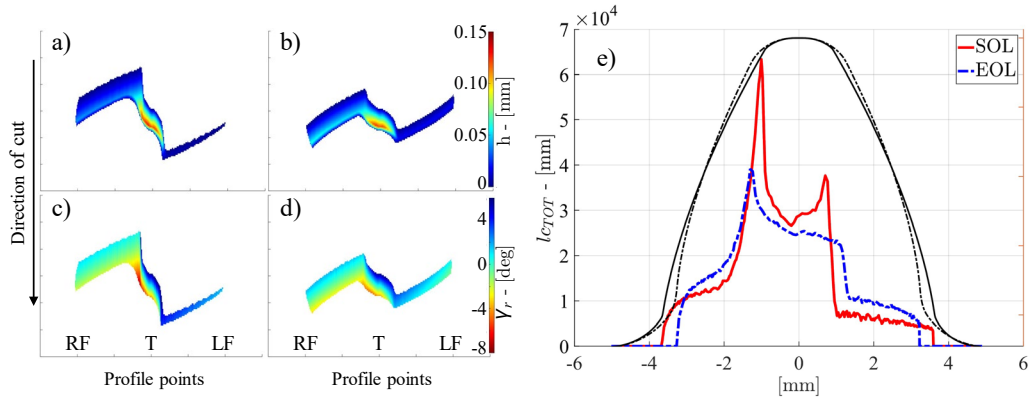


**Figure 3.20.** Comparison of working parameters of tool 1 at SOL (left side) and EOL (right side): a) – b) working chip thickness of pass n° 15; c) – d) working rake angle of pass n° 15; e) cumulative machined total cutting length  $l_{cTOT}$ .

In addition, the corresponding process experiments are conducted to assess the validity of the simulation results. For each case study the same number of workpieces is machined with the tool at the SOL and that at the EOL. The process parameters related to each case study are reported in Table 3.7. The table shows that the number of parts machined as well as the process parameters, are different for the two case studies. This is due not only to the fact that tool 1 and tool 2 are different in design, but also because the machined parts have different geometries and are made of different materials (Table 3.6). Specifically, the workpiece material of Case study 1 contains Vanadium an alloying element that is known for making machining challenging.

Therefore, it is important to bear in mind that the following analysis is not intended to compare the performances of tool 1 with those of tool 2, but to compare in each case study the performances of the tool at the SOL and at the EOL.

**Table 3.7.** Process data of the two case studies.

Data	Case study 1	Case study 1 new process	Case study 2
$NoP$	23	14	13
$h_{MAX}$ [mm]	0.15	0.12	0.15
Cross-axis angle $\Sigma$ [deg]	20	20	20
Cutting velocity [m/min]	60	60	80
Cooling	Oil	Oil	Oil
N° of machined parts	30	30-38	50
Cycle time $t$ [min sec]	21' 40''	20' 11''	5' 08''

#### 3.3.4 Comparison of cutting performances between SOL and EOL: Case study 1

As it was shown in Figure 3.18a) and Figure 3.19, the tool 1 of Cases study 1, undergoes a significant change in its cutting profile between its SOL and EOL. Therefore, it is natural to also expect differences on the cutting conditions. The process data employed are those of the first column of Table 3.7.

Some relevant results of the two simulations for the tool at SOL and that at the EOL, are shown in Figure 3.20. Particularly, Figure 3.20 a) and c) portray respectively, the values of the working chip thickness and of the working rake angle, relative to the tool at SOL for the process pass n° 15. Figure 3.20 c) and d) instead, show the same working parameters, respectively, for the tool at EOL at the same pass. From the figures, several differences on the cutting conditions between

### 3 Process optimisation based on the proposed numerical model

the tool at the SOL and at the EOL can be observed. The tool at the SOL cuts with its tip a larger maximum chip thickness than the tool at the EOL. Also, comparing the working rake angle values the smallest minimum rake angle is reached by the tool tip relative to the SOL.

Such a difference could be explained by analysing the implications that the value of the tool tip diameter at the SOL has on the operating tool pitch diameter of each pass and compare them to the tool at the EOL. This topic will be taken up in Chapter 4. For now, it can be stated the following.

Due both to the bigger tool tip diameter and to the different cutting trajectory it yields, the tool at the SOL begins earlier and ends later to cut the gear gap, resulting in a longer engagement of each pass. This, in turn, as explained in Paragraph 2.2.8, translates in a bigger  $l_{cSING}$  of each pass and in the observed lower values of working rake angle. In addition, referring to Figure 3.20a) and c), it may be observed that when the cutting profile points are close to the highest localised load conditions, namely when the chip thickness reaches its maximum and the rake angle its minimum, the tool at the SOL only works with a limited portion of the tip profile. Also, such a critical condition is maintained for longer in the direction of cut. This can be observed by comparing the longer shape of the engagement points at the tool tip along the direction of cut of Figure 3.20a) and c) with respect to Figure 3.20b) and d).

In contrast, the tool at the EOL works with a larger portion of the tip profile. Furthermore, due both to the smaller tip diameter and to the different cutting trajectory it yields, the tool at the EOL remains in engagement for less cutting positions, hence working with more positive values of  $\gamma_r$  and smaller values of  $l_{cSING}$ .

For an overall view of the process, the comparison between the cumulative machined total cutting length  $l_{cTOT}$  relative to all the passes, cut by the profile at the SOL and at the EOL is

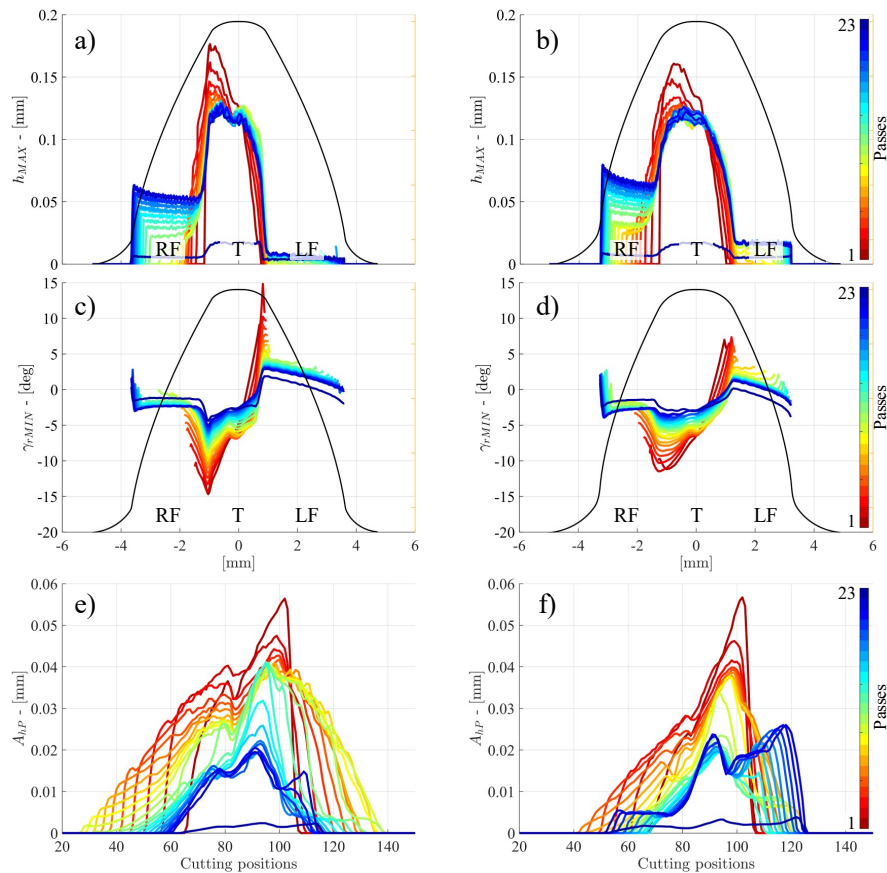


**Figure 3.21.** Comparison of working parameters of tool 1 at SOL (left side) and at EOL (right side) for all the process passes: a) – b) values of  $h_{MAX}$ ; c) - d) values of  $\gamma_{rMIN}$ ; e) – f) values of  $A_{hP}$ .

### 3.3 Application 2: on the implications resulting from re-sharpening of conical skiving tools

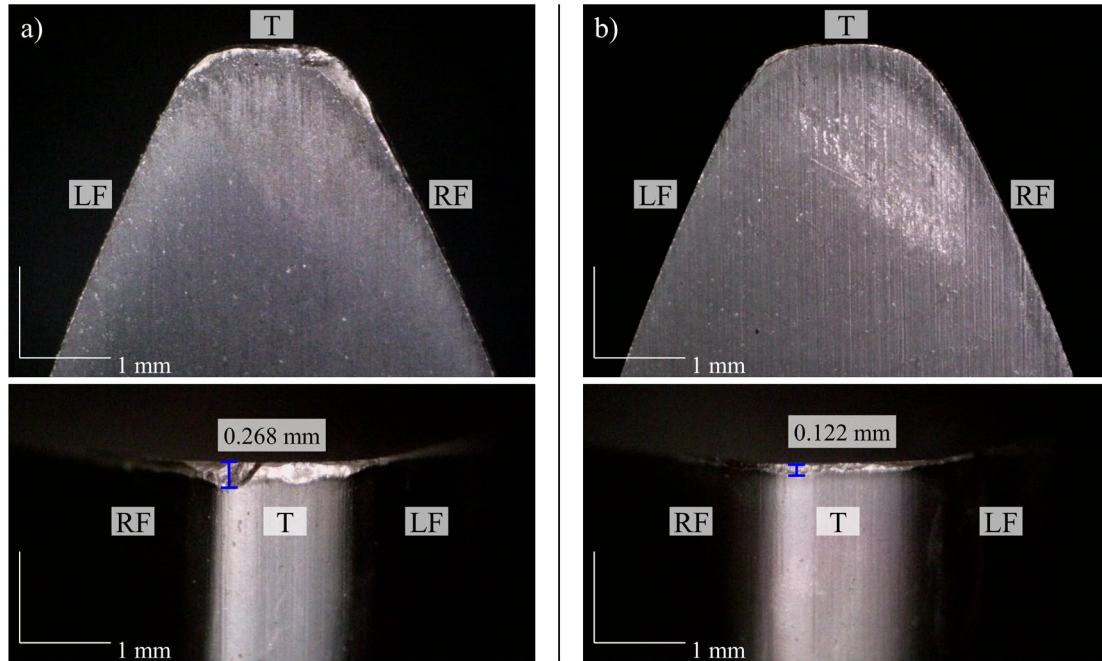


**Figure 3.22.** Tool wear from the rake face and the tip view, after machining 30 workpieces with: a) the tool at the SOL; b) the tool at the EOL.

shown in Figure 3.20e), in red and blue, respectively. Also, the two tool profiles have been reported in the figure. The tool at SOL is depicted in continuous line, while that at the EOL in dashed line. The portion of the cutting profile that machines most material is the right radius of the tip. Remarkably, the tool at SOL machines about 60% more material with respect to the tool at EOL in the corresponding profile portion. Recalling Eq. 2.24, such a marked difference in  $l_{cTOT}$  is caused by the difference of  $l_{cSING}$  between the tool at the SOL and the tool at the EOL, discussed above. Indeed, the two tools employ the same values of axial feed and the  $NoC$  of each pass is the same.

The bigger values of machined  $l_{cTOT}$  along with the longer permanence at high localised load conditions are expected to yield a significant difference in how the tool at the SOL wears compared to that at the EOL.

It should be remarked, that pass n° 15 reported in Figure 3.20, yields nothing special compared to other passes. The behaviour discussed above may be observed in all 23 passes of the process. To show this, reference can be made to Figure 3.21. The figure shows a comparison of the simulated values, for all the passes, of the maximum chip thickness  $h_{MAX}$ , the minimum working rake angle  $\gamma_{rMIN}$  and the working normalised chip area  $A_{hP}$ . The values relative to the tool at the SOL, are shown respectively in Figures 3.21 a), c) and e) whereas those for the tool at the EOL in Figures 3.21 b), d) and f).

By comparing the values of  $h_{MAX}$  and  $\gamma_{rMIN}$  it may be noticed that especially at the first passes there is a remarkable difference, with the tool at the SOL working in more critical cutting conditions. Additionally, comparing the values of  $A_{hP}$  a significant discrepancy can be observed. This may be associated to higher loads per length of tool profile during each pass for the tool at SOL with respect to the tool at EOL.

It is worth noting that the simulation results of the present case study are in accordance with the experiment shown in [14]; i.e. a tool with lower profile shift coefficient, in this case the tool 1 at the EOL, have reduced length of cut, smaller maximum chip thickness and bigger minimum values of rake angle. In Chapter 4, this topic will be taken up when addressing the implications on cutting conditions of the selection of the tool tip diameter value. Specifically, from the study

### 3 Process optimisation based on the proposed numerical model

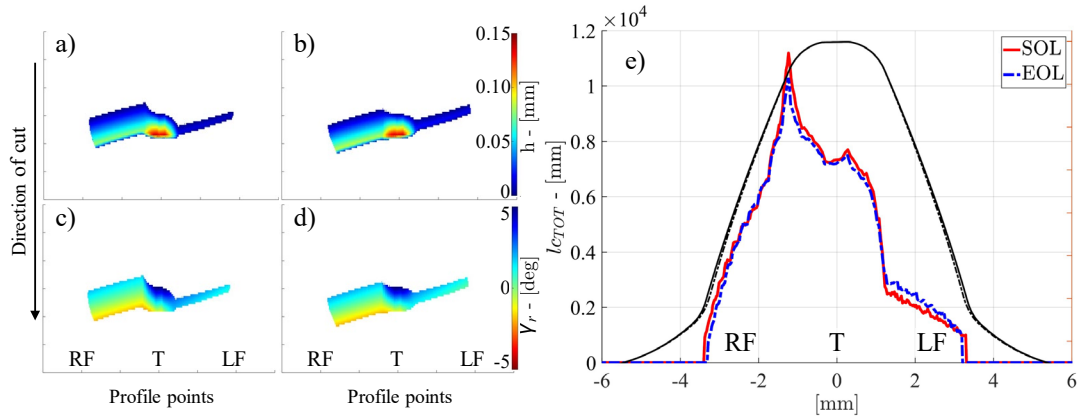


**Figure 3.23.** Comparison of working parameters of tool 2 at SOL (left side) and EOL (right side): a) – b) working chip thickness of pass n° 9; c) – d) working rake angle of pass n° 9; e) cumulative machined total cutting length  $l_{cTOT}$ .

proposed in the next chapter, it can be anticipated that a significant role is played by the implications that tool tip diameter has on the operating pitch diameter of the tool while machining. This relationship influences the cutting trajectory of each pass and heavily affects the cutting conditions.

In order to assess the validity of the simulation results, experiments for case study 1 are carried out. Figure 3.22 reports the wear conditions of the rake face and the tip for tool 1 at both the SOL (Figure 3.22a) and at the EOL (Figure 3.22b), after machining 30 workpieces. The cutting profile portions, right flank (RF), tip (T), and left flank (LF) are also reported in the figure. As observed also in the previous experiments, the tip results the most worn profile part, which is typical of the skiving process. Specifically, the right radius of the tip is highly worn. Indeed, according to the simulation results of Figure 3.21, it is the most highly loaded portion of the profile, and it is the one which machine most material.

Notably, there is a marked difference in the amount of wear on the rake face as well as on the tip for the tool at the SOL with respect to the EOL. Specifically, the tool at the SOL results to be twice as worn compared to the one at the EOL, despite having machined both 30 workpieces with the same process parameters. The experiment has been repeated several times producing the same results.

The experiment outcomes suggest the correctness of the simulation results and are in line with what was observed in Paragraph 3.3.2, i.e. tool 1 is subject to a significant change in the shape of its profile during its service life which leads to significant differences on cutting performances.

Recalling the discussion at the beginning of Section 3.2, two main scenarios arise when analysing tool wear at the company shop floor. The first scenario, in which the tool profile wears rather homogeneously and loses its sharpness, has been shown in the previous section where a novel cutting strategy to reduce this type of wear has been presented.

However, by observing Figure 3.22a), the wear distribution is far from being homogeneous. From the discussion above, the key factors causing this phenomenon are attributed to  $h_{MAX}$ ,  $\gamma_{rMIN}$  and  $l_{cTOT}$ . Indeed, the tool presents cracks and craters along the profile, which are associated to high localised load given by the extreme values of  $h_{MAX}$ ,  $\gamma_{rMIN}$ . Additionally, the exceptionally high values of  $l_{cTOT}$  contributes in terms of abrasive wear. After Case study 2 is addressed, a novel cutting strategy to homogenise such type of wear is presented based on the implications derived in Section 3.1.

#### 3.3.5 Comparison of cutting performances between SOL and EOL: Case study 2

In Case Study 2 the tool exhibits minimal changes of profile shape throughout its service life (Figure 3.18b). As mentioned, this is attributed to a smaller variation in the profile shift coefficient

### 3.3 Application 2: on the implications resulting from re-sharpening of conical skiving tools

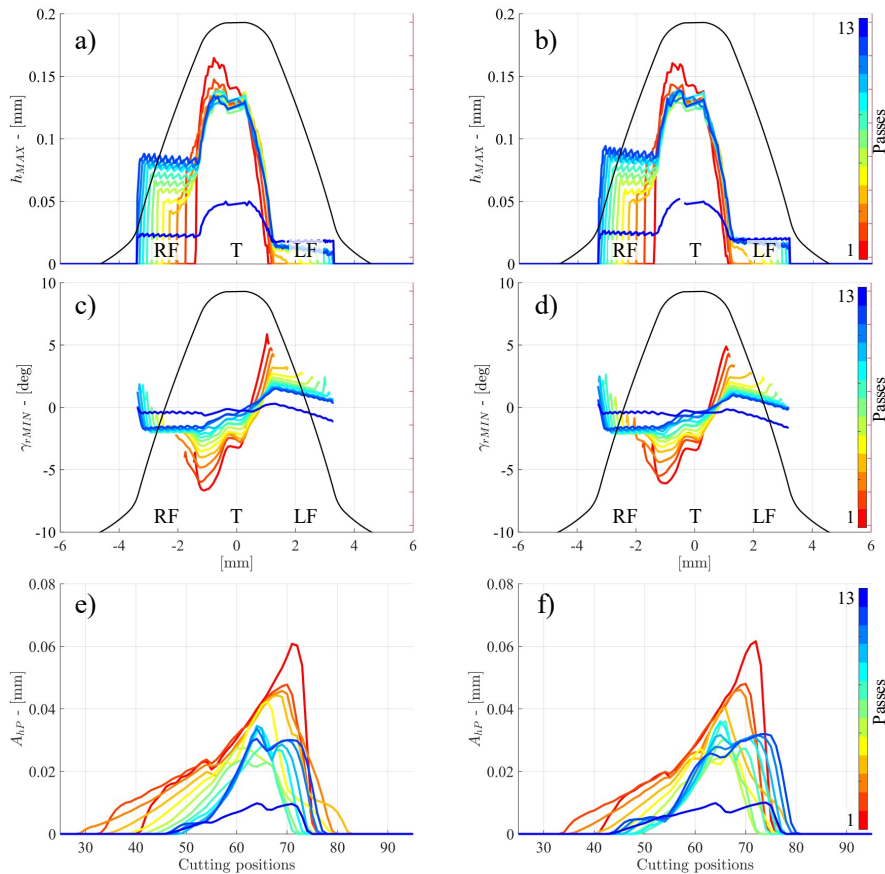


**Figure 3.24.** Comparison of working parameters of tool 2 at SOL (left side) and at EOL (right side) for all the process passes: a) – b) values of  $h_{MAX}$ ; c) - d) values of  $\gamma_{rMIN}$ ; e) – f) values of  $A_{hP}$ .

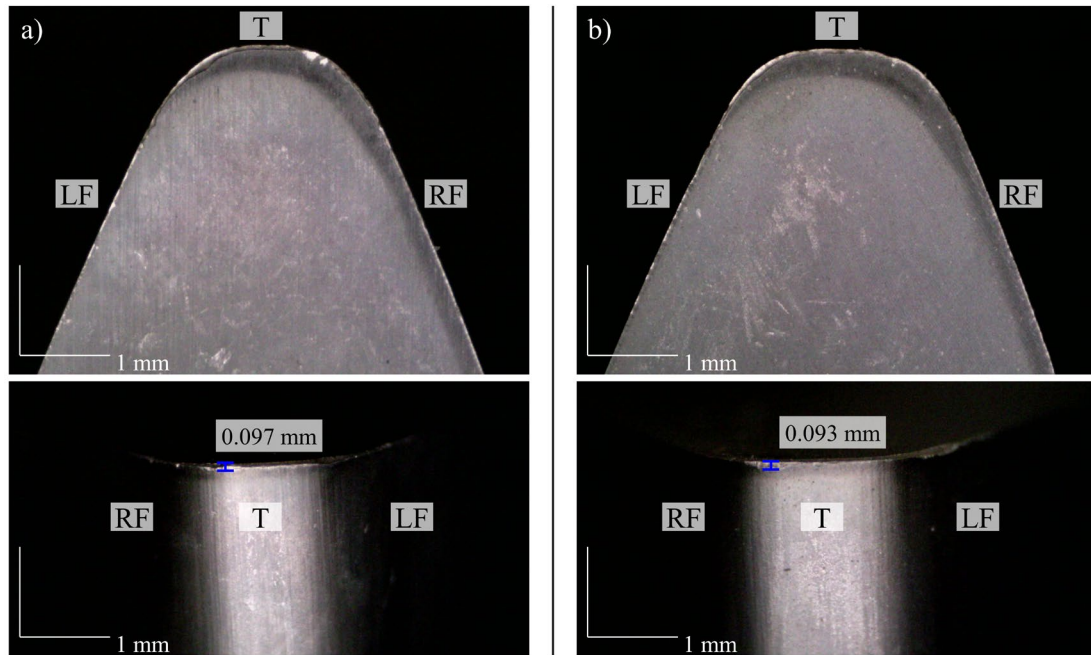
but primarily to the tool high number of teeth. As a result, the cutting conditions are expected to not vary significantly from SOL to EOL. The process data employed are shown in the third column of Table 3.7.

Figure 3.23 confirms the prediction. Specifically, Figures 3.23a) and c) portray respectively, the values of the working chip thickness and of the working rake angle, relative to the tool at SOL for the process pass n° 9. Figures 3.20 c) and d) on the other hand, show the same working parameters, respectively, for the tool at EOL at the same pass. From the figures, no substantial differences can be spotted. Also, by comparing the values of the cumulative machined total cutting length  $l_{cTOT}$ , for the tool at the SOL and at the EOL, portrayed in Figure 3.23e), there is no remarkable difference.

As it was for Case study 1, the pass n° 9 yields nothing special compared to other passes. By observing the simulation results relative to the whole process, of  $h_{MAX}$ ,  $\gamma_{rMIN}$  and  $A_{hP}$ , no appreciable difference can be spotted between the tool at SOL and at the EOL. For the sake of completeness these results are shown respectively in Figures 3.24 a), c), e) for the tool at the SOL and in Figures 3.24b), d) f) for that at the EOL.

Figure 3.25 shows the wear conditions of the rake face and of the tip for tool 2, after machining 50 workpieces, for both the tool at the SOL (Figure 3.25a) and at the EOL (Figure 3.25b). Overall, the wear is distributed rather evenly over the tip and, there are no substantial differences in the way the tool has worn at the SOL compared to the EOL. This is both in accordance with the simulation results and to what observed in Paragraph 3.3.1, i.e. the cutting profile of tool 2 does not change significantly during its service life and consequently neither do the cutting performances. Hence differently from Case study 1, there is no need to balance the cutting conditions of the tool 2, depending on its re-sharpening stage.





**Figure 3.25.** Tool wear from the rake face and the tip view, after machining 30 workpieces with: a) the tool at the SOL; b) the tool at the EOL.

### 3.3.6 Homogenisations of cutting performances between SOL and EOL: Case study 1

The aim of this paragraph is to propose a cutting strategy to homogenize the cutting performances, between the tool at the SOL and the tool at the EOL of Case study 1.

In general, a significant difference in the level of tool wear between tools of the same type at the SOL and at the EOL can cause issues in the production of large batches since tools should be replaced at different times to avoid failures. Specifically, for Case study 1, the tool at the SOL operates in worse cutting conditions respect to the tool at the EOL and it wears twice as much. If the upper limit for tool replacement is determined by the tool at SOL, the full potential of the tool at the EOL is not utilized, leading to premature tool substitution. Conversely, by using the tool at EOL as a reference, there is a risk of causing excessive damage to the tool at SOL (Figure 3.22a).

Since tool 1 has significantly different profile shapes depending on the re-sharpening stage (Figure 3.18a), it is convenient to consider tool 1 at the SOL as a different tool design respect to tool 1 when at the EOL. Therefore, the tool at the SOL should be operated with a different cutting strategy with respect to the tool at the EOL.

At a first thought, to improve the performances of the tool at the SOL, it may be thought to apply the novel cutting strategy presented in Section 3.2. By doing so the value of  $h_{MAX}$  should be increased as well that of  $NoP$  in order to yield a reduction in  $l_{cTOT}$  for the same cycle time and similar load conditions. Furthermore, the values of  $\gamma_{rMIN}$  would also increase. However, to balance the difference of  $l_{cTOT}$  shown in Figure 3.20e), would require an increase of  $h_{MAX}$  up to more than 0.40 mm. Such values of  $h_{MAX}$  cannot be tolerated by the tool at the SOL since as it is visible from the craters of Figure 3.22a) it suffers already from too high localised load.

Therefore, using the simulation model a different and novel cutting strategy is devised. Specifically, in order to reduce the high localised load condition at the tip, the nominal maximum chip thickness is reduced from 0.15 mm to 0.12 mm. However, a reduction of nominal chip thickness also reduces the value of the axial feed, increasing the  $NoC$  of each pass and consequently also the value of  $l_{cTOT}$  which is already high. Additionally, the cycle time would also rise. Therefore, in the new process, the  $NoP$  is also reduced from 23 to 14. By doing so, the

### 3.3 Application 2: on the implications resulting from re-sharpening of conical skiving tools

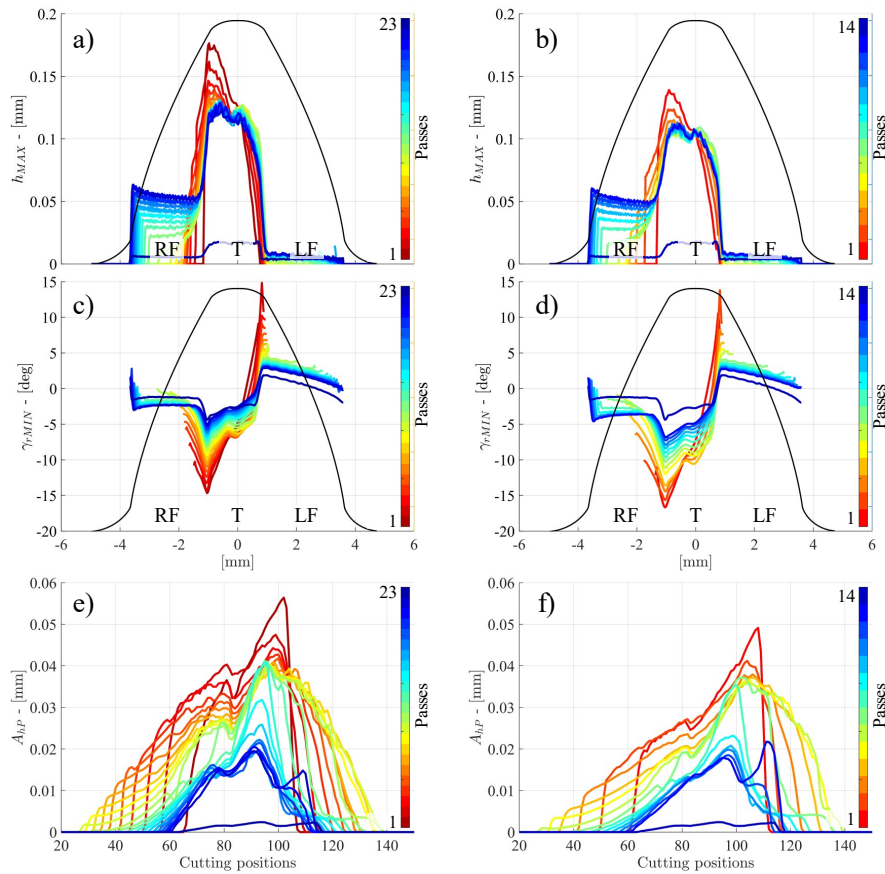


**Figure 3.26.** Comparison of working parameters of tool 1 at SOL with the standard process (left side), and with the new process (right side), for all the process passes: a) – b) values of  $h_{MAX}$ ; c) – d) values of  $\gamma_{rMIN}$ ; e) – f) values of  $A_{hP}$ .

value of  $l_{cTOT}$  remains approximately the same and the localised load on the profile points should decrease. The data relative to the new process employed with tool 1 at SOL are shown in the second column of Table 3.7. It can be seen that the cycle time has been reduced of more than 1 minute.

In Figure 3.26 the simulated values of  $h_{MAX}$ ,  $\gamma_{rMIN}$  and  $A_{hP}$  are compared between the tool at the SOL employed with the standard process, (Figure 3.26a), c) e) and the tool at the SOL employed with the new process (Figure 3.26b), d) f). As it can be seen, the values of  $h_{MAX}$  have been significantly decreased in the new process. This causes a significant reduction in the localised tool load on the tool profile points. On the other hand, in the new process the lower  $NoP$  causes bigger values of radial infeed of the passes and a longer engagement at each pass which cause a reduction of  $\gamma_{rMIN}$ . However, the loss given by the worsened values of  $\gamma_{rMIN}$  is supposed to be minor than the gain obtained with the reduced values of  $h_{MAX}$ . Observing the values of  $A_{hP}$ , the load per profile length has remained approximately the same for the two strategies.

For what concern the cumulative machined total cutting length, in Figure 3.27a) the values of  $l_{cTOT}$  relative to the standard process are compared to those relative to the new process. As aimed, the values have been kept on the same level.

With the new process, the tool at SOL maintains its inherently non-uniformity in the amount of material machined by the tip on the right radius. However, the localised load with which it operates is expected to be significantly reduced. In Figure 3.27b) are compared the values of working chip thickness relative to homologous passes for the two process. Being the  $NoP$  different

### 3 Process optimisation based on the proposed numerical model

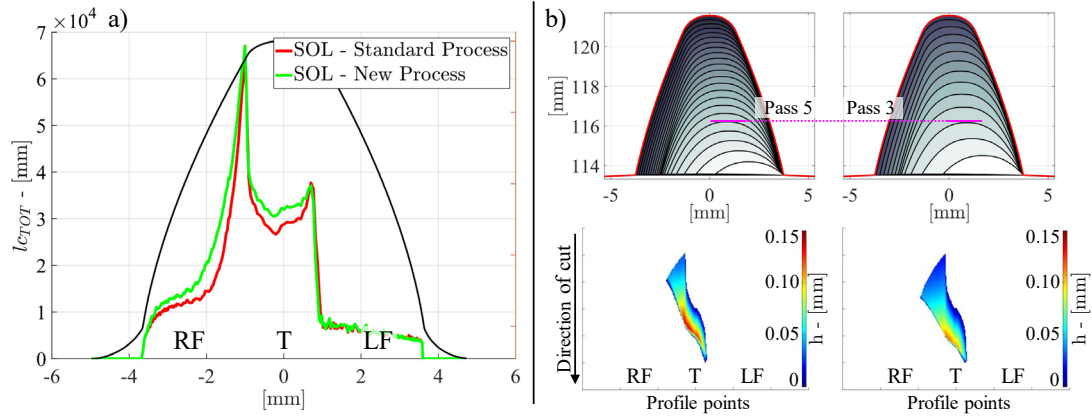


**Figure 3.27.** a) Comparison of the values of machined  $l_{COT}$  using the tool at the SOL with the standard process and with the new process; b) comparison of the working chip thickness machined by the tool at the SOL, during two different passes with same radial infeed relative to the two compared processes.

for the two considered process, pass n° 5 of the standard process has the same radial infeed of pass n° 3 of the new process, as shown in the figure. Observing the values of the working chip thickness machined by the right radius of the tip it can be seen that the values relative to the new process are significantly reduced.

To prove the effectiveness of the new cutting strategy, two trials have been carried out using the tool at SOL with the new process. In the first and second trial, 30 and 38 workpieces have been respectively machined. The resulting tool wear of the first trial after machining 30 workpieces are shown in Figure 3.28a).

By comparing Figure 3.28a) with Figure 3.22a), relative to the tool at SOL after machining the same number of workpieces, a significant reduction in terms of tool wear can be observed. Moreover, by comparing Figure 3.28a) with Figure 3.22b), it appears that the wear values of the tool at the SOL operated with the new process parameters match those of the tool at the EOL operated with the standard process parameters. From Figure 3.28a) it can be observed that the

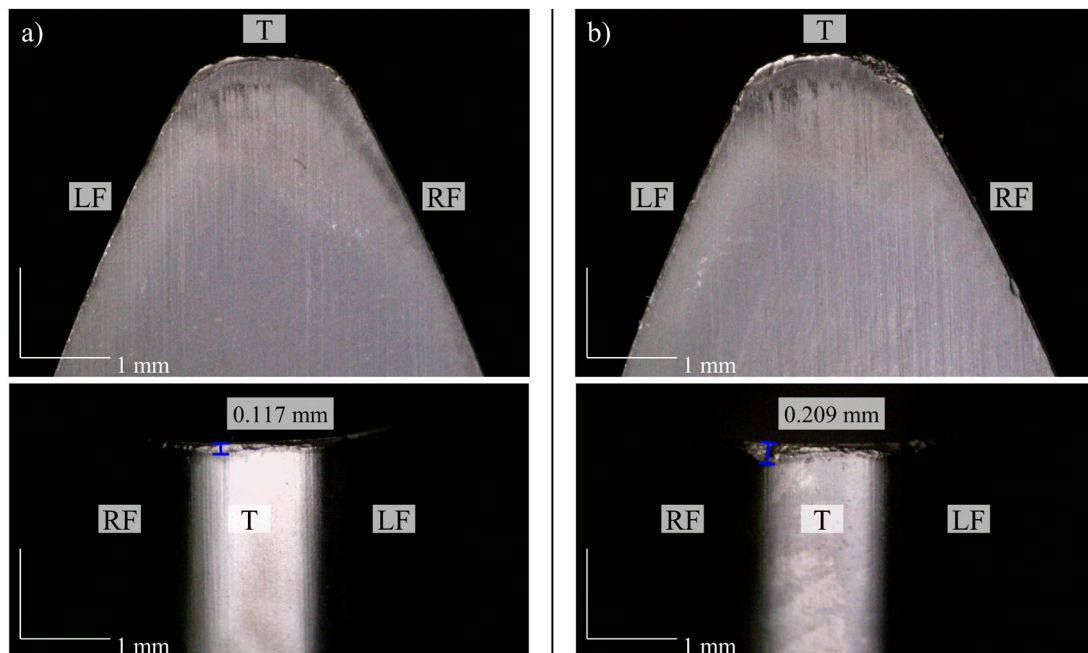


**Figure 3.28.** Tool wear from the rake face and the tip view, after machining: a) 30 workpieces with the tool at SOL using the new process; b) 38 workpieces with the tool at SOL using the new process.



right radius at the tip, in accordance with the simulation, remains the most worn part. However, the wear level has been significantly reduced with respect to the standard process.

For what concern the second cutting trial it can be seen from the comparison between Figure 3.28b) and Figure 3.22a) that with the new process, the tool at SOL can machine about 25% more workpieces with respect to the standard process while wearing less. However, such level of wear is not convenient in terms of a cost-effective re-sharpening and the trial has been used only as a demonstration.

Overall, it can be concluded that by adopting two different sets of process parameters, one for the tool at the SOL and one for the tool at the EOL, the cutting performances may be effectively homogenized.

### 3.4 Conclusions and future perspectives

In this chapter, by using the numerical program presented in Chapter 2, novel implications linking set-up parameters to working parameters were investigated (Section 3.1). Based on the studied implications, novel ad-hoc cutting strategies have been devised to address two distinct applications of the gear skiving process. The rationale employed in both applications is the same, namely reducing tool wear while maintaining the cycle time unchanged or even reduce it.

In the first application, discussed in Section 3.2, it was demonstrated with the aid of the numerical program, that by simultaneously increasing the values of  $h_{MAX}$  and of  $NoP$ , a reduction in terms of  $l_{cTOT}$  could be achieved. This was achieved while either maintaining or reducing the cycle time and by minimally increasing the tool load. Regarding the last point, the parameter  $A_{hP}$  has proved to be crucial (Figure 3.13). Through experiments, the effectiveness of the proposed technique was demonstrated. Specifically, a reduction in terms of tool wear for skiving of annealed steel gears up to 50% was observed in two case studies. The novel cutting strategy proves to be effective for different workpiece geometries and across different cutting speeds.

In future studies, by employing the proposed strategy, through experiments, a limiting value for  $h_{MAX}$  across several cutting speeds may be investigated for major gear materials. Investigating such a relationship depending on the geometry of the tool-workpiece pair, would allow for the definition of simplified charts for devising cutting strategies without requiring numerical simulations. Furthermore, by adding up the values of  $A_{hP}$  considering the tool teeth in engagement with the workpiece at different phases, and also considering the relevant values of the working angles, would allow for new precise models aimed at force and wear prediction.

Regarding the application presented in Section 3.3, this is tied to theoretical aspects concerning the design of skiving tools. Specifically, it has been shown that during the service life, conical tools may undergo a significant change in the cutting profile which affect the cutting performance. For the same usable height and the same clearance angle, conical tools with a small module and few teeth are the most sensitive to the change in cutting profile.

Then, with the aid of the numerical program, two case studies were analysed. In case study 1, a considerable change in the tool cutting profile was observed, whereas in case study 2 the change was negligible. The simulation revealed that for case study 1 with the same process parameters, the tool at the SOL is operated in more severe cutting conditions with respect to the tool at the EOL. To prove the validity of the simulation results, experiments have been conducted for both case studies. In case study 1, for the same number of parts machined, the tool at the SOL wore twice as much than at the EOL. In case study 2 the difference in tool wear between SOL and EOL was negligible.

Considering the marked difference in performance of the tool in case study 1, with the aid of the simulation model and of the implications presented in Section 3.1, a new set of process parameters for the tool at the SOL was proposed. The rationale was to reach similar cutting

### 3 Process optimisation based on the proposed numerical model

conditions to those met at the EOL. The new process parameters have been tested by experiment showing the effectiveness of the new process strategy and of the simulation model.

The idea of using two different process strategies, one for tools toward the SOL and one for tools closer to the EOL, is strongly recommended when the tool is sensitive to major change of the cutting profile. If only one set of process parameters that works well for the tool at the EOL is used, it may lead to poor performances of the tool at the SOL (Figure 3.22a). On the other hand, the new process designed for the tool at the SOL may not be suitable for a tool at the EOL. Indeed, the tool at the EOL features both a reduced thickness at the tooth root and a low usable height, both features that compromise the bending strength of the tool teeth. Since the process parameters proposed for the tool at the SOL may yield higher bending load to the tool due to bigger radial infeed, they may trigger vibrations that may result in low workpiece quality, and eventually to tool breakage in extreme cases.

The presented study is not only significant for the field of gear manufacturing, but also from the perspective of tool design. Indeed, by demonstrating that tool performances can be balanced despite a remarkable change in the profile shape, opens the possibility to design conical skiving tools with longer service life. In future studies a parameter that limits the maximum variation of cutting profile shape during the tool service life depending on tool geometry will be proposed and used for optimal design of conical skiving tools.

Overall, as suggested in [5], adopting a multi-parameter variation has allowed for the discovery of new cutting strategies to enhance the process. The results of the experiments strongly agree with those of the numerical model in all the presented case study of both applications, suggesting its validity.

## 4 Towards a parameter selection method for conical skiving tools

During several trials carried out at the company, it was observed that the main problem causing machining difficulties was frequently rooted in poor tool design. After the development of a numerical program to compute the tool geometry and to carry out the corresponding process simulation, it is natural to wonder how to predict, among all possible tool designs for a given workpiece, which is the most suitable. This is the topic that the last chapter of this work aim to address.

As detailed in the literature review, there are several issues of gear skiving that still need to be explored. Among these, the optimal selection of the tool design parameters still deserves further investigations since they heavily affect the process. Several studies have analysed some of their effects on gear skiving [7,36,39]. However, especially in industrial practice, the choice of the tool design parameters is usually based on practical experience and analytical methods to select them are still lacking in the literature.

A first idea that might be thought of, in order to compare the performances of different tool designs for machining the same workpiece, would be to carry out a simulation for each design. However, even assuming to use geometric simulations such as that shown in this work, the amount of data to be compared would make the procedure too slow and cumbersome.

The objective of this chapter is to outline a novel design methodology that allows, given a workpiece to be machined, the definition of tool design parameters that meet specific cutting conditions and productivity requirements.

The methodology consists in dividing the tool design parameters into two subsets: the tool kinematic parameters, which alter the kinematics of the process, and the tool constructive parameters, which are independent from the former and only affect the cutting conditions.

The idea is to select the tool kinematic parameters by means of qualitative indices representing, respectively, the cutting conditions and the productivity of each tool design. These indices must be computed over a domain of possible tool design parameters, i.e. design parameters relative to actually feasible tools. The indices may be plotted on charts to allow an immediate comparison among all possible tool design in terms of performance and productivity limiting the use of simulation. By selecting the tool kinematic parameters with the proposed methodology, the tool macro-geometry would be established. Then, by fine-tuning the tool constructive parameters with the aid of simulation, the micro geometry of the selected tool can also be determined.

It must be remarked that this chapter does not delve into each point of the methodology, which is still under investigation. Some sections are discussed in depth, while others are only briefly summarised.

The methodology outlined is considered highly relevant. It represents a novelty in the gear skiving arena in both the selection method for the tool design parameters and the kinematic concepts it is based on. It lays foundation on screw theory, which is widely used in the literature related to gear design [89,104–107]. However, apart from a previous publication conducted as part of the contribution of this PhD [74], that this chapter aims to expand and rectify, screw theory has not been exploited in the study of gear skiving.

The main advantages of using the proposed approach are that the resulting tool design can fulfil specific performances, both in terms of productivity and of cutting conditions to be met, that a parameter selection based on practical experience cannot consider. Furthermore, this method is time-efficient, avoiding extensive simulations and their subsequent post-processing for comparison. Instead, it enables the graphical visualization and summarized presentation of the performance of the different possible tool design.

The chapter is structured as follows. Section 4.1 recalls the tool design parameters and introduces the rationale by which these are classified as well as their relevance in the methodology. In Section 4.2 the instantaneous kinematics of helical gears with skew axes is exploited to derive original equations for the operating pitch diameters of skiving tools. Then, the implications of the tool tip diameter on the profile shape and on the cutting conditions are explored. Section 4.3 presents the concept of the common machining operation which allow comparison between different tool designs. The remaining sections are briefly summarised to convey the logic of the full methodology. Specifically, Section 4.4 introduces tentative qualitative indices and Section 4.5 describes the main design constraints that the method should consider.

### 4.1 The tool design parameters

The tool design parameters have already been defined in Paragraph 2.2.3 when the tool profile calculation was presented. Here they are briefly recalled. The procedure for the tool profile calculation, however, is assumed to be known. The reader may refer to the relevant paragraph for further details.

Generally, the tool parameters are defined as those describing the tool shape. However, in this work, reference is made to the tool design parameters. These parameters are defined as those that uniquely determine the geometry of the tool and that must be set as input in the tool calculation routine.

In centred gear skiving three elements concur in determining the geometry of the tool: the geometry of the workpiece to machine, the relative kinematics between the tool and the gear and the tool constructive angles. Since the workpiece geometry is given as the input, the tool design depends uniquely on the parameters affecting the relative kinematics and, on the tool constructive angles. Hence, the tool design parameters in this work are divided in two subsets. The first subset, here referred to as the tool kinematic parameters, includes the tool number of teeth  $z_T$ , the tool helix angle  $\beta_T$ , and the tool tip diameter  $d_{tT}$ . The second subset, addressed here as the tool constructive parameters, comprises the tool constructive angles, namely the constructive rake angle  $\gamma_{r0}$ , the constructive clearance angle  $\alpha_{c0}$ , and the constructive step angle  $\tau_{s0}$ .

The tool kinematics parameters and the constructive parameters are independent from each other. However, they concur in determining the cutting conditions on which depends the outcome of the machining process.

Specifically, the tool kinematic parameters are of particular significance. To show this, reference is made to the numerical model of Chapter 2. In the tool design phase, the tool kinematic parameters determine the shape of the generating gear, which is then sectioned by the rake plane, whose orientation is determined by the tool constructive parameters (Figure 2.4). In this way the tool profile shape is computed. However, once the tool profile has been designed, the tool kinematic parameters also determine the shape of the surface swept by the tool (Figure 2.6). Based on the shape of the surface swept by the tool, and on its relative position with respect to the gear gap, the engagement points are computed (Figures 2.9, 2.12). The engagement points and their relevant cutting conditions determine the outcome of the process.

The contribution of each of the two sets of tool design parameters on the cutting conditions cannot be entirely isolated. However, their practical range of variability suggests that tool kinematic parameters exert a stronger influence on tool profile shape. Furthermore, since they also determine the shape of the surface swept by the tool, it can be inferred that the geometry of the penetration of each pass and the corresponding cutting conditions depend primarily on the tool kinematic parameters.

Consequently, the proposed parameter selection method prioritizes tool kinematic parameters, aiming to select the optimal set for the process. This involves computing qualitative indices solely based on tool kinematic parameters. Once chosen, the tool kinematic parameters determine the tool macro-geometry. Notably the tool constructive parameters are held constants for all designs.

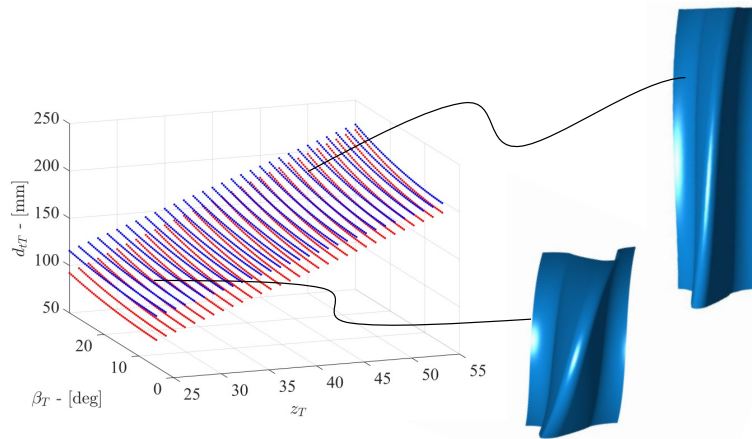


**Figure 4.1.** The domain of the tool kinematic parameters relative to one workpiece.

Particularly, the constructive rake angle and clearance angle are assumed to be zero and the step angle is taken equal to the tool helix angle  $\beta_T$ . After the tool kinematic parameters have been chosen, a fine-tuning phase for the selection of the constructive parameters aided by simulation may be carried out. However, this part is not dealt in this chapter.

Reversing the procedure order, starting with constructive parameters, carries risks. It may result in tools designed with sub-optimal process kinematics, often observed in practice. Consequently, large tool constructive angles might be employed to offset poor kinematics, leading to drawbacks like undesirable tool profile changes after re-sharpening with a large constructive clearance angle or a weak tool wedge with a large constructive rake angle, complicating tool production.

#### 4.1.1 The domain of the tool kinematic parameters

In order to portray the domain corresponding to the several combinations of tool kinematic parameters, a chart as the one shown in Figure 4.1 may be employed. On the x-axis is reported the number of tool teeth  $z_T$ , on the y-axis the nominal helix angle  $\beta_T$ , and on the z-axis the tool tip diameter  $d_{tT}$ . It is worth noticing that the number of tool teeth must be an integer number. Hence, while on the y and z axes the tool kinematic parameters are continuous, on the x-axis the values for  $z_T$  are discrete.

Figure 4.1 may be interpreted as the following. Each point on the x-y grid represents a pair of parameters  $(z_T, \beta_T)$ . For each pair, there are two distinct points along the z-axis, denoted in blue and red, indicating the maximum and minimum limit values for the tip diameter of that pair.

A discussion on the limiting values will be addressed in the next section. For now, it is important to convey that for each pair  $(z_T, \beta_T)$  there are several values, with which to select the tool tip diameter  $d_{tT}$ .

Hence, the design domain is three-dimensional, with each combination of parameters  $(z_T, \beta_T, d_{tT})$  representing a unique tool profile operating under unique cutting conditions. Figure 4.1 also illustrates two surfaces swept by the tool, corresponding to different tool designs for machining the same gear. These surfaces exhibit different shapes, with one being more twisted and curved than the other, which appears longer and straighter. Consequently, the geometry of penetration associated with the two surfaces will differ, resulting in significantly different cutting conditions for the two tools.

In the subsequent section, considerations are made to reduce the three-dimensional design domain into a two-dimensional design domain. Additionally, it is important to note that not all

combinations of  $(z_T, \beta_T, d_{iT})$  correspond to practically feasible tools. Therefore, design constraints must be introduced to address this issue.

## 4.2 Implications of the tool tip diameter on the gear skiving process

The model proposed in this section enables the derivation of equations for the operating pitch diameters based solely on the tool kinematic parameters, which is crucial for tool design. However, before delving into this discussion, a preliminary overview is necessary.

In the field of gear skiving, there is no standard method for computing operating process parameters like the tool operating pitch diameter. This is due to the specific meshing characteristic of the skiving process, where a two-dimensional tool cutting profile engages with the gear gap flanks, unlike in conventional skew axis gear pairs where the pinion and gear have three-dimensional flanks. Additionally, the theoretical profile of a skiving tool is not involute [44,61], posing challenges in associating it with geometric parameters common in traditional gears, such as the profile shift coefficient and the pressure angle. Nevertheless, the knowledge of the operating parameters remains crucial. While in the case of common gears it allows the optimisation of gear drive operation, in the skiving process it may allow the optimisation of the cutting conditions.

For the case of common skew axis gears, in order to compute the operating pitch diameters, a coupled system of equations must be solved, where several gear geometric parameters, such as the profile shift coefficients and the pressure angle of the gear pair, are set as input [92]. This approach is derived using the condition of backlash-free meshing tooth contact. It stems from the fact that in the gear design models, the geometric parameters of each of the two gears are fully known. Conversely, the assembly parameters such as the resulting centre distance  $a$  and cross-axis angle  $\Sigma$ , are unknown beforehand and must be determined as a result of the geometric parameters of the gearset.

Oppositely, in the case of gear skiving, once the tool design parameters are chosen, the assembly parameters are immediately defined by Eq. 1.1. However, a standard parametric description of the geometry of the corresponding tool profile is lacking. The precise determination of the tool profile shift coefficient and the pressure angle is challenging and may potentially lead to approximations. This is because the theoretical tool profile is not defined by a conventional rack, but directly by the workpiece gap, which has its own corrections and profile modifications. Simultaneously, the profile is defined on the rake plane which is not a standard plane. As a result, a precise standard for a parametric description of the tool profile geometry has not yet been established in the literature.

Recently, a model based on parameters of profile shifted conical gears that allows the computation of operating parameters in off-centred gear skiving was proposed [14]. However, such model follows the logic of [92], and the value of the tool profile shift coefficient and its pressure angles are required inputs. Given the inherent ambiguity in defining and accurately determining such parameters within the context of a gear skiving tool, the requirement to use them as entries in the model raise concern about the applicability of the method. Moreover, within the method presented in [14], lacks a direct relationship between operating parameters and tool kinematic parameters. Consequently, to attain the desired operating parameters and tool kinematic parameters, an iterative adjustment of the input parameters and the resolution of a system of non-linear equations is required. In light of these considerations, the practical implementation of the recently proposed method could encounter difficulties in tool design practice.

The methodology proposed in the following, in contrast, enables the derivation of formulas for the operating pitch diameter directly from the tool kinematic parameters. This eliminates the need for solving a coupled equations system or having prior knowledge of the profile shift coefficient and pressure angle of the tool.

### 4.2.1 Formulas for the operating pitch diameters

The discussion presented in the following lays foundation on the work of Phillips [89,104], where screw theory is used to describe the relative kinematics between skewed-axis gears. The employment of screw theory is widely used in the literature related to gear design, however, despite offering several advantages, it has not been exploited yet in the study of gear skiving. Particularly, kinematics concepts such as the instantaneous screw axis (ISA) of relative motion aid the visualisation of the implications that the tool kinematic parameters have on the process. In addition, entities such as the distance along the centre distance between the ISA and the operating pitch diameter, referred to as the departure [89], may be used to define the performance indices addressed in the next paragraphs.

For brevity, a summary of the main model and relevant equations is provided in Appendix B. Figure 4.2a) illustrates a schematic diagram of a gearset consisting of a tool and the internal workpiece it machines during the final pass. Notably, the notation employed here aligns with that of Appendix B. The tool and the gear in Figure 4.2a) correspond to the pinion 1 and the gear 2 of Figure B.1, respectively.

In the diagram, only one tooth of the tool and a single traversal section of a gear gap are depicted, shown in light blue and grey colours, respectively, at the moment when the tool profile aligns with the centre of the gear gap. The two rotation axes are set at the centre distance  $a$  and are inclined about the cross-axis angle  $\Sigma$ . In the figure are shown the instantaneous screw axis ISA, the pitch of relative motion  $p_{rel}$ , and the relative velocity vectors of points P, Q, and R on the centre distance line. Specifically, points P, Q, and R denote the intersection points between the centre distance and: the ISA, the two operating pitch diameters, and the gear root diameter, respectively. The infinitesimal tooth tangent to the operating pitch diameters  $d_{opT}$  and  $d_{opG}$  of the tool and the gear, respectively, has been also portrayed.

In Appendix B, the analogy between relative velocity and the concept of infinitesimal tooth departed from the ISA, is discussed. The infinitesimal tooth represents the common tangent direction to the helices which results from the intersection of the physical gearset teeth with the operating pitch diameter, while in tangency along the centre distance line. With reference to Figure 4.2a), by moving along the centre distance from point P to point R, the direction of the infinitesimal tooth evolves following the helical velocity field, whose vectors increase in magnitude. Specifically, the velocity of point R can be expressed as:

$$\mathbf{v}_R = p_{rel} \cdot \boldsymbol{\omega}_{rel} + \boldsymbol{\omega}_{rel} \times (\mathbf{R} - \mathbf{P}) \quad 4.1$$

When the infinitesimal tooth becomes tangent to the flank of the gear gap, namely when it reaches point Q, its location in relation to the tool and the gear centre,  $O_T$  and  $O_G$  respectively, defines the operating pitch diameters. To compute such condition, Eqs. (B.7), (B.10), and (B.12) are combined and the equation of the gear operating pitch diameter  $d_{opG}$  is derived:

$$d_{opG} = 2 \cdot [r_{aG} + p_{rel} \cdot \tan(\beta_{oG} - \psi_{aG})] \quad 4.2$$

In Eq. 4.2  $r_{aG}$  is the gear axode radius measured along the centre distance,  $\beta_{oG}$  is the gear helix angle at  $d_{opG}$  and  $\psi_{aG}$  is the helix angle of the gear axode at radius  $r_{aG}$ . Furthermore,  $\beta_{oG}$  may be written as a function of  $d_{opG}$  and of the gear screw parameters  $p_G = \frac{H_G}{2\pi}$ , where  $H_G$  is the gear lead, as follows:

$$\beta_{oG} = \tan^{-1} \left( \frac{d_{opG}}{2 \cdot p_G} \right) \quad 4.3$$

#### 4 Towards a parameter selection method for conical skiving tools

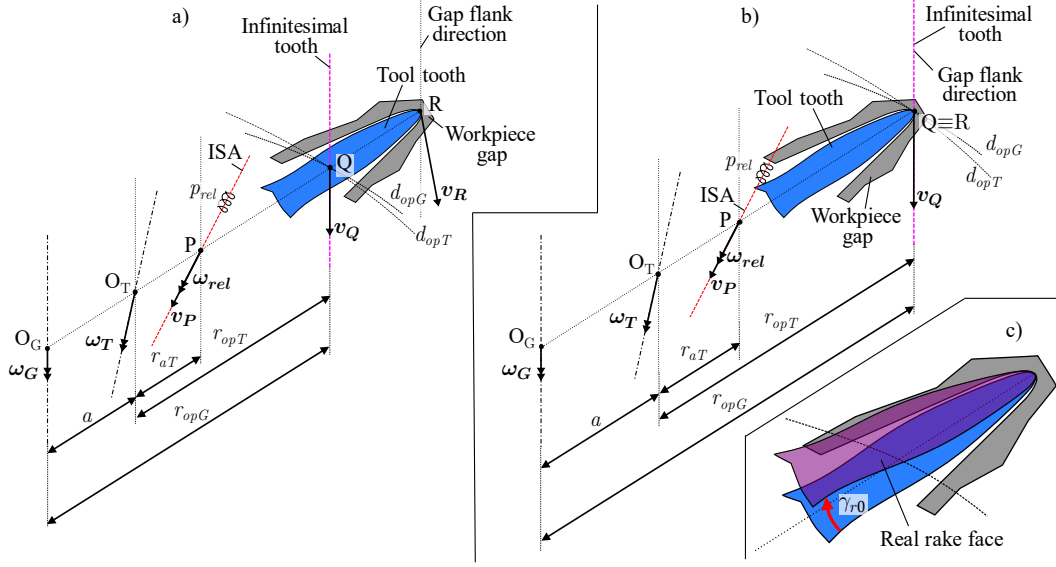


**Figure 4.2.** a) Schematic of a generic gearset made up of a skiving tool and an internal gear; b) schematic of a gearset made up of a skiving tool and an internal gear in the particular case where the tool has been designed to have the tip diameter equal to the operating pitch diameter; c) comparison of the rake face orientation between the theoretical case used to derive the equation for the operating pitch diameter and the real case.

Hence, by combining Eqs. 4.2-4.3 and considering Eqs. (B.2) and (B.4), Eq. 4.2 may be written as:

$$\varepsilon_z \cdot \sin(\Sigma) \cdot \left(\frac{d_{opG}}{2}\right)^2 + [k \cdot p_G + \varepsilon_z \cdot \cos(\Sigma) \cdot p_G - \varepsilon_z \cdot a \cdot \sin(\Sigma)] \cdot \left(\frac{d_{opG}}{2}\right) - \varepsilon_z \cdot a \cdot \cos(\Sigma) \cdot p_G = 0 \quad 4.4$$

Equation 4.4 follows the convention used throughout this work, i.e.  $\varepsilon_z = 1$  in case of external gear and  $\varepsilon_z = -1$  in case of internal gear, the sign of  $\Sigma$  depends on the relative orientation of the reference frames of Figure 2.3, whereas  $p_G$  is positive for left-hand gears and negative for right-hand gears. Equation 4.4 is a second-degree equation in  $d_{opG}$  and yields two solutions. However, only one solution is physically meaningful since the other is either negative or results in an enormous and not feasible value, which is hence easily discarded. In case the workpiece is a spur gear,  $p_G$  rises to infinity, and Eq. 4.4 simplifies to an equation of first-degree:

$$d_{opG} = \frac{2 \cdot \varepsilon_z \cdot a \cdot \cos(\Sigma)}{\varepsilon_z \cdot \cos(\Sigma) + k} \quad 4.5$$

Once the value of  $d_{opG}$  is computed, it is possible to compute the value of the gear helix angle at the operating pitch diameter  $\beta_{oG}$ , through Eq. 4.3.

The step described above, leading to Equation 4.2, can be viewed as the enforcement of the well-known equation of meshing [93]. In fact, the infinitesimal tooth has the direction of the relative velocity vector, which for correct meshing must be parallel to the gear flank direction at the considered instant.

It must be highlighted that the model presented assumes that the two teeth of the gearset make contact at the operating pitch diameters along the centre distance line. This assumption is valid for standard non-modified skew axis gearsets with three-dimensional flanks in point contact. However, for a gearset composed of a skiving tool and its workpiece, the tool profile meshes with the gear flanks with its two-dimensional cutting profile oriented on the rake plane (Figure 4.2c). In this scenario, contact at the operating pitch diameters along the centre distance line only occurs



in a specific case, i.e. when the tool tip diameter is coincident with the operating pitch diameter (Figure 4.2b). In all other cases as the one shown in Figure 4.2a), the equations proposed result in a slight approximation.

In the following it will be demonstrated that selecting the tool tip diameter equal to the operating pitch diameter may be advantageous. However, even when not considering this special case, the approximation introduced by Eqs. 4.4-4.5 is negligible for tool design, and the derived equations remain effective.

Recalling that for external and internal gearing, the operating pitch diameters must add and subtract respectively, to equal the centre distance:

$$a = \frac{(d_{opG} + \varepsilon_z \cdot d_{opT})}{2} \quad 4.6$$

from Eqs. 4.4-4.6, it is possible to derive a unique formula for the tool operating pitch diameter:

$$d_{opT} = \frac{d_{opG} \cdot k}{\cos(\Sigma) + \tan(\beta_{oG}) \cdot \sin(\Sigma)} \quad 4.7$$

Remarkably, equations 4.4, 4.5 and 4.7 for the operating pitch diameters uniquely depend on the known workpiece geometry and on  $(k, a, \Sigma)$ . Hence, they do not require tool geometric parameters such as the profile shift coefficient or the pressure angle. The parameters  $(k, a, \Sigma)$  in turn, directly depend on the tool kinematic parameters  $(z_T, \beta_T, d_{tT})$  through Eq. 1.1. This formulation, linking the tool kinematic parameters with the operating pitch diameter offers significant advantages in tool design. It enables adjustments of process kinematics and cutting conditions by directly manipulating the tool geometry.

### 4.2.2 Implications on the tool profile shape

For a specific pair of  $(z_T, \beta_T)$ , there is a range of values within which to select the tool tip diameter  $d_{tT}$ , as depicted in Figure 4.1. The equations for the operating pitch diameters help understand how by altering the tool tip diameter the profile shape is affected. For simplicity reference is made to Eq. 4.5, relative to the simpler case of gear skiving of a spur workpiece. Nevertheless, the conclusions that are drawn are also valid for helical workpieces.

From Eqs. 4.5-4.7, an increase of the centre distance  $a$ , leads to a larger operating pitch diameter of the gear and of the tool, regardless of whether the workpiece is external or internal. However, the variation of the centre distance with respect to  $d_{tT}$  is opposite for the two cases. Based on Eq. 4.6, for internal gears a reduction in  $d_{tT}$  corresponds to a bigger centre distance, whereas for external gears, the centre distance increases with  $d_{tT}$ .

Consequently, for internal workpieces, reducing the tool tip diameter  $d_{tT}$  causes the corresponding operating pitch diameter  $d_{opT}$  to increase, potentially exceeding the tool tip diameter. Conversely, as  $d_{tT}$  increases,  $d_{opT}$  decreases, moving towards the tool center. This behavior is illustrated in Figure 4.3a), where the values of  $d_{opT}$  (plotted in red) are shown against  $d_{tT}$  (depicted in blue) for a specific pair  $(z_T, \beta_T)$  relative to a skiving tool designed for machining a spur internal gear.

For external workpieces, reducing the tool tip diameter,  $d_{tT}$ , leads to a decrease in the operating pitch diameter,  $d_{opT}$ . However,  $d_{tT}$  decreases at a faster rate, causing  $d_{opT}$  to reach and potentially exceed  $d_{tT}$ . Conversely, increasing  $d_{tT}$  causes  $d_{opT}$  to increase as well, but at a slower rate, which shifts the operating pitch diameter towards the root of the tool profile. This behavior is depicted in Figure 4.3b), which relates to a skiving tool designed for machining a spur

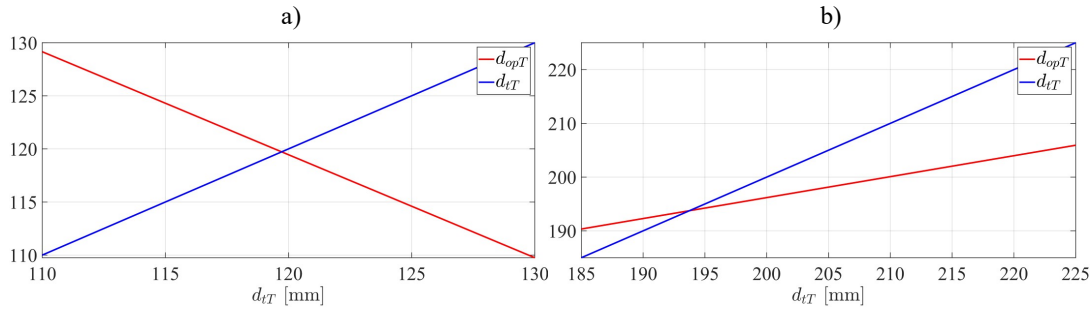


**Figure 4.3.** Variation of the tool operating pitch diameter as a function of the tool tip diameter: a) for a spur internal gear; b) for a spur external gear.

external gear. In the figure, the slope of the red line representing the values assumed by  $d_{opT}$  as a function of  $d_{tT}$  is less steep than the blue line representing  $d_{tT}$ .

By considering the workpiece as the rack generating the tool profile on the operating pitch diameter, the observed trend mirrors what is seen in standard gears when altering the profile shift coefficient. In gear skiving, reducing the tool tip diameter for both external and internal gears, resembles reducing the profile shift coefficient, resulting in an undercut tool profile. Conversely, increasing the tool tip diameter is akin to increasing the profile shift coefficient, shifting the tool profile towards the condition of pointed teeth.

From what reported, it may be deduced the existence of an upper and a lower limit for the value of the tool tip diameter for a given pair of the tool kinematic parameters ( $z_T, \beta_T$ ). In fact, a too small tool tip diameter causes strongly undercut profiles and too large a tip diameter causes pointed teeth. If such limits are reached and exceeded, the tool profile degenerates and is no longer able to produce the desired gap; not to mention, the tool profile becomes unpractical to produce.

### 4.2.3 Implications on the cutting conditions

The focus is now set in comprehending the impact of selecting different values for the tool tip diameter on the resulting cutting conditions, for a generic pair ( $z_T, \beta_T$ ) of tool kinematic parameters. Reference is made to Figures 4.2a) and b), which refers to the case of skiving of an internal gear. However, the conclusions that are drawn are discussed also for the skiving of external gears.

Despite the two schematics are relative to a single instant, they are indicative of the process kinematics. Indeed, the machining action primarily occurs in the vicinity of the portrayed position. The cutting trajectory and the surface swept by the tool (Figure 2.6) are tangent to the relative velocity vectors of the profile points. Hence, the dimension of the tool operating pitch diameters in relation to the tool tip diameter will determine the cutting trajectory. Particularly, the direction of the velocity vector of point R, coinciding with the tip of the tool profile, allows speculations on the shape of the surface swept by the tool, which, determines the cutting conditions.

Referring to the tool in Figure 4.2a), its tip diameter has a generic value, and the infinitesimal tooth and the operating pitch diameter lie in the middle of the tool tooth. Here the velocity  $v_Q$  is tangent to the gap flank direction, which for simplicity has been taken straight in the figures. By further moving the tool tip at R, the relative velocity deviates from the gap flank direction. Conversely Figure 4.2b) illustrates the special case where the tool tip diameter and the corresponding operating pitch diameter are coincident. This translates in the velocity vector  $v_R$  which lies parallel to the gear gap flank at the root.

Therefore, it can be inferred that the shape of the surface swept by the tool, relative to the case of Figure 4.2a), will exhibit a twisted trajectory with respect to the gear gap at the tool tip, whereas that relative to Figure 4.2b) will tend to remain parallel to the gap at this tool profile portion. An example of this is shown in Figures 4.4a) and b), where the surfaces swept by two tools with the

## 4.2 Implications of the tool tip diameter on the gear skiving process

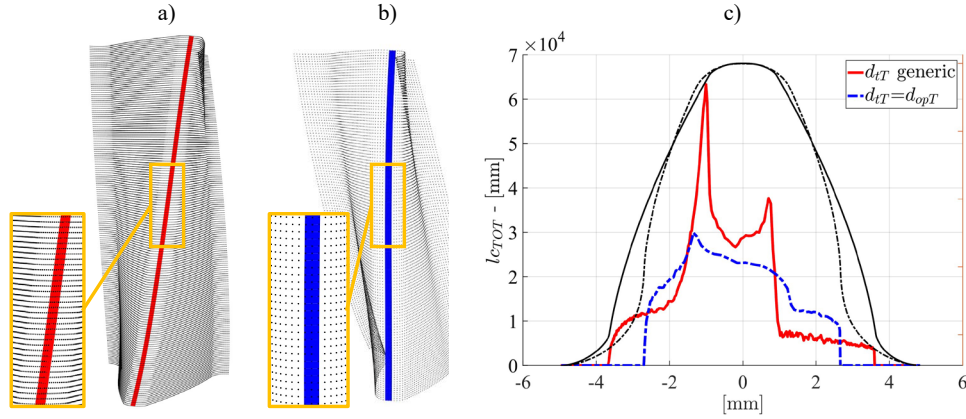


**Figure 4.4.** a) Cutting trajectory of a tool designed with the tip diameter bigger than the operating pitch diameter; b) cutting trajectory of a tool designed with tip diameter equal to the operating pitch diameter; c) comparison between the values of  $l_{cTOT}$  machined by the two tools.

same  $(z_T, \beta_T)$  but different diameters have been portrayed. Specifically, the tool in Figure 4.4a), corresponding to the scenario in Figure 4.2a), exhibits a twisted trajectory at the tip diameter. This is further highlighted by the trajectory of the midpoint at the tool tip, marked in red. On the other hand, the tool in Figure 4.4b), which aligns with the scenario in Figure 4.2b) where  $d_{tT}$  equals to  $d_{opT}$ , follows a straighter cutting trajectory at the tip (depicted in blue).

The deviation in the direction of the cutting trajectory with respect to the gear gap, which is spur in the case considered, will reflect on the cumulative machined cutting length. The tool of Figures 4.2a) and 4.4a) will work with larger values of  $l_{cSING}$  under the same set-up parameters with respect to the tool of Figures 4.2b) and 4.4b).

This trend will also repeat in the roughing passes preceding the last one, to which Figure 4.2 refers. In the roughing passes, the parameters  $(k, \Sigma)$  remain unchanged and only the centre distance varies. Therefore, the ISA does not change direction, but assumes a different position along the centre distance line at each pass and a different pitch (Eqs. B.1-B.5). This causes a deviation of the tool tip trajectory in the early passes from the desired gap direction for both the tools of Figures 4.4a) and 4.4b). It is also for this reason, that at initial passes, prolonged engagement with the workpiece is recorded, leading to a higher value of  $l_{cSING}$  and lower values of  $\gamma_{rMIN}$ .

Hence, the tool referenced in Figures 4.2b) and 4.4b), which has  $d_{tT} = d_{opT}$ , operates with lower values of  $l_{cSING}$  and higher values of  $\gamma_{rMIN}$  at each pass. Overall, it achieves a smaller value of  $l_{cTOT}$  compared to the tool depicted in Figures 4.2a) and 4.4a), which features a generic tool tip diameter. The simulated values for  $l_{cTOT}$  machined by the two tools, operating under the same process parameters, are presented in Figure 4.4c). It has been observed that choosing  $d_{tT} = d_{opT}$  leads to a significant reduction in  $l_{cTOT}$ , a factor demonstrated in Chapter 3 to be closely related to tool wear.

It is worth mentioning that the two scenarios illustrated in Figures 4.2 and 4.4 may be suitable to distinct applications of the gear skiving process. Specifically, the scenario of Figure 4.4a) should benefit the case of hard gear skiving, whereas that of Figure 4.4b) might enhance the conventional skiving process. In the case of hard gear skiving, the tool is constructed using a hard and brittle core material such as carbide, with the objective of removing a small quantity of hardened machining stock from the flanks of a previously machined gear gap. Typically, the root diameter of the gap is pre-machined to prevent tool tip breakage. Consequently, the tool profile portions which work the most are the flanks. Positioning the operating pitch diameter at the midpoint of the tooth height minimizes the trajectory covered by the tool flanks, thereby  $l_{cTOT}$

on the flanks. On the other hand, in conventional gear skiving, the tool tip is the primary profile portion responsible for material removal and consequently is the portion who wears the most, as it has been shown throughout the experiments of Chapter 3.

In light of what discussed, Eq. 4.7 may be specialised by setting the operating tip diameter coincident with the desired diameter, depending on the specific case at hand. In the following discussion reference is made to the case of conventional skiving where it is convenient to set  $d_{tT} = d_{opT}$ . However, it must be remarked that the equations derived in this section, allow the operating pitch diameter to be set at any desired value by adjusting the tool kinematic parameters, which is of great advantage in tool design. The approximation arising when  $d_{opT}$  is set at a different value than the tool tip diameter is negligible.

For conventional skiving, starting by Eq. 4.7 and setting  $d_{rG} = d_{opG}$  the equation that yields an operating pitch diameter coincident with the tip diameter is obtained as follows:

$$d_{tT} \Big|_{d_{tT}=d_{opT}} = \frac{d_{rG} \cdot k}{\cos(\Sigma) + \tan(\beta_{oG}) \cdot \sin(\Sigma)} \quad 4.8$$

where  $\beta_{oG}$  is coincident to the helix angle measured at the root diameter. Additionally, Eq. 4.8 simplifies in case of spur workpiece:

$$d_{tT} \Big|_{d_{tT}=d_{opT}} = \frac{d_{rG} \cdot k}{\cos(\Sigma)} \quad 4.9$$

By proceeding as shown, one of the three tool kinematic parameters ( $z_T, \beta_T, d_{tT}$ ), namely  $d_{tT}$  becomes a function of the other two. As a result, the three-dimensional domain of possible tool design may be restricted to a two-dimensional domain for the parameters ( $z_T, \beta_T$ ). Additionally, each pair of ( $z_T, \beta_T$ ), is linked to a pair ( $k, \Sigma$ ) by Eq. 1.1. Hence, the tool designs may be analysed over charts ( $k, \Sigma$ ). The choice of using pairs ( $k, \Sigma$ ) instead of pairs ( $z_T, \beta_T$ ) to compare the different tool designs, comes from the fact that the former yields an absolute depiction of the design-related kinematic conditions, whereas the latter must be put into the context of the specific workpiece geometry at hand. Overall, to each pair ( $k, \Sigma$ ) corresponds a unique tool tip diameter, computed according to Eq. 4.8 and a unique macro-geometry of tool design. By comparing the performances of each design over charts ( $k, \Sigma$ ) by means of qualitative indices allow to optimise the process for the specific case at hand.

Before briefly introducing the tentative qualitative indices, it is necessary to define a methodology that allows a fair comparison between each different tool design. Therefore, the concept of common machining operation is introduced in the next section.

### 4.3 The common machining operation

In order to carry out a comparative analysis of the cutting performances of different tool designs, it is necessary to establish a suitable methodology for comparison. While there are a few studies in the literature examining the effects of different tool designs on working parameters, some of the assumptions made in these studies may not be completely adequate for ensuring a fair comparison of tool performances in terms of cutting conditions. Additionally, only a few implications on working parameters have been addressed in each study.

In [7], the impact of tool design parameters on working parameters were only qualitatively explored, including chip thickness, cutting velocity, and sliding velocity, among others. The tool design comparison was made by equalizing the tools productivity, which was accomplished by employing the same axial feed and workpiece rotation speed across the different tool designs. As a result, each tool design was operated with different chip thickness and cutting velocities as well

as different cutting conditions. In [36], a simulative investigation on the effect that a different tool teeth number and helix angle have on the working rake angle was carried out. Similarly, in [38,39] the effect of employing tools with different helix angle on working parameters was analysed.

In all these studies, the same axial feed was employed for comparison, which resulted in a different chip thickness for each tool design. However, in gear skiving, the cutting velocity and chip thickness significantly influence the tool load and its wear as it was shown in Chapter 3. The comparison method employed in [7,36,38,39] entails the risk of favouring, during experimental trials, one design over another due to the more favourable cutting speed or chip thickness, rather than to the superior working parameters. Furthermore, in none of those studies a standard for the value of the tool tip diameter was set. Thus, one design may prevail over another due to a more fortunate choice of the tool tip diameter, e.g. closer to the operating pitch diameter, rather than due to a better choice of the values  $(k, \Sigma)$ .

For a given workpiece to be machined, it exists a limited range of chip thickness and cutting velocities within which a skiving tool exhibits optimal performance. Such a range is primarily influenced by the material properties of the workpiece, the material and coating of the tool, and lubrication.

Therefore, in the comparison method proposed in this section, the same tool materials and coatings are assumed across different designs, as well as identical lubrication conditions. Also, a unique standard is employed for the selection of the tool tip diameter of the different tool designs, which consist in setting the tool tip diameter equal to the operating pitch diameter, as mentioned in the previous section. Then, for all tool designs, an equal chip thickness and cutting velocity are selected, along with an identical number of radial passes. With this approach, performance differences among different tool designs stem solely from differences in working parameters, such as local rake angle or cutting length. As a consequence of the proposed approach, discrepancies in productivity among tool designs will occur.

This results of great advantage as it allows the tool performances to be split in two components one relating to working parameters and one relating to productivity. Having two performance components would allow for a more accurate choice in tool design based on the requirements of the case at hand. This is the reason why two types of qualitative indices of performance, one relating to cutting conditions and one to productivity, are introduced.

## 4.4 Tentative tool design quality indices

### 4.4.1 Productivity indices

In this paragraph the implications that different tool designs have on factors influencing productivity are briefly analysed. Reference is made to Eq. 1.5 determining the cycle time. In the context of the common machining operation, the same  $h_{MAX}$  is assumed to be machined by each tool design. As discussed in Chapter 2, tools with higher  $k$  and higher  $\Sigma$  can operate with higher  $f_A$ . For the proposed comparison method, an empirical index  $K_{f_A}$  has been developed, which provides the trend, in percentage, of the average value of  $f_A$  among the passes, in relation to the different tool designs. This index is unrelated to  $h_{MAX}$  or  $NoP$  since it is assumed that each tool design operates with the same parameters, so the differences in  $f_A$  between one design and another remain approximately the same by changing  $h_{MAX}$  and  $NoP$ . The index for the axial feed is defined as follows:

$$K_{f_A} = \frac{k \cdot \sin(|\Sigma|) \cdot (1 + \tan(|\beta_G|) \cdot \tan(|\beta_T|))}{\|k \cdot \sin(|\Sigma|) \cdot (1 + \tan(|\beta_G|) \cdot \tan(|\beta_T|))\|} \cdot 100 \quad 4.10$$

The higher the value of  $(k, \Sigma)$  the higher the axial feed. Referring to Eq. 1.5, the axial feed appears to greatly influence the cycle time. Therefore, it can be concluded that tool designs resulting in higher gear ratio and bigger cross-axis angle allow higher productivity.

Another factor that influences the cycle time is the sum of the tool run-in and run-out path,  $l_{IN}$  and  $l_{OUT}$  respectively. They ensure that the tool is freed from the engagement with the workpiece and allow avoidance of abrupt impacts at the beginning of the pass and also the prevention from not fully machined gap at the end of the pass. Few approximated models can be found in the literature for the calculation of  $l_{IN}$  and  $l_{OUT}$ . The run-in and run-out path depend on the trace that the surface swept by the tool leave on the gap after penetration. This suggests that a simulation is needed to accurately compute the tool run-in/out. From simulation it appears that the average value among the passes for the sum  $l_{IN} + l_{OUT}$  with respect to the different tool designs, has a similar trend to that shown for the axial feed. Hence, tool designs that realize higher  $(k, \Sigma)$  will need higher tool run-in and run-out path, which increase the cycle time. However, the impact on the cycle time of  $l_{IN}$  and  $l_{OUT}$  is limited compared to the other factors for common values of the gear width  $b_G$  and may be neglected.

The last factor that influences the cycle time is the workpiece angular velocity  $\omega_G$ . With the assumptions of the tool operating pitch diameter equal to the tip diameter, the relationship linking the tool angular velocity  $\omega_T$  with the cutting velocity at the tip  $v_{cut}$  may be written as follows:

$$\omega_T = \frac{2 \cdot v_{cut}}{d_{rG} \cdot k} \cdot \left( \frac{\cos(\Sigma) \cdot \cos(\beta_{oG}) + \sin(\Sigma) \cdot \sin \beta_{oG}}{\sin(\Sigma)} \right) \quad 4.11$$

Eq. 4.11 follows the convention adopted throughout this work for  $\Sigma$  and  $\beta_{oG}$ . For a given  $v_{cut}$  chosen as suitable to carry out the skiving process of the workpiece at hand, and hence for making the comparison across different tool designs, the tool rotational speed depends uniquely on  $(k, \Sigma)$ . From Eq. 4.11 it can be observed that for lower value of  $(k, \Sigma)$  a higher  $\omega_T$  is required to generate the same  $v_{cut}$ . The value of  $\omega_T$  must not exceed the limit speed value of the electric motor powering the tool holder, which is about 1500 rpm for skiving machine tools on the market. This is a basic requirement that each tool design must satisfy in order to be considered suitable for the process. For this reason, it is very common to see tools designed such that  $\Sigma=20^\circ$ . However, choosing tool design with such a value for  $\Sigma$  may yield sub-optimal performances in terms of productivity. Considering the gear ratio  $k$ , the relevant equation for the workpiece angular velocity is obtained as follows:

$$\omega_G = \frac{2 \cdot v_{cut}}{d_{rG}} \cdot \left( \frac{\cos(\Sigma) \cdot \cos(\beta_{oG}) + \sin(\Sigma) \cdot \sin \beta_{oG}}{\sin(\Sigma)} \right) \quad 4.12$$

From Eq. 4.12 it can be seen that for a given workpiece and a chosen cutting velocity,  $\omega_G$  does not depend on the gear ratio  $k$  and the lower  $\Sigma$  the higher  $\omega_G$  which decreases the cycle time. In other words, for a given cutting velocity and a given number of teeth for the tool, the smaller the value of  $\Sigma$  the higher the productivity. From a productivity point of view, it is convenient to design tools that generate higher gear ratio, in order to reach the desired cutting velocity while not exceeding the motor limit, with cross-axis angle that are, theoretically, as small as possible.

The productivity indices should be hence proposed based on Eqs. 4.11, 4.12 and after having developed an analytical index for the run-in, run-out paths. In this way the productivity of several tool design over the design domain  $(k, \Sigma)$  can be compared.

#### 4.4.2 Performance indices

The performance indices should effectively summarize each tool design's performance without relying on simulation data. The goal is to define these indices in a way that accurately reflects the working parameters. This can be achieved by basing the indices on the kinematic entities of the skew axis gearset.

A remarkable correlation emerges between the magnitude of  $v_{rel}$ , computed as in Eq. B.8, and the minimum working rake angle  $\gamma_{rMIN}$  with which the tool operates. Specifically, tool designs with higher  $v_{rel}$  tend to operate with higher  $\gamma_{rMIN}$ . Additionally, there is a strong correlation between the departure  $\Delta r$  from Equation B.7 and  $l_{cSING}$ .

Considering the shape of the axodes, it is evident that those with a smaller throat radius lead to higher values of  $\Delta r$  and  $l_{cSING}$ . Tool designs associated with this type of axode can accommodate higher axial feeds while maintaining the same maximum chip thickness, and overall, they tend to machine a reduced  $l_{cTOT}$ . Moreover, this axode shape facilitates more homogeneous cutting conditions during a single pass, from the beginning to the end of the cutting action.

However, designs with excessively high  $\Delta r$  correspond to extremely high values of  $(k, \Sigma)$ . Such designs are more sensitive to changes in kinematics across different passes, which may lead to issues with the homogeneity of material removal along various profile portions. Consequently, designs with extreme values of  $\Delta r$  should be avoided.

### 4.5 The tool design constraints

Here are briefly listed the tool design constraints that should be considered to reduce the domain of pairs  $(k, \Sigma)$ . For some of these constraints, an analytical form has already been derived, while for others, simulation is still required. The goal is to rely solely on equations to constrain the design domain  $(k, \Sigma)$ , enabling the assessment of quality indices for tools that meet specific process requirements without the need for simulation.

The first constraint comes from the risk of collision between tool holder and the workpiece when machining internal gears. For a given size of the tool holder, there are values of  $(k, \Sigma)$  which can't be met since they would determine a collision of the tool holder with the gear tip diameter.

Additionally, tools which results in too small centre distance must be discarded since their kinematics deviate significantly among passes up to a point where the first passes machine portions of the desired gear gap. Also, tools that result in pointed tip or strongly undercut, which are not practical to produce must be discarded. Finally, as previously mentioned, pairs  $(k, \Sigma)$  should be discarded in case the corresponding design does not meet the required cutting velocity for the process.

### 4.6 Conclusions and future perspectives

In this Chapter a novel design methodology for the selection of the tool kinematic parameters has been outlined. Original equations linking the tool operating pitch diameter with kinematic parameters have been derived which are of great relevance for tool design. Then, the implications of selecting different tool tip diameter values on the profile shape and on the cutting conditions in which the tool operate have been introduced. The concept of a common machining operation has also been outlined, proving suitable for a fair comparison of cutting performances across different tool designs. Additionally, foundational ideas for defining qualitative indices and tool design constraints have been presented. Future studies will complete the methodology in all its aspects. Investigations will also be conducted to establish a precise limit for the tool tip diameter and to define the profile shift coefficient for a skiving tool.



# Appendix

## A. Numerical routine for the calculation of the constructive clearance angle of a conical skiving tool

This section presents a numerical routine implemented in Matlab environment to compute the tool constructive clearance angle  $\alpha_{c0}$  of conical skiving tools. As shown below, the routine is rather cumbersome and could be optimised. However, the purpose for which it is presented is to explain the main logic behind the computation of the constructive clearance angle.

In Paragraph 2.2.3.1, it has been discussed that conical tools varies their tip diameter along the tool flanks, based on their constructive clearance angle (Eq. 2.7). This allows interference avoidance with the flanks of the gear being machined.

In the same paragraph it was presented the theoretical calculations of the tool flanks of a conical skiving tool from the point of view of replicating a tool already designed, and  $\alpha_{c0}$  was already provided. In the calculation, at each re-sharpening step, due to the variation of the tip diameter given by  $\alpha_{c0}$  (Figure 2.5), the centre distance was reported to vary. As a result, the relative kinematics varies with re-sharpening and so does the generating gear. Hence, the tool flanks calculation resulted in iteratively computing the tool profile, relative to the different tool tip diameters, of the considered re-sharpening step, and extruding them along the tool flank based on the tool lead (Eq. 2.8).

From the design point of view, the problem is more complicated. It is necessary to determine, for the whole tool service life considered, a unique value of  $\alpha_{c0}$  that allows interference free tool flanks. Since at each re-sharpening step the tip diameter varies according to  $\alpha_{c0}$  (Eq. 2.7), it is necessary to assess multiple times, one for each re-sharpening step considered, that the generating gear does not collide with the designed tool flanks. Indeed, the generating gear, represents the locus of points occupied by the gear gap in relative motion with the respect to the tool.

However, since  $\alpha_{c0}$  is unknown, the starting value of  $\alpha_{c0}$  with which the calculation is carried out might assure interference avoidance only up to an insufficient tool service life. In that case the starting value of  $\alpha_{c0}$  must be increased iteratively to assure interference avoidance for the required tool service life.

Referring to the schemes of Figure 2.3, it is useful to visualise the problem from the tool mobile reference frame  $O_T(x_T, y_T, z_T)$ . The first goal is to compute the generating gear numerically, which is not trivial. To do this, the function [95], based on the algorithm proposed in [96], is employed. The function enables the computation of the intersection points between a triangular mesh and a beam of rays which intersect it. Such technique is the same introduced in Paragraph 2.2.6.1 for the calculation of the chip thickness machined by the profile points (Figure 2.11).

In this case the triangulated mesh is the gear gap surface. Specifically, it is necessary to consider all the family of gear gap surfaces written in the tool reference frame  $\{\mathcal{S}_G(\psi)\}_T(\phi_G)$ . Hence the several triangular meshes representing  $\{\mathcal{S}_G(\psi)\}_T(\phi_G)$  are intersected by a beam of rays. The rays connect each of the points of  $\{\mathcal{S}_G(\psi)\}_T(\phi_G)$  to the origin of the tool mobile reference frame  $O_T(x_T, y_T, z_T)$ , where the point of  $\{\mathcal{S}_G(\psi)\}_T(\phi_G)$  are written. Then, for each ray, it is kept only the intersection point closest to the origin  $O_T$ . This is because the points of  $\{\mathcal{S}_G(\psi)\}_T(\phi_G)$  closest to the origin are those which cause interference with the tool flanks. By doing so, a point cloud, resulting from the intersection points of each ray, is computed. Then the point cloud is meshed with a triangulation technique. The meshed point cloud obtained is the generating gear computed numerically. Such procedure must be iterated for each re-sharpening step considered, in order to carry out the collision check with the tool flanks.

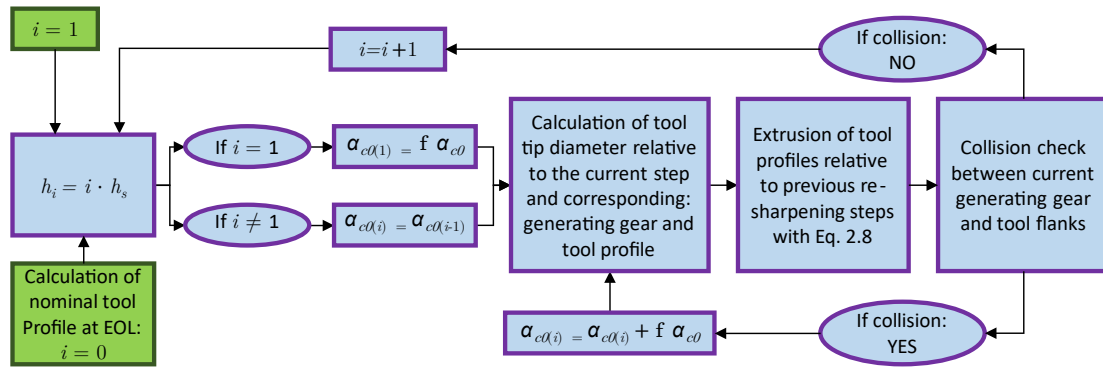


**Figure A.1.** Block diagram representing the workflow of the numeric routine for the calculation of the constructive clearance angle.

The scheme representing the numerical routine workflow is shown in the block diagram of Figure A1 and is summarised in the following. The tool service life that must be guaranteed is split into a discrete number of re-sharpening steps  $h_s$ . Additionally, a discrete clearance angle step  $\Delta\alpha_{c0}$  is defined and is set as the initial value for the constructive clearance angle  $\alpha_{c0}$ . In the figure, the letter  $i$  stands for the  $i$ -th re-sharpening step considered. The tool profile at the EOL is taken as the input. It corresponds to the zero-re-sharpening step. This is the starting point for the calculation. It must be noted that the first iteration will be referred to as the first re-sharpening step. However, when the tool is already designed and employed in practice, such re-sharpening step will be the final one as brings the tool at the end of life.

The routine starts with the first iteration, relative to the first re-sharpening step, and  $i = 1$ . The tool height value relative the first re-sharpening step is  $h_1 = h_s$ . Considering  $h_1$  and the initial values of  $\alpha_{c0}$  the tool tip diameter at the first re-sharpening step  $d_{tT1}$  is computed using Eq. 2.7, where  $d_{tT1} = d_{tTEOL} + \Delta_{dtT1}$ . Then, the generating gear and the tool profile corresponding to  $d_{tT1}$  are computed. The tool profile relative to  $d_{tT1}$  will be used in the next iteration, whereas the generating gear, numerically computed as reported above, is used to carry out the collision check for the current iteration. The profile at the EOL, is extruded along the tool flank using Eq. 2.8, based on the relevant tool lead. By doing so the first layer of the tool flank is generated.

Using the algorithm based on ray intersection, it is checked if the rays starting from the points on the extruded tool flanks intersect the generating gear of the current iteration. For  $i = 1$  the interference check is done between the points of the tool profile at EOL, which are part of the so far extruded tool flank, with those of the numerical generating gear relative to the  $d_{tT1}$ . If the generating gear intersects with the tool flank layer at height  $h_1$ , the clearance angle  $\alpha_{c01}$  is increased of a step  $\Delta\alpha_{c0}$  and a new tool tip diameter  $d_{tT1}$  is computed as well as the corresponding new generating gear and tool profile. Then interference with tool flank is checked again. This procedure is iterated until there is no interference. At this point the tool profile of the first re-sharpening step becomes part of the tool flank together with the profile at the EOL.

Now the iteration relative to the second re-sharpening step, i.e.  $i = 2$ , may begin. The tool height relative the second re-sharpening step is  $h_2 = 2 \cdot h_s$ . Based on the value of  $h_2$  and the last computed value at the previous iteration for  $\alpha_{c0}$ , the tool tip diameter of the second iteration  $d_{tT2}$  is determined as  $d_{tT2} = d_{tT1} + \Delta_{dtT1}$ . The corresponding generating gear to  $d_{tT2}$  is computed, as well as the corresponding tool profile which will be used in the third iteration. At this second iteration, the collision check is carried out between the generating gear corresponding to  $d_{tT2}$  and the so far extruded tool flank. For  $i = 2$  the flank is made up of two profile points layers: the tool profile at EOL, and the tool profile of first iteration. The profile at the EOL is placed at a re-sharpening depth of  $h_2$  from the current profile, and the tool profile of first iteration is placed at a distance  $h_1$ . Again, if no interference is detected the value of  $\alpha_{c0}$  remains that of the last

iteration, otherwise it is increased iteratively of  $\Delta\alpha_{c0}$  until collision is avoided. Then the third re-sharpening step may be computed, and the procedure can be iterated for the whole tool width.

It is worth noticing that, based on the presented routine, the value of the constructive clearance  $\alpha_{c0}$  angle may only increase from its starting value, with iterations.

Some clarification must be made. The final value of  $\alpha_{c0}$  determined as above, still does not assure an interference free tool in operation. Indeed, the routine must be iterated for intermediate passes where the centre distance is not at its nominal value and where additional workpiece side rotation *Crot* may be used. These factors alter the relative kinematics and also the shape of the numerically determined generating gears, hence affect the collision check, which must be repeated. Finally, as mentioned regarding the practical production of a conical skiving tool in Paragraph 2.2.3.1, from a practical point of view it may also be worth considering, in the routine just presented, the eventual change in the operating cross-axis angle due to the constant lead of the real tool since this also alters the kinematics and the generating gear.

## B. Kinematics of helical gear with skew axes

This section briefly reviews a few basic concepts from [89,104]. The schematic of a gearset consisting of a pinion 1 and its mating gear 2, with skew axes and the frame 3 is depicted in Figure B.1a), where only the axes of the two gears are represented for clarity. Here  $\omega_1$  and  $\omega_2$  are the shaft absolute angular velocities. The shapes of the real gear teeth are irrelevant for the considerations that follow.

The relative position of the two shafts is described by the centre distance  $a$ , defined by the points  $O_1$  and  $O_2$ , and the shaft angle  $\Sigma$  between them. For a given gearset the relative motion between the pinion and the gear, can be described by the instantaneous screw axis (ISA) that results from the linear combination of the two screws of zero pitch of the two gears. The relative motion is a skew motion performed about the ISA with pitch  $p_{rel}$ .

The ISA lies on the plane  $\pi$  orthogonal to  $O_1O_2$  and passing through the point P. Its pose is described by the distance  $r_{a1}$  from the shaft of pinion 1 to point P and by the angle  $\psi_{a1}$  between the shaft of pinion 1 and the ISA (see Figure B.1a). By selecting the triplet  $(k, a, \Sigma)$ , where  $k$  is the gear ratio, the gearset kinematics is fully determined. Indeed, the pose of the ISA and its relative pitch  $p_{rel}$  depend uniquely on  $(k, a, \Sigma)$ .

Here are reported as a reference, the relevant formulas to compute the position and the orientation of the ISA in relation to the axes of the gearset shown in Figure B.1a). The formula to compute the pitch of relative motion is also reported. Notably, all the equations below uniquely depend on the triplet  $(k, a, \Sigma)$ .

$$r_{a1} = a \cdot \frac{k^2 + k \cdot \cos(\Sigma)}{1 + 2 \cdot k \cdot \cos(\Sigma) + k^2} \quad \text{B.1}$$

$$r_{a2} = a \cdot \frac{1 + k \cdot \cos(\Sigma)}{1 + 2 \cdot k \cdot \cos(\Sigma) + k^2} \quad \text{B.2}$$

$$\psi_{a1} = \tan^{-1} \left( \frac{k \cdot \sin(\Sigma)}{1 + k \cdot \cos(\Sigma)} \right) \quad \text{B.3}$$

$$\psi_{a2} = \tan^{-1} \left( \frac{\sin(\Sigma)}{k + \cos(\Sigma)} \right) \quad \text{B.4}$$

$$p_{rel} = -a \cdot \frac{k \cdot \sin(\Sigma)}{1 + 2 \cdot k \cdot \cos(\Sigma) + k^2} \quad \text{B.5}$$

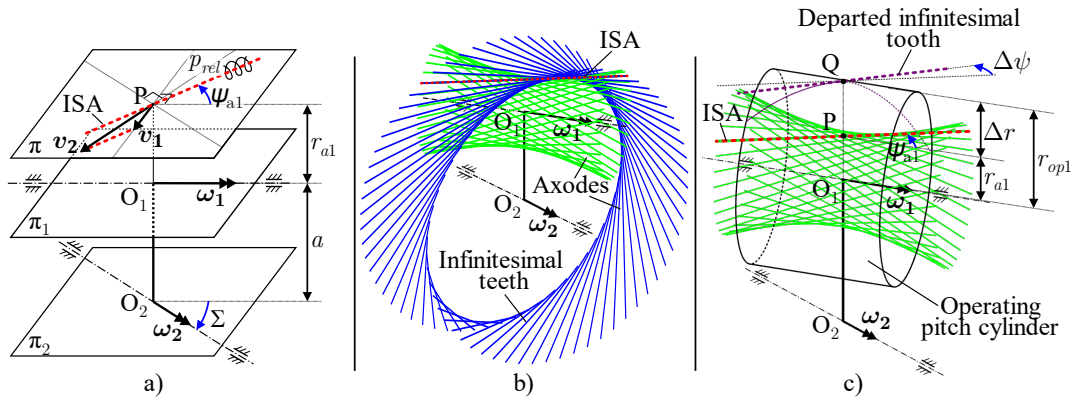


**Figure B.1** a) Schematic of a skew axis gearset; b) gearset axodes; c) schematic of the infinitesimal tooth departed from the ISA.

### Infinitesimal teeth

Revolving the ISA about each gear shaft generates two hyperboloids, which are the axodes of the gearset (Figure B.1b). The radii of the axodes, measured along the centre distance, and their respective helix angles at these radii are denoted as  $r_{a1}$ ,  $r_{a2}$  and  $\psi_{a1}$ ,  $\psi_{a2}$ , for the pinion and the gear, respectively. The two hyperboloids, in line contact, roll and slide over each other about and along the ISA. After selection of the normal module, an integer number of equidistant lines can be drawn on the axodes (Figure B.1b). These lines can be thought as straight small teeth of infinitesimal depth and thickness called infinitesimal teeth. In this scenario, the two axodes can be viewed as a pair of solid surfaces rotating about their shaft axes, transmitting motion one to another with gear ratio  $k$ , while being in line contact along the ISA. On the centre distance, the direction of the infinitesimal teeth is coincident with that of the ISA and parallel to the relative velocity vector. The magnitude of the relative velocity of the points along the ISA may be computed as:

$$v_{rel} = p_{rel} \cdot \omega_{rel} \quad \text{B.6}$$

where  $\omega_{rel}$  is the magnitude of the gear relative angular velocity,  $\omega_{rel} = \omega_1 - \omega_2$ . Differently from the case of parallel or intersecting axes, for skew axes helical gears it is possible to define a new pair of solid surfaces for motion transmission through infinitesimal teeth. In fact, the infinitesimal teeth passing from the ISA at point P can be moved to another point Q at an arbitrarily chosen distance apart  $\Delta r$  on the common perpendicular (Figure B.1c), while leaving unchanged the triplet  $(k, a, \Sigma)$ . The distance  $\Delta r$  between P and Q is addressed as departure. To maintain the meshing of the new pair of solid surfaces, while an infinitesimal tooth is moved from P to Q, its direction must be twisted of an angle  $\Delta\psi$  with respect to the ISA, according to the following relation:

$$\Delta r = p_{rel} \cdot \tan(\Delta\psi) \quad \text{B.7}$$

This is because, when in contact along the centre distance, the infinitesimal teeth must remain tangent to the relative velocity vector for proper motion transmission. The ISA and the hyperboloids remain the same because the triplet  $(k, a, \Sigma)$  is not changed. However, the departure from P involves several issues. It is worth mentioning that the new pair of solid surfaces, which exchange motion through the shifted infinitesimal teeth at Q, undergoes a transformation in shape, ultimately becoming cylindrical. The resulting solid cylinders, still transmit motion one to another

## Appendix

with gear ratio  $k$ , but are now in point contact at Q. Additionally the relative velocity in B increases in magnitude according to the following relation:

$$v_{rel} = p_{rel} \cdot \omega_{rel} \cdot \sqrt{1 + \tan(\Delta\psi)^2} \quad \text{B.8}$$

such cylinders are the well-known operating pitch cylinders [93] and the angle that the departed infinitesimal tooth at Q forms with the shaft axis is the operating helix angle of the real gear. Specifically, the radii of the operating pitch cylinders  $r_{op1}$ ,  $r_{op2}$  differ from those of the axodes  $r_{a1}$ ,  $r_{a2}$  by the departure  $\Delta r$  (Figure B.1c). Similarly, the operating helix angle of the real gears  $\beta_{op1}$ ,  $\beta_{op2}$ , differ from the helix angle of the axodes  $\psi_{a1}$ ,  $\psi_{a2}$  of the quantity  $\Delta\psi$ . Considering that the values of  $a$  and  $\Sigma$  remain unchanged, the following equations must hold:

$$r_{op1} = r_{a1} + \Delta r \quad \text{B.9}$$

$$r_{op2} = r_{a2} - \Delta r \quad \text{B.10}$$

$$\beta_{op1} = \psi_{a1} + \Delta\psi \quad \text{B.11}$$

$$\beta_{op2} = \psi_{a2} - \Delta\psi \quad \text{B.12}$$

A clarification must now be made. In a skew axes gearset, both pairs of what have been here described as solid surfaces, exist. One pair is formed by the axodes, which describe the relative motion of the gearset, and depend solely on kinematics, specifically on the triplet  $(k, a, \Sigma)$ . The other pair is formed by the operating pitch surfaces whose definition comes as well from kinematics. Practitioners, however, define these surfaces to depict the kinematic behaviour of actual gear teeth. As a result, the operating pitch surfaces are commonly established using the geometric parameters of gears, such as the normal module and the pressure angle. For the cases of parallel and intersecting axes gearsets, the axodes and the operating pitch surface coincide since there is no possibility for departure. The only distinction is made between operating pitch cylinders and pitch cylinders. The former concern the kinematic of the gearset in assembly, the latter concern the relative kinematic between the gear and the rack who defines it.

The departed infinitesimal teeth are indicative of the relative motion between the real teeth of the gear and the tool nearby point Q. Hence, since the kinematics of the axodes can be exploited for gear synthesis as reported in [107], the same can be done for the kinematics of the departed teeth on the operating pitch cylinders.

# References

- [1] V.W. Pittler, Verfahren zum Schneiden von Zahnrädern mittels eines zahnradartigen, an den Stirnflächen der Zähne mit Schneidkanten versehenen Schneidwerkzeugs, 1910.
- [2] K.D. Bouzakis, E. Lili, N. Michailidis, O. Friderikos, Manufacturing of cylindrical gears by generating cutting processes: A critical synthesis of analysis methods, *CIRP Ann. - Manuf. Technol.* 57 (2008) 676–696. <https://doi.org/10.1016/j.cirp.2008.09.001>.
- [3] B.C. Kobialka, AGMA Technical Paper Contemporary Gear Solutions, Am. Gear Manuf. Assoc. (2012).
- [4] H.J. Stadtfeld, Power Skiving of Cylindrical Gears on Different Machine Platforms, *Gear Technol.* (2014) 52–62.
- [5] E. Olivoni, R. Vertechy, V. Parenti-Castelli, Power skiving manufacturing process : a review, *Mech. Mach. Theory.* 175 (2022). <https://doi.org/10.1016/j.mechmachtheory.2022.104955>.
- [6] E. Guo, R. Hong, X. Huang, C. Fang, Research on the design of skiving tool for machining involute gears, *J. Mech. Sci. Technol.* 28 (2014) 5107–5115. <https://doi.org/10.1007/s12206-014-1133-z>.
- [7] F. Klocke, C. Brecher, C. Löpenhaus, P. Ganser, J. Staudt, M. Krömer, Technological and Simulative Analysis of Power Skiving, *Procedia CIRP.* 50 (2016) 773–778. <https://doi.org/10.1016/j.procir.2016.05.052>.
- [8] T. Bergs, A. Georgoussis, C. Löpenhaus, Development of a numerical simulation method for gear skiving, *Procedia CIRP.* 88 (2020) 352–357. <https://doi.org/10.1016/j.procir.2020.05.061>.
- [9] B. Vargas, V. Schulze, Three-dimensional modeling of gear skiving kinematics for comprehensive process design in practical applications, *CIRP Ann.* 70 (2021) 99–102. <https://doi.org/10.1016/j.cirp.2021.04.075>.
- [10] V. Schulze, C. Kühlewein, H. Autenrieth, 3D-FEM modeling of gear skiving to investigate kinematics and chip formation mechanisms, *Adv. Mater. Res.* 223 (2011) 46–55. <https://doi.org/10.4028/www.scientific.net/AMR.223.46>.
- [11] D. Spath, A. Hühsam, Skiving for high-performance machining of periodic structures, *CIRP Ann. - Manuf. Technol.* 51 (2002) 91–94. [https://doi.org/10.1016/S0007-8506\(07\)61473-5](https://doi.org/10.1016/S0007-8506(07)61473-5).
- [12] C. Janßen, J. Brimmers, T. Bergs, Simulative Study of the Applicability of Topological Modifications for Gear Skiving, *Procedia CIRP.* 118 (2023) 465–470. <https://doi.org/10.1016/j.procir.2023.06.080>.
- [13] C. Janßen, J. Brimmers, T. Bergs, Validation of the plane-based penetration calculation for gear skiving, *Procedia CIRP.* 99 (2021) 220–225. <https://doi.org/10.1016/j.procir.2021.03.034>.
- [14] A. Hilligardt, V. Schulze, A holistic approach for gear skiving design enabling tool load homogenization, *CIRP Ann.* 71 (2022) 85–88. <https://doi.org/10.1016/j.cirp.2022.03.029>.
- [15] A. Hilligardt, V. Schulze, Gear skiving with minimum twist errors: Modeling and optimization of flank twist in gear skiving, *Forsch. Im Ingenieurwesen/Engineering Res.* 87 (2023) 997–1007. <https://doi.org/10.1007/s10010-023-00695-2>.
- [16] T. Nishikawa, S. Shimada, G. Kobayashi, R. Zongwei, N. Sugita, Using Power Skiving to Increase the Efficiency and Precision of Internal Gear Cutting, *Komatsu Tech. Rep.* 64 (2018) 1–7.
- [17] Z. Ren, Z. Fang, T. Arakane, T. Kizaki, T. Nishikawa, Y. Feng, J. Kugo, E. Nabata, N. Sugita, Parametric modeling of uncut chip geometry for predicting crater wear in gear skiving, *J. Mater. Process. Technol.* 290 (2021) 116973. <https://doi.org/10.1016/j.jmatprotec.2020.116973>.
- [18] P. McCloskey, A. Katz, L. Berglind, K. Erkorkmaz, E. Ozturk, F. Ismail, Chip geometry and cutting forces in gear power skiving, *CIRP Ann.* 68 (2019) 109–112. <https://doi.org/10.1016/j.cirp.2019.04.085>.

## References

- [19] M. Inui, Y. Huang, H. Onozuka, N. Umezu, Geometric simulation of power skiving of internal gear using solid model with triple-dexel representation, *Procedia Manuf.* 48 (2020) 520–527. <https://doi.org/10.1016/j.promfg.2020.05.078>.
- [20] Z. Fang, Z. Ren, T. Kizaki, Y. Feng, J. Kugo, Y. Komatsu, N. Sugita, Construction of uncut chip geometry in gear skiving using level contours, *Precis. Eng.* 73 (2021) 93–103. <https://doi.org/10.1016/j.precisioneng.2021.08.013>.
- [21] Z. Ren, Z. Fang, T. Kizaki, Y. Feng, T. Nagata, Y. Komatsu, N. Sugita, Understanding local cutting features affecting surface integrity of gear flank in gear skiving, *Int. J. Mach. Tools Manuf.* 172 (2022). <https://doi.org/10.1016/j.ijmachtools.2021.103818>.
- [22] A. Antoniadis, N. Vidakis, N. Bilalis, A simulation model of gear skiving, *J. Mater. Process. Technol.* 146 (2004) 213–220. <https://doi.org/10.1016/j.jmatprotec.2003.10.019>.
- [23] A. Antoniadis, Gear skiving - CAD simulation approach, *CAD Comput. Aided Des.* 44 (2012) 611–616. <https://doi.org/10.1016/j.cad.2012.02.003>.
- [24] N. Tapoglou, Calculation of non-deformed chip and gear geometry in power skiving using a CAD-based simulation, *Int. J. Adv. Manuf. Technol.* 100 (2019) 1779–1785. <https://doi.org/10.1007/s00170-018-2790-3>.
- [25] N. Tapoglou, Development of Cutting Force Model and Process Maps for Power Skiving Using CAD-Based Modelling, *Machines.* 9 (2021) 95. <https://doi.org/10.3390/machines9050095>.
- [26] A. Marinakis, P. Alevras, A. Antoniadis, A systematic analysis of the power skiving process using a novel gear manufacturing simulation software, *Simul. Model. Pract. Theory.* 123 (2023) 102711. <https://doi.org/10.1016/j.simpat.2022.102711>.
- [27] J. Li, P. Wang, Y.Q. Jin, Q. Hu, X.C. Chen, Cutting force calculation for gear slicing with energy method, *Int. J. Adv. Manuf. Technol.* 83 (2016) 887–896. <https://doi.org/10.1007/s00170-015-7630-0>.
- [28] Z. Guo, S.M. Mao, L. Huyan, D.S. Duan, Research and improvement of the cutting performance of skiving tool, *Mech. Mach. Theory.* 120 (2018) 302–313. <https://doi.org/10.1016/j.mechmachtheory.2017.08.004>.
- [29] B. Vargas, M. Zapf, J. Klose, F. Zanger, V. Schulze, Numerical modelling of cutting forces in gear skiving, *Procedia CIRP.* 82 (2019) 455–460. <https://doi.org/10.1016/j.procir.2019.04.039>.
- [30] H. Onozuka, F. Tayama, Y. Huang, M. Inui, Cutting force model for power skiving of internal gear, *J. Manuf. Process.* 56 (2020) 1277–1285. <https://doi.org/10.1016/j.jmapro.2020.04.022>.
- [31] X. Wu, J. Li, Y. Jin, S. Zheng, Temperature calculation of the tool and chip in slicing process with equal-rake angle arc-tooth slice tool, *Mech. Syst. Signal Process.* 143 (2020). <https://doi.org/10.1016/j.ymssp.2020.106793>.
- [32] L. Zhang, J. Liu, X. Wu, C. Zhuang, Digital twin-based dynamic prediction of thermomechanical coupling for skiving process, *Int. J. Adv. Manuf. Technol.* (2022). <https://doi.org/10.1007/s00170-022-08908-8>.
- [33] M. Kojima, On the Clearance Angles of Skiving Cutter, *Bull. JSME.* 17 (1974) 401–408. [https://www.jstage.jst.go.jp/article/bpb1993/17/11/17\\_11\\_1460/\\_pdf/-char/ja](https://www.jstage.jst.go.jp/article/bpb1993/17/11/17_11_1460/_pdf/-char/ja).
- [34] X. Chen, J. Li, B. Lou, J. Shi, Q. Yang, Effect of the cutter parameters and machining parameters on the interference in gear slicing, *Chinese J. Mech. Eng. (English Ed.)* 26 (2013) 1118–1126. <https://doi.org/10.3901/CJME.2013.06.1118>.
- [35] X.Q. Li, J. Li, P. Wang, Y. Zou, Calculation and analysis of the interference amount in gear slicing, *Appl. Mech. Mater.* (2014) 7–12. <https://doi.org/10.4028/www.scientific.net/AMM.687-691.7>.
- [36] E. Guo, R. Hong, X. Huang, C. Fang, Research on the cutting mechanism of cylindrical gear power skiving, *Int. J. Adv. Manuf. Technol.* 79 (2015) 541–550. <https://doi.org/10.1007/s00170-015-6816-9>.
- [37] C.Y. Tsai, Mathematical model for design and analysis of power skiving tool for involute gear cutting, *Mech. Mach. Theory.* 101 (2016) 195–208. <https://doi.org/10.1016/j.mechmachtheory.2016.03.021>.
- [38] I. Moriwaki, T. Osafune, M. Nakamura, M. Funamoto, K. Uriu, T. Murakami, E. Nagata,



- N. Kurita, T. Tachikawa, Y. Kobayashi, Cutting Tool Parameters of Cylindrical Skiving Cutter with Sharpening Angle for Internal Gears, *J. Mech. Des. Trans. ASME*. 139 (2017). <https://doi.org/10.1115/1.4035432>.
- [39] K. Uriu, T. Osafune, T. Murakami, M. Nakamura, D. Iba, M. Funamoto, I. Moriwaki, Effects of shaft angle on cutting tool parameters in internal gear skiving, *J. Mech. Sci. Technol.* 31 (2017) 5665–5673. <https://doi.org/10.1007/s12206-017-1107-z>.
- [40] P. Wang, F. Liu, J. Li, Analysis and optimization of gear skiving parameters regarding interference and theoretical machining deviation based on chaos map, *Int. J. Adv. Manuf. Technol.* 112 (2021) 2161–2175. <https://doi.org/10.1007/s00170-020-06562-6>.
- [41] Z. Fang, Z. Ren, L. Shu, T. Kizaki, N. Sugita, A parametric modeling for fast radial infeed planning process in gear skiving, *Mech. Mach. Theory*. 174 (2022) 104909. <https://doi.org/10.1016/j.mechmachtheory.2022.104909>.
- [42] A. Hillgardt, J. Klose, M. Gerstenmeyer, V. Schulze, Modelling and prevention of meshing interference in gear skiving of internal gears: Conference Proceedings, *Forsch. Im Ingenieurwesen/Engineering Res.* (2021). <https://doi.org/10.1007/s10010-021-00520-8>.
- [43] T. Tachikawa, N. Kurita, M. Nakamura, D. Iba, I. Moriwaki, Calculation Model for Internal Gear Skiving With a Pinion-type Cutter Having Pitch Deviation and a Run-Out, in: *Proc. ASME 2015 Int. Des. Eng. Tech. Conf. Comput. Inf. Eng. Conf.*, Boston, Massachusetts, USA, 2015.
- [44] E. Guo, R. Hong, X. Huang, C. Fang, A novel power skiving method using the common shaper cutter, *Int. J. Adv. Manuf. Technol.* 83 (2015) 157–165. <https://doi.org/10.1007/s00170-015-7559-3>.
- [45] E. Guo, N. Ren, Z. Liu, X. Zheng, Influence of sensitive pose errors on tooth deviation of cylindrical gear in power skiving, *Adv. Mech. Eng.* 11 (2019) 1–12. <https://doi.org/10.1177/1687814019843759>.
- [46] J. Li, P. Wang, X.C. Chen, T.J. Yang, A study on the optimal selection of spur slice cutter parameters and machining parameters, *Int. J. Adv. Manuf. Technol.* 82 (2016) 407–417. <https://doi.org/10.1007/s00170-015-7369-7>.
- [47] Z. Guo, S.M. Mao, X.E. Li, Z.Y. Ren, Research on the theoretical tooth profile errors of gears machined by skiving, *Mech. Mach. Theory*. 97 (2016) 1–11. <https://doi.org/10.1016/j.mechmachtheory.2015.11.001>.
- [48] Z. Guo, S.M. Mao, X.F. Du, Z.Y. Ren, Influences of tool setting errors on gear skiving accuracy, *Int. J. Adv. Manuf. Technol.* (2017) 3135–3143. <https://doi.org/10.1007/s00170-017-9988-7>.
- [49] C.Y. Tsai, Simple mathematical approach for analyzing gear tooth profile errors of different gears cut using same power-skiving tool, *Mech. Mach. Theory*. 177 (2022) 105042. <https://doi.org/10.1016/j.mechmachtheory.2022.105042>.
- [50] F. Zheng, M. Zhang, W. Zhang, X. Guo, Research on the tooth modification in gear skiving, *J. Mech. Des. Trans. ASME*. 140 (2018) 1–9. <https://doi.org/10.1115/1.4040268>.
- [51] M. Trübswetter, M. Otto, K. Stahl, Evaluation of Gear Flank Surface Structure Produced by Skiving, *Forsch. Im Ingenieurwesen/Engineering Res.* 83 (2019) 719–726. <https://doi.org/10.1007/s10010-019-00348-3>.
- [52] K. Jia, J. Guo, T. Ma, S. Wan, Mathematical Modelling of Power Skiving for General Profile based on Numerical Enveloping, *Int. J. Adv. Manuf. Technol.* 116 (2021) 733–746. <https://doi.org/10.1007/s00170-021-07485-6>.
- [53] Z. Ren, Z. Fang, G. Kobayashi, T. Kizaki, N. Sugita, T. Nishikawa, J. Kugo, E. Nabata, Influence of tool eccentricity on surface roughness in gear skiving, *Precis. Eng.* 63 (2020) 170–176. <https://doi.org/10.1016/j.precisioneng.2020.02.007>.
- [54] Z. Guo, R. Xie, W. Guo, W. Han, F. Gao, Y. Zhang, A Novel Method for Improving the Skiving Accuracy of Gears with Profile and Lead Modifications, *Machines*. 11 (2023). <https://doi.org/10.3390/machines111010087>.
- [55] I.P. Balabanov, V.N. Gilman, T.S. Timofeeva, A.I. Faskhutdinov, Modeling of the cutting edge rounding influence on the tool life in processing a gear wheel by the Power Skiving method, *Int. J. Eng. Technol.* 7 (2018) 71–73. <https://doi.org/10.14419/ijet.v7i4.7.20386>.

## References

- [56] V.I. Astashchenko, I.N. Gilazov, A comparative analysis of machining of parts from 38H2MYuA by cutting tool of different materials, *IOP Conf. Ser. Mater. Sci. Eng.* 570 (2019) 4–7. <https://doi.org/10.1088/1757-899X/570/1/012007>.
- [57] T. Arndt, J. Klose, M. Gerstenmeyer, V. Schulze, Tool wear development in gear skiving process of quenched and tempered internal gears, *Forsch. Im Ingenieurwesen/Engineering Res.* (2021). <https://doi.org/10.1007/s10010-021-00544-0>.
- [58] E. Olivoni, R. Vertechy, V. Parenti-Castelli, On the profile change of conical skiving tools after re-sharpening, in: *17th CIRP Conf. Intell. Comput. Manuf. Eng.*, Elsevier, 2023: pp. 12–14.
- [59] S.P. Radzevich, *Gear Cutting Tools - fundamentals of design and computation*, CRC Press, Boca Raton, 2010.
- [60] X.C. Chen, J. Li, B.C. Lou, A study on the design of error-free spur slice cutter, *Int. J. Adv. Manuf. Technol.* 68 (2013) 727–738. <https://doi.org/10.1007/s00170-013-4794-3>.
- [61] J. Jing, An Analytical Theory of Gear Turning - Gear Skiving for Internal Gears and Gear Generating for External Gears, *Int. J. Mach. Tool Des. Res.* 22 (1982) 125–130.
- [62] P. Wang, J. Li, Y.Q. Jin, A study on the design of slicing cutter for cycloid gear based on conjugate theory, *Int. J. Adv. Manuf. Technol.* 98 (2018) 2057–2068. <https://doi.org/10.1007/s00170-018-2115-6>.
- [63] Y.P. Shih, Y.J. Li, Y.C. Lin, H.Y. Tsao, A novel cylindrical skiving tool with error-free flank faces for internal circular splines, *Mech. Mach. Theory.* 170 (2022) 104662. <https://doi.org/10.1016/j.mechmachtheory.2021.104662>.
- [64] P. Wang, J. Li, L. Han, Research on the cutting principle and tool design of gear skiving based on the theory of conjugate surface, *Math. Probl. Eng.* 2021 (2021). <https://doi.org/10.1155/2021/5469020>.
- [65] K. Jia, S. Zheng, J. Guo, J. Hong, A surface enveloping-assisted approach on cutting edge calculation and machining process simulation for skiving, *Int. J. Adv. Manuf. Technol.* 100 (2019) 1635–1645. <https://doi.org/10.1007/s00170-018-2799-7>.
- [66] K. Jia, J. Guo, S. Zheng, J. Hong, A general mathematical model for two-parameter generating machining of involute cylindrical gears, *Appl. Math. Model.* 75 (2019) 37–51. <https://doi.org/10.1016/j.apm.2019.05.021>.
- [67] M. Kojima, K. Nishijima, Gear Skiving of Involute Internal Spur Gear, *Bull. JSME.* 17 (1974) 511–518. [https://www.jstage.jst.go.jp/article/bpb1993/17/11/17\\_11\\_1460/\\_pdf-char/ja](https://www.jstage.jst.go.jp/article/bpb1993/17/11/17_11_1460/_pdf-char/ja).
- [68] E. Guo, R. Hong, X. Huang, C. Fang, A correction method for power skiving of cylindrical gears lead modification, *J. Mech. Sci. Technol.* 29 (2015) 4379–4386. <https://doi.org/10.1007/s12206-015-0936-x>.
- [69] T.T. Luu, Y.R. Wu, A novel correction method to attain even grinding allowance in CNC gear skiving process, *Mech. Mach. Theory.* 171 (2022) 104771. <https://doi.org/10.1016/j.mechmachtheory.2022.104771>.
- [70] E. Guo, N. Ren, X. Ren, C. Liu, An efficient tapered tool having multiple blades for manufacturing cylindrical gears with power skiving, *Int. J. Adv. Manuf. Technol.* 102 (2019) 2823–2832. <https://doi.org/10.1007/s00170-018-03239-z>.
- [71] T. Monden, T. Kikuchi, Y. Chihara, Y. Nakamura, MHI Super-Skiving System for Longer Tool Life and Enhanced Efficiency in Internal Gear Cutting, *Mitsubishi Heavy Ind. Tech. Rev.* 52 (2015) 101–105.
- [72] T. Monden, T. Kikuchi, K. Yoshikawa, N. Fujimura, G. Adrianos, Super Skiving Cutter An Innovative Process Modification of Gear Skiving, *Mitsubishi Heavy Ind. Tech. Rev.* 56 (2018) 1–32.
- [73] E. Guo, Z. Shi, L. Hu, E. Zhang, X. Ren, Design method of a multi-blade skiving tool for gear skiving, *Mech. Mach. Theory.* 173 (2022) 104848. <https://doi.org/10.1016/j.mechmachtheory.2022.104848>.
- [74] E. Olivoni, R. Vertechy, V. Parenti-Castelli, A New Parameter Selection Method for Power Skiving Tools, in: *Rom. 24 - Robot Des. Dyn. Control*, Springer, Udine, 2022: pp. 322–331.
- [75] Y.P. Shih, Y.J. Li, A Novel Method for Producing a Conical Skiving Tool with Error-Free

- Flank Faces for Internal Gear Manufacture, *J. Mech. Des. Trans. ASME*. 140 (2018) 1–9. <https://doi.org/10.1115/1.4038567>.
- [76] C.Y. Tsai, Power-skiving tool design method for interference-free involute internal gear cutting, *Mech. Mach. Theory*. 164 (2021) 104396. <https://doi.org/10.1016/j.mechmachtheory.2021.104396>.
- [77] E. Guo, L. Hu, E. Zhang, C. Liu, J. Xu, W. He, A cylindrical skiving tool design method based on a conjugate surface for internal gear manufacture, *J. Manuf. Process*. 101 (2023) 1538–1550. <https://doi.org/10.1016/j.jmapro.2023.07.019>.
- [78] C.-Y. Tsai, Algebraic modeling of cylindrical interference-free power-skiving tool for involute internal gear cutting with tilt angle, *J. Manuf. Sci. Eng.* (2023) 1–26. <https://doi.org/10.1115/1.4062312>.
- [79] P. Wang, Slicing principle and cutter design for the arc internal tooth of pin gear housing in RV reducer, *Proc. - 2019 2nd World Conf. Mech. Eng. Intell. Manuf.* (2019) 335–338. <https://doi.org/10.1109/WCMEIM48965.2019.00072>.
- [80] P. Wang, L. Han, J. Li, F. Liu, Research on design and manufacturing of gear slicing cutter for circular arc tooth, *Int. J. Adv. Manuf. Technol.* 113 (2021) 2017–2029. <https://doi.org/10.1007/s00170-021-06757-5>.
- [81] X.C. Chen, J. Li, Y. Zou, P. Wang, A study on the grinding of the major flank face of error-free spur slice cutter, *Int. J. Adv. Manuf. Technol.* 72 (2014) 425–438. <https://doi.org/10.1007/s00170-014-5626-9>.
- [82] C.Y. Tsai, Integrated mathematical approach for design and manufacturing of power-skiving tool for interference-free involute internal gear cutting, *Mech. Mach. Theory*. 180 (2023) 105172. <https://doi.org/10.1016/j.mechmachtheory.2022.105172>.
- [83] C.Y. Tsai, P.D. Lin, Gear manufacturing using power-skiving method on six-axis CNC turn-mill machining center, *Int. J. Adv. Manuf. Technol.* 95 (2018) 609–623. <https://doi.org/10.1007/s00170-017-1154-8>.
- [84] T. Tachikawa, D. Iba, N. Kurita, M. Nakamura, I. Moriwaki, Basic study on calculation of cutting forces useful for reducing vibration in skiving, *J. Mech. Des. Trans. ASME*. 139 (2017) 1–6. <https://doi.org/10.1115/1.4037625>.
- [85] Z. Han, C. Jiang, X. Deng, Machining and meshing analysis of face gears by power skiving, *J. Adv. Mech. Des. Syst. Manuf.* 16 (2022) 1–15. <https://doi.org/10.1299/JAMDSM.2022JAMDSM0002>.
- [86] S. Mo, S. Wang, B. Luo, H. Bao, G. Cen, Y. Huang, Research on the skiving technology of face gear, *Int. J. Adv. Manuf. Technol.* 121 (2022) 5181–5196. <https://doi.org/10.1007/s00170-022-09663-6>.
- [87] J.F. Hochrein, M. Trübswetter, M. Otto, K. Stahl, Direct flank geometry calculation for face gears, *Forsch. Im Ingenieurwesen/Engineering Res.* 86 (2022) 617–625. <https://doi.org/10.1007/s10010-021-00505-7>.
- [88] H. Guo, T. Ma, S. Zhang, N. Zhao, A. Fuentes-Aznar, Computerized generation and surface deviation correction of face gear drives generated by skiving, *Mech. Mach. Theory*. 173 (2022) 104839. <https://doi.org/10.1016/j.mechmachtheory.2022.104839>.
- [89] J. Phillips, *Freedom in Machinery*, Cambridge University Press, 2007. <https://doi.org/10.1017/CBO9780511751745>.
- [90] KISSsoft AG, KISSsoft, (2023). <https://www.kisssoft.com/en>.
- [91] D.T. Lee, B.J. Schachter, Two algorithms for constructing a Delaunay triangulation, *Int. J. Comput. Inf. Sci.* 9 (1980) 219–242. <https://doi.org/10.1007/BF00977785>.
- [92] F.L. Litvin, A. Fuentes, *Gear geometry and applied theory*, Second edi, Cambridge :University Press, 2004.
- [93] F.L. Litvin, *Theory of Gearing, Theory of Gearing.* (1989). <https://doi.org/10.1201/b12727>.
- [94] U. Reif, SurfPart, (n.d.). <https://www.mathworks.com/matlabcentral/fileexchange/50186-surfpart> (accessed January 6, 2024).
- [95] T. Jaroslaw, Triangle/Ray Intersection, (n.d.). <https://www.mathworks.com/matlabcentral/fileexchange/33073-triangle-ray-intersection>.
- [96] T. Möller, B. Trumbore, Fast, minimum storage ray/triangle intersection, *ACM*

## References

- SIGGRAPH 2005 Courses, SIGGRAPH 2005. (2005) 37–41. <https://doi.org/10.1145/1198555.1198746>.
- [97] A. Katz, K. Erkorkmaz, F. Ismail, Virtual model of gear shaping-Part I: Kinematics, cutter-workpiece engagement, and cutting forces, *J. Manuf. Sci. Eng. Trans. ASME*. 140 (2018) 1–15. <https://doi.org/10.1115/1.4039646>.
- [98] Y. Altintas, *Manufacturing Automation*, Second ed., Cambridge University Press, 2012. <https://doi.org/10.1201/9781420039733.ch26>.
- [99] H. Saglam, F. Unsacar, S. Yaldiz, Investigation of the effect of rake angle and approaching angle on main cutting force and tool tip temperature, *Int. J. Mach. Tools Manuf.* 46 (2006) 132–141. <https://doi.org/10.1016/j.ijmachtools.2005.05.002>.
- [100] G. V. Stabler, The Fundamental Geometry of Cutting Tools, *Proc. Inst. Mech. Eng.* 165 (1951) 14–26. [https://doi.org/10.1243/PIME\\_PROC\\_1951\\_165\\_008\\_02](https://doi.org/10.1243/PIME_PROC_1951_165_008_02).
- [101] L. Vedmar, C. Andersson, J.E. Ståhl, A parametric analysis of the undeformed chip geometry in gear hobbing, *J. Manuf. Sci. Eng.* 131 (2009) 0610031–0610038. <https://doi.org/10.1115/1.4000334>.
- [102] Mohsen Habibi, Z.C. Chen, An accurate and efficient approach to undeformed chip geometry in face-obbing and its application in cutting force prediction, *J. Mech. Des.* 138 (2016) 1–11. <https://doi.org/10.1115/1.4032090>.
- [103] A.R. Albert, Influence of the gear geometry and the machine on the power-skiving cutter design, (2017) 0–2.
- [104] J. Phillips, *General Spatial Involute Gearing*, Springer, 2003. <https://doi.org/10.1007/978-3-642-56680-6>.
- [105] D.B. Dooner, *Kinematic Geometry of Gearing*, 2012. <https://doi.org/10.1002/9781119942474>.
- [106] G. Figliolini, H. Stachel, J. Angeles, The role of the orthogonal helicoid in the generation of the tooth flanks of involute-gear pairs with skew axes, *J. Mech. Robot.* 7 (2015) 1–9. <https://doi.org/10.1115/1.4029287>.
- [107] G. Figliolini, J. Angeles, The synthesis of the pitch surfaces of internal and external skew-gears and their racks, *J. Mech. Des. Trans. ASME*. 128 (2006) 794–802. <https://doi.org/10.1115/1.2202875>.